ABSTRACT

CONSTITUTIVE MODELING OF THE THERMO-MECHANICS ASSOCIATED WITH CRYSTALLIZABLE SHAPE MEMORY POLYMERS

by
Gautam Barot

This research addresses issues central to material modeling and process simulations. Here, issues related for developing constitutive model for crystallizable shape memory polymers are addressed in details. Shape memory polymers are novel material that can be easily formed into complex shapes, retaining memory of their original shape even after undergoing large deformations. The temporary shape is stable and return to the original shape is triggered by a suitable mechanism such heating the polymer above a transition temperature. Crystallizable shape memory polymers are called crystallizable because the temporary shape is fixed by a crystalline phase, while return to the original shape is due to the melting of this crystalline phase.

A set of constitutive equations has been developed to model the thermo-mechanical behavior of crystallizable shape memory polymers using elements of thermodynamics, continuum mechanics and polymer science. Models are developed for the original amorphous phase, the temporary semi-crystalline phase and transition between these phases. Modeling of the crystallization process is done using a framework that was developed recently for studying crystallization in polymers and is based on the theory of multiple natural configurations. Using the same frame work, the melting of the crystalline phase to capture the return of the polymer to its original shape is also modeled. The developed models are used to simulate a range of boundary value problems commonly encountered in the use of these materials. Predictions of the model are verified

against experimental data available in literature and the agreement between theory and experiments are good. The model is able to accurately capture the drop in stress observed on cooling and the return to the original shape on heating. To solve complex boundary value problems in realistic geometries a user material subroutine (UMAT) for this model has been developed for use in conjunction with the commercial finite element software ABAQUS. The accuracy of the UMAT has been verified by testing it against problems for which the results are known. The UMAT was then used to solve complex 2-D and 3-D boundary value problems of practical interest.

CONSTITUTIVE MODELING OF THE THERMO-MECHANICS ASSOCIATED WITH CRYSTALLIZABLE SHAPE MEMORY POLYMERS

by
Gautam Barot

A Dissertation
Submitted to the Faculty of
New Jersey Institute of Technology
in Partial Fulfillment of the Requirements for the Degree of
Doctor of Philosophy in Mechanical Engineering

Department of Mechanical Engineering

August 2006

APPROVAL PAGE

CONSTITUTIVE MODELING OF THE THERMO-MECHANICS ASSOCIATED WITH CRYSTALLIZABLE SHAPE MEMORY POLYMERS

Gautam Barot

Dr. I. J. Rao, Dissertation Advisor   Date
Associate Professor of Mechanical Engineering, NJIT

Dr. Anthony Rosato, Committee Member   Date
Professor of Mechanical Engineering, NJIT

Dr. Ernest Geskin, Committee Member   Date
Professor of Mechanical Engineering, NJIT

Dr. Pushpendra Singh, Committee Member   Date
Professor of Mechanical Engineering, NJIT

Dr. Chien-Yueh (Michael) Huang, Committee Member   Date
Assistant Professor of Chemical Engineering

BIOGRAPHICAL SKETCH

Author: Gautam Barot

Degree: Doctor of Philosophy

Date: August 2006

Date of Birth:

Place of Birth:

Undergraduate and Graduate Education:

- Doctor of Philosophy in Mechanical Engineering,
  New Jersey Institute of Technology, Newark, NJ, 2006

- Master of Science in Mechanical Engineering,
  New Jersey Institute of Technology, Newark, NJ, 2004

- Bachelor of Science in Mechanical Engineering,
  SVRCET, Surat, Gujarat, India, 2000

Major: Mechanical Engineering

Publications and Presentations:

G. Barot and I. J. Rao
    "Three-Dimensional, Non-Isothermal Modeling and Simulation of Shape Memory Polymers", in preparation.

G. Barot, K. R. Rajagopal and I. J. Rao
    "Constitutive Modeling of the Thermo-Mechanics Associated with Crystallizable Shape Memory Polymers", in preparation.

G. Barot and I. J. Rao
    "Constitutive modeling of the mechanics associated with crystallizable shape memory polymers," *ZAMP*, March 2006, Pages 1-30.

G. Barot and I. J. Rao
    "Modeling the Film Casting Process using Continuum Model for Crystallization in Polymer," *International Journal of Non-Linear Mechanics*, Volume 40, Issue 7, September 2005, Pages 939-955.

G. Barot and I. J. Rao
    "Constitutive Modeling and Simulation of the Thermo-Mechanics Associated with Crystallizable Shape Memory Polymers", *McMat2005,*

Mechanics and Material conference, Baton Rouge, LA, June 2005.

G. Barot and I. J. Rao

"Constitutive Modeling of Crystallizable Shape Memory Polymer," *Frontier in Applied and Computational Mathematics*, May 2004, NJIT, Newark.

G. Barot and I. J. Rao

"Analysis of the Film Casting Process Using a Continuum Model for Crystallization", *39ᵗʰ Annual Technical Meeting of the Society of Engineering Science*, State College, PA, 2002. (Refereed Abstract)

"Ya Devi Sarvabhuteshu
Budhi Rupena Sansthita
Namastasyai Namastasyai Namastsyai
Namo Namaha"

Which means:
Prostrations unto Thee O Devi (Ma) who resides in all beings as Intelligence (Wisdom)

Dedication:

To,

My dearest brother: Ripal Barot and his family: Mrs. Falguni Barot and Neil

"Who has first thought of the task and wished for successful completion before it started"

My kind parents: Mr. Jashvant Barot and Mrs. Anila Barot

"For their love, support and encouragement"

My lovely wife Jenny

"For her unconditional love, faith and endurance to tolerate beyond limits"

We all die. The goal isn't to live forever; the goal is to create something that will.

-Chuck Palahnuik

ACKNOWLEDGMENT

TABLE OF CONTENTS

TABLE OF CONTENTS
(Continued)

LIST OF TABLES

LIST OF FIGURES

CHAPTER 1

INTRODUCTION

1.1 Research Objective

This study focuses on the modeling the thermo mechanics and phase change occurring in crystallizable shape memory polymers (CSMP) undergoing large deformations in to transient shape. Shape memory polymers (SMP) are a relatively new material and have novel properties. These kinds of polymers are able to 'remember' their original shape even after undergoing large deformations. Because of this they are finding use in applications ranging from biomedical devices to space technology. Currently there are no models available that can accurately characterize their behavior and this is partly because of modeling crystallization and melting process coupled with shape change in polymers is a difficult yet important one. This requires elements of mechanics, thermodynamics and polymer science and a proper combination of these elements is necessary to develop the accurate models. The aim of this research is to formulate fully invariant three dimensional constitutive equations in a thermodynamic setting that are capable of predicting the thermal and mechanical behavior of CSMP under a variety of conditions. The model developed will be implemented in to a finite element program to simulate the behavior of shape memory polymers in realistic geometries and conditions. This work will help speed up the use of this novel material in production of different plastic products in a variety of applications.

1.2   Introduction to Shape Memory Polymers

A new class of materials called 'smart material' has emerged as a result of rapid technological advancements. Material scientists predict a prominent role for such kinds of materials in the future to come. Smart materials are those whose one or more properties can be dramatically altered such as piezoelectric materials, magneto-rheostatic materials, electro-rheostatic materials, shape memory alloys and shape memory polymers.

Polymeric materials have become the integral part of human life in 21st century. Wide range of applications varying from technologically important to ones those are of commonplace everyday use. Shape memory polymers are new type of polymers that has been first developed by group of researchers in Japan and later introduced in USA. These kinds of polymers posses a unique property, they remember their original shape even after undergoing large deformation into a temporary shape. Return to the original shape is activated by the suitable external trigger. Based on the external stimuli used as triggering mechanism, shape memory polymer can be classified in to thermo responsive, photo-responsive and chemo-responsive shape memory polymers. Photo-responsive shape memory polymers uses light source as an external stimulus that is capable to induce the photochromic reaction causing geometrical rearrangement of the monomers that leads to large shape change at bulk level. Where as in case of chemo responsive, another chemical is used as an external stimulus and shape recovery can be caused by changing the pH value of the reactive environment it is in. Thermo responsive materials are those which use heat as the external stimulus. Shape memory alloys and shape memory polymers are good examples of thermo responsive shape memory materials. However, mechanisms for shape fixity and shape recovery are totally different in each case. Detailed descriptions of the mechanism that is responsible for shape fixity and shape recovery are discussed for both the cases in following chapters.

1.3   Thermo Responsive Shape Memory Polymers

Thermo responsive shape memory material can be classified in to two groups: shape memory alloys and shape memory polymers. First time shape memory was observed in Nickel-Titanium alloys broadly known as Nitinol in the year of 1958 (Müllner (1999)). Solid state phase change that occurs in metal alloys is responsible for the exhibition of this unique property in nickel-titanium alloys. To have better understanding of the mechanism, responsible for shape memory in nickel-titanium alloys, knowledge of phases associated with alloys is necessary. There are two phases associated with the alloys: austenite structure and martensite structure. Even though austenite structure and deformed martensite structure has different molecular configurations, on the macroscopic level they can have similar shape as shown in Figure 1.1. Cooling alloy below certain temperature (martensite phase transformation end temperature) 100% austenite structure converts in to 100% martensite structure. Martensite structure can be deformed easily when comparing it with austenite structure. After distorting, undeformed martensite structures will take a permanent deform structure and even after load removal it will remain in a deformed shape due to rearrangement of molecules. This deformed shape is the transient shape for shape memory alloys. Heat is the driving force for the molecular rearrangements and so upon heating deformed martensite structure will then converted in to more ordered austenite structure transforming the transient shape back to its original shape as shown in Figure 1.2.

Macroscopic View

Austenite   Twinned Martensite   Deformed Martensite

Microscopic View

Austenite   Twinned Martensite   Deformed Martensite
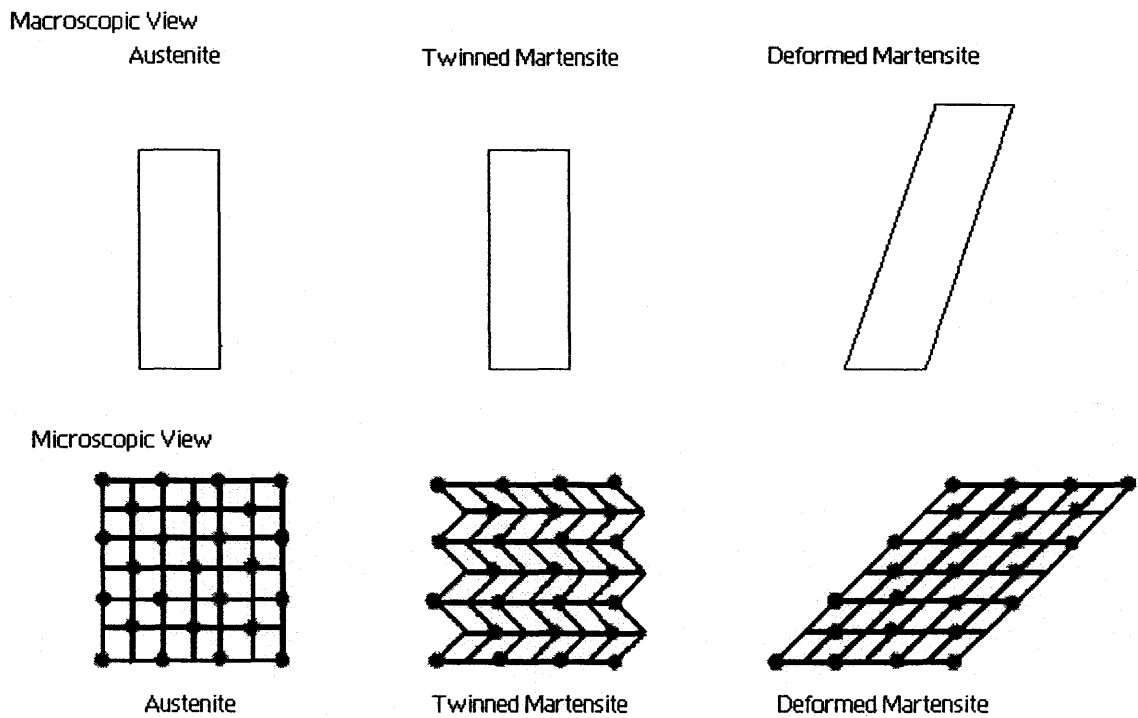
Figure 1.1 Microscopic and macroscopic views of the two phases of shape memory alloys.
(Source: Oulu University - http://herkules.oulu.fi/isbn9514252217/html/x317.html date: Dec 26, 2005)
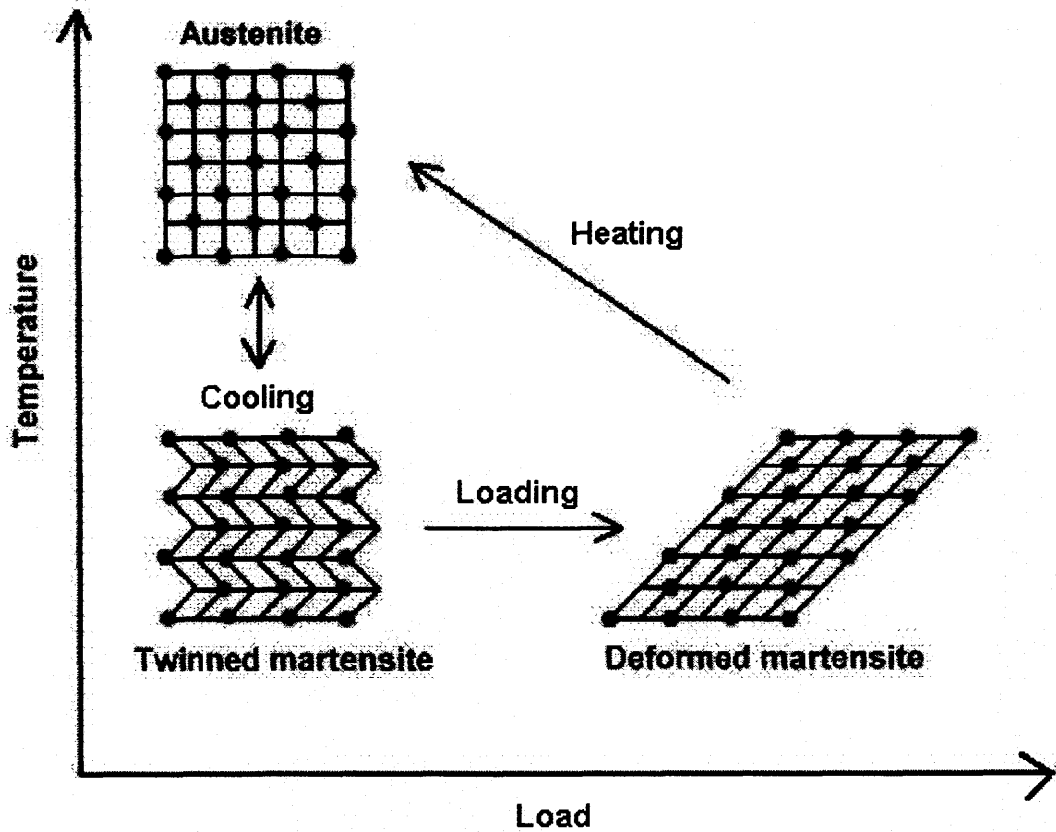
Figure 1.2 Microscopic diagram of the shape memory effect.
(Source : Oulu University - http://herkules.oulu.fi/isbn9514252217/html/x317.html date: Dec 26, 2005)

Shape memory alloys are being used in various applications in different fields including aerospace, robotics, bio-engineering etc. for example vascular stents, sensors and actuators, space shuttles, hydraulic fittings for aeroplane and many more. Even though shape memory alloys have many applications, they do however have some limitations. Shape memory alloys are expensive to use due to its expensive manufacturing process that requires special treatments and expensive metals. Moreover, Shape memory alloys cannot under go large deformation and they cannot be made bio-degradable, these reasons put restrictions on their usage.

Shape memory polymers can be a good alternative to shape memory alloys in many cases where shape memory alloys can not be used. According to Monkman (2000), Shape memory polymers can be used as actuators and various other applications and can be a good alternative to expensive shape memory alloys. Making shape memory polymers bio-degradable, follow up surgery required with the use of metallic implants can be avoided (Lendlein et al. (2002(b))). Shape memory polymers are cheaper to produce than shape memory alloys as they can be easily processed in to a variety of different shapes and sizes using standard processing methods such as extrusion, molding forming etc., that are routinely used in the manufacture of plastics. Moreover, by adjusting their chemical structure and composition by a small amount, their transient temperature can be set to any temperature with in a large window (Davis et al. (2003), Jeong et al. (2000), Lendlein et al. (2001), Liu et al. (2002)). Because of the above mentioned properties there are potential applications for shape memory polymers, ranging from actuators, MEMS devices, temperature sensors to damping elements in structure to name a few. Due to their bio-friendly nature, these materials have the potential to be used in biomedical applications, many of which are in their early stages of development. Fibers and films made from shape memory polymers have good insulating

properties at low temperatures and high gas permeability at higher temperatures preventing the build up of heat. Work on making smart clothing, which, do not require frequent ironing and changes the texture according to environment, is going on. Other applications include digital storage media that can be easily re-written, intravenous needles and other implantable medical devices that soften in the body. The applications are in the process of development such as their use in deployment of space structures in simple manner at very low costs and with a much smaller storage volume as compared to other deployment mechanisms. For more detail on these and other applications see (Tobushi et al. (1996), Monkman (2000), Poilane et al. (2000) and Tey et al. (2001)).

1.4   Driving Mechanisms for Shape Fixity and Shape Recovery

Although heat is used in both cases as an external stimulus, the driving mechanism that is responsible for shape memory is different in both: shape memory alloys and shape memory polymers. The mechanisms responsible for memorizing or fixing the original shape or transient shape is shape memory polymers are: entanglements of the polymer molecules, cross-linking, crystalline state and glassy state (see Lin et al. (1999), Irie (1998), Kim et al. (2000)). Depending on the specific polymer, one of these four mechanisms is responsible for fixing the transient shape. If glass transition is responsible for the transient shape, then glass transition temperature, θ_g, is the recovery temperature, θ_R, If it is due to crystallization the melting temperature, θ_m, is the recovery temperature. If transient shape is fixed due to crystallization then such shape memory polymers are called crystallizable shape polymer and if transient shape is fixed due to glass transition temperature such shape memory polymer are called amorphous shape memory polymer. In this work, only crystallizable shape memory polymers are discussed.

Crystallizable shape memory polymers can be either thermosets or thermoplastics. Thermoplastic crystallizable shape memory polymers are block copolymers consisting of alternating chains of two different polymers (A and B) linked end to end. The polymers A and B are chosen so that the copolymer exhibits shape memory behavior. One of the constituent polymers, say A, is chosen to have a high melting or glass transition temperature, which is denoted by θ_h while the other polymer, represented by B, has a lower melting temperature, which for reasons to be made apparent shortly, by θ_R (for recovery temperature). When the polymer is cooled from a melt like state the polymer with the higher melting / glass transition temperature, here polymer A, solidifies first forming segregated hard domains. These hard domains are linked together by polymer B, which crystallizes at a lower temperature (θ_R). *Between these two temperatures $(\theta_R < \theta < \theta_h)$ the materials behavior is rubber-like, with the hard domains acting as cross-links due to which the polymer returns to its original shape even after undergoing large deformations.* If the polymer is cooled below θ_R, polymer B *partially crystallizes* and the material stiffens, losing its rubber like behavior. If the material is cooled while it is in a deformed configuration, polymer B crystallizes in this deformed configuration, and these newly formed crystallites act as temporary cross-links which prevent the shape memory polymer from returning to its original shape. On unloading the specimen below θ_R a small amount of recovery is observed as the polymer has its original cross-links still in place. On subsequent heating above θ_R the crystalline phase associated polymer B melts and the shape memory polymer returns to its original shape. On further heating above θ_R the hard domains also melt and the material returns to the melt-like state.

The orientation of the crystals formed below θ_R depends on the deformation undergone by the polymer just prior to cooling (see Wang et al. (1999)). These crystals will have a preferred direction depending on the deformation that will cause the material properties to be anisotropic. Thermoset shape memory polymers also show similar behavior, except the permanent shape is a result of chemically cross-linking a crystallizable polymer and not due to the presence of hard domains. Vulcanization of rubber is a common example of such a process, wherein the introduced Sulphur reacts with natural rubber forming a network structure. Above the melting temperature of the polymer, which is again denoted by θ_R, the SMP has a rubber like behavior due to the presence of chemical cross-links, however upon cooling below θ_R, polymer crystallization takes place. These newly formed crystals act to stiffen the SMP with the crystallites acting as cross-links. If the polymer is deformed prior to cooling, the crystallites, which act as temporary cross-links are formed in the deformed configuration and as a result the polymer retains its transient shape. The original shape is recovered on heating above the melting temperature. The behavior of these two types of SMPs, i.e., thermosets and thermoplastic SMPs is hence, very similar.

The shape memory behavior of SMPs is illustrated schematically in Figure 1.3 along with a typical uni-axial stress-strain curve, Figure 1.4 (see Kim et al. (1996, 1998) and Lendlein et al. (2001)). In Figure 1.3, the filled circles represent the cross-links (they could be the hard domains or chemical cross-links), the wavy line connecting the cross-links represents the crystallizable polymer in its amorphous state while the rectangular blocks represent the crystallizable polymer in a crystalline state. State 1 in both figures denotes the undeformed configuration. Above the recovery temperature θ_R the polymers behavior is rubber-like and its elastic behavior is driven by changes in entropy. On

deforming above θ_R, the polymer molecules between the cross-links stretch (state 2). If the polymer is now cooled to a temperature below θ_R, crystallization takes place and the crystals are formed in this deformed configuration. The onset of crystallization is accompanied by a sharp drop in the stress (from state 2 to state 3). *After unloading (state 3 to state 4) the polymer remains in a deformed configuration with a small amount of recovery. This recovery is due to the presence of two components (amorphous and crystalline) each with their own stress-free states.* The amorphous part has a tendency to retract to its original configuration while the crystalline part prefers the deformed configuration. As the crystalline part is a lot stiffer, the recovery strain is small (see Figure. 1.4). The mechanical response of the polymer in this state is similar to that of a semi-crystalline polymer with oriented crystallites, i.e., it is relatively stiff and the mechanical behavior is anisotropic. Usually when this semi-crystalline polymer is subject to small deformations it exhibits elastic behavior, energetic in origin. If however, the polymer is subject to large deformations, inelastic behavior caused by reorientation of the crystallites and secondary crystallization takes place. During these inelastic processes degradation of the original cross-links can occur reducing the ability of the polymer to return to its original shape on heating. When the polymer is heated to above θ_R, (from state 4 to state 1) the crystallites melt returning to their original amorphous state, if the cross-links originally present in the polymer remain the polymer retracts to its original shape. This retractive force depends on the extent to which the polymer was deformed prior to cooling and is an important parameter when shape memory polymers are used in actuators.
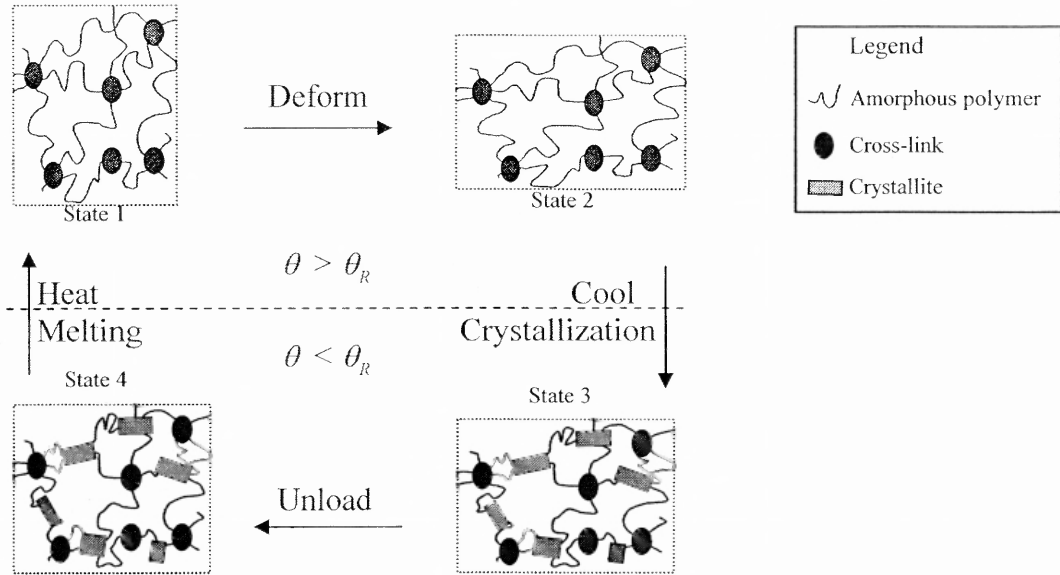
Figure 1.3 Schematic illustration of the shape memory effect in polymers.
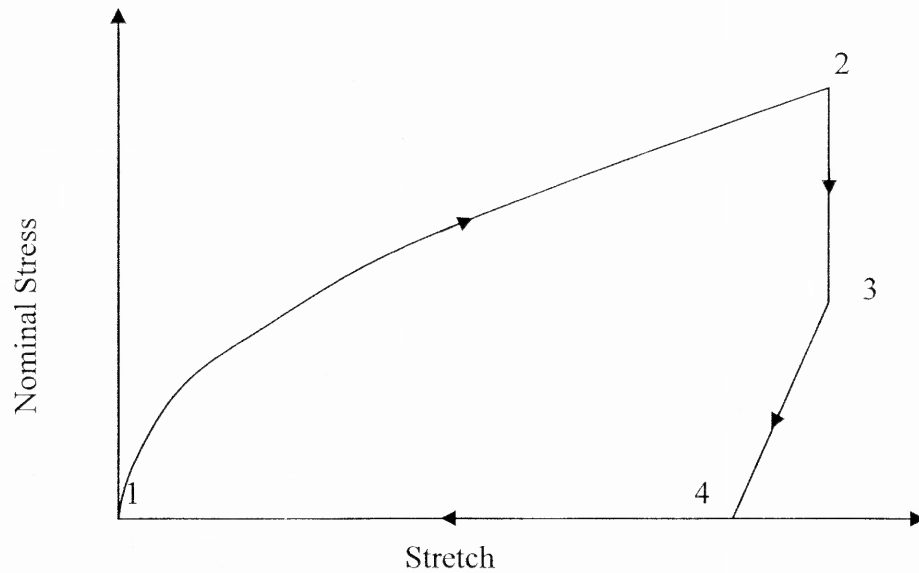
Figure 1.4 Typical stress versus strain curve for shape memory polymer.

1.5 Outline of the Dissertation

In Chapter 2, prescribes the discussion of the work of other research groups whose works are important for the current research. Also, it includes various attempts made to model shape memory polymers, phase transition and crystallization. Significant experimental observations will be noted and simplifying assumptions, solution methods and results of simulations of will be outlined. In Chapter 3, some important concepts of Continuum Mechanics and Thermodynamics will be presented concisely. Chapter 4 presents the details of the continuum framework for the crystallizable shape memory polymers. Thermo-mechanics associate with each phase of the crystallizable shape memory polymers will be modeled using the concepts of Continuum Mechanics and Thermodynamics. Crystallization and Melting includes phase transition phenomenon, and using the frame work developed for the crystallization in polymers this phenomenon will be incorporated in to the model.

In Chapter 5, simulation of standard, one dimensional deformation processes such as uni-axial extension and circular shear will be carried out. For each process required kinematical quantities and balance laws will be derived in their proper form. A numerical method to develop the computer code that is required for simulations will be programmed. In Chapter 6, using the model developed in Chapter 4 and MATLAB simulation of 1-D, non-isothermal process will be carried out. Simulations of this process will be helpful to understand thermo-mechanics associated with the CSMPs. In Chapter 7, some basic concepts of FEM are prescribed along with the procedure to create a user subroutine (UMAT) for a user material. Further, the developed user subroutine is tested with standard suggested tests in ABAQUS/CAE. Chapter 8 is about the finite element analysis of various processes where the material used in the process is CSMP. These

analyses will be done using ABAQUS/CAE and it will show the applicability of the developed UMAT based on the constitutive equation derived in Chapter 4.

The summary of the dissertation with an outline of original contributions of this research are presented in Chapter 9 along with recommendations for the future work.

CHAPTER 2

BACKGROUND

2.1 Introduction

In this chapter, related works in the area of shape memory polymer are discussed. Each work is studied in depth to understand the critical issues presented. A brief description of the materials used for making shape memory polymer along with, experimental methods that is used for various tests and material characterization is also discussed. The study on various modeling techniques and different analysis done for the shape memory polymers is described and critical finding of their works is mentioned.

Crystallization is the most important phenomenon in case of crystallizable shape memory polymers. A separate section in this chapter is devoted to studies related to crystallization. The section mainly discusses the various modeling approaches to crystallization.

2.2 Related Work

Wang et al. (1999), used poly(ether ester)s consisting of poly(ethylene oxide) and poly(terephthalate) segments, EOET co-polymer as shape memory polymers and showed that only oriented and/or extended chains are contributive to recovery of deformation and these chains in stretch direction will result in crystalline morphology similar to 'shish-kebab' upon cooling.

Shape memory technology for polymers needs optimum combination of two components out of which one is responsible for polymer architecture or morphology to fulfill certain structural requirement and other require for programming technology for

shape fixity and recovery. Shape memory polymer elongation is possible up to 1100% (see Lendlein et al. (2002(a))).

In the work of Jeong and Kim (Jeong et al. (2000), Kim et al. (1996, 1998, 2000)), detail description of both phases of shape memory polymer namely: amorphous phase and crystalline phase can be found. Optimized ratio of both co-polymers is essential for maximizing the crystallinity and with the increasing crystallinity hysterisis can also be increased. Transition temperature of shape memory polymer can also be adjusted using proper combination of the copolymer used.

C. Poilane et al. (2000), quantified the mechanical characteristic of shape memory polymers using three different techniques namely nanoindentation, bulging and membrane point deflection. Nanoindentation and bulging test can be useful when the simple tensile tests are difficult to perform. Lendlein et al. (2001), used $\varepsilon -$ caprolactone, bio-degradable copolymer, for making crystalline shape memory polymer and showed in thermocyclic experiments that a recovery rate more than 99% can be achieved.

Tobushi et al. (2001), developed non-linear thermomechanical model of crystallizable shape memory polymer. It is assumed that shape fixity is caused due to glass transition temperature and final solid after cooling is amorphous in nature. The equation is as follows:

$$\dot{\varepsilon} = \frac{\dot{\sigma}}{E} + m\left(\frac{\sigma - \sigma_y}{k}\right)^{m-1}\frac{\dot{\sigma}}{k} + \frac{\sigma}{\mu} + \frac{1}{b}\left(\frac{\sigma}{\sigma_c} - 1\right)^n - \left(\frac{\varepsilon - \varepsilon_s}{\lambda}\right) + \alpha\dot{T}, \qquad (2.2.1)$$

where, ε, σ and T denote strain, stress and temperature respectively. E, μ, λ and α represent modulus of elasticity, viscosity, retardation time and co-efficient of thermal expansion. k, b, σ_c, σ_y & ε_s are constants of the equation. Similar work can be found in work of Lin et al. (1999). These models are merely 1-D curve fitting and models are not

frame invariant and can not be used for three-dimensional geometries as it is not applicable for large deformation.

Based on the thermodynamic concepts of entropy and internal energy, it is possible to interpret the thermomechanical behavior of SMPs from a macroscopic viewpoint without explicitly incorporating details of the molecular interactions. Liu et al. (2006) developed model using the same concept for amorphous shape memory polymers. The model quantifies the storage and release of the entropic deformation during thermo-mechanical processes. The fraction of the material freezing a temporary entropy state is a function of temperature, which can be determined by fitting the free strain recovery response. A free energy function for the model is formulated and thermodynamic consistency is ensured. However, as the model was for amorphous shape memory polymers both phases were considered as isotropic, hyperelastic solid and transition from rubbery phase to glassy phase were done my increasing shear modulus only. The main difference between modeling amorphous shape memory polymers and crystalline shape memory polymer is the modeling phase transition. Phase transition in CSMP involves crystallization. Properties of the semicrystalline phase or temporary shape depend on what happens during the crystallization.

2.3   Study on the Crystallization Process in Polymers

Heat conduction was dominant mechanism to study the phase transition such studies cane be traced back to the works of Lame et al. (1831) and Stefen (1891), in which temperature is considered to be basic variable (see Bankoff (1964), Crank (1984), Fasano et al. (1979) and Rubinstein (1971)). One approach to model the phase transition is the 'phase field' model. The model includes a parameter, along with conduction, called the

order parameter whose value determines the state of the material. The parameter takes on extreme values of +1 for pure liquid and -1 for pure solid. The heat conduction equation is modified to incorporate the effect of the order parameter that leads to an additional equation whose origin can be traced back to Landau-Ginzburg theory of phase transitions (see Landau (1967)). Both the Stefen approach and the phase field approach does not include the issues related to symmetry of the final solid and this issue only can resolved with the addition of kinematic fields.

A known approach in polymer physics to study the crystallization kinetics is an Avarami approach. Avarami approach is based on the notion of filling space through the nucleation and growth of one phase in to another. It is assumed in this approach that nucleation initiated at certain location known as nucleation sites. On set of the nucleation the growth of crystalline material is then prescribed by growth rate. The problems in which exact instant when crystallization is initiated in not known, such as non-isothermal processes it is difficult to apply the Avarami equation. Moreover, Avarami approach does not address issue of important thermodynamic quantities such as the internal energy and the entropy in straight forward manner. These are major drawbacks with this approach. Also, there are certain polymers such as polyethylene terephthalate which at temperatures just above the glass transition temperature crystallize only due to deformation. The Avarami equation fails to predict such kind to behavior and not general enough to capture the various types of crystallization behavior observed in polymers. Due to such reasons, this approach is not used in this work (more information on the Avarami approach can be found in Eder et al. (1990), Mandelkern L (1964) and Wunderlich (1976)).

The other approach that is useful for modeling the thermo mechanics associated with crystallization is the notion of the natural configuration. Usually, stress-free configuration is considered as natural configuration of a material. For elastic materials,

elastic response can be fully described by the deformation of the body from a single natural configuration. The stress at a material point is determined by a functional of the history of the density and the deformation gradient, at a material point where stress free configuration is considered as reference configuration. For materials exhibiting inelastic response, such as polymers, single natural configuration is not sufficient for the full description of the behavior. Rajagopal (1995) has demonstrated the central role played by natural configuration in a variety of dissipative processes with associated symmetry changes and the change of response characteristics of the body. The work covers large class of materials under one frame work: multi network theory (see Rajagopal et al. (1992)), classical metal plasticity (see Rajagopal et al. (1998)), twinning (see Rajagopal et al. (1995)), solid to solid phase transition (Rajagopal et al. (1999)), viscoleastic liquids (Rajagopal et al. (2000)), anisotropic fluids (Rajagopal et al. (2001)) and geological materials (Muralikrishna et al. (2004)). Rao et al. (2000) introduced the utility of the framework to capture transition, from viscous rate type of fluid to anisotropic hyper elastic solid, due to solidification and crystallization in polymers with purely mechanical settings. Rao et al. (2002) used this approach because of its robustness to model crystallization in process and created a thermodynamic framework for the study crystallization in polymers. The key feature of this framework is that a body can exist, stress free, in numerous natural configurations, the underlying natural configuration of the body changing during the process, with the response of the body being elastic from these evolving natural configurations. This framework has been successfully utilized to simulate various polymer processes involving crystallization phenomena (Barot et al. (2005, 2006), Rao (2002, 2004), Rao et al. (2005)).

CHAPTER 3

PRELIMINARIES

3.1   Introduction

In this chapter, the familiar concepts of Continuum Mechanics are prescribed. The review includes introduction to all the required kinematical quantities as well as the measures of stress and study of the other physical laws which requires a general approach that includes Thermodynamics.   Roughly, the review comprises the following basic ingredients:

- A brief description of motion and deformation.

- A brief discussion of stress in continuum.

- A brief description of the fundamental laws of physics governing the motion of a continuum.

All the results are given here without proof; the proof can be found in some of the classical work of Truesdell (1991), Truesdell et al. (1965), Holzapel G (2000), Rajagopal et al. (1999), Green et al. (1977) and Rao et al. (2002).

3.2   Kinematics

3.2.1 Body, Motion and Deformation

A continuum theory has been developed independently of the molecular and atomistic theory. A body B may be viewed as continuous distribution of matter in a topological space $\aleph$ and time t, over which a non-negative measure M, called mass, is defined. Large numbers of molecules makes a typical continuum particle and the behavior of such continuum particle reflects a collective behavior of all the molecules constituting a

continuum particle. An invertible mapping κ from the space of bodies $\aleph$ to a three-dimensional Euclidean space $\Im$ is called a *placer*. The image of B through the placer, $\kappa(B)$ is a *Configuration* or shape of the body.

A mass of any part of the body B, say P can be expressed with the help of a scalar function ρ called *density*:

$$M(P) = \int_{\kappa(P)} \rho_\kappa dV, \tag{3.1.1}$$

where κ is the certain configuration of B.

Consider a body B in a configuration $\kappa_R(B)$, let X denote a typical position of a material point in κ_R. Let κ_t be the configuration at a time t, and then the *motion* χ_κ assigns to each particle in configuration κ_R a position in the configuration κ_t at time t, i.e.

$$\text{x} = \chi_\kappa(\text{X}, t). \tag{3.1.2}$$

The *velocity* of the particle is given by

$$\text{V}(\text{X}, t) = \frac{\partial \chi_\kappa(\text{X}, t)}{\partial t}, \tag{3.1.3}$$

while its *acceleration* is

$$\text{A}(\text{X}, t) = \frac{\partial^2 \chi_\kappa(\text{X}, t)}{\partial t^2}. \tag{3.1.4}$$

The velocity and the acceleration here are expressed here by denoting the position of a particle in reference configuration such description is often called as the *Lagrangian* description or *Material* description. Since, the motion χ_κ is invertible,

$$\text{X} = \chi_\kappa^{-1}(\text{x}, t), \tag{3.1.5}$$

It is possible to express velocity and acceleration and other quantities that depend on particle by denoting the particle with its current configuration also. The way of describing

quantities using its current configuration is known as *Eulerain* description or *Spatial* description. The velocity and the acceleration field in spatial description can be written as

$$
\begin{aligned}
\mathbf{v}(\mathbf{x},t) &= \mathbf{V}\left[\chi_\kappa^{-1}(\mathbf{X},t),t\right], \\
\mathbf{a}(\mathbf{x},t) &= \mathbf{A}\left[\chi_\kappa^{-1}(\mathbf{X},t),t\right].
\end{aligned}
\tag{3.1.6}
$$

Eulerian approach is suitable for studying the mechanics of fluids where as for the solid mechanics Lagrangian representation is preferred.

The deformation gradient $\mathbf{F}_{\kappa_R}$, with respect to reference configuration, is defined through

$$
\mathbf{F}_{\kappa_R} := \frac{d\chi_{\kappa_R}}{d\mathbf{X}}.
\tag{3.1.7}
$$

Using polar decomposition theorem for $\mathbf{F}_{\kappa_R}$ following can be showed

$$
\mathbf{F}_{\kappa_R} = \mathbf{R}_{\kappa_R}\mathbf{U}_{\kappa_R} = \mathbf{V}_{\kappa_R}\mathbf{R}_{\kappa_R},
\tag{3.1.8}
$$

where $\mathbf{R}_{\kappa_R}$ is a proper orthogonal tensor, $\mathbf{U}_{\kappa_R}$ and $\mathbf{V}_{\kappa_R}$ are symmetric, positive definite tensors. The physical meaning of equation(3.1.8) is that every deformation can be decomposed locally as rotation followed by a pure stretch or in a pure stretch followed by a rotation. The *left* and *right Cauchy-Green stretch tensors* $\mathbf{B}_{\kappa_R}$ and $\mathbf{C}_{\kappa_R}$ are defined through

$$
\begin{aligned}
\mathbf{B}_{\kappa_R} &:= \mathbf{V}_{\kappa_R}^2 = \mathbf{F}_{\kappa_R}\mathbf{F}_{\kappa_R}^T = \sum_{a=1}^{3}\lambda_a^2\hat{\mathbf{n}}_a\otimes\hat{\mathbf{n}}_a, \\
\mathbf{C}_{\kappa_R} &:= \mathbf{U}_{\kappa_R}^2 = \mathbf{F}_{\kappa_R}^T\mathbf{F}_{\kappa_R} = \sum_{a=1}^{3}\lambda_a^2\hat{\mathbf{N}}_a\otimes\hat{\mathbf{N}}_a.
\end{aligned}
\tag{3.1.9}
$$

where, λ_a is principal Eigen values of tensor $\mathbf{U}_{\kappa_R}$ and $\hat{\mathbf{n}}_a$ and $\hat{\mathbf{N}}_a$ are the principal spatial directions and principal referential directions respectively.

As the information of the stretch inside the body is given by Cauchy-Green tensors the measures of strains are usually defined in terms of either $\mathbf{B}_{\kappa_R}$ or $\mathbf{C}_{\kappa_R}$, e.g. The Green-St. Venant strain, strain form in Lagrangian form,

$$\mathbf{E}_{\kappa_R} := \frac{\mathbf{C}_{\kappa_R} - \mathbf{I}}{2}, \tag{3.1.10}$$

where, $\mathbf{I}$ is an identity tensor. Similarly, Eulerian measure of strain, known as Almansi-Hamel strain, can be prescribed by

$$\mathbf{e}_{\kappa_t} := \frac{\mathbf{I} - \mathbf{B}_{\kappa_R}^{-1}}{2}. \tag{3.1.11}$$

The spatial gradient or velocity is given by:

$$\mathbf{L} := \frac{\partial v}{\partial x} = \dot{\mathbf{F}}_{\kappa_R} \, \mathbf{F}_{\kappa_R}^{-1}. \tag{3.1.12}$$

$\mathbf{L}$ can be decomposed in to its symmetric part $(\mathbf{D})$, which represents the rate of deformation tensor, and skew-symmetric part $(\mathbf{W})$, which represents the rate of rotation tensor or vorticity tensor by following expression

$$\mathbf{L} = \mathbf{D} + \mathbf{W} \tag{3.1.13}$$

3.2.2 Stress Tensor

There are two types of the forces a body can observe. First, the arbitrary force, known as *external forces,* that acts on the parts or the whole of the boundary surface S and second, known as *internal forces,* acts on a surface within the interior of the body in some distributed manner. These forces are also known as traction $\mathbf{t}$ and body forces $\mathbf{b}$ respectively. The unit of the traction force is fore per unit area while, body force has the dimension of fore per unit volume. Using Cauchy stress theorem, the dependence of the traction on the surface can be prescribed by as follows:

$$\mathbf{t}(x,t,S) = \sigma^T(x,t)\mathbf{n}. \tag{3.1.14}$$

Where, σ^T is true stress or Cauchy stress and **n** is the unit normal vector to the surface S.

In material representation, it is known as Piola-Kirchoff stress and it can be given in terms of Cauchy stress as follows:

$$\mathbf{P} := (\det \mathbf{F})\sigma \mathbf{F}^{-T} \tag{3.1.15}$$

In practical, first Piola-Kirchoff stress is also known as nominal stress or engineering stress. Two other measures of stress are the second Piola-Kirchoff stress tensor

$$\hat{\mathbf{P}} := (\det \mathbf{F})\mathbf{F}^{-1}\sigma \mathbf{F}^{-T,} \tag{3.1.16}$$

and the Kirchoff stress

$$\overset{k}{\sigma} = (\det \mathbf{F})\sigma. \tag{3.1.17}$$

This form is useful for developing finite element code particularly, one that is used with ABAQUS.

3.2.3 Conservation Laws and Thermodynamics

Physical meaning of any of the balance law is the fact that a physical quantity under consideration does not change its value during the process. Any acceptable process has to satisfy the appropriate balance laws. Conservation laws of Continuum Mechanics include the conservation of mass, momentum and angular momentum. There are cases, where the modeling cannot be done with the aid of laws of Continuum Mechanics and one has to use the conservation laws of Thermo-mechanics such as first and second laws of thermodynamics which requires the knowledge of the concepts of energy and entropy.

The conservation of mass states the fact that the mass of any part P of the body remain unaltered irrespective of the motion the body undergoes. The spatial form of the conservation of mass is:

$$\frac{\partial \rho}{\partial t} + div(\rho \mathbf{v}) = 0, \tag{3.1.18}$$

while the referential form of the same principle is:

$$\rho_0 = \rho \det \mathbf{F}, \tag{3.1.19}$$

where, ρ_0 is the density in reference configuration. Incompressible material can only undergo the volume preserving motion in which case the density remains constant. The conservation of mass for an incompressible material reduces to

$$div(\mathbf{v}) = 0, \tag{3.1.20}$$

or in referential form using equation(3.1.19)

$$\det \mathbf{F} = 1. \tag{3.1.21}$$

The conservation of linear momentum is equivalent of Newton's second law for the continua. Its Eulerian local form is:

$$\rho \left[\frac{\partial \mathbf{v}}{\partial t} + [\nabla \mathbf{v}] \mathbf{v} \right] = div\sigma^T + \mathbf{b}, \tag{3.1.22}$$

where $\mathbf{b}$ is the body force. The balance of linear momentum in referential form can be written as:

$$\rho_0 \left[\frac{d\mathbf{v}}{dt} \right] = Div\mathbf{P} + \mathbf{B}, \tag{3.1.23}$$

where the Div is the divergence taken in the reference configuration and $\mathbf{B}$ is the body force in reference configuration.

For an incompressible material the stress tensor σ reduces to

$$\sigma = -p\mathbf{I} + \sigma^E, \tag{3.1.24}$$

where p is the Lagrange multiplier due to the constraints of incompressibility, and σ^E is the constitutively determined extra stress. The balance of angular momentum for a body in the absence of internal couples requires that the stress tensor be symmetric.

$$\sigma = \sigma^T. \tag{3.1.25}$$

Concept of energy can be related to its conservation directly as no one has no knowledge of what energy is (see Feynman (1989)). Energy neither can be produce nor it

can be destroyed and it can only be transformed in to one form to its other several forms. Talking about mechanical energy only, the balance of mechanical energy known as power theorem can be written as:

$$\frac{D}{Dt}\mathcal{K}(t) + \mathcal{P}_{int}(t) = \mathcal{P}_{ext}(t) \qquad (3.1.26)$$

where, $\mathcal{K}$ is kinetic energy, $\mathcal{P}_{int}$ is rate of internal mechanical work or stress power and $\mathcal{P}_{ext}$ represents rate of external mechanical work. Equation (3.1.26) can be written in more general form that is suitable for continuum occupying some arbitrary region Ω as

$$\frac{d}{dt}\int_{\Omega}\frac{1}{2}\rho\mathbf{v}\cdot\mathbf{v}\,dv + \int_{\Omega}\sigma\cdot\mathbf{L}\,dv = \int_{\partial\Omega}\sigma^{T}\mathbf{n}\cdot\mathbf{v}\,da + \int_{\Omega}\rho\mathbf{b}\cdot\mathbf{v}\,dv \qquad (3.1.27)$$

The first law of Thermodynamics can be thought of as implicit definition of energy. This law of Thermodynamics correlates between mechanical energy and the other form of energy known as 'heat'. There exists a physical quantity known as 'internal energy', ε, that closes the energy balance equation. A statement for the first law can be then stated as "The sum of the variations of kinetic energy, $\mathcal{K}$, and of internal energy ε (the sum of two can be depicted as $(\dot{\mathcal{E}})$) is equal to sum of the rate at which work is done by the external forces, $\mathcal{W}$, and of the energy per unit time that enter the system as heat transfer, $\mathcal{Q}$ ". Mathematical representation of the statement is as follows:

$$\dot{\mathcal{E}} = \dot{\mathcal{Q}} + \dot{\mathcal{W}} \qquad (3.1.28)$$

where,

$$\dot{\mathcal{E}} = \frac{d}{dt}\int_{\Omega}\frac{1}{2}\rho\mathbf{v}\cdot\mathbf{v}\,dv + \frac{d}{dt}\int_{\Omega}\rho\varepsilon\,dv,$$

$$\dot{\mathcal{Q}} = \frac{d}{dt}\int_{\Omega}\rho r\,dv + \frac{d}{dt}\int_{\partial\Omega}\mathbf{q}\cdot\mathbf{n}\,da, \qquad (3.1.29)$$

$$\dot{\mathcal{W}} = \int_{\partial\Omega}\sigma^{T}\mathbf{n}\cdot\mathbf{v}\,da + \int_{\Omega}\rho\mathbf{b}\cdot\mathbf{v}\,dv,$$

and r is the radiant heating, q is the heat flux through the surface Ω. As Ω is arbitrary surface, combining the power theorem and the first law of thermodynamics the local form of the balance of energy for a continuum can be written as follows

$$\rho \dot{\varepsilon} + div\mathbf{q} = \boldsymbol{\sigma} \cdot \mathbf{L} + \rho r. \tag{3.1.30}$$

The second law of Thermodynamics identifies the fundamental difference between the two forms of energy namely mechanical energy in form of work and thermal energy in form of heat. The second law of Thermodynamics can be stated, according to Kelvin, (see Pippard (1957)) as follows: "*It is impossible to devise an engine which, working in a cycle, shall produce no effect other than extraction of hear from a reservoir and the performance of an equivalent amount of mechanical work.*" This observation cannot be deduced from the first law. Only second law can indicates the direction of an energy transfer process.

The useful form for the second law is known as entropy inequality principle. It is important to introduce the concept of entropy before writing the statement. Entropy, $\mathcal{S}$, is defined as fundamental state variable. Assuming the entropy is possessed by continuum body Ω occupying some region is defined to be

$$\mathcal{S} = \int_{\Omega} \rho \eta dv, \tag{3.1.31}$$

where η is entropy per unit mass. The production of entropy is the difference between the rate of change on entropy and the rate of entropy input in to body at an absolute temperature θ. According to the second law of thermodynamics, this rate of entropy production for all the thermodynamics process is never negative. The mathematical expression for the statement is

$$d\mathcal{S} - \frac{dQ}{\theta} = d\xi \geq 0. \tag{3.1.32}$$

where $d\xi$ is entropy produced. For reversible process $d\xi$ is equal to zero and for irreversible process $d\xi$ is positive. Hence, for any realistic process Equation (3.1.32) can also be written as

$$\frac{d\mathcal{S}}{dt} - \frac{1}{\theta}\frac{dQ}{dt} = \frac{d\xi}{dt}.$$
(3.1.33)

It can be showed that using Equation (3.1.31), second term in Equation (3.1.29) and Equation (3.1.33) the balance law for entropy can have following form

$$\rho\dot{\eta} + div\left(\frac{q}{\theta}\right) = \rho\frac{r}{\theta} + \rho\xi$$
(3.1.34)

Combining the balance of energy, Equation (3.1.30), and the balance of entropy, Equation (3.1.34) results in the reduced energy-dissipation equation. The reduced energy-dissipation equation is

$$\sigma\cdot\mathbf{L} - \rho\dot{\varepsilon} + \rho\theta\dot{\eta} - \frac{\mathbf{q}\cdot grad\theta}{\theta} = \rho\theta\xi := \zeta \geq 0,$$
(3.1.35)

where ζ is defined as the rate of dissipation. Both ξ and ζ are constrained to be non-negative for an acceptable process. Here it should be noted that the rate of dissipation is positive if and only if the rate of entropy production is positive. As the entropy production can take place because of the variety reasons, for e.g., due to phase change, chemical reactions, heat conductions etc., the rate of dissipation as defined through Equation (3.1.35) is non-zero whenever entropy production is zero. Equation (3.1.35) can also be written as

$$\sigma\cdot\mathbf{L} - \rho\dot{\Psi} + \rho\eta\dot{\theta} - \frac{\mathbf{q}\cdot grad\theta}{\theta} = \rho\theta\xi := \zeta \geq 0,$$
(3.1.36)

where ψ is the Helmholtz potential and is given by $\Psi = \varepsilon - \theta\eta$. This form of reduced energy dissipation equation is useful to place restriction for the constitutive equations. As mentioned above, for any realistic process the rate of entropy production is zero and so

consequently the rate of dissipation will also be zero. Most thermo-mechanical processes are irreversible process and for that entropy production is greater than zero. It can also be assumed that the rate of dissipation can be split in to a part that is due to heat conduction and another part that is a consequence of other irreversible affects, i.e.,

$$\boldsymbol{\sigma} \cdot \mathbf{L} - \rho \dot{\Psi} + \rho \eta \dot{\theta} - \frac{\mathbf{q} \cdot grad\theta}{\theta} = \rho \theta \xi := \zeta = \zeta_c + \zeta_d \geq 0. \tag{3.1.37}$$

where ζ_c is the rate of dissipation due to heat conduction and ζ_d is the rate of dissipation due to other processes. The rate of dissipation due to conduction is assumed to be given by

$$\zeta_c = -\frac{\mathbf{q} \cdot grad\theta}{\theta} \geq 0. \tag{3.1.38}$$

Substituting Equation (3.1.38) in to Equation (3.1.37), following can be obtained

$$\boldsymbol{\sigma} \cdot \mathbf{L} - \rho \dot{\Psi} + \rho \eta \dot{\theta} = \zeta_d \geq 0. \tag{3.1.39}$$

CHAPTER 4

CONSTITUTIVE MODELING

4.1   Introduction

The Constitutive equation provides a material its distinguished identity. As a matter of fact, all materials obeys the balance law; and hence, to differentiate one material from another, it is necessary to include information about the typical characteristics of the material in to the model. The Constitutive equation of the material contains such information. The constitutive equations relate quantities like the stress tensor and the Helmholtz potential with the history of the deformation that the body has undergone. The problem can be solved if this piece of information is known.

4.2   Phases Associated with Crystallizable Shape Memory Polymer

As painted out earlier, a typical cycle consists of four different processes namely: loading, cooling/crystallization, unloading and heating/melting. The morphology of the shape memory polymer changes during each of these processes. It is essential to understand the changes that occur to the polymer at the molecular level and then quantify their effects on the polymer for the changes that occur at the continuum level. The mechanical properties of the same polymer can vary widely depending on the phase description.   Following is a description of each phase associated with each process described above for shape memory polymers.

4.2.1   Isotropic Rubbery Phase

Above the recovery temperature (θ_r), shape memory polymers exhibit the characteristics of rubber. In literature, it is also referred to as the amorphous phase due to the

morphology of the state. In the amorphous state, polymer chains take up a completely random distribution in the matrix. For a rubber, the retractive force is determined by changes in the entropy and the internal energy does not change significantly with deformation at all. Hence, this type of behavior is also known as 'entropic elasticity'. In a stress free state, a linear amorphous polymer chain will adopt the conformation with the maximum entropy (see Flory (1953)).

Above the recovery temperature, polymer chains have a higher degree of freedom and this situation enables the chains to take up one of the possible energetic equivalent conformations without disentangling itself significantly. The compact coil type of conformation is entropically favored, and so the majority of the macromolecules will form the compact coil type of conformation instead of the stretched conformation. This is the reason why a piece of rubber will shrink upon heating and expand upon cooling. In this state, the material has the same the strength in all directions and will get stretched in the direction of the external force. For a force that is applied for a short time, the entanglements of the polymer chains with their direct neighbors puts restrictions on large movements of these chains. Due to this restriction, upon unloading or removal of external force, the polymer goes back to its original shape. This recovery is sometimes referred as 'memory effect' (Lendlein et al. (2002(a))). For a force that is applied for a longer time, a relaxation process will take place which results in a plastic, irreversible deformation of the sample. A longer time enables the polymer chains to disentangle and slip off each other. These rearrangements of the polymer chains will end up in more entropically favored random coils and this phenomenon is known as the relaxation process.

In the crystallizable shape memory polymers, the amorphous region contains randomly oriented networks of the polymer chain segments along with the randomly oriented hard blocks that act as connecting points. The presence of these hard blocks or

connecting points is due to one of the co-polymers used to form crystallizable shape memory polymers. The co-polymer used can have a higher glass transition temperature or a higher crystallization temperature than the transition temperature of the crystallizable shape memory polymers. These hard blocks are actually are responsible for remembering the 'original shape' above the transition temperature. Due to their presence, soft polymer chain segments do not undergo complete relaxation. The cumulative strength of these hard blocks and soft segments of polymer chains is considered as the strength of the amorphous phase of the crystallizable shape memory polymers. Besides the hard blocks, the network has flexible components in the form of amorphous chain segments. If the transition temperature is below the working temperature, the network will be elastic in nature. Stretching these segments results in loss of entropy. Upon removal of the load, the material, returns to its original shape and regains the lost entropy. This is a typical characteristic of hyper elastic materials.

In a nutshell, a crystallizable shape memory polymers above the recovery temperature is modeled as a hyper-elastic incompressible isotropic solid that is capable of strain hardening for large deformations. Constitutive equations for the stress in isotropic hyper elastic solids are widely available and fit easily into our theory based on natural configurations.

In Figure 4.1, κ_R is a reference configuration and $\kappa_{c(t)}$ is the configuration currently occupied by the material. It is assumed here that the material does not undergo any relaxation process, and so there is no relaxation mechanism included in this work. Since the behavior is elastic, it has only one natural configuration, which is the reference configuration and it has an instantaneous elastic response from this configuration.
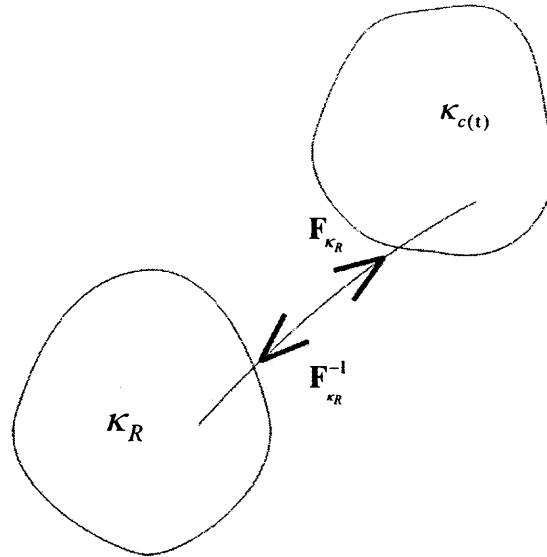
Figure 4.1 Natural configuration associated with the amorphous (or rubbery) phase.

The deformation gradient $\mathbf{F}_{\kappa_R}$ denotes the mapping between the tangent space

associated with κ_R, at a point in the reference configuration and the tangent space

associated with $\kappa_{c(t)}$. The natural configuration is fixed and does not change as in the case

of a viscous fluid, and hence there will be no dissipation of energy.

A so called 'hyperelastic material' postulates the existence of a Helmholtz free-

energy function Ψ, which is defined per unit reference volume. The Helmholtz potential

is also referred to as the strain-energy function or stored-energy function. It is assumed

that the amorphous region is homogenous since the distribution of the internal

constituents is assumed to be uniform on the continuum scale. For this type of material,

the strain-energy function depends only upon the deformation gradient $\mathbf{F}$. $\Psi = \Psi(\mathbf{F})$ is a

typical example of a scalar value function of a tensor variable $\mathbf{F}$, which is assumed to be

continuous. Stress response of hyper elastic materials is derived from a given scalar-valued energy function, which implies that hyperelasticity has a conservative structure. Different types of constitutive models can be found in the following texts (Treolar (1976), Ogden (1984) and Holpzafel (2000)). In general, for a hyperelastic incompressible material the Cauchy stress σ is given by:

$$\sigma = -p\mathbf{I} + 2\rho\mathbf{F}_{\kappa_a} \frac{\partial \Psi_a}{\partial \mathbf{C}_{\kappa_a}} \mathbf{F}_{\kappa_a}^T, \qquad (4.2.1)$$

where, p is the Lagrange multiplier due to the constraints of incompressibility, $\mathbf{F}_{\kappa_a}$ is the deformation gradient measured from reference configuration $\kappa_R = \kappa_a$ associated with the amorphous rubbery phase, ρ is the density, Ψ_a is the Helmholtz potential. The Helmholtz potential is related to the entropy, η_a through the following equation:

$$\frac{\partial \Psi_a}{\partial \theta} = -\eta_a. \qquad (4.2.2)$$

Also, Equation (4.2.2) is equivalent to the following relation between the internal energy and the entropy:

$$\frac{\partial \varepsilon_a}{\partial \theta} = \theta \frac{\partial \eta_a}{\partial \theta}. \qquad (4.2.3)$$

Here, it is important to note that it is assumed that the internal energy and the entropy of the amorphous phase depend on the temperature and the mapping $\mathbf{F}_{\kappa_a}$. For an isotropic incompressible phase, the form for the internal energy and the entropy depend on $\mathbf{F}_{\kappa_a}$ through the first two invariants of $\mathbf{B}_{\kappa_a}$. i.e.,

$$I_{\mathbf{B}_a} = I_{\mathbf{C}_a} = tr\left(\mathbf{B}_{\kappa_a}\right) = tr\left(\mathbf{C}_{\kappa a}\right), II_{\mathbf{B}_a} = II_{\mathbf{C}_a} = tr\left(\mathbf{B}_{\kappa_a}^2\right) = tr\left(\mathbf{C}_{\kappa_a}^2\right) \qquad (4.2.4)$$

therefore the internal energy, the entropy and, consequently, the Helmholtz potential can have the forms:

$$\varepsilon_a = \varepsilon_a \left(\theta, I_{C_a}, II_{C_a} \right), \tag{4.2.5}$$

$$\eta_a = \eta_a \left(\theta, I_{C_a}, II_{C_a} \right), \tag{4.2.6}$$

$$\Psi_a = \Psi_a \left(\theta, I_{C_a}, II_{C_a} \right). \tag{4.2.7}$$

In rubber-like materials, the internal energy is a weak function of deformation and is mainly a function of temperature. Specific models to describe the behavior of the rubbery phase of the shape memory polymers will be chosen by picking forms for the internal energy and entropy consistent with the experimental results. In this project, a model chosen is the simplest hyperelastic model which often serves as a prototype for rubber-like materials due to the absence of accurate material data. The model chosen for the rubbery-amorphous region is referred to as the Neo-Hookean model in the literature. The Neo-Hookean model has some theoretical relevance since the mathematical representation is analogous to that of an ideal gas: "the Neo-Hookean potential represents the Helmholtz free energy of a molecular network with Gaussian chain-length distribution" (ABAQUS user manual). The form chosen for the internal energy is

$$\varepsilon_a = C_a \theta + A_a, \tag{4.2.8}$$

where, C_a is the specific heat of the amorphous phase and A_a is a constant. The corresponding form for the entropy reduces to

$$\eta_a = C_a \ln(\theta) + B_a - \bar{\mu}_a \left(I_{C_a} - 3 \right) \tag{4.2.9}$$

where, B_a is constant and $\bar{\mu}_a$ is the constant related to the shear modulus of the amorphous phase. Because of the chosen form for the internal energy and the entropy, the Helmholtz potential is now just a function of the temperature and the first invariant of the stretch tensor only, and so Equation (4.2.7) reduces to:

$$\Psi_a = \Psi_a\left(\theta, I_{\mathbf{C}_a}\right). \tag{4.2.10}$$

It is also assumed that the viscous dissipation ζ_d in this phase is also a function of temperature and deformation.

$$\zeta_d = \zeta_a\left(\theta, \mathbf{B}_{\kappa_a}\right). \tag{4.2.11}$$

where, ζ_a is the rate of dissipation. However, the amorphous phase is modeled as an elastic solid and so the rate of the dissipation is expected to be identically zero. Substituting these forms in the reduced energy dissipation equation (Equation (3.1.39)) and using Equation (4.2.10), Equation (4.2.11) we get

$$\left(\sigma - 2\rho\left[\frac{\partial\Psi_a}{\partial I_{\mathbf{C}_a}}\mathbf{B}_{\kappa_a}\right]\right)\cdot\mathbf{D}_{\kappa_a} - \left(\frac{\partial\Psi_a}{\partial\theta} + \eta_a\right)\dot{\theta} = \zeta_a = 0. \tag{4.2.12}$$

Since, one is looking for the form that can satisfy the above equation, it is reasonable to assume that the stress is given by

$$\sigma = -p\mathbf{I} + 2\rho\left[\frac{\partial\Psi_a}{\partial I_{\mathbf{C}_a}}\right]\mathbf{B}_{\kappa_a} \tag{4.2.13}$$

Note that the form is similar to the one given by Equation (4.2.1). The Cauchy stress can be written using Equation (4.2.2), Equation (4.2.3) and Equation (4.2.13) as

$$\sigma = -p\mathbf{I} + \mu_a\mathbf{B}_{\kappa_a}, \tag{4.2.14}$$

where, $\mu_a(= 2\rho\theta\overline{\mu}_a)$ is the shear modulus of the amorphous region.

The aim of this study is to model a particular class of polymers rather than any individual polymer. Hence, in the absence of accurate data a three-dimensional, frame invariant model requires compensation for compressibility. Some materials behave differently in bulk and shear. In such cases the idea of splitting the deformation locally into two parts, namely: 'volumetric part' and 'isochoric part', would be quite beneficial,

and has been successfully applied within the context of isothermal finite strain elasticity (see Holpzafel (2000)). The idea was originally proposed by Flory (1961). The unique decoupled representation of the strain-energy function for compressible isotropic hyperelastic materials is given by: (see Holpzafel (2000))

$$\Psi(\mathbf{B}) = \Psi_{vol}(J) + \Psi_{iso}(\overline{\mathbf{B}}), \tag{4.2.15}$$

where, J is the volume ratio and can be found using $J = \det(\mathbf{B})^{\frac{1}{2}}$ and $\overline{\mathbf{B}}$ is the volume preserving component of a deformation and can be found using $\overline{\mathbf{B}} = (J)^{-\frac{2}{3}}\mathbf{B}$. The specific form of the Neo-Hookean model for the compressible, isotropic, hyperelastic material can be written as follows:

$$\psi_a = C_{10}(\overline{I}_{C_a} - 3) + \frac{1}{D_1}(J - 1)^2. \tag{4.2.16}$$

ψ_a is the strain energy function for the rubbery phase , $C_{10}\ \& D_1$ are co-efficients of the equation related to shear modulus(μ_a) and bulk modulus(K_a) of the amorphous region respectively, and they can be correlated as $C_{10} = \frac{\mu_a}{2}\ \& K_a = \frac{2}{D_1}$, and

$\overline{I}_{C_a} = tr(\overline{\mathbf{C}}_{\kappa_a}) = tr(\overline{\mathbf{B}}_{\kappa_a})$. The reason for choosing this particular form for the model is the compatibility it provides with finite element analysis using the available software like ABAQUS.

4.2.2   Phase Transition: Amorphous Phase to Semi-Crystalline Phase

Below the recovery temperature(θ_r), crystallization begins in the CSMP's. During the phase transition, one can find both, the amorphous phase and the crystalline phase, at the same time. This mixture of phases is considered as a constrained mixture. As in

traditional mixture theory (see Truesdell(1957), Bowen (1975), Atkin and Craine(1976), Rajagopal and Tao(1995)), co-occupancy is allowed, in a homogenized sense, of the phase at a point. However, it is important to note that unlike traditional mixture theory, it is assumed that the displacement in both phases is equal. The assumption is based on the fact that in polymeric materials same molecule traverses both the amorphous phase and crystalline phase. Hence, both the phase are constrained to move together.

The newly formed crystalline material is also an elastic solid. The stress in the current configuration can be calculated by finding the deformation gradient from a configuration of known stress to the current configuration. In this case, the configuration of the deformed amorphous solid, when the crystal is formed, is the known configuration. This is the natural configuration of the newly born crystal.
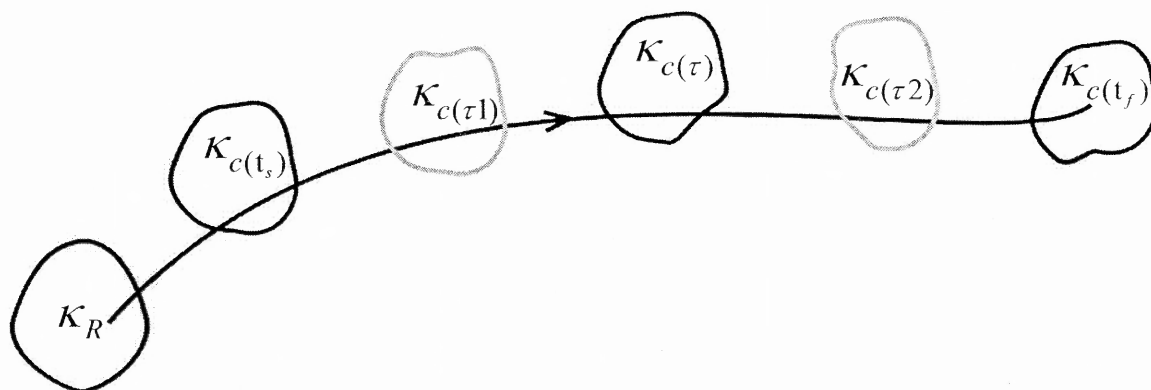
Figure 4.2 At time t_s crystallization begins and stops at time t_f. Between these times newly formed crystals are formed with different natural configurations.

With further deformation of the material, this newly formed crystalline phase also deforms. The subsequently formed crystals are also born in their own natural configurations as described above. This transient phase can be thought of as a mixture of a crystalline phase with different natural configurations and an amorphous phase in a deformed configuration with respect to the original stress free configuration. Furthermore, the natural configuration of the crystalline solid fraction born at some time t is the configuration of the body at the time t. If crystallization begins at time t_s, in Figure 4.2, let τ be the some time later than t_s at which crystals starts forming. It is assumed that the thermodynamic quantities, the internal energy and entropy (at a time t) in the body due to a crystalline fraction born at time τ is determined by the deformation gradient from the configuration of the body at time τ to the current configuration at time t, i.e. $\mathbf{F}_{\kappa_{c(\tau)}}$. With these assumptions the internal energy, entropy and the Helmholtz potential of the newly formed crystalline phase are given by: (see Rao and Rajagopal (2002))

$$\varepsilon_c = \varepsilon_c(\theta, \mathbf{C}_{\kappa_{c(\tau)}}), \tag{4.2.17}$$

$$\eta_c = \eta_c(\theta, \mathbf{C}_{\kappa_{c(\tau)}}), \tag{4.2.18}$$

$$\Psi_c = \Psi_c(\theta, \mathbf{C}_{\kappa_{c(\tau)}}), \tag{4.2.19}$$

while the internal energy and entropy of the amorphous phase are determined by $\mathbf{F}_{\kappa_a}$ through $\mathbf{B}_{\kappa_a}$.

The internal energy and the entropy of the mixture are assumed to be additive and can be given by:

$$\varepsilon = i_\varepsilon + (1-\alpha)\varepsilon_a + \int_{t_s}^{\tau} \varepsilon_c \frac{d\alpha}{d\tau} d\tau, \tag{4.2.20}$$

$$\eta = i_\eta + (1-\alpha)\eta_a + \int_{t_s}^{\tau} \eta_c \frac{d\alpha}{d\tau} d\tau, \tag{4.2.21}$$

where, α is crystallinity, i_ε is the interfacial energy per unit mass of the amorphous-crystalline mixture and i_η is the interfacial entropy per unit mass of the amorphous-crystalline mixture. These interfacial components are added to take into account the presence of phase boundaries. This is because their presence will change the structure of the amorphous and crystalline regions in the vicinity of the interface. In polymers, this term is expected to be important, as the crystalline lamellae are small and there is a substantial amount of material in the interfacial region in between the crystalline and amorphous regions (see Mandelkern L. et al. (1981), Flory P. J. et al. (1984), Kuwabara K. et al. (1997)). Also, ε_a and η_a are assumed to have the same form as that for the amorphous phase and are given by Equation (4.2.5) and Equation (4.2.6). Using Equation (4.2.20) and Equation (4.2.21), the Helmholtz potential for the mixture is then given by

$$\Psi = i_\Psi + (1-\alpha)\Psi_a + \int_{t_s}^{\tau} \Psi_c \frac{d\alpha}{d\tau} d\tau. \tag{4.2.22}$$

The presence of the integral in the Equation (4.2.22) above is because the crystalline phase is formed gradually and not instantaneously.

As mentioned earlier, the semi-crystalline solid that is formed is an anisotropic solid. The anisotropy depends on the orientation of the crystal that is formed. The tensors $\mathbf{B}_{\kappa_{a(i)}}$, $i = t_s < \tau_1 < \tau < \tau_2 < t_f$, give us information about the orientation of the crystals in the mixture at any give time t, albeit in an averaged sense. Experiments suggest that one can use the mutually perpendicular principal directions to determine the directions of the anisotropic solid. The principal directions can be quantified by any two of the three eigenvectors of $\mathbf{B}_{\kappa_{a(i)}}$, namely $\mathbf{n}_{\kappa_{c(\tau)}}$ and $\mathbf{m}_{\kappa_{c(\tau)}}$ (see Rao and Rajagopal

(2000)). At every instant, depending upon the loading conditions, there can be an unequal stretch in the principal directions. The symmetry group of an orthotropic solid is determined by three mutually perpendicular directions hence, this form of anisotropy seems reasonable to assume for the crystalline phase of the solid. The three principal direction can change with time and are determined by $\mathbf{n}_{\kappa_{c(t)}}$ and $\mathbf{m}_{\kappa_{c(t)}}$. The directions associated with $\mathbf{n}_{\kappa_{c(t)}}$ and $\mathbf{m}_{\kappa_{c(t)}}$ are used in order to incorporate the dependence of anisotropy in the elastic response of the crystalline phase. Hence, it is assumed that Helmholtz potential of an incompressible orthotropic elastic solid is consistent with the configuration $\kappa_{c(t)}$. For an incompressible orthotropic elastic solid, the Helmholtz potential depends on the first two invariants of the right Cauchy-Green tensor, $\mathbf{C}_{\kappa_{c(t)}}$, which is denoted by $I_{\mathbf{C}_c}, II_{\mathbf{C}_c}$ and the following scalars (see Spencer (1972))

$$J_1 = \mathbf{n}_{\kappa_{c(t)}} \cdot \mathbf{C}_{\kappa_{c(t)}} \mathbf{n}_{\kappa_{c(t)}}, \tag{4.2.23}$$

$$K_1 = \mathbf{m}_{\kappa_{c(t)}} \cdot \mathbf{C}_{\kappa_{c(t)}} \mathbf{m}_{\kappa_{c(t)}}, \tag{4.2.24}$$

The Helmholtz potential for an incompressible orthotropic elastic solid then can be written as:

$$\Psi_c = \Psi_c\left(\theta, I_{\mathbf{C}_c}, II_{\mathbf{C}_c}, J_1, K_1\right), \tag{4.2.25}$$

where the invariants depend on t and τ. It is important to note here that there are alternate ways to include anisotropy.

Before choosing a specific form for the entropy and the internal energy, it is important to discuss the rate of dissipation. There can be dissipation in the material due to the presence of the amorphous phase. However, in this case it is assumed that it is an elastic solid and hence, there will be negligible dissipation associated with this phase. Moreover, it is observed in the experiments carried out on polyethylene that the

temperature at which majority of the quiescent crystallization takes place is lower than the temperature at the melting takes place. This observation indicates that crystallization is an entropy producing process as the state of the melt before and after crystallization-melting cycle is the same. It is assumed that the rate of dissipation can be split into two parts, the first related to the dissipation associated with the amorphous phase and the second related to the phase change.

$$\zeta_d = \zeta_a + \zeta_p \geq 0, \tag{4.2.26}$$

where, ζ_p is the rate of dissipation associated with the phase change. It is assumed that ζ_p depends on the crystallinity, α, crystallization rate, $\dot{\alpha}$ and temperature, θ. It can also be depend on the other kinematic variables i.e.,

$$\zeta_p = \zeta_p\left(\alpha, \dot{\alpha}, \theta, \ldots\right) \geq 0. \tag{4.2.27}$$

It is obvious to assume that the rate of dissipation ζ_p is exactly zero when no crystallization is taking place i.e.,

$$\zeta_P\big|_{\dot{\alpha}=0} = 0. \tag{4.2.28}$$

Substituting the Helmholtz potential from Equation (4.2.22) with Ψ_a given by Equation (4.2.10) and Ψ_c given by Equation (4.2.25) and ζ_p given by Equation (4.2.27) in to the reduced energy dissipation Equation (3.1.39), we obtain

$$\left(\sigma - (1-\alpha)2\rho\left[\frac{\partial\Psi_a}{\partial I_{C_a}}\mathbf{B}_{\kappa_a}\right] - 2\rho\left[\int_{t_s}^{\tau}\mathbf{F}_{\kappa_{c(t)}}\frac{\partial\Psi_c}{\partial I_{C_c}}\mathbf{F}_{\kappa_{c(t)}}^T\right]\right)\cdot\mathbf{D} +$$

$$-\left(\frac{\partial\Psi}{\partial\theta} + \eta\right)\dot{\theta} + \rho\left(\Psi_a - \Psi_c\big|_{C_{\kappa_{c(t)}}=\mathbf{I}} - \frac{\partial i_\Psi}{\partial\alpha}\right)\dot{\alpha} = \zeta_p \geq 0. \tag{4.2.29}$$

It is assumed that the following form for the stress that satisfies the above equation:

$$\sigma = -p\mathbf{I} + 2(1-\alpha)\rho\left[\frac{\partial \Psi_a}{\partial I_{C_a}}\mathbf{B}_{\kappa_a}\right] + 2\rho\left[\int_{t_s}^{\tau} \mathbf{F}_{\kappa_{c(t)}}\frac{\partial \Psi_c}{\partial I_{C_c}}\mathbf{F}^T_{\kappa_{c(t)}}\frac{d\alpha}{d\tau}d\tau\right]. \qquad (4.2.30)$$

It is also noted that for a Helmholtz potential consistent with that of an orthotropic elastic solid with Ψ_c given by Equation (4.2.25), we obtain the following representation

$$\mathbf{F}_{\kappa_{c(t)}}\frac{\partial \Psi_c}{\partial I_{C_c}}\mathbf{F}^T_{\kappa_{c(t)}} = \frac{\partial \Psi_c}{\partial I_{C_c}}\mathbf{B}_{\kappa_{c(t)}} - \frac{\partial \Psi_c}{\partial II_{C_c}}\mathbf{B}^{-1}_{\kappa_{c(t)}} +$$

$$\mathbf{F}_{\kappa_{c(t)}}\left(\frac{\partial \Psi_c}{\partial J_1}\mathbf{n}_{\kappa_{c(t)}}\otimes \mathbf{n}_{\kappa_{c(t)}} + \frac{\partial \Psi_c}{\partial K_1}\mathbf{m}_{\kappa_{c(t)}}\otimes \mathbf{m}_{\kappa_{c(t)}}\right)\mathbf{F}^T_{\kappa_{c(t)}}. \qquad (4.2.31)$$

The entropy and the Helmholtz potential are related through

$$\frac{\partial \Psi}{\partial \theta} = -\eta. \qquad (4.2.32)$$

For crystalline materials, there is not significant change in the configurational entropy with the deformation, while the internal energy does depend on the deformation, because of which, the following forms for the internal energy and the entropy of the crystalline phase are assumed,

$$\varepsilon_c = C_c\theta + A_c + \frac{1}{2\rho}\left(\mu_c\left(I_{C_c}-3\right) + \mu_{c1}\left(J_1-1\right)^2 + \mu_{c2}\left(K_1-1\right)^2\right) \qquad (4.2.33)$$

$$\eta_c = C_c\ln(\theta) + B_c, \qquad (4.2.34)$$

where C_c is the specific heat associated with the crystalline phase, A_c and B_c are constants and μ_c, μ_{c1} and μ_{c2} are material moduli associated with the crystalline phase. It is important to mention here that the internal energy is represented as a linear function of the temperature and chosen form for the entropy follows Equation (4.2.32).

The Cauchy stress in a constrained mixture of phases from Equation (4.2.30) can be seen to be:

$$\sigma = -p\mathbf{I} + (1-\alpha)\sigma_a + \int_{t_s}^{\tau}\sigma_c\frac{d\alpha}{d\tau}d\tau. \qquad (4.2.35)$$

In the Equation (4.2.35) above, σ_a is the stress due to the amorphous region and can be described as in Equation (4.2.13), where as σ_c is the stress due to the crystalline region. Using Equation (4.2.1), Equation (4.2.33) and Equation (4.2.34) The Cauchy stress for the crystalline region at any given time t can be written as follows

$$\int_{t_s}^{\tau} \sigma_c \frac{d\alpha}{d\tau} d\tau = \int_{t_s}^{\tau} \mu_c \mathbf{B}_{\kappa_{c(t)}} \frac{d\alpha}{d\tau} d\tau +$$

$$\int_{t_s}^{\tau} \left(\mathbf{F}_{\kappa_{c(t)}} \left(\mu_{c1}(J_1-1)\mathbf{n}_{\kappa_{c(t)}} \otimes \mathbf{n}_{\kappa_{c(t)}} + \mu_{c2}(K_1-1)\mathbf{m}_{\kappa_{c(t)}} \otimes \mathbf{m}_{\kappa_{c(t)}} \right) \mathbf{F}^T_{\kappa_{c(t)}} \right) \frac{d\alpha}{d\tau} d\tau. \tag{4.2.36}$$

Using Equation (4.2.13), Equation (4.2.35) and Equation (4.2.36) the Cauchy stress for the transition phase can then be given by

$$\sigma = -p\mathbf{I} + (1-\alpha)\mu_a \mathbf{B}_{\kappa_a} + \int_{t_s}^{\tau} \mu_c \mathbf{B}_{\kappa_{c(t)}} \frac{d\alpha}{d\tau} d\tau +$$

$$\int_{t_s}^{\tau} \left(\mathbf{F}_{\kappa_{c(t)}} \left(\mu_{c1}(J_1-1)\mathbf{n}_{\kappa_{c(t)}} \otimes \mathbf{n}_{\kappa_{c(t)}} + \mu_{c2}(K_1-1)\mathbf{m}_{\kappa_{c(t)}} \otimes \mathbf{m}_{\kappa_{c(t)}} \right) \mathbf{F}^T_{\kappa_{c(t)}} \right) \frac{d\alpha}{d\tau} d\tau. \tag{4.2.37}$$

The internal energy for the mixture is given by Equation (4.2.20) and the form for the internal energy in the amorphous phase and the crystalline phase is given by Equation (4.2.8) and Equation (4.2.33), respectively. The energy equation for the mixture is derived by substituting the internal energy into the energy equation (Equation (3.1.30)) with the assumption that the amorphous phase is non-dissipative,

$$\rho\left((1-\alpha)C_a + \alpha C_c \right)\dot{\theta} + div\mathbf{q} =$$

$$(1-\alpha)\mu_a \mathbf{B}_{\kappa_a} \cdot \mathbf{L} + \rho\left(C_a\theta + A_a - C_c - A_c - \frac{\partial i_\varepsilon}{\partial \alpha} \right)\dot{\alpha} + \rho r. \tag{4.2.38}$$

This completes the development of the constitutive equations for the phase transition.

For a compressible orthotropic Neo-Hookean solid, using arguments similar to those used for equation(4.2.15), The Helmholtz potential can be prescribed as follows:

$$\Psi_c = \Psi_c\left(\theta, J, \overline{I}_{C_c}, \overline{J}_1, \overline{K}_1\right), \tag{4.2.39}$$

where, $\overline{I}_{C_c} = J^{-\frac{2}{3}} I_{C_c}, \overline{J}_1 = J^{-\frac{2}{3}} J_1$ and $\overline{K}_1 = J^{-\frac{2}{3}} K_1$. The specific form for the stored energy

function, which is chosen for writing the UMAT for ABAQUS, in order to simulate the

crystalline phase, is given below:

$$\psi_c = C_{20}(\overline{I}_{C_c} - 3) + \frac{1}{D_2}(J-1)^2 + C_{201}(\overline{J}_1 - 1)^2 + C_{202}(\overline{K}_1 - 1)^2. \tag{4.2.40}$$

ψ_c is the strain energy function for the crystalline phase, C_{20} & D_2 are the co-efficients of

the equation related to the shear and bulk modulus of the crystalline region respectively,

and they can be correlated as $C_{20} = \frac{\mu_c}{2}$ and $K_c = \frac{2}{D_2}$. $C_{201} = \mu_{c1}$ and $C_{202} = \mu_{c2}$ are the

shear moduli related to the anisotropic crystalline phase. Using arguments similar to

those used for Equation (4.2.22), the stored energy function for the mixture can be

written using Equation (4.2.16), Equation (4.2.22) and Equation (4.2.40) as follows:

$$\psi = (1-\alpha)\psi_a + \int_{t_s}^{\tau} \psi_c \frac{d\alpha}{d\tau} d\tau. \tag{4.2.41}$$

4.2.3 Semi-Crystalline Phase

With a decrease in temperature, crystallinity increases up to a certain extent. With the

increase in crystallinity, the amorphous fraction of the polymer chain will loose mobility

which will result in cessation of the crystallization in the material. If the temperature

drops to the glass transition temperature, the polymer chain looses its mobility and

crystallization stops. Thus, after the cessation of the crystallization, the temporary shape

is always the mixture of the amorphous solid and the crystalline solid. Sometimes

crystallization, as in case of polyethylene, stops between the glass transition temperature

and the melting temperature. Between those temperatures, the solid consists of rigid

crystals and a flexible amorphous fraction making the resultant solid both tough and flexible. Also, as described earlier, due to the deformation the crystals formed have an orientation which causes anisotropy. Hence, the solid formed after the cessation of the crystallization is tough, flexible and anisotropic.

As shown in Figure 4.3, after the cessation of the crystallization, stress in the material can be found out by the mapping between the current configuration and the original configuration, along with the summation of all the mappings between configurations of the body at every instant that a new crystal was born to the current configuration. The Helmholtz potential for such a hyperelastic solid can be then given by

$$\Psi = i_\Psi + (1-\alpha)\Psi_a + \int_{t_s}^{t_f} \Psi_c \frac{d\alpha}{d\tau} d\tau. \tag{4.2.42}$$

Note that Equation (4.2.42) is very similar to Equation (4.2.22) with a little change in the limits of the integral. This is due to the fact that crystallization stops at time t_f, after which no configuration will evolve from which mapping is possible. Therefore, The Cauchy stress in the material will also have a form similar to that as of Equation (4.2.37) with a change in the limits. The Cauchy stress in the solid at this point can be prescribe by

$$\sigma = -p\mathbf{I} + (1-\alpha)\mu_a \mathbf{B}_{\kappa_a} + \int_{t_s}^{t_f} \mu_c \mathbf{B}_{\kappa_{c(\tau)}} \frac{d\alpha}{d\tau} d\tau +$$

$$\int_{t_s}^{t_f} \left(\mathbf{F}_{\kappa_{c(\tau)}} \left(\mu_{c1}(J_1-1)\mathbf{n}_{\kappa_{c(\tau)}} \otimes \mathbf{n}_{\kappa_{c(\tau)}} + \mu_{c2}(K_1-1)\mathbf{m}_{\kappa_{c(\tau)}} \otimes \mathbf{m}_{\kappa_{c(\tau)}} \right) \mathbf{F}^T_{\kappa_{c(\tau)}} \right) \frac{d\alpha}{d\tau} d\tau. \tag{4.2.43}$$

The required stored energy function for modeling the compressible crystallizable shape memory polymers using ABAQUS can be then prescribe by

$$\psi = (1-\alpha)\psi_a + \int_{t_s}^{t_f} \psi_c \frac{d\alpha}{d\tau} d\tau. \tag{4.2.44}$$
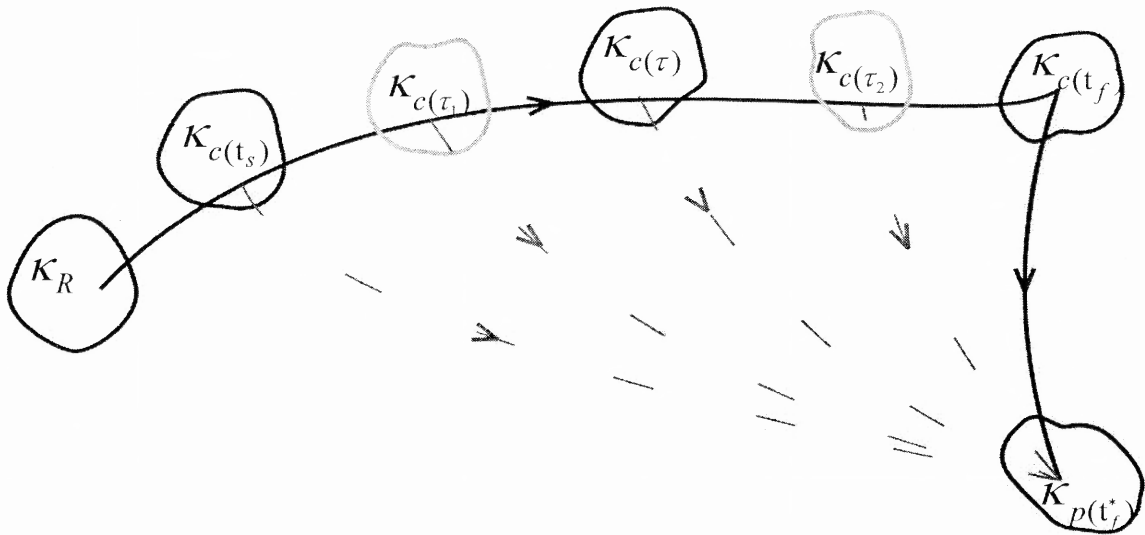
Figure 4.3 The figure shows the natural configuration of the unloaded material ($\kappa_{p(\mathrm{t}_f)}$) after crystallization.

4.2.4 Phase Transition: Semi-Crystalline Phase to Amorphous Phase

The return to the original shape is accomplished by heating the material above the recovery temperature. Once the temperature reaches above the recovery temperature, the crystals start melting. Due to the melting of these crystals the crystalline phase will start disappearing and the material will become more and more rubbery. Due to unloading, there will be no stress in the material and eventually all the crystalline material will transform into the amorphous phase taking the material back into its original shape. To track the evolution of the shape as it evolves from the temporary to the permanent shape, it is necessary to track which fraction of the crystalline phase is melting at any given time. This is particularly true for the case where crystallization takes place under constant stress, as different crystals are formed at different stretches, and hence can have different stress-free states. Therefore, when a crystallite that is more stressed melts the polymer as

a whole will retract towards its original shape more than if a less stressed crystallite melted. For the constant stretch case, all the crystals were formed in the same configuration so the order in which the crystals melt does not impact the intermediate shapes occupied by the polymer. However, for crystallization under constant stress, or for a more general case wherein crystallization takes place under conditions of varying stress, the order in which the crystallites melt is important. The assumption made with regards to the melting process is that the crystallites formed last melt first. This assumption is supported by experiments in which crystallites formed farthest from the equilibrium melting temperature (i.e. crystallites that were formed last) are thinner and melt at lower temperatures (i.e. melt first)(see Gedde (1995)).

At the beginning of heating, the two phases will have different stress-free states because of which shape fixity is possible. Figure 4.4 shows that after unloading material is in stress free configuration $\kappa_{p(t_f)}$. Due to the melting of the crystals, the material will pass through all the different stress free configurations, ending up in the stress free configuration of the permanent shape. Assuming that the melting of the crystals begins at some time t_{ms}, the configuration of the material at time t_{ms} is given by $\kappa_{t_{ms}} = \kappa_{p(t_f)}$. The Helmholtz potential of the mixture during the melting at any given point of time can be then calculated using following equation:

$$\Psi = i_\Psi + (1-\alpha)\Psi_a + \int_{t_s}^{\overset{\cdot}{\tau}} \Psi_c \frac{d\alpha}{d\tau} d\tau,$$

$$\text{with } \overset{\cdot}{\tau} \in \left[t_s, t_f \right] \quad \text{and} \quad \alpha(\overset{\cdot}{\tau}) = \alpha(t).$$

(4.2.45)

Note, in the above equation the time is tagged when the material has crystallinity during melting to the actual times when the material had the same crystallinity during the

crystallization i.e., $\tau \in \left[t_s, t_f \right]$. From the rate equation for melting, which will be described in detail later in this section the current value of crystallinity is known, and therefore, the amount that has melted is also known. Since, crystallinity can be tracked as a function of time during crystallization, through interpolation between known values of crystallinity and the times at which those values occur, one can determine the time during the crystallization process, denoted by $\overset{*}{\tau} \in \left[t_s, t_f \right]$, when the amount of crystalline material present equals the current level of crystallinity during melting, i.e., $\alpha(\overset{*}{\tau}) = \alpha(t)$. This is possible because of the assumption that crystallites formed later are the first to melt.
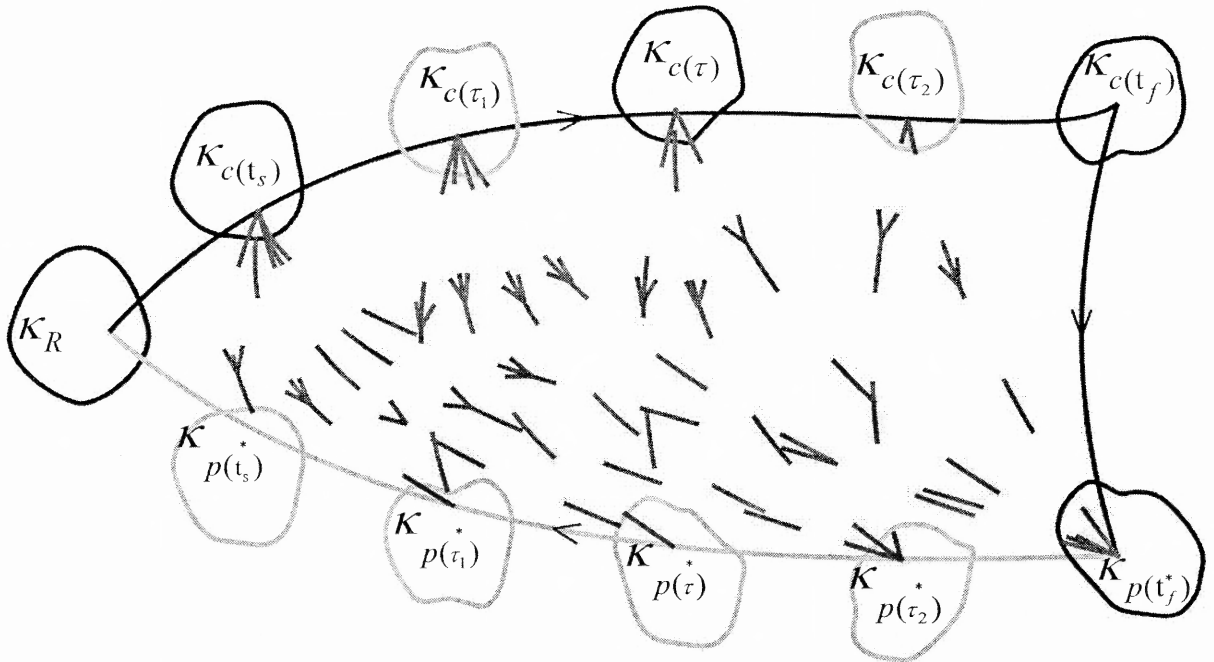
Figure 4.4 The figure shows that upon heating, the CSMP is achieving its original stress-free configuration.

The rate of dissipation, ζ_d, as discussed above, during melting can be divided into two parts. The first part is the rate of dissipation due to the presence of the amorphous phase, ζ_a, that can be prescribed as in Equation (4.2.11) which has negligible value in this case and the second part is the rate of dissipation due to the phase change, ζ_m. The rate of dissipation due to the phase change during crystallization and melting depends on the same parameters. However, it is important to note that they are not same. The rate of dissipation associated with the phase change during melting can be give by:

$$\zeta_m = \zeta_m\left(\alpha,\dot{\alpha},\theta,...\right) \geq 0. \tag{4.2.46}$$

Moreover, it is reasonable to assume that if melting rate is zero then the rate of dissipation associated with the phase change during melting is also exactly equal to zero.

$$\zeta_m\big|_{\dot{\alpha}=0} = 0. \tag{4.2.47}$$

With this information it is now possible to write the reduced energy dissipation Equation (3.1.39) for the melting process with the aid of Equation (4.2.10), Equation (4.2.45), Equation (4.2.25), Equation (4.2.11) and Equation (4.2.46) as follows

$$\left(\sigma - (1-\alpha)2\rho\left[\frac{\partial \Psi_a}{\partial I_{\mathbf{C}_a}}\mathbf{B}_{\kappa_a}\right] - 2\rho\left[\int_{t_s}^{\tau}\mathbf{F}_{\kappa_{c(t)}}\frac{\partial \Psi_c}{\partial \mathbf{C}_{\kappa_{c(t)}}}\mathbf{F}^T_{\kappa_{c(t)}}\right]\right)\cdot\mathbf{D} +$$

$$-\left(\frac{\partial \Psi}{\partial \theta}+\eta\right)\dot{\theta}+\rho\left(\Psi_c\big|_{\mathbf{C}_{\kappa_{c(t)}}} - \Psi_a\big|_{\mathbf{C}_{\kappa_a}} - \frac{\partial i_{\Psi}}{\partial \alpha}\right)\dot{\alpha} = \zeta_m \geq 0, \tag{4.2.48}$$

with $\dot{\tau} \in \left[t_s, t_f\right]$ and $\dot{\alpha}(\tau) = \alpha(t)$.

For Equation (4.2.48) to hold a sufficient condition is that the Cauchy stress satisfy the following

$$\sigma = -p\mathbf{I} + 2(1-\alpha)\rho\left[\frac{\partial \Psi_a}{\partial I_{\mathbf{C}_a}}\mathbf{B}_{\kappa_a}\right] + 2\rho\left[\int_{t_s}^{\dot{\tau}}\mathbf{F}_{\kappa_{c(t)}}\frac{\partial \Psi_c}{\partial I_{\mathbf{C}_c}}\mathbf{F}^T_{\kappa_{c(t)}}\frac{d\alpha}{d\tau}d\tau\right],$$

$$(4.2.49)$$

with $\dot{\tau} \in \left[t_s, t_f\right]$ and $\dot{\alpha}(\tau) = \alpha(t)$.

The stress in the polymer during melting is exactly equal to zero due to the fact that the material is totally unloaded. Yet, it is important to prescribe the equation of the Cauchy stress because it is useful to find the shape of the material at any given time during the melting process. Using Equation (4.2.8), Equation (4.2.9), Equation (4.2.33), Equation (4.2.34), Equation (4.2.36) and Equation (4.2.49), the Cauchy stress can be given by:

$$\sigma = 0 = -p\mathbf{I} + (1-\alpha)\mu_a\mathbf{B}_{\kappa_a} + \int_{t_s}^{\dot{\tau}}\mu_c\mathbf{B}_{\kappa_{c(t)}}\frac{d\alpha}{d\tau}d\tau +$$

$$\int_{t_s}^{\dot{\tau}}\left(\mathbf{F}_{\kappa_{c(t)}}\left(\mu_{c1}(J_1-1)\mathbf{n}_{\kappa_{c(t)}}\otimes\mathbf{n}_{\kappa_{c(t)}} + \mu_{c2}(K_1-1)\mathbf{m}_{\kappa_{c(t)}}\otimes\mathbf{m}_{\kappa_{c(t)}}\right)\mathbf{F}^T_{\kappa_{c(t)}}\right)\frac{d\alpha}{d\tau}d\tau, \quad (4.2.50)$$

with $\dot{\tau} \in \left[t_s, t_f\right]$ and $\dot{\alpha}(\tau) = \alpha(t)$.

The energy equation for the mixture is derived by substituting the internal energy into the energy equation (Equation (3.1.30)). Moreover, it is also known that during heating the material is totally unloaded, and hence, there is no stress in the material. For this situation the energy equation can be prescribed as:

$$\rho\left((1-\alpha)C_a + \alpha C_c\right)\dot{\theta} + div\mathbf{q} =$$

$$(1-\alpha)\mu_a\mathbf{B}_{\kappa_a}\cdot\mathbf{L} + \rho\left(C_a\theta + A_a - C_c - A_c - \frac{\partial i_\varepsilon}{\partial\alpha}\right)\dot{\alpha} + \rho r. \quad (4.2.51)$$

Using arguments similar to those made in the previous sections, for the compressible hyper elastic solid, the required stored energy function for writing the UMAT for ABAQUS can be prescribe by

$$\psi = (1-\alpha)\psi_a + \int_{t_s}^{\tau} \psi_c \frac{d\alpha}{d\tau} d\tau,$$

(4.2.52)

with $\dot\tau \in \left[t_s, t_f \right]$ and $\dot{\alpha(\tau)} = \alpha(t)$.

4.3   Activation Criterion for Crystallization and Crystallization Rate

It is essential for the crystallizable shape memory polymers to have an activation criterion for crystallization and a crystallization rate (or the growth criterion). A mathematical representation of conditions that indicates the beginning of the crystallization is called the activation criterion, where as, the growth criterion is an equation which gives the amount of material converted in the crystalline phase.

Crystallizable shape memory polymers have, as discussed above, two phases namely the amorphous phase and crystalline phase. Both the phases are modeled as elastic processes and will show virtually no dissipation. Hence, entropy production takes place only after the onset of crystallization. Usually, amorphous polymers in a melted form show a viscous effect. This can be another reason for entropy production. Hence, the rate of dissipation can be split into two parts, the first related to the dissipation due to the viscous effects in the amorphous phase, ζ_a, and the second related to the phase change, ζ_p, i.e. (see equation from section 4.2).

$$\rho \left(\Psi_a - \Psi_c \big|_{C_{\kappa_{c(\tau)}} = I} - \frac{\partial i_\psi}{\partial \alpha} \right) \dot\alpha = \zeta_p > 0.$$

(4.3.1)

This is a useful equation for prescribing the activation criterion and the crystallization rate. The term in the bracket of Equation (4.3.1) shows the difference between the Helmholtz potentials of the amorphous and the crystalline phase. And this term acts as the driving force, D_f, for crystallization. It can be defined as

$$D_f := \left(\Psi_a - \Psi_c \big|_{\mathbf{C}_{\kappa_{c(r)}} = \mathbf{I}} - \frac{\partial i_\psi}{\partial \alpha} \right).$$
(4.3.2)

When crystallization is initiated, the crystallinity is identically zero, and the driving force is given by

$$D_f \big|_{\alpha=0} := \left(\Psi_a - \Psi_c \big|_{\mathbf{C}_{\kappa_{c(r)}} = \mathbf{I}} - \frac{\partial i_\psi}{\partial \alpha} \bigg|_{\alpha=0} \right).$$
(4.3.3)

The activation function can be defined through the driving force as

$$\phi\left(\theta, \mathbf{B}_{\kappa_a}\right) = D_f \big|_{\alpha=0} - A,$$
(4.3.4)

where A is the initiation barrier and is a positive constant. Crystalline material does not form in a stress free state and hence the activation criterion depends on the temperature θ and tensor $\mathbf{B}_{\kappa_a}$. If the activation function has a negative value then it does not exceed the initiation barrier and crystallization cannot take place. If, at a material point, the activation function is taking a zero value then it indicates that crystallization is about to begin and that that material point is on the activation surface. Increasing the value of the activation function above zero causes crystallization to initiate. The mathematical presentation of the fact then can be prescribed as follows:

$$\phi\left(\theta, \mathbf{B}_{\kappa_a}\right) > 0 \quad \text{or}$$

$$\phi\left(\theta, \mathbf{B}_{\kappa_a}\right) = 0, \frac{\partial \phi}{\partial \theta}\dot{\theta} + \frac{\partial \phi}{\partial \mathbf{B}_{\kappa_a}}\dot{\mathbf{B}}_{\kappa_a} > 0.$$
(4.3.5)

Depending on the chosen forms of the various thermodynamic quantities for the amorphous phase in this work, the activation function for crystallization can be written as:

$$\phi\left(\theta, \mathbf{B}_{\kappa_a}\right) = \left(\frac{\theta_r - \theta}{\theta_r}\right) - \frac{1}{\Delta H_a}\frac{\partial i_\psi}{\partial \alpha}\bigg|_{\alpha=0} + \frac{\mu_a\left(I_{\mathbf{B}_{\kappa_a}} - 3\right)}{2\rho\Delta H_a},$$
(4.3.6)

where, ΔH_a is the latent heat. Note, in the Equation (4.3.6) the latent energy near the vicinity of the equilibrium melting temperature of the crystals has been derived assuming that the energy and entropy of the two phases are independent in this temperature range (see Rao and Rajagopal (2002)).

Using Equation (4.3.2), Equation (4.3.1) can be rewritten as follows:

$$\rho D_f \dot{\alpha} = \zeta_p. \tag{4.3.7}$$

The crystallization rate can be obtained using the Equation (4.3.7). As Equation (4.3.7) is in general non-linear, more than one value of $\dot{\alpha}$ is possible. The value of $\dot{\alpha}$ chosen is the one that maximizes the rate of dissipation. Consequently, to derive the rate of crystallization, it is necessary to prescribe the rate of dissipation. In this work, the form chosen is

$$\zeta_p = \frac{\dot{\alpha}^m}{\overline{G}(\alpha_0 - \alpha)^k}, \tag{4.3.8}$$

where the constant α_0 represents the maximum crystallinity and $\overline{G}$, k and m are constants. For the chosen form of rate of the dissipation, as crystallinity reaches its maximum value, the rate of dissipation becomes very large, effectively curtailing any further crystallization. Also, this form satisfies the required conditions as in equation(4.2.28). For the chosen form of the rate of dissipation the crystallization rate takes the following form:

$$\dot{\alpha} = G(\alpha_0 - \alpha)^{k/m-1} \left(\left(\frac{\theta_r - \theta}{\theta_r} \right) - \frac{1}{\Delta H_a} \frac{\partial i_\psi}{\partial \alpha} + \frac{\mu_a \left(I_{B_{\kappa_a}} - 3 \right)}{2\rho \Delta H_a} \right)^{1/m-1}, \tag{4.3.9}$$

where G is a constant.

4.4 Activation Criterion for Melting and Melting Rate

The melting of crystals in CSMP is an irreversible process, just like crystallization. The difference between the Helmholtz potentials of the crystalline and amorphous phase acts as the driving force for melting. Using the reduced energy dissipation equation for melting that is given by Equation (4.2.48), the driving force for the melting process can be prescribed by

$$D_f := \left(\Psi_c \big|_{C_{\kappa_{c(t)}}} - \Psi_a \big|_{C_{\kappa_a}} - \frac{\partial i_\psi}{\partial \alpha} \right). \tag{4.4.1}$$

Moreover, for the forms selected for Ψ_a, Ψ_c, ζ_a and ζ_m, it is clear that the following relationship holds,

$$-\rho \left(\Psi_c \big|_{C_{\kappa_{c(t)}}} - \Psi_a \big|_{C_{\kappa_a}} - \frac{\partial i_\psi}{\partial \alpha} \right) \dot{\alpha} = \zeta_m \geq 0. \tag{4.4.2}$$

At the instant melting is initiated, both phases can be in a deformed state, As a result, the activation function will depend on the deformation variables associated with both the amorphous and crystalline phases. In such a case activation function through the driving force can be defined as

$$\phi_m \left(\theta, \mathbf{B}_{\kappa_a}, \mathbf{B}_{\kappa_{c(t)}} \right) = D_f \big|_{\alpha = \alpha_0} - B, \tag{4.4.3}$$

where B is the initiation barrier and is a positive constant.

The activation function will take negative values when there is no melting and it will take exactly zero when melting is about to begin. Once the activation function exceeds zero, melting begins. The activation criterion for the initiation of melting can be stated more precisely as follows:

$$\phi_m \left(\theta, \mathbf{B}_{\kappa_a}, \mathbf{B}_{\kappa_{c(t)}} \right) > 0 \quad \text{or}$$

$$\phi_m \left(\theta, \mathbf{B}_{\kappa_a}, \mathbf{B}_{\kappa_{c(t)}} \right) = 0, \frac{\partial \phi_m}{\partial \theta} \dot{\theta} + \frac{\partial \phi_m}{\partial \mathbf{B}_{\kappa_a}} \dot{\mathbf{B}}_{\kappa_a} + \frac{\partial \phi_m}{\partial \mathbf{B}_{\kappa_{c(t)}}} \dot{\mathbf{B}}_{\kappa_{c(t)}} > 0. \tag{4.4.4}$$

This completes the specification of the initiation criterion for the melting process.

Depending on the chosen forms of the various thermodynamic quantities for the amorphous phase and the crystalline phase in this work, the activation function for the melting process can be written as:

$$\phi_m\left(\theta, \mathbf{B}_{\kappa_a}, \mathbf{B}_{\kappa_{c(t)}}\right) = \left(\frac{\theta - \theta_r}{\theta_r}\right) - \frac{1}{\Delta H_a}\frac{\partial i_\psi}{\partial \alpha}\bigg|_{\alpha = \alpha(t)} +$$

$$\frac{\mu_c\left(I_{\mathbf{B}_{\kappa_{c(t)}}} - 3\right) + \mu_{c1}\left(J_1 - 1\right)^2 + \mu_{c2}\left(K_1 - 1\right)^2 - \mu_a\left(I_{\mathbf{B}_{\kappa_a}} - 3\right)}{2\rho\Delta H_a},$$

(4.4.5)

For deriving the rate of melting, it is important to prescribe the rate of dissipation associated with the phase change during the melting process. In this work, the simplest form that depends on the crystallinity and the crystallization rate has been chosen.

$$\zeta_m = \frac{|\dot{\alpha}^m|}{\overline{G}(\alpha)^k},$$

(4.4.6)

It is important to note that the chosen form for ζ_m is very similar to the rate of dissipation associated with the phase transition during crystallization i.e. ζ_p. When the last crystal melts, crystallinity takes a zero value and ζ_m will take the maximum value. Further heating, above the melting temperature of the CSMP, will cause decomposition of the material. For the chosen form for ζ_m, the melting rate can be prescribed using Equation (4.4.2) and Equation (4.4.5) as follows:

$$\dot{\alpha} = G(\alpha)^{k/m-1}\left(\frac{\left(\frac{\theta - \theta_r}{\theta_r}\right) - \frac{1}{\Delta H_a}\frac{\partial i_\psi}{\partial \alpha} + }{\mu_c\left(I_{\mathbf{B}_{\kappa_{c(t)}}} - 3\right) + \mu_{c1}\left(J_1 - 1\right)^2 + \mu_{c2}\left(K_1 - 1\right)^2 - \mu_a\left(I_{\mathbf{B}_{\kappa_a}} - 3\right)}{2\rho\Delta H_a}\right)^{1/m-1}$$

.(4.4.7)

This is the necessary equation required to complete the model. In the following chapters, this model will be evaluated by simulating various processes.

CHAPTER 5

APPLICATION OF THE MODEL TO ONE-DIMENSIONAL PROBLEM

5.1   Introduction

In this chapter, the shape memory behavior in CSMP's is modeled in a mechanical setting with the understanding that this is the first step in developing a full thermodynamic model for these materials. The aim of this study is to clarify the mechanical issues relating to these shape memory polymers.

This chapter presents the effects of the chosen constitutive equations for the amorphous phase and the semi-crystalline phase as well as the implications of the natural configuration associated with the crystalline phase on the temporary shape and return to its original shape. Specific problem solved here that the model that arises using the assumption that the polymer crystallizes in a stress-free state, is able to capture the experimental observations accurately. To illustrate the efficacy of the model developed a typical uni-axial cycle of deformation is simulated using MATLAB code and compare its result with experimental data. For the uni-axial cycle of deformation, two cases studied are crystallization under constant strain and crystallization under constant stress. In addition, another problem solved is circular shear of a hollow cylinder. This is an inhomogeneous deformation for which also, two cases are considered, namely crystallization under constant shear and crystallization under constant moment. For both these deformations, the rates are slow and so, inertial terms have been ignored.

5.2 Kinematics

5.2.1 Uni-Axial Stretching

The first deformation cycle modeled is a uni-axial cycle of deformation. As mentioned earlier, for a shape memory polymer, the study of only the loading process is not sufficient. To capture the complete behavior, the whole cycle which consists of four distinct phases, namely loading, crystallization (cooling), unloading and melting (heating) is simulated. For the uni-axial cycle of deformation two commonly encountered cases are studied. The first involves crystallization under constant strain. The shape memory polymer is stretched to a prescribed length, and while the length is kept constant, crystallization is initiated by cooling. In the second case, the behavior of the polymer is studied when crystallization is initiated, while keeping the stress constant.

Uni-axial extension for an incompressible material is given by:

$$x = \Lambda(t)X, \quad y = \frac{1}{\sqrt{\Lambda(t)}}Y, \quad z = \frac{1}{\sqrt{\Lambda(t)}}Z. \tag{5.2.1}$$

where, X, Y, Z are the co-ordinates in the undeformed configuration and x, y, z are the co-ordinates in the deformed configuration and $\Lambda(t)$ is the stretch ratio. Here, the polymer is extended in the x-direction. For such a motion, the tensors $\mathbf{F}_{\kappa_a}$ and $\mathbf{F}_{\kappa_{c(\tau)}}$ are given by:

$$\mathbf{F}_{\kappa_a} = diag\left(\Lambda(t), \sqrt{\frac{1}{\Lambda(t)}}, \sqrt{\frac{1}{\Lambda(t)}}\right), \tag{5.2.2}$$

$$\mathbf{F}_{\kappa_{c(\tau)}} = diag\left(\frac{\Lambda(t)}{\Lambda(\tau)}, \sqrt{\frac{\Lambda(\tau)}{\Lambda(t)}}, \sqrt{\frac{\Lambda(\tau)}{\Lambda(t)}}\right). \tag{5.2.3}$$

Other kinematical tensors, namely $\mathbf{B}_{\kappa_a}, \mathbf{B}_{\kappa_{c(\tau)}}$, $\mathbf{C}_{\kappa_a}$ and $\mathbf{C}_{\kappa_{c(\tau)}}$ are also diagonal and are given by:

$$\mathbf{B}_{\kappa_a} = \mathbf{C}_{\kappa_a} = diag\left(\left(\Lambda(t)\right)^2, \frac{1}{\Lambda(t)}, \frac{1}{\Lambda(t)} \right), \tag{5.2.4}$$

$$\mathbf{B}_{\kappa_{c(\tau)}} = \mathbf{C}_{\kappa_{c(\tau)}} = diag\left(\left(\frac{\Lambda(t)}{\Lambda(\tau)}\right)^2, \frac{\Lambda(\tau)}{\Lambda(t)}, \frac{\Lambda(\tau)}{\Lambda(t)} \right). \tag{5.2.5}$$

For a uni-axial extension, if the lateral surfaces are stress free, the stress in the directions other than the direction of extension is assumed to be zero. Moreover, the stress tensor can be written as

$$\sigma = -p\mathbf{I} + \sigma^{\mathrm{E}} \tag{5.2.6}$$

where p is the Lagrangian multiplier and σ^{E} is the constitutively determined extra stress. Using equation(5.2.6) and the above mentioned assumptions, stress in the direction of stretch can be written as follows:

$$\sigma_{11} = \sigma_{11}^E - \sigma_{22}^E \tag{5.2.7}$$

5.2.2 Circular Shear

In this section, the cycle of circular shear of a shape memory polymer is presented. The geometry of the problem is illustrated in Figure 5.1. It is a long, hollow, circular cylinder which is fixed to a rigid support at its inner radius R_1, and to a rigid sleeve at its outer radius R_2. A moment per unit length of the cylinder is applied to the outer sleeve, causing it to rotate about the center-line of the cylinder. Because of this, the hollow cylinder is subject to circular shear. The hollow cylinder is subjected to two cycles of deformation, similar to the ones used for the uni-axial example. For the first cycle, the cylinder is sheared and then while the moment is kept constant, crystallization is initiated.

Moment applied at outer surface keeping inner surface of cylinder rigidly fixed.
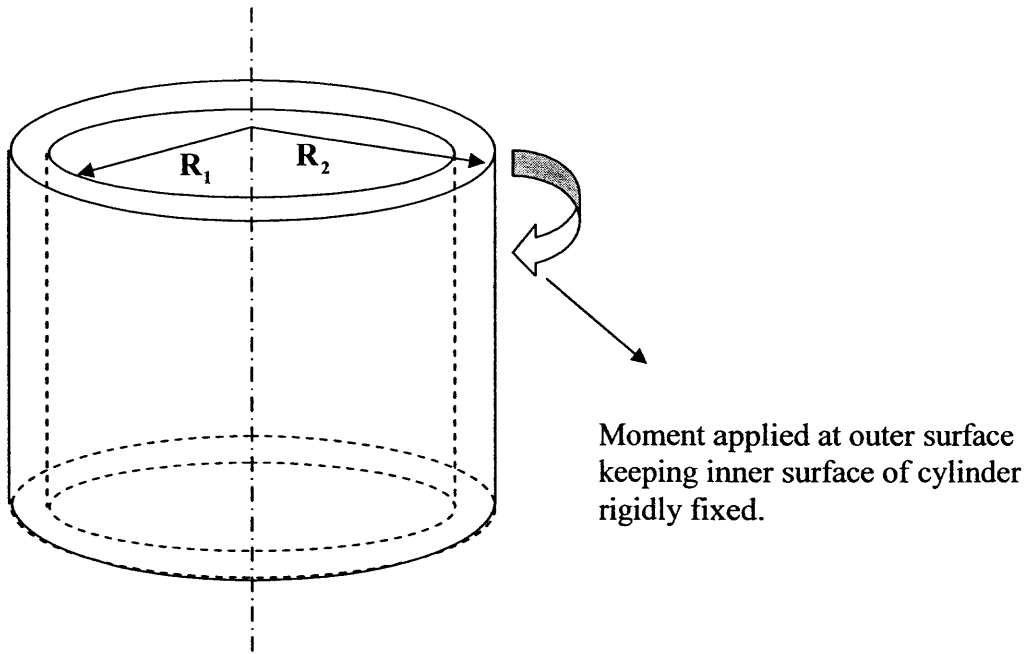
Figure 5.1 Schematic associated with the circular shear geometry.

Following this, the cylinder is unloaded and then melting of the crystalline phase returns the cylinder to its original shape. In the second type of deformation, the shear is kept constant as crystallization takes place. Note, this is an inhomogeneous deformation in which the shear components of stress are non zero and in addition the directions of anisotropy can evolve, depending on the conditions under which crystallization takes place. Furthermore, the shear varies through the thickness of the cylinder. For this deformation, the two vectors that characterize the direction of anisotropy, $\mathbf{n}_{\kappa_{c(t)}}$ and $\mathbf{m}_{\kappa_{c(t)}}$, evolve. The deformation for circular shear in cylindrical co-ordinates is given by:

$$
\begin{aligned}
r &= R, \\
\theta &= \Theta + f(R, \mathrm{t}), \\
z &= Z,
\end{aligned}
\tag{5.2.8}
$$

where (R,Θ,Z) and (r,θ,z) denotes the coordinates of the material particle in the reference and current configuration respectively and $f(R,t)$ denotes the rotation at time t and radius R. For such a motion, the deformation gradient, denoted by $\mathbf{F}_{\kappa_a}$ is given by

$$\mathbf{F}_{\kappa_a} = \begin{pmatrix} 1 & 0 & 0 \\ k(t,r) & 1 & 0 \\ 0 & 0 & 1 \end{pmatrix}, \tag{5.2.9}$$

while the relative gradient, $\mathbf{F}_{\kappa_{c(t)}}$ is given by:

$$\mathbf{F}_{\kappa_{c(t)}} = \begin{pmatrix} 1 & 0 & 0 \\ \Delta k & 1 & 0 \\ 0 & 0 & 1 \end{pmatrix}, \tag{5.2.10}$$

where, $\Delta k = k(t,r) - k(\tau,r)$ and $k = r\dfrac{\partial f}{\partial r}$, which is the local shear at any given radial location in the cylinder. From now, we will suppress the variable r in the local shear k and the incremental local shear Δk with the tacit understanding that it varies with radius.

$\mathbf{B}_{\kappa_a}$ is the important tensor for finding stress in the amorphous region, and that along with $\mathbf{C}_{\kappa_a}$ can be prescribe by:

$$\mathbf{B}_{\kappa_a} = \begin{pmatrix} 1 & k(t) & 0 \\ k(t) & 1+k(t)^2 & 0 \\ 0 & 0 & 1 \end{pmatrix},$$

$$\mathbf{C}_{\kappa_a} = \begin{pmatrix} 1+k(t)^2 & k(t) & 0 \\ k(t) & 1 & 0 \\ 0 & 0 & 1 \end{pmatrix}. \tag{5.2.11}$$

The other important kinematic tensors for finding stress in the crystalline phase are $\mathbf{B}_{\kappa_{c(t)}}$ and $\mathbf{C}_{\kappa_{c(t)}}$ and can be written as:

$$\mathbf{B}_{\kappa_{c(\tau)}} = \begin{pmatrix} 1 & \Delta k & 0 \\ \Delta k & 1 + \Delta k^2 & 0 \\ 0 & 0 & 1 \end{pmatrix},$$

$$\mathbf{C}_{\kappa_{c(\tau)}} = \begin{pmatrix} 1 + \Delta k^2 & \Delta k & 0 \\ \Delta k & 1 & 0 \\ 0 & 0 & 1 \end{pmatrix}. \tag{5.2.12}$$

The direction of anisotropy in the crystalline phase formed at time τ is determined by the unit vectors $\mathbf{n}_{\kappa_{c(\tau)}}$ and $\mathbf{m}_{\kappa_{c(\tau)}}$, which in turn are the eigenvectors of $\mathbf{B}_{\kappa_a}$ at the time of formation of the crystalline phase. Moreover, $\mathbf{n}_{\kappa_{c(\tau)}}$ and $\mathbf{m}_{\kappa_{c(\tau)}}$ are in the $r - \theta$ plane. The third eigenvector is perpendicular to the $r - \theta$ plane and is the unit vector in $z -$ direction. One can define $\mathbf{n}_{\kappa_{c(\tau)}}$ and $\mathbf{m}_{\kappa_{c(\tau)}}$ through:

$$\mathbf{n}_{\kappa_{c(\tau)}} = \begin{pmatrix} a \\ b \\ 0 \end{pmatrix}, \qquad \mathbf{m}_{\kappa_{c(\tau)}} = \begin{pmatrix} c \\ d \\ 0 \end{pmatrix}. \tag{5.2.13}$$

In the above equation, a, b, c and d are functions of τ and their values needed to be calculated. The invariants J_1 and K_1 can be calculated using Equation (4.2.23) and Equation (4.2.24) as follows:

$$J_1 = \left(1 + \Delta k^2\right)a^2 + 2\Delta kab + b^2,$$
$$K_1 = \left(1 + \Delta k^2\right)c^2 + 2\Delta kcd + d^2. \tag{5.2.14}$$

An inverse solution method is utilized to solve this problem. For the deformation described it possible to find stress components that satisfy the balance of linear momentum, the appropriate boundary conditions and have the following structure:

$$\sigma = -p(r, \mathrm{t})\mathbf{I} + \sigma^E (r, \mathrm{t}) \tag{5.2.15}$$

It is needed to search for stress components that depend on the radius and time that will satisfy the balance of linear momentum. The balance of linear momentum reduces to:

$$\frac{\partial \sigma_{rr}}{\partial r} + \frac{\sigma_{rr} - \sigma_{\theta\theta}}{r} = 0,$$

$$\frac{\partial \sigma_{r\theta}}{\partial r} + 2\frac{\sigma_{r\theta}}{r} = 0. \tag{5.2.16}$$

Integrating the above equation for the shear stress, and utilizing the inner radius of the cylinder to non-dimensionalized radius, we obtain:

$$\sigma_{r\theta} = \frac{M_0(t)}{2\pi r^2}, \quad \text{and} \quad M_0(t) = \frac{\bar{M}_0(t)}{\mu_a R_1^2} \tag{5.2.17}$$

where $\sigma_{r\theta}$ is the dimensionless shear stress at the radial location r and at time t. $\bar{M}_0$ is the moment per unit length applied to the outer surface of the cylinder, while M_0 is a dimensionless quantity related to the moment applied. This is the key equation used to solve for the variation of local shear with time and radius as the polymer undergoes a cycle of deformation.

5.3   Solution Method

5.3.1 Uni-axial Stretching

Next, the set of equations for each stage of the shape memory process is derived for this uni-axial cycle.

1. The Loading Process: During the loading process, the material is above the transition temperature and is totally amorphous in nature. Hence, $\alpha = 0$ and the stress in the direction of stretch can be written using Equation (4.2.13), Equation (5.2.4) and Equation (5.2.7) as follows:

$$\sigma_{11} = \left(\Lambda(t)^2 - \frac{1}{\Lambda(t)} \right). \tag{5.3.1}$$

For the case when the final stretch is known, by prescribing the stretch as a function of time, the progression of stress is readily known from Equation (5.3.1). Conversely, for the case when the final stress is known, by prescribing the stress as a function of time, the algebraic equation for stretch can be readily solved.

2. The Cooling Process: Once crystallization is initiated, the rate of crystallization is given by the appropriate crystallization kinetics, which are intimately related to the temperature and thermodynamics of the problem. Typically, for polymers, different forms of the Avrami equation are used, and recently Rao et al. (2004, 2005) have derived rate equations based on thermodynamic considerations. However, in this work, issues with regards to the mechanical behavior of shape memory polymers is only considered, there is no need to delve into the thermodynamics of the problem. And that will be the topic of the next chapter. Here, It is assumed that the rate at which crystallization takes place is given by a crystallization rate equation, with the tacit understanding that such an equation can be derived from a firm basis in thermodynamics (see Rao et al. (2002)). The specific equation chosen to mimic the rate of crystallization is given through a differential equation for the mass fraction of the crystalline phase and is given by:

$$
\begin{aligned}
\alpha &= 0, &\quad for \quad & 0 < t < t_s, \\
\frac{d\alpha}{dt} &= G(t - t_s)(\alpha_0 - \alpha), &\quad for \quad & t_s < t < t_f,
\end{aligned}
\tag{5.3.2}
$$

where, G is a constant, α_0 is the maximum crystallinity possible in the material and t_s is the time at which crystallization is initiated. The above equation is solved numerically using a standard numerical scheme for ordinary differential equations. Once crystallization ceases, i.e., when, $\alpha = \alpha_0$ at a later time denoted by t_f, the material is unloaded.

Crystallization can be done either under constant strain or constant stress. Depending on how the crystallization takes place, the solution methodology changes slightly. Both cases should be discussed separately.

Crystallization under constant strain: When crystallization is done under constant strain, there is no change in the stretch i.e.:

$$\Lambda(\tau) = \Lambda(t_s), \quad t_s < \tau < t < t_f \tag{5.3.3}$$

Using Equation (4.2.37), Equation (5.2.4), Equation (5.2.5), Equation (5.3.3) and noting that the crystalline phase is formed in a stress free state and hence the contribution to the stress from the crystalline phase, while the stretch is kept constant, is zero results in the following equation for the stress:

$$\sigma_{11} = (1 - \alpha(t))\left(\Lambda(t)^2 - \frac{1}{\Lambda(t)} \right). \tag{5.3.4}$$

Crystallization under constant stress: When the polymer crystallizes under constant stress the mechanical behavior is quite different. Because the newly crystallized material is formed in a stress free state, while the stress on the polymer is kept constant, the polymer will stretch as crystallization proceeds. Explained differently, when part of the amorphous polymer crystallizes, the ability of the amorphous polymer to carry the stress diminishes, as there is less amorphous polymer available. However, the newly formed crystalline polymer is formed in a stress free state and is unable to carry the load either. The only way the polymer can sustain this stress is to stretch as the already present crystalline phase and the remaining amorphous phase take on the additional stress. The crystalline phase is a lot stiffer than the original amorphous phase and hence the magnitude of this incremental stretch is much smaller than the original stretch.

The stress in direction of extension can be found using Equation (4.2.37), Equation (5.2.4), Equation (5.2.5), and Equation (5.2.7), and is prescribed by:

$$\sigma_{11} = \left(1-\alpha(t)\right)\mu_a \left(\Lambda(t)^2 - \frac{1}{\Lambda(t)} \right) + \mu_1 \int_{t_s}^{t} \left(\left(\frac{\Lambda(t)}{\Lambda(\tau)}\right)^2 - \frac{\Lambda(\tau)}{\Lambda(t)} \right) \frac{d\alpha}{d\tau} d\tau$$

$$+ \mu_2 \int_{t_s}^{t} \left(\left(\frac{\Lambda(t)}{\Lambda(\tau)}\right)^2 - 1 \right) \left(\frac{\Lambda(t)}{\Lambda(\tau)}\right)^2 \frac{d\alpha}{d\tau} d\tau \qquad (5.3.5)$$

Rearranging Equation (5.3.5), the variation of the stretch with time can be prescribed as

$$\sigma_{11} = \left(1-\alpha(t)\right)\left(\Lambda(t)^2 - \frac{1}{\Lambda(t)} \right) + \mu_1 \left(\Lambda(t)\right)^2 L_1 - \mu_1 \left(\frac{1}{\Lambda(t)}\right) L_2$$

$$+ \mu_2 \left(\Lambda(t)\right)^4 L_3 - \mu_2 \left(\Lambda(t)\right)^2 L_1, \qquad (5.3.6)$$

where, L_1, L_2 and L_3 are integrals that are defined through:

$$L_1 = \int_{t_s}^{t-d\tau} \frac{1}{\left(\Lambda(\tau)\right)^2} \frac{d\alpha}{d\tau} d\tau,$$

$$L_2 = \int_{t_s}^{t-d\tau} \Lambda(\tau) \frac{d\alpha}{d\tau} d\tau, \qquad (5.3.7)$$

$$L_3 = \int_{t_s}^{t-d\tau} \frac{1}{\left(\Lambda(\tau)\right)^4} \frac{d\alpha}{d\tau} d\tau.$$

The values of these integrals are known at time t as all past values of stretch and crystallization rates are known. To solve for the current value of stretch, $\Lambda(t)$, the values of these three integrals are first evaluated numerically and then substituted into Equation (5.3.6). Now, in Equation (5.3.6) the only unknown variable is the current stretch $\Lambda(t)$. The resulting equation is a polynomial equation of order five, which is solved numerically utilizing the fact that out of the five possible solutions, only one is physically possible. For this problem, the conditions that the correct root had to be real and greater than unity (as the polymer is stretched) sufficed to identify the physically realizable solution.

3. The Unloading Process: It is important to note that during unloading, the material is a mixture of two different phases, the crystalline and amorphous phases, with each having

different stress-free states. Hence both phases will not unload to a stress-free state, though the mixture will be stress-free. The equation for the stress during unloading reduces to

$$\sigma_{11} = \left(1 - \alpha_0\right)\left(\Lambda(t)^2 - \frac{1}{\Lambda(t)}\right) + \mu_1 \int_{t_s}^{t_f}\left(\left(\frac{\Lambda(t)}{\Lambda(\tau)}\right)^2 - \frac{\Lambda(\tau)}{\Lambda(t)}\right)\frac{d\alpha}{d\tau}\,d\tau$$
$$+ \mu_2 \int_{t_s}^{t_f}\left(\left(\frac{\Lambda(t)}{\Lambda(\tau)}\right)^2 - 1\right)\left(\frac{\Lambda(t)}{\Lambda(\tau)}\right)^2 \frac{d\alpha}{d\tau}\,d\tau. \tag{5.3.8}$$

In the above equation the limit of the integral is now t_f, the time at which crystallization ended and α_0 is the final crystallinity. Again, re-writing equation(5.3.8) in a manner identical manner to Equations (5.3.6) and Equation (5.3.7) we obtain:

$$\sigma_{11} = \left(1 - \alpha_0\right)\left(\Lambda(t)^2 - \frac{1}{\Lambda(t)}\right) + \mu_1\left(\Lambda(t)\right)^2 L_1 - \mu_1\left(\frac{1}{\Lambda(t)}\right)L_2$$
$$+ \mu_2\left(\Lambda(t)\right)^4 L_3 - \mu_2\left(\Lambda(t)\right)^2 L_1, \tag{5.3.9}$$

$$L_1 = \int_{t_s}^{t_f}\frac{1}{\left(\Lambda(\tau)\right)^2}\frac{d\alpha}{d\tau}\,d\tau,$$

$$L_2 = \int_{t_s}^{t_f}\Lambda(\tau)\frac{d\alpha}{d\tau}\,d\tau, \tag{5.3.10}$$

$$L_3 = \int_{t_s}^{t_f}\frac{1}{\left(\Lambda(\tau)\right)^4}\frac{d\alpha}{d\tau}\,d\tau.$$

where, L_1, L_2 and L_3 are integrals identical to those given by Equation (5.3.7), except that the upper limit is t_f. The values of these integrals remain unchanged during the unloading process as their integrands only depend on the stretches and crystallization rates during crystallization, i.e. between times t_s to t_f. To determine the variation of stretch during the unloading process, the stress value brought down to zero from its value at the end of crystallization. For each intermediate value of stress, the value of stretch can be obtained by solving the resulting polynomial Equation (5.3.9) in a manner identical to

that described earlier, keeping in mind that out of the multiple roots, the right root is the one that has physical significance.

4. The Melting Process: After unloading, the polymer is in its temporary shape. Return to the original shape is accomplished by melting the crystalline phase. This is done by heating the polymer above the melting temperature of the crystalline phase. As described earlier, the temporary shape of the polymer is retained because the two phases have different stress-free states. As the crystalline phase melts, the shape of the polymer slowly returns to its original shape as the crystalline phase is no longer present to keep it in its temporary shape. To track the evolution of the shape as it evolves from the temporary to permanent shape it is necessary to track which fraction of the crystalline phase is melting at any given time. This is particularly true for the case where crystallization takes place under constant stress as different crystals form at different stretches, and for this reason, the crystalline phase has different stress-free states. So, when a crystallite that is more stressed melts, the polymer as a whole will retract towards its original shape more than if a less stressed crystallite melted. For the constant stretch case all the crystals form in the same configuration, and therefore, the order in which the crystals melt does not impact the intermediate shapes occupied by the polymer. However, for crystallization under constant stress, or for a more general case wherein crystallization takes place under conditions of varying stress, the order in which the crystallites melt is important. The assumption made with regards to the melting process is that the crystallites formed last melt first, this assumption is supported from experiments as crystallites formed farthest from the equilibrium melting temperature (i.e. crystallites that were formed last) are thinner and melt at lower temperatures (i.e. melt first). During the melting process, the crystalline phase begins to melt at some time denoted in this study

by t_{ms}. The stress in the polymer is zero and the equation for determining the stretch simplifies to:

$$\sigma_{11} = 0 = \left(1 - \alpha(t)\right)\left(\Lambda(t)^2 - \frac{1}{\Lambda(t)}\right) + \mu_1 \int_{t_s}^{\dot{\tau}} \left(\left(\frac{\Lambda(t)}{\Lambda(\tau)}\right)^2 - \frac{\Lambda(\tau)}{\Lambda(t)}\right)\frac{d\alpha}{d\tau}d\tau$$

$$+ \mu_2 \int_{t_s}^{\dot{\tau}} \left(\left(\frac{\Lambda(t)}{\Lambda(\tau)}\right)^2 - 1\right)\left(\frac{\Lambda(t)}{\Lambda(\tau)}\right)^2 \frac{d\alpha}{d\tau}d\tau,$$

$$\text{with} \quad \dot{\tau} \in \left[t_s, t_f\right] \quad \text{and} \quad \dot{\alpha}(t) = \dot{\alpha}(\tau).$$

(5.3.11)

The above equation can be re-written as an algebraic equation of the order of five as follows:

$$\sigma_{11} = 0 = \left(1 - \alpha(t)\right)\left(\Lambda(t)^2 - \frac{1}{\Lambda(t)}\right) + \mu_1 \left(\Lambda(t)\right)^2 L_1 - \mu_1 \left(\frac{1}{\Lambda(t)}\right)L_2$$

$$+ \mu_2 \left(\Lambda(t)\right)^4 L_3 - \mu_2 \left(\Lambda(t)\right)^2 L_1,$$

(5.3.12)

where the integrals have integrands identical to Equation (5.3.7) and Equation (5.3.10) with different limits and are given by:

$$L_1 = \int_{t_s}^{\dot{\tau}} \frac{1}{\left(\Lambda(\tau)\right)^2} \frac{d\alpha}{d\tau}d\tau,$$

$$L_2 = \int_{t_s}^{\dot{\tau}} \Lambda(\tau)\frac{d\alpha}{d\tau}d\tau,$$

(5.3.13)

$$L_3 = \int_{t_s}^{\dot{\tau}} \frac{1}{\left(\Lambda(\tau)\right)^4} \frac{d\alpha}{d\tau}d\tau.$$

Incremental values of crystallinity are obtained from the prescribed melting equation for crystallinity, which is given by:

$$\frac{d\alpha}{dt} = G(t - t_{ms})(0 - \alpha) \qquad \text{for} \qquad t_{ms} < t < t_{mf}$$

(5.3.14)

where, G is a constant, t_{ms} is the time at which melting is initiated and t_{mf} is the time at which melting ceases, i.e. when $\alpha = 0$. This is the last equation required to complete the cycle. Here, the melting rate equation is prescribed as an empirical equation because the

primarily focus is on the mechanical implications. One can determine the incremental decrease in crystallinity and the net crystallinity after each time step by solving Equation (5.3.14). Using the interpolation procedure described above the value of $\dot{t}$ can be determined. Using the value of $\dot{t}$, the values of integrals in Equation (5.3.13) can be determined. The values of the integrals are substituted into Equation (5.3.12) and the resulting polynomial equation is solved for the appropriate value of stretch. This completes the solution procedure for the uni-axial cycle of deformation.

5.3.2 Circular Shear

The solution methodology closely follows what is developed for the uni-axial problem.

1. The Loading Process: The cylinder is loaded by gradually increasing the applied moment at the outer radius, which produces shearing. Since during the loading process the polymer is amorphous, from Equation (4.2.13), Equation (5.2.11), Equation (5.2.15) and Equation (5.2.17), the local shear inside the cylinder is given by:

$$\sigma_{r\theta} = \frac{M_0(t)}{2\mu_a \pi r^2} = k(t). \tag{5.3.15}$$

Note, the shear varies with radius and time as the applied moment is increased.

2. The Cooling Process: As presented two cases for the uni-axial extension cycle earlier, here also, two different cases are described. The first is crystallization under constant shear and the second is crystallization under constant moment.

Crystallization with constant local shear: Once the maximum moment is applied, crystallization begins keeping the local shear constant. As the new crystals form in a stress free state during the crystallization process, the moment required to maintain a state of constant shear decreases. During the crystallization process the local shear remains constant, i.e.

$$\kappa(\tau) = \kappa(t_1) \quad for \quad \tau \in [t_s, t_f] \tag{5.3.16}$$

Therefore, using Equation (4.2.37), Equation (5.2.11), Equation (5.2.12), Equation (5.2.17) and Equation (5.3.16) the shear stress can be written as:

$$\sigma_{r\theta} = \frac{M_0(t)}{2\pi r^2} = (1 - \alpha(t))k(t). \tag{5.3.17}$$

It is important to note that it is possible from Equation (5.3.17) to calculate how the applied moment has to vary in order to maintain constant shear. The crystallization rate equation is identical to the one chosen earlier in Equation (5.3.2).

Crystallization with constant applied moment: In this second case, after loading, the moment is kept constant, and crystallization is initiated. Because the newly crystallized material is formed in a stress free state, while the applied moment is kept constant, the polymer will continue to shear as crystallization proceeds for exactly the same reasons explained earlier for the uni-axial case, where in crystallization taking place under constant stress were investigated. The equation for shear stress can be written using Equation (4.2.37), Equation (5.2.11), Equation (5.2.12), Equation (5.2.14) and Equation (5.2.17) as follows:

$$\sigma_{r\theta} = (1 - \alpha(t))k + \mu_1 \int_{t_s}^{t} \Delta k \frac{d\alpha}{d\tau} d\tau + \mu_2 \int_{t_s}^{t} \left[(J_1 - 1)(\Delta k^2 a^2 + ab) \right] \frac{d\alpha}{d\tau} d\tau$$
$$+ \mu_3 \int_{t_s}^{t} \left[(K_1 - 1)(\Delta k^2 c^2 + cd) \right] \frac{d\alpha}{d\tau} d\tau \tag{5.3.18}$$

Hence, during crystallization under constant moment, the local shear at each radial location can be obtained rearranging and expanding Equation (5.3.18)

$$\sigma_{r\theta} = \frac{M_0(t)}{2\pi r^2} = k^3(t)I_1 + k^2(t)I_2 + k(t)(1 - \alpha(t) + I_3) + I_4, \tag{5.3.19}$$

where I_1, I_2, I_3 and I_4 are integrals and are given by:

$$I_1 = \int_{t_s}^{t-d\tau} \left[\mu_2 a^4 + \mu_3 c^4 \right] \frac{d\alpha}{d\tau} d\tau,$$

$$I_2 = \int_{t_s}^{t-d\tau} \left[3\mu_2 a^2 b + 3\mu_3 c^2 d - 3\mu_2 a^4 k(\tau) - 3\mu_3 c^4 k(\tau) \right] \frac{d\alpha}{d\tau} d\tau,$$

$$I_3 = \int_{t_s}^{t-d\tau} \begin{bmatrix} \mu_1 + \mu_2 \left(3a^2 b^2 + a^4 - a^2 \right) + \mu_3 \left(3c^2 d^2 + c^4 - c^2 \right) \\ -6\mu_2 a^2 bk(\tau) - 6\mu_3 c^2 dk(\tau) + 3\mu_2 a^4 k^2(\tau) + 3\mu_3 c^4 k^2(\tau) \end{bmatrix} \frac{d\alpha}{d\tau} d\tau, \qquad (5.3.20)$$

$$I_4 = \int_{t_s}^{t-d\tau} \begin{bmatrix} -\mu_1 k(\tau) - \mu_2 \left(3a^2 b^2 + a^4 - a^2 \right) k(\tau) - \mu_3 \left(3c^2 d^2 + c^4 - c^2 \right) k(\tau) \\ +3\mu_2 a^2 bk^2(\tau) + 3\mu_3 c^2 dk^2(\tau) - \mu_2 a^4 k^3(\tau) - \mu_3 c^4 k^3(\tau) \end{bmatrix} \frac{d\alpha}{d\tau} d\tau.$$

The values of the integrals only depend on kinematic variables at times prior to the current time and hence, can be directly evaluated. Once, these integrals are evaluated numerically for each radial location, the current value of shear at that radial location is obtained by solving the resulting cubic Equation (5.3.20). The correct root is identified by examining the physical validity of the result (it has to be real and greater than zero).

3. The Unloading Process: To determine the shape recovery on unloading it is noted that the relationship between the local shear at any radius and the applied moment is given by Equation (5.3.19) and Equation (5.3.20) with the exception that the limits of the integrals are now fixed from time t_s (the time crystallization began) to time t_f (when crystallization ended). Substituting these integrals into Equation (5.3.19) the variation of local shear at any radial location with time is determined by solving the cubic equation for different decreasing values of moment, till the applied moment is zero.

4. The Melting Process: Here as in the uni-axial case it is assumed that the crystallites formed at the end of the crystallization process melt first. The local shear during the melting process is again given by Equation (5.3.19) with the integrals given by Equation (5.3.20) with a part of the integral not contributing to the stress as it has melted. The methodology and reasoning are identical to the uni-axial case and will not be reiterated

again. The stress in the polymer is zero and the equation for determining the stretch simplifies to

$$\sigma_{r\theta} = \frac{M_0(t)}{2\pi r^2} = 0 = k^3(t)I_1 + k^2(t)I_2 + k(t)\left(1 - \alpha(t) + I_3\right) + I_4, \qquad (5.3.21)$$

where,

$$I_1 = \int_{t_s}^{t_f} \left[\mu_2 a^4 + \mu_3 c^4\right]\frac{d\dot{\alpha}}{d\tau}d\tau,$$

$$I_2 = \int_{t_s}^{t_f} \left[3\mu_2 a^2 b + 3\mu_3 c^2 d - 3\mu_2 a^4 k(\tau) - 3\mu_3 c^4 k(\tau)\right]\frac{d\dot{\alpha}}{d\tau}d\tau,$$

$$I_3 = \int_{t_s}^{t_f} \begin{bmatrix} \mu_1 + \mu_2\left(3a^2 b^2 + a^4 - a^2\right) + \mu_3\left(3c^2 d^2 + c^4 - c^2\right) \\ -6\mu_2 a^2 bk(\tau) - 6\mu_3 c^2 dk(\tau) + 3\mu_2 a^4 k^2(\tau) + 3\mu_3 c^4 k^2(\tau) \end{bmatrix}\frac{d\dot{\alpha}}{d\tau}d\tau, \qquad (5.3.22)$$

$$I_4 = \int_{t_s}^{t_f} \begin{bmatrix} -\mu_1 k(\tau) - \mu_2\left(3a^2 b^2 + a^4 - a^2\right)k(\tau) - \mu_3\left(3c^2 d^2 + c^4 - c^2\right)k(\tau) \\ +3\mu_2 a^2 bk^2(\tau) + 3\mu_3 c^2 dk^2(\tau) - \mu_2 a^4 k^3(\tau) - \mu_3 c^4 k^3(\tau) \end{bmatrix}\frac{d\dot{\alpha}}{d\tau}d\tau.$$

with $\dot{\tau} \in \left[t_s, t_f\right]$ *and* $\alpha(t) = \alpha(\dot{\tau})$

As noted earlier, the time is tagged when the crystals were formed with the actual times when they were formed, i.e., $\dot{\tau} \in \left[t_s, t_f\right]$. The melting rate equation is identical to the one used in the uni-axial case and is given by Equation(5.3.14) and the methodology for solving for the local shear is identical with the exception that now the equations are solved for each radial location at which the variation of local shear with time is desired. This completes the solution methodology used, in the next section; results of the calculations are discussed.

5.4 Results

The calculations were performed for two geometries, namely, uni-axial extension and circular shear, the first being homogenous while the second inhomogeneous. In each geometries, two types of results were obtained. For the uni-axial case, crystallization

under constant strain and crystallization under constant stress were studied. In the case of circular shear, the two cases investigated are: crystallization under constant shear and crystallization under constant moment. In addition the results of the calculation from the uni-axial simulation are compared against experimental data.

The first set of results is for uni-axial extension with crystallization taking place while the strain is kept constant. The graph of true stress versus strain (in %) for different values of final crystallinity are shown in Figure 5.2. Note that the stress increases when the polymer is deformed above the recovery temperature. After the onset of crystallization the stress drops as the newly formed crystalline phase is formed in a stress free state. Note that the drop in stress observed during crystallization increases for larger final values of crystallinity. Finally on unloading there is a small amount of retraction, the new material is significantly stiffer than the original amorphous material. Also, the material with more crystalline material is stiffer than the material with less amount of crystalline material, this can be discerned by looking at the slope during unloading.
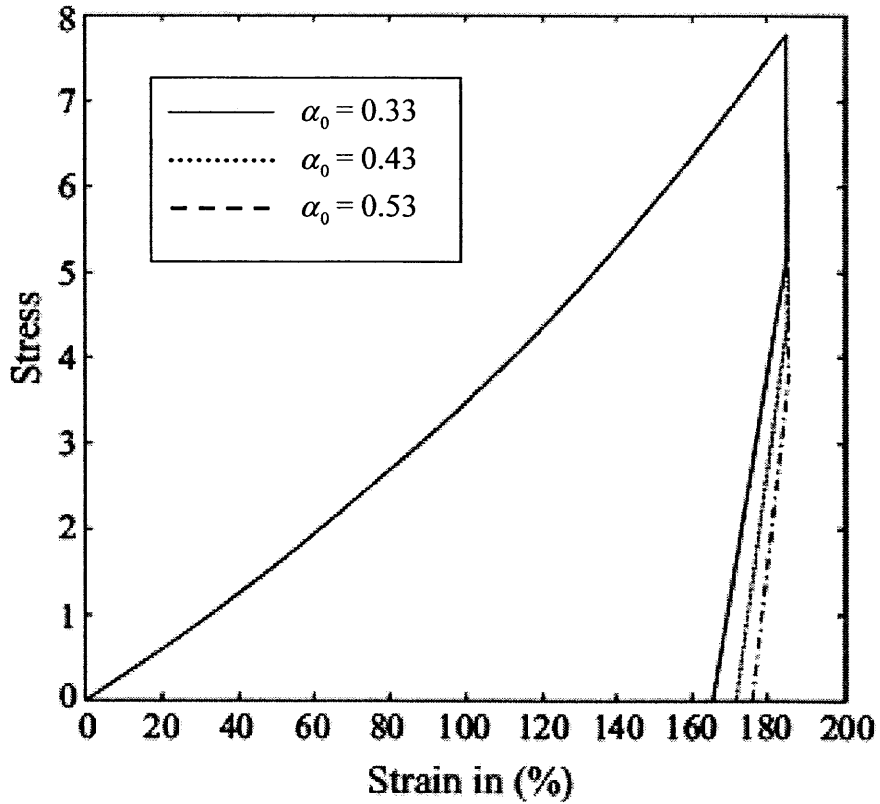
Figure 5.2 Plot of stress versus strain for uni-axial extension with crystallization taking place at constant strain for three different crystallinity values. The constants used for simulation are mentioned in Table 5.1.

Table 5.1 Data Used for Simulating Circular Shear in Cylinder (Constant Strain Process)

t_s	t_{ms}	G (in sec^{-2})	μ_a (in Mpa)	μ_1	μ_2
120	800	0.00007	0.256	50	30
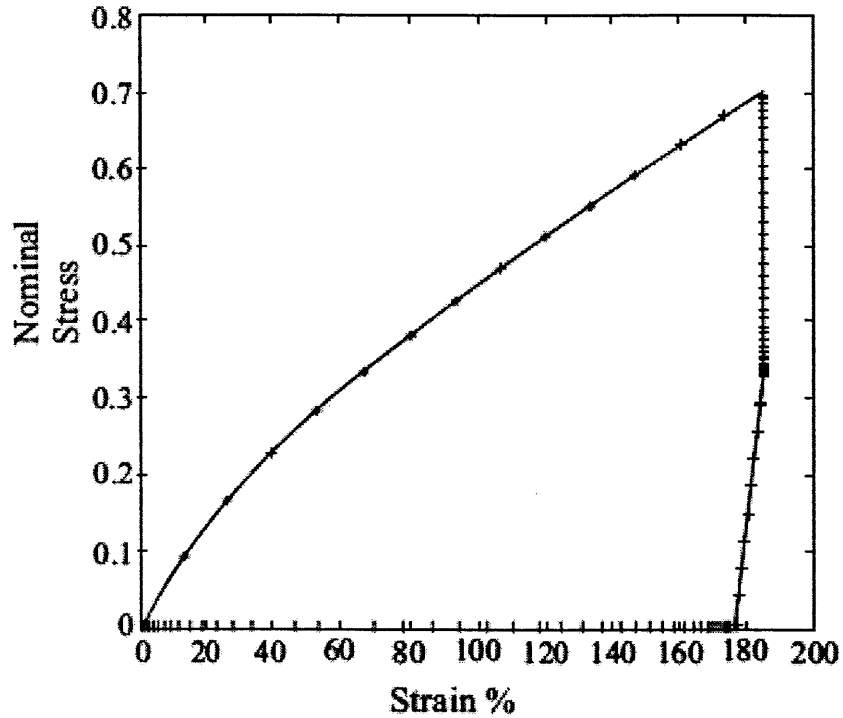
Figure 5.3 Plot of nominal stress versus strain for uni-axial extension with crystallization taking place at constant strain. + indicates experimental data (Lendlein et al. 2001). The constants used are mentioned in Table 5.2.

Table 5.2 Data Used for Simulation of Verification Process

α_0	t_s	t_{ms}	G (in sec^{-2})	μ_a (in Mpa)	μ_1	μ_2
0.53	120	800	0.00007	0.256	50	30
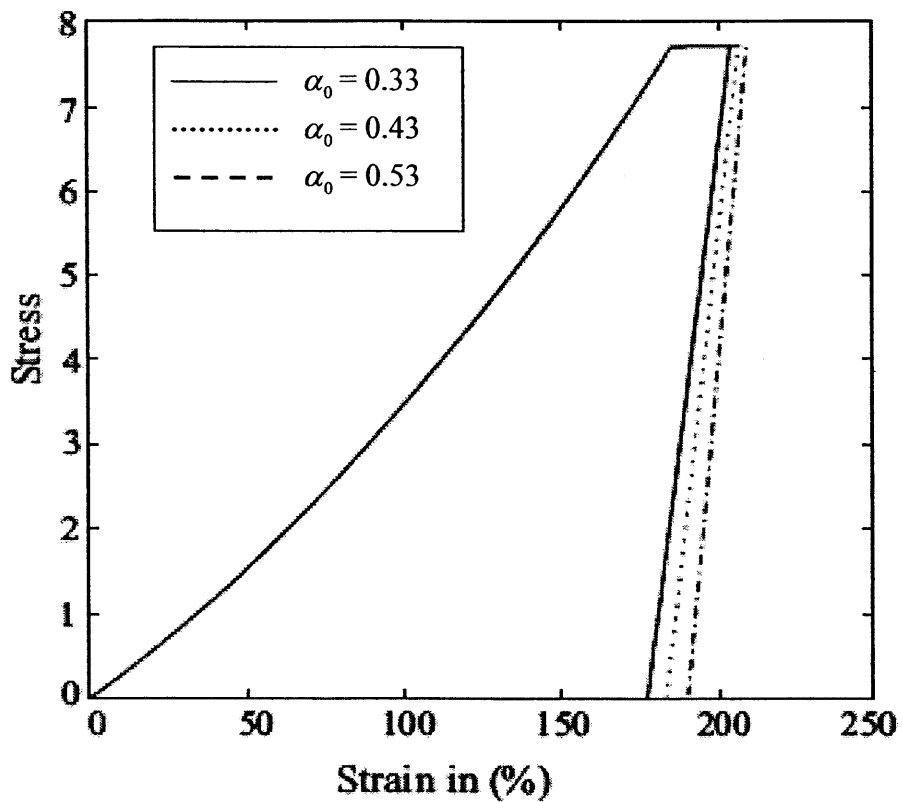
Figure 5.4 Plot of stress versus strain for uni-axial extension with crystallization taking place at constant stress for three different crystallinities. Constant used in the simulation are mentioned in Table 5.1.

For uni-axial extension, the behavior of the model were compared with data presented in Lendlein et al. 2001.The material constants are consistent with the data presented. The stress in this case is the nominal stress, and the plot is of nominal stress versus the strain and is shown in Figure 5.3. As you can see the data points compare very well with the model predictions.

In the uni-axial geometry, the results were also obtained for a case when crystallization takes place while the stress is kept constant. This case is shown in Figure 5.4 Again, three sets of curves are plotted, each corresponding to a different level of final crystallinity. Note that as the crystalline phase is formed in a stress free state, for the stress to be held constant, the polymer will have to immediately undergo a small extension. This is clearly observed in Figure 5.4, where as crystallization proceeds the material extends. The maximum stretch is directly correlated with the final crystallinity, with its magnitude increasing with the final crystallinity. On unloading the sample retracts by a small but finite amount because of the increase in stiffness. Also, note as the final crystallinity increases the stiffness also increases.

The second geometry investigated was circular shear of a hollow cylinder. The first case studied in this geometry was a deformation cycle in which a moment was applied above the recovery temperature, as a result of which the cylinder underwent a shearing deformation. When a prescribed value of moment has been reached, the moment is held constant and crystallization is initiated. Then the cylinder is unloaded to zero moment. The variation of moment with time is shown in Figure 5.5, it is ramped up to the prescribed value and then ramped down to zero. The variation of moment with shear is shown in Figure 5.6. Note that the shear at the inner radius of the cylinder is maximum while at the outer radius it is minimum.

Figure 5.5 Plot of time versus applied moment for circular shear geometry. During crystallization, moment is kept constant. Constant used for simulation are mentioned in Table 5.3.

Table 5.3 Data used for Simulating Circular Shear in Cylinder (Constant Moment Process)

α_0	t_s	t_{ms}	G (in sec^{-2})	μ_a (in Mpa)	μ_1	μ_2	μ_3
0.33	120	1200	0.00007	0.256	50	30	30

Figure 5.6 Plot of applied moment versus shear for circular shear geometry. During crystallization, moment is kept constant. The constants used in simulation are mentioned in Table 5.3.
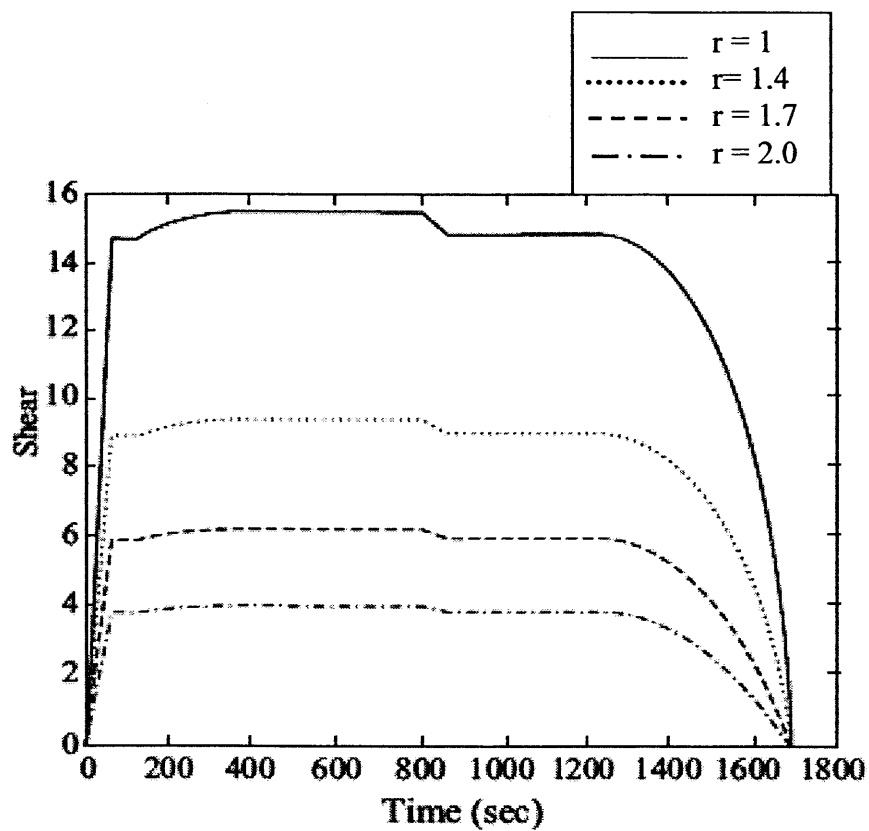
Figure 5.7 Plot of time versus shear for circular shear geometry. During crystallization, moment is kept constant. The constants used for simulation are mentioned in Table 5.3.

After the onset of crystallization, the shear at all locations increases because the crystalline phase is formed in a stress free state and to support the same moment, the cylinder has to shear further. During unloading a small retraction in deformation is observed and as it is noted that the material is a lot stiffer after crystallization. Figure 5.7 plots the shear versus time for the whole process for different radii, the different stages are marked. Initially the shear increases. After the onset of crystallization, there is further increase in shear at each location for reasons explained earlier. During the unloading process there is a small decrease in shear with the decrease being larger at the inner radius of the cylinder where the shear is the maximum. Finally as the crystalline phase melts, the shear again returns to zero.

The second case investigated in the cylindrical geometry was the case where after loading the shear was kept constant during the crystallization process. The variation of moment with time is shown in Figure 5.8, note that the after the onset of crystallization, the moment drops and finally returns to zero on unloading. The plot of moment versus shear is shown in Figure 5.9. Note that, the shear is maximum at the inner cylinder and after the onset of crystallization the moment drops. Also, similar to the other cases, on unloading a small retraction is observed. Finally in Figure 5.10 the shear versus time graph was plotted. Initially the shear increases as the moment is increased, then during crystallization the shear is kept constant. On unloading a small amount of retraction can be seen in Figure 5.10. During melting of the crystalline phase, the shear drops back to zero.
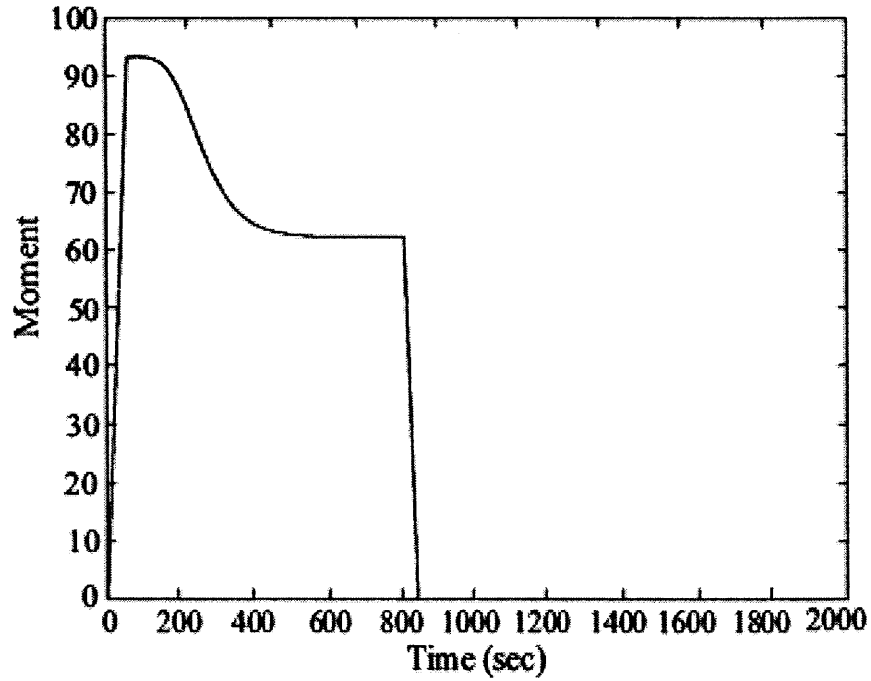
Figure 5.8 Plot of time versus applied moment for circular shear geometry. During crystallization, shear is kept constant. The constants used for simulation are mentioned in Table 5.3.
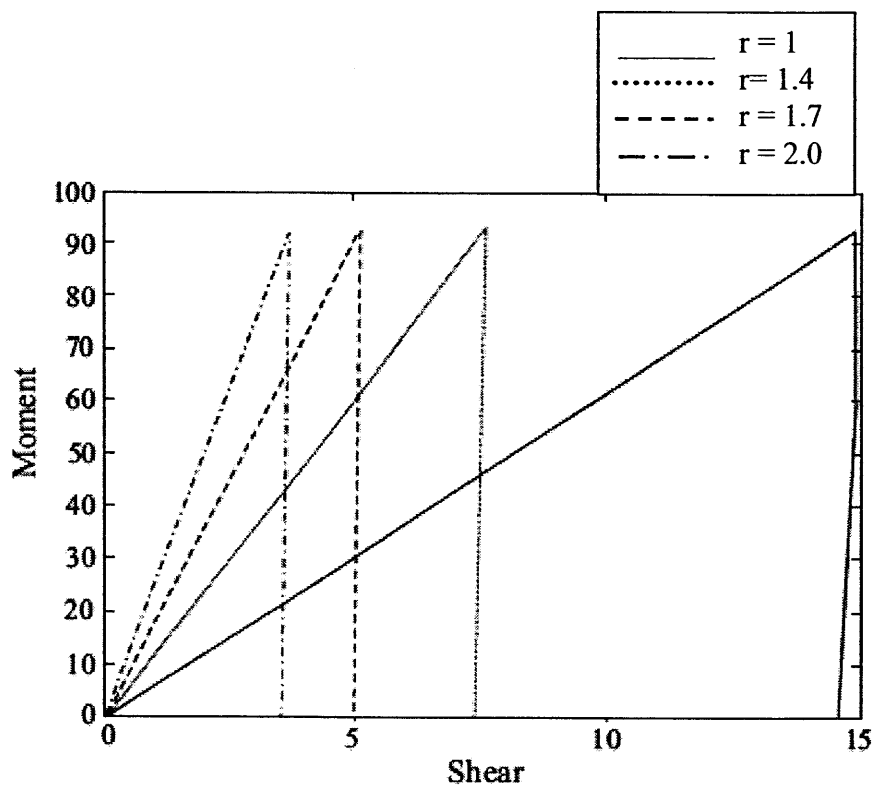
Figure 5.9 Plot of applied moment versus shear for circular shear geometry. During crystallization, shear is kept constant. The constants used for the simulation are mentioned in Table 5.3.
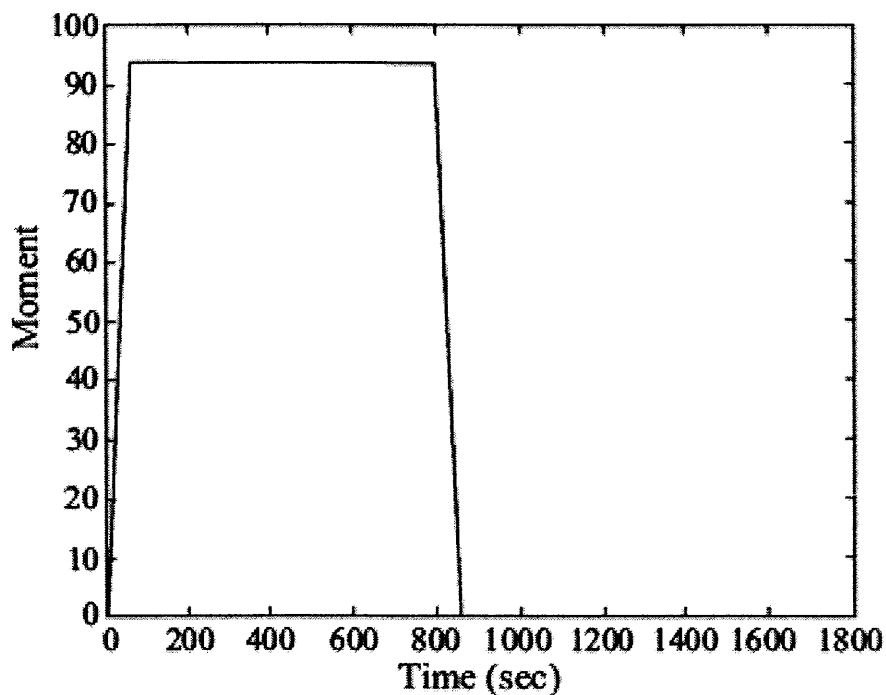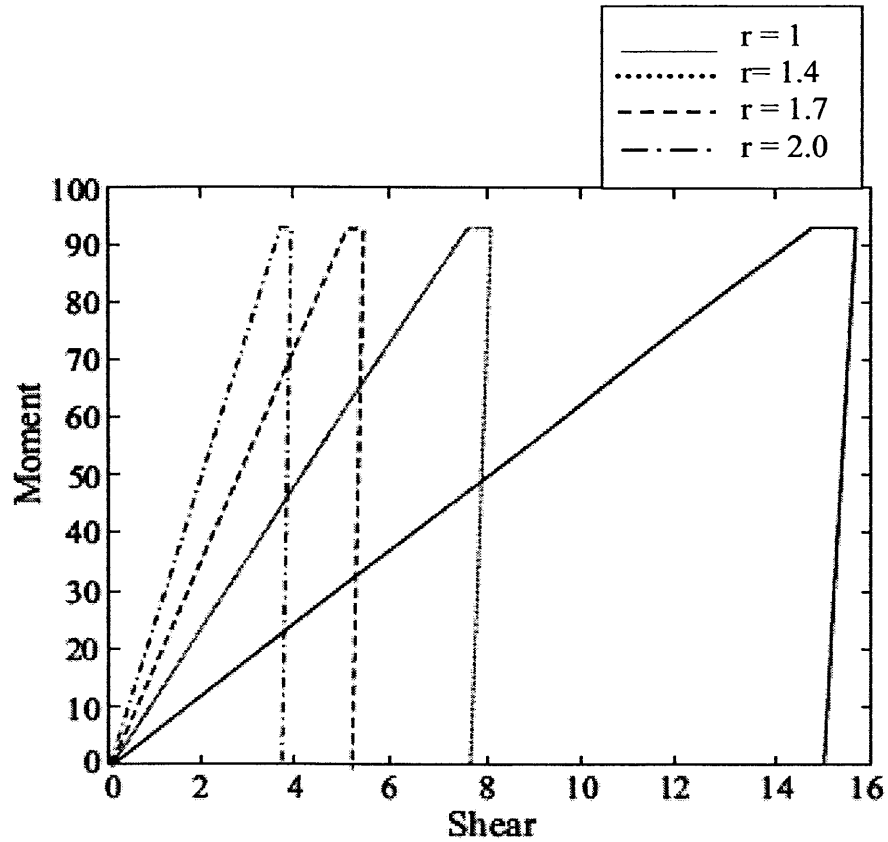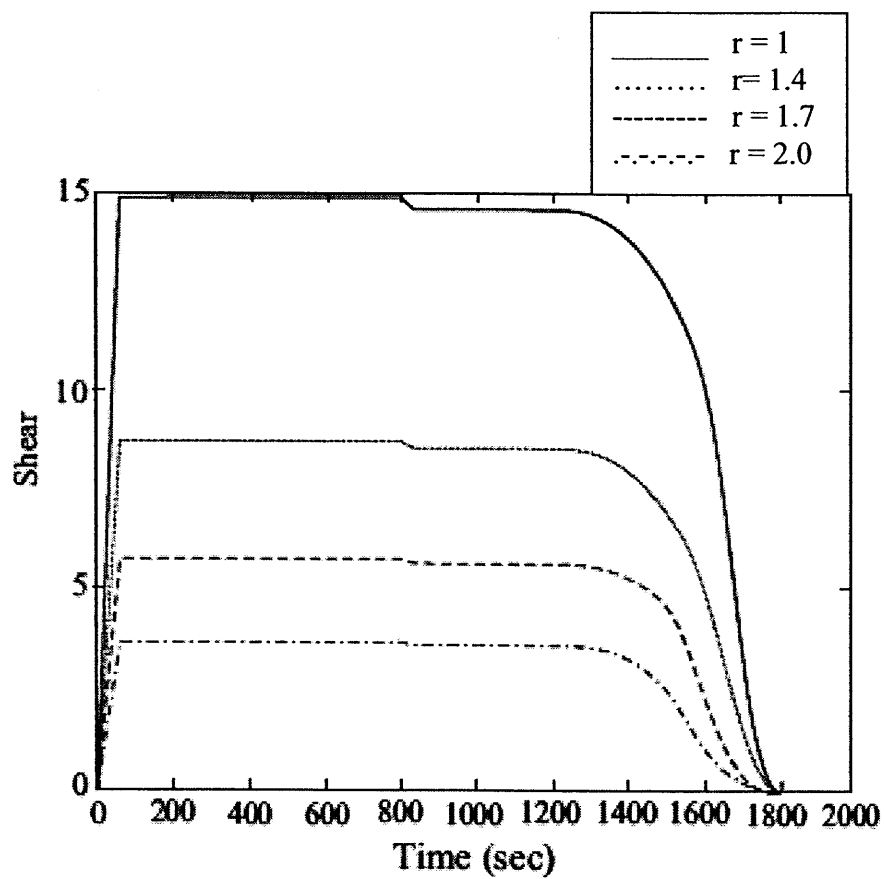
Figure 5.10 Plot of time versus shear for circular shear geometry. During crystallization, shear is kept constant. The constants used for simulation are mentioned in Table 5.3.

CHAPTER 6

APPLICATION OF THE MODEL TO THERMALLY COUPLED SYSTEM: INFLATION AND EXTENSION OF HOLLOW CYLINDER

6.1   Introduction

In this chapter, description about the work that is needed to be done for the fulfillment of the requirements of the current study is presented. So far, thermo-mechanics associated with CSMP is well understood. It have been shown in the previous chapter that using the developed model (described in Chapter 4) it is possible to model phase transitions (the amorphous phase to semi-crystalline phase and vice versa) with in mechanical settings for one-dimensional processes. The future study will be more comprehensive and the aim is to be able to simulate more realistic processes with more complex geometries.

6.2   Simulation of Non-isothermal and Inhomogeneous Deformation Cycle

The representative deformation cycle chosen is inflation and extension of the tube. In this process the material undergoes large inhomogeneous deformation and heat transfer process can be prescribed with realistic boundary conditions. Figure 6.1 shows the schematic of the process in which the primary mode of the heat transfer inside the material is heat conduction. It is assumed that inner surface of the cylinder is insulated and outer surface of the cylinder is having convective boundary condition. In this case physical quantities for which attention must be paid are radius of the cylinder, pressure difference that is applied and the stretch-ratio. For this case, it is assumed that the rates are slow and hence, inertial terms have been ignored and the stretch ratio $\left(\Lambda\left(t\right)\right)$ is kept constant in all processes loading, cooling, unloading and heating.
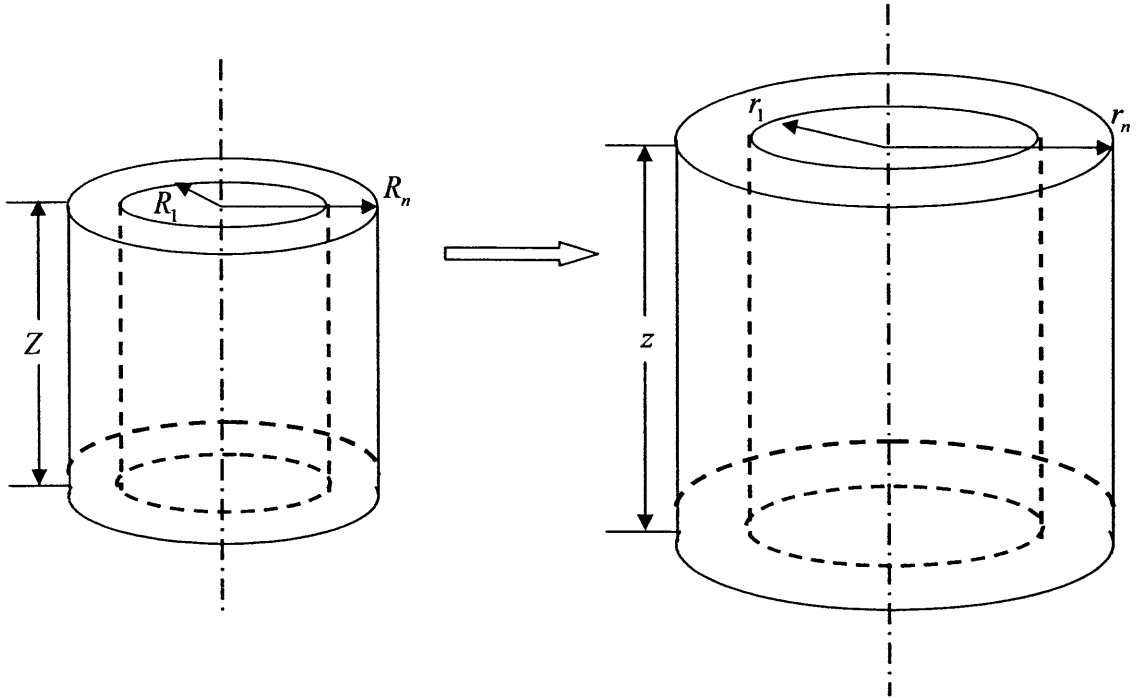
Figure 6.1 Schematic associated with the inflation and extension of a tube.

6.2.1 Motion

Consider the Figure 6.1 showing hollow cylinder with internal radius R_1, external

radius R_2 and height H at time t=0. The cylindrical co-ordinates (R, Θ, Z) are used for

analysis purpose. Material is stretched in z direction and the tube is pressurized gradually

to inflate tube such a way that motion of the processes can be stated as follows:

$$
\begin{aligned}
r &= r(R, \mathrm{t}), \\
\theta &= \Theta, \\
z &= \Lambda Z.
\end{aligned}
\tag{6.2.1}
$$

For the given case deformation gradients $\mathbf{F}_{\kappa_a}$ and $\mathbf{F}_{\kappa_{c(t)}}$ can be written as:

$$
\mathbf{F}_{\kappa_a} = \begin{pmatrix} \dfrac{dr(R,\mathrm{t})}{dR} & 0 & 0 \\ 0 & \dfrac{r(R,\mathrm{t})d\Theta}{Rd\Theta} & 0 \\ 0 & 0 & \Lambda(\mathrm{t}) \end{pmatrix},
\tag{6.2.2}
$$

$$\mathbf{F}_{\kappa_{c(\tau)}} = \begin{pmatrix} \dfrac{dr(R,t)}{dr(R,\tau)} & 0 & 0 \\ 0 & \dfrac{r(R,t)}{r(R,\tau)} & 0 \\ 0 & 0 & \dfrac{\Lambda(t)}{\Lambda(\tau)} \end{pmatrix}, \tag{6.2.3}$$

For the given case, equation for the conservation of mass is

$$\det(\mathbf{F}) = 1. \tag{6.2.4}$$

According to the conservation of mass given by Equation (6.2.4) and based on the assumption that stretch ratio remains constant through out the deformation cycle, deformation gradients take the following forms

$$\mathbf{F}_{\kappa_a} = \begin{pmatrix} \dfrac{R}{\Lambda r(R,t)} & 0 & 0 \\ 0 & \dfrac{r(R,t)}{R} & 0 \\ 0 & 0 & \Lambda \end{pmatrix}, \tag{6.2.5}$$

$$\mathbf{F}_{\kappa_{c(\tau)}} = \begin{pmatrix} \dfrac{r(\tau)}{r(t)} & 0 & 0 \\ 0 & \dfrac{r(t)}{r(\tau)} & 0 \\ 0 & 0 & 1 \end{pmatrix}. \tag{6.2.6}$$

The other important kinematic tensors such as $\mathbf{B}_{\kappa_a}, \mathbf{C}_{\kappa_a}, \mathbf{B}_{\kappa_{c(t)}}$ and $\mathbf{C}_{\kappa_{c(t)}}$ can be prescribed as

$$\mathbf{B}_{\kappa_a} = \mathbf{C}_{\kappa_a} = \begin{pmatrix} \left(\dfrac{R}{\Lambda r(R,t)}\right)^2 & 0 & 0 \\ 0 & \left(\dfrac{r(R,t)}{R}\right)^2 & 0 \\ 0 & 0 & (\Lambda)^2 \end{pmatrix}, \qquad (6.2.7)$$

$$\mathbf{B}_{\kappa_{c(\tau)}} = \mathbf{C}_{\kappa_{c(\tau)}} = \begin{pmatrix} \left(\dfrac{r(\tau)}{r(t)}\right)^2 & 0 & 0 \\ 0 & \left(\dfrac{r(t)}{r(\tau)}\right)^2 & 0 \\ 0 & 0 & 1 \end{pmatrix}. \qquad (6.2.8)$$

The directions associated with the anisotropy in the crystalline phase formed at time τ is determined by the unit vectors $\mathbf{n}_{\kappa_{c(t)}}$ and $\mathbf{m}_{\kappa_{c(t)}}$, which in turn are the eigenvectors of $\mathbf{B}_{\kappa_a}$ at the time of formation of the crystalline phase. One can define $\mathbf{n}_{\kappa_{c(t)}}$ and $\mathbf{m}_{\kappa_{c(t)}}$ through:

$$\mathbf{n}_{\kappa_{c(t)}} = \begin{pmatrix} 1 \\ 0 \\ 0 \end{pmatrix}, \qquad \mathbf{m}_{\kappa_{c(t)}} = \begin{pmatrix} 0 \\ 1 \\ 0 \end{pmatrix}. \qquad (6.2.9)$$

These values eigenvectors are required to find invariants associated with anisotropy such as J_1 and K_1.

6.2.2 Mass Conservation

For the current problem, the mass conservation principle is given by Equation (6.2.4) but a more useful form of the principle can be written using Equation (6.2.2) and Equation (6.2.4) and applying proper limits. We obtain,

$$r^2 - r_1^2 = \frac{1}{\Lambda}\left(R^2 - R_1^2\right). \qquad (6.2.10)$$

This is a useful equation because knowing R_1 and r_1 one can map the radius of each particle from the reference configuration to the deform configuration or the current configuration.

6.2.3 Balance of Linear Momentum

For the current geometry the balance of linear momentum in cylindrical co-ordinates can be written as follows:

$$\frac{d\sigma_{rr}}{dr} = \frac{1}{r}\left(\sigma_{\theta\theta} - \sigma_{rr}\right). \tag{6.2.11}$$

But it is also known that

$$\sigma_{rr}(r_1) = -P_{i,}$$
$$\sigma_{rr}(r_1) = -P_{o.} \tag{6.2.12}$$

Where, P_i is internal pressure and P_o is ambient pressure that applies to the outer wall of the cylinder. Using Equation (6.2.11) and the boundary conditions given in Equation (6.2.12) a relation between pressure difference and radii as give below.

$$\Delta P = P_i - P_o = \int_{r_1}^{r_2} \frac{\sigma_{\theta\theta} - \sigma_{rr}}{r} dr. \tag{6.2.13}$$

This is an important equation for simulating the process.

6.2.4 Heat Transfer

It is assumed that there is no heat transfer possible from the top and the bottom of the cylinder. Hence, at a particular radius r in all $r - \theta$ planes, material points will have the same temperature. In one cycle of deformation, there are two processes: the crystallization and the melting both of which are non-isothermal. For both the cases, it is needed to be prescribed a heat transfer rate separately.

1. Heat Transfer Rate for the Cooling Process

Considering the geometry and the boundary conditions for the cooling process, use of the standard diffusion equation in cylindrical co-ordinates should be enough for prescribing the cooling rate

$$\frac{\partial \theta}{\partial t} = \gamma \left(\frac{\partial^2 \theta}{\partial r^2} + \frac{1}{r} \frac{\partial \theta}{\partial r} \right) + \frac{\Delta H}{C} \dot{\alpha} + \frac{\mu_a (1-\alpha) \mathbf{B}_{\kappa_a} \cdot \mathbf{L}}{C}, \tag{6.2.14}$$

with the following initial and boundary conditions

$$\theta(r,0) = \theta_{initial},$$
$$\frac{\partial \theta(r = r_1, t)}{\partial r} = 0, \tag{6.2.15}$$
$$\frac{\partial \theta(r = r_2, t)}{\partial t} = f(t) = -kt,$$

where, $\gamma, \Delta H$ and C are the diffusivity, the latent heat and the specific heat of the material respectively and k is some constant. The required crystallization rate, $\dot{\alpha}$ necessary to find the heat transfer rate is given by Equation (4.3.9).

2. Heat Transfer for the Melting Process

The heating rate can also be given using the same equation but there will be change in boundary conditions.

$$\frac{\partial \theta}{\partial t} = \gamma \left(\frac{\partial^2 \theta}{\partial r^2} + \frac{1}{r} \frac{\partial \theta}{\partial r} \right) + \frac{\Delta H}{C} \dot{\alpha}, \tag{6.2.16}$$

with the following initial and boundary conditions

$$\theta(r,0) = \theta_{t-\Delta t},$$
$$\frac{\partial \theta(r = r_1, t)}{\partial r} = 0, \tag{6.2.17}$$
$$\frac{\partial \theta(r = r_2, t)}{\partial t} = f(t) = kt.$$

The required crystallization rate, $\dot{\alpha}$ necessary to find the heat transfer rate is given by Equation (4.4.7).

6.3 Solution Method

In this section, the key equations for all four processes are prescribed in non-dimensional form and then discussion about the solution procedure for each equation is also discussed. As, it is assumed here; that the stretch ratio remains constant during the entire cycle, the actual computational domain is in the $r - \theta$ plane only.

6.3.1 The Loading Process

The key parameters in non-dimensional form are prescribed below,

$$\Delta P^* = \frac{\Delta P}{\mu_a}, r_i^* = \frac{r}{R_1} \text{ and } R_1^* = \frac{R}{R_1} \qquad i = 1, 2..., n. \qquad (6.3.1)$$

Here, n is total number of nodes. For the sake of clarity we will drop * sign for non-dimensional form.

Key equation for the loading process is one that correlates pressure difference and the radius at any given time. The equation in non-dimensional form can be written as

$$\Delta P = \int_{r_1}^{r_2} \frac{\left(\left(\frac{r}{R} \right)^2 - \left(\frac{R}{\Delta r} \right)^2 \right)}{r} dr. \qquad (6.3.2)$$

The loading can be prescribed either by an internal pressure which is a function of time or by incrementing the values of inner radius at every time step. If the loading process is prescribed by the internal pressure, then in the above equation, the value of the term on right hand side of the equation is known. Now guessing values for r_1, using Equation (6.2.10) numerical values of the radius at any point and at any given moment of time can

be found. For each assumed value for the inner radius, using trapezoidal rule for calculating integration on the left hand side of the equation, verification of the assumption is possible. If the loading is defined by defining inner radius as a function of time then using Equation (6.2.10), numerical values of radii for each node can be found. Once, known all the values; using trapezoidal rule for integration, pressure difference can be found easily.

6.3.2 The Cooling Process

For the cooling process important equations are the energy equation, the crystallization rate equation and the balance of momentum. The non-dimensional form is given by:

$$\theta^* = \frac{\theta - \theta_{min}}{\Delta\theta_{max}} \& \Delta\theta_{max} = \theta_{max} - \theta_{min},$$

$$t^* = \frac{t}{\left(R_1^2 \middle/ \gamma\right)}, \tag{6.3.3}$$

$$\mu_c^* = \frac{\mu_c}{\mu_a}, \qquad \mu_{c1}^* = \frac{\mu_{c1}}{\mu_a} \quad \text{and} \quad \mu_{c2}^* = \frac{\mu_{c2}}{\mu_a}.$$

Using Equation (6.3.3), following equations for the cooling rate with the initial condition and boundary conditions can be written as stated below.

$$\frac{\partial\theta}{\partial t} = \left(\frac{\partial^2\theta}{\partial r^2} + \frac{1}{r}\frac{\partial\theta}{\partial r}\right) + \frac{\Delta H}{C}\dot{\alpha}, \tag{6.3.4}$$

$$\theta(r,0) = \theta_{initial},$$

$$\frac{\partial\theta(r_1,t)}{\partial r} = 0, \tag{6.3.5}$$

$$\frac{\partial\theta(r_n,t)}{\partial t} = -kt.$$

The crystallization equation in the non-dimensional form can be written as,

$$\dot{\alpha} = \hat{G}(\alpha_0 - \alpha)^{k/m-1}\left(\frac{\theta_r - \theta}{\theta_r + \theta_{min}/\Delta\theta_{max}}\right)^{1/m-1} \qquad \text{where } \hat{G} = G\frac{R_1^2}{\gamma}. \qquad (6.3.6)$$

And the equation for the pressure difference can be prescribed as

$$\Delta P = \int_{r_1}^{r_2}\frac{\left[\begin{array}{l}(1-\alpha(t))\mu_a\left(\left(\frac{r}{R}\right)^2 - \left(\frac{1}{\Lambda}\frac{R}{r}\right)^2\right) + \mu_c\int_s^r\left(\left(\frac{r(t)}{r(\tau)}\right)^2 - \left(\frac{r(\tau)}{r(t)}\right)^2\right)\frac{d\alpha}{d\tau}d\tau + \\ \int_s^r\left[\mu_{c2}\left(\left(\frac{r(t)}{r(\tau)}\right)^4 - \left(\frac{r(t)}{r(\tau)}\right)^2\right) - \mu_{c1}\left(\left(\frac{r(\tau)}{r(t)}\right)^4 - \left(\frac{r(\tau)}{r(t)}\right)^2\right)\right]\frac{d\alpha}{d\tau}d\tau\end{array}\right]}{r}dr. \qquad (6.3.7)$$

The computational domain is divided and it ranges from inner radius R_1 to outer radius R2 of the cylinder, in several parts. Using this grid and the explicit scheme for the diffusion equation one can find the temperature at every node. Once the temperature is known, crystallinity can be found solving ordinary differential equation (Equation (6.3.6)) using the Euler's method. While cooling the material shape is kept fixed and hence, there will be no change in the values of radii at different nodes. In such scenario, Equation (6.3.7) will be reduced to

$$\Delta P = \int_{r_1}^{r_2}\frac{\left[(1-\alpha(t))\left(\left(\frac{r}{R}\right)^2 - \left(\frac{1}{\Lambda}\frac{R}{r}\right)^2\right)\right]}{r}dr. \qquad (6.3.8)$$

Knowing the values of all radii from the last time step, using trapezoidal rule it is easy to find the pressure difference.

6.3.3 The Unloading Process

The unloading process is assumed to be isothermal and so there will be no change in the crystallinity i.e. no phase transition will occur. The pressure difference gradually decreases as the internal pressure lowers to match the external pressure. With this concept

of unloading of the material, it is very difficult to find the values of radius at each node point at any time during the unloading process. The equation that connects the pressure difference to the radius can be presented in dimensionless form

$$\Delta P = \int_{r_1}^{r_2} \frac{\begin{bmatrix} \left[(1-\alpha(t))\mu_a \left(\left(\frac{r}{R}\right)^2 - \left(\frac{1}{\Lambda}\frac{R}{r}\right)^2 \right) + \mu_c \int_s^{t_f} \left(\left(\frac{r(t)}{r(\tau)}\right)^2 - \left(\frac{r(\tau)}{r(t)}\right)^2 \right) \frac{d\alpha}{d\tau} d\tau + \right] \\ \left[\int_s^{t_f} \left[\mu_{c2} \left(\left(\frac{r(t)}{r(\tau)}\right)^4 - \left(\frac{r(t)}{r(\tau)}\right)^2 \right) - \mu_{c1} \left(\left(\frac{r(\tau)}{r(t)}\right)^4 - \left(\frac{r(\tau)}{r(t)}\right)^2 \right) \right] \frac{d\alpha}{d\tau} d\tau \right] \end{bmatrix}}{r} dr. \quad (6.3.9)$$

Guessing the values of inner radius one can find the values of radii at each nodal point using Equation(6.2.10). Only for the right guess for the value of inner radius, Equation(6.3.9) will be satisfied.

6.3.4 The Heating Process

For the heating process, the heating rate equation along with the initial condition and boundary conditions in non-dimensional form can be written as

$$\frac{\partial \theta}{\partial t} = \left(\frac{\partial^2 \theta}{\partial r^2} + \frac{1}{r} \frac{\partial \theta}{\partial r} \right) - \frac{\Delta H}{C} \dot\alpha. \tag{6.3.10}$$

$$\theta(r,0) = \theta_{t-\Delta t,}$$

$$\frac{\partial \theta(r_1,t)}{\partial r} = 0, \tag{6.3.11}$$

$$\frac{\partial \theta(r_n,t)}{\partial t} = kt.$$

Solving the diffusion equation using explicit scheme gives the temperature at every nodal point. Once the temperature is known, using the Euler's method, below mentioned non-dimensional crystallization equation can be solved for the crystallinity at each point.

$$\dot\alpha = \hat{G}(\alpha)^{k/m-1} \left(\frac{\theta_r - \theta}{\theta_r + \theta_{min}/\Delta\theta_{max}} \right)^{1/m-1} \quad \text{where } \hat{G} = G\frac{R_1^2}{\gamma}. \tag{6.3.12}$$

The balance of momentum equation in non-dimensional form can be prescribed as

$$\Delta P = 0 = \int_{r_1}^{r_2} \frac{\left[\begin{array}{c} (1-\alpha(t))\mu_a\left(\left(\frac{r}{R}\right)^2 - \left(\frac{1}{\Lambda}\frac{R}{r}\right)^2\right) + \mu_c \int_{t_s}^{t} \left(\left(\frac{r(t)}{r(\tau)}\right)^2 - \left(\frac{r(\tau)}{r(t)}\right)^2\right)\frac{d\alpha}{d\tau}d\tau + \\ \int_{t_s}^{t}\left[\mu_{c2}\left(\left(\frac{r(t)}{r(\tau)}\right)^4 - \left(\frac{r(t)}{r(\tau)}\right)^2\right) - \mu_{c1}\left(\left(\frac{r(\tau)}{r(t)}\right)^4 - \left(\frac{r(\tau)}{r(t)}\right)^2\right)\right]\frac{d\alpha}{d\tau}d\tau \end{array} \right]}{r} dr. (6.3.13)$$

Using the same technique that used for finding the radii in the unloading process, Equation (6.3.13) can be solved.

6.4 Results

Using the set of equations developed for inflation and extension of the tube, the process has been simulated. Here, some of the interesting results that were found during these simulations are discussed. Two different set of results are developed for two different cases of processes simulations. In first case, it was assumed that the deformed shape is not deforming further during the cooling process. Figure 6.2 shows the temperature variation through out the cycle. From Figure 6.3, it can be said that at every point when the temperature drops below the transition temperature, the crystallinity increases and once it attains the highest value it remains there until the temperature takes higher values than the transition temperature. With the increase in temperature the crystals start melting and the semi-crystalline phase transforms in to the amorphous decreasing the crystallinity in the material. Figure 6.4, shows the plot between the pressure and the radii of nodes. With the increase in pressure radius is also increasing. During crystallization as per our assumptions, there will be no change in the values of radii of different node points, yet the pressure drop can be observed. The pressure should drops because the new crystals are stronger than the amorphous chains and so there will be less pressure required to

retain the shape of the material. As the material is unloaded due to the presence of the rigid crystals material will retain its shape. However, it can also be seen that due to presence of the amorphous phase there is a small strain recovery. During the melting process, strained crystal melts and transfers in to the amorphous phase and as there is no pressure difference exists, it will go back to its original shape as shown in Figure 6.4.
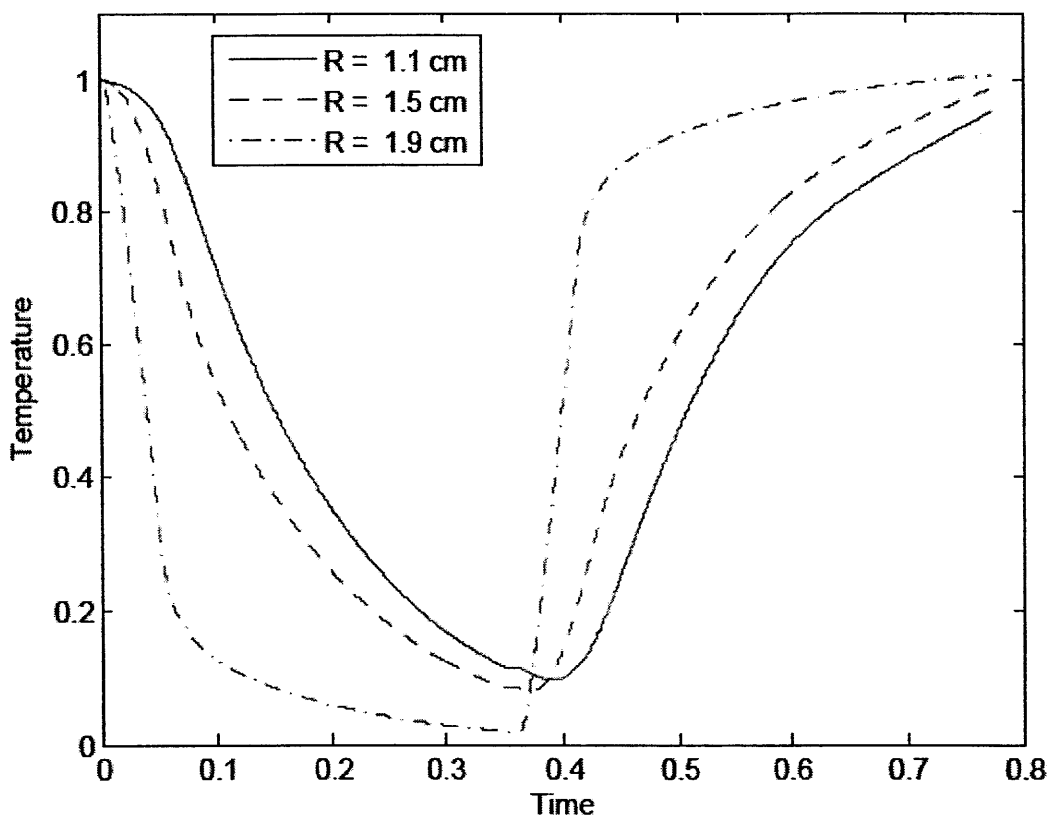
Figure 6.2 The temperature variation plot for inflation and extension of the tube where there is no change in the shape during the cooling process. (see Table 6.1 for the constant used)

Table 6.1 Data used for Simulating Process of Inflation and Expansion of the Hollow Tube

Initial temperature in K	438
Minimum temperature in K	388
Transition temperature in K	413
Latent heat(J/Kg)	27000
Specific heat (J/Kg-K)	3100
Initial crystallinity	0
Maximum crystallinity	0.4
G	0.05
Initial pressure difference	0
μ_c	100
μ_{c1}	2
μ_{c2}	2
Shear modulus of amorphous region in Pa	4×10^{-6}

Figure 6.3 The crystallinity variation with time in the inflation and extension of the tube where there is no change in the shape during the cooling process.
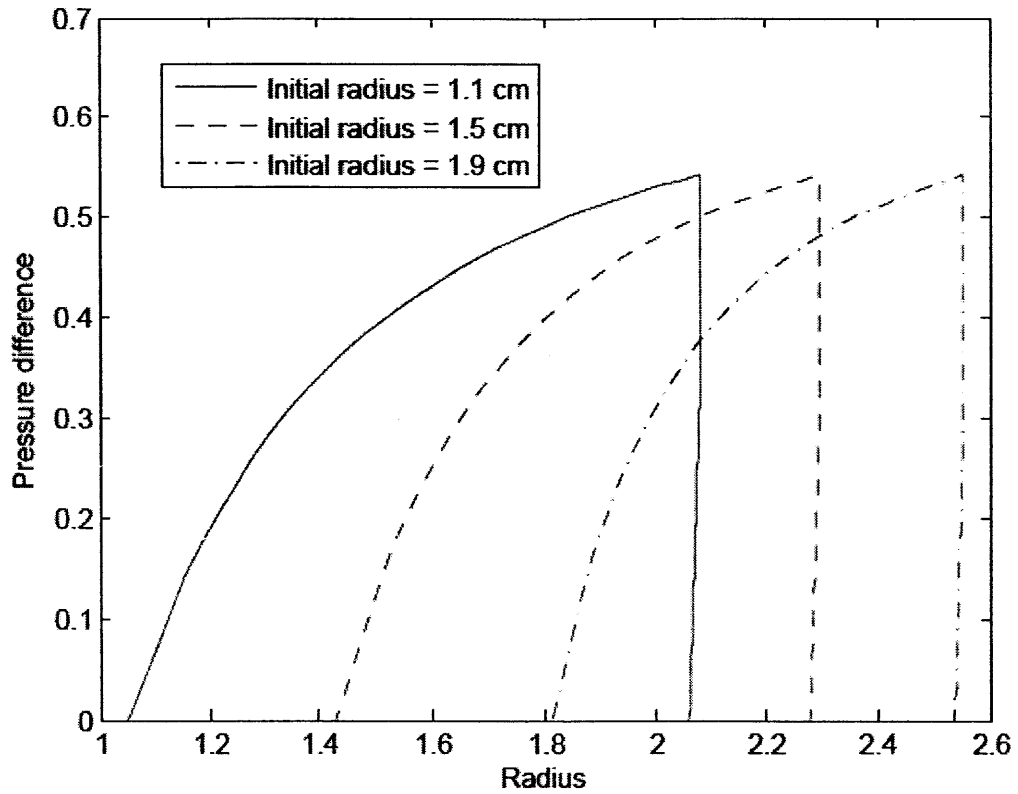
Figure 6.4 The pressure difference versus radius plot for the inflation and extension of the tube where there is no change in the shape during the cooling process.

For the other case also, the similar graphs were plotted between the respective quantities. However, the difference in this case is that during the cooling pressure it is assumed that the pressure remains the constant. Figure 6.5 and Figure 6.6 shows the temperature and crystallinity plots for the cycle and it show similar pattern as of the other case. Figure 6.7 shows the plot between the pressure and the radius of a node. In this case, as the pressure remains constant, with the formation of new crystals in their natural configuration it will start deforming. This deformation will cause the increase in radius as new crystals form. At the end of the unloading process, pressure difference is zero and so, due to the presence of the soft amorphous phase there can be small strain recovery can be seen in the Figure 6.7 And because of above mentioned reasons here also one can see 100% shape recovery at the end of the heating process.
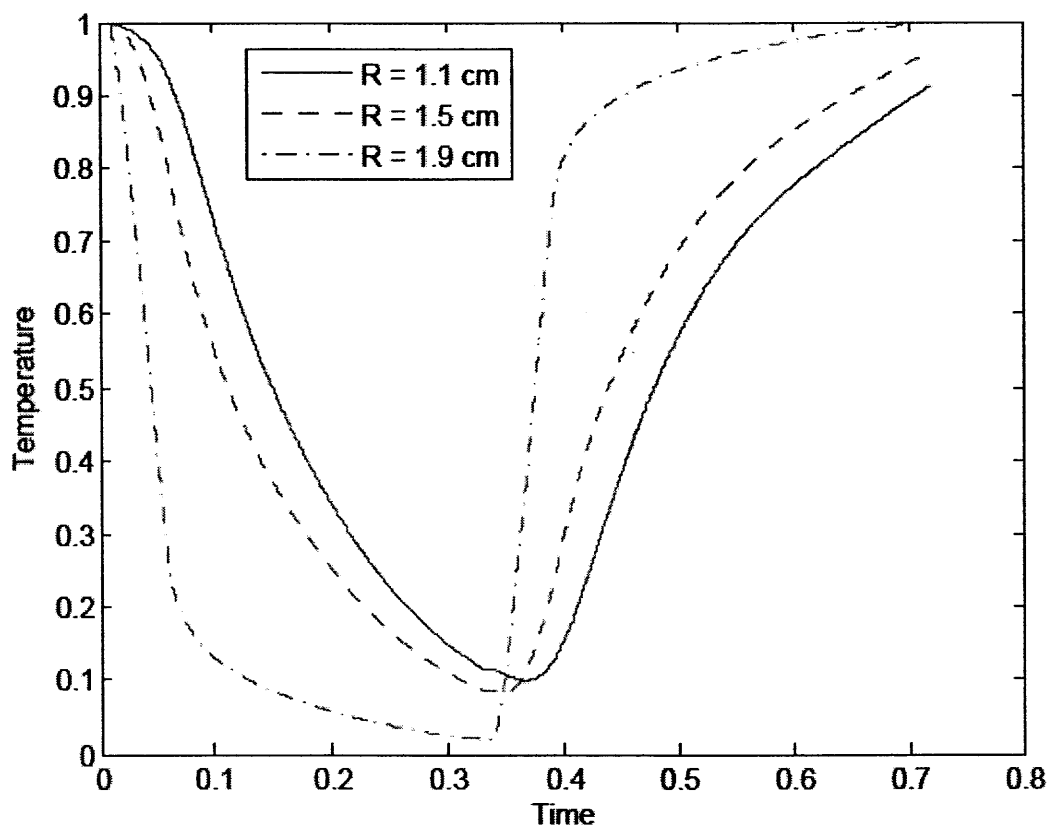
Figure 6.5 The temperature variation plot for the inflation and extension of the tube where there is no change in the pressure difference during the cooling process.
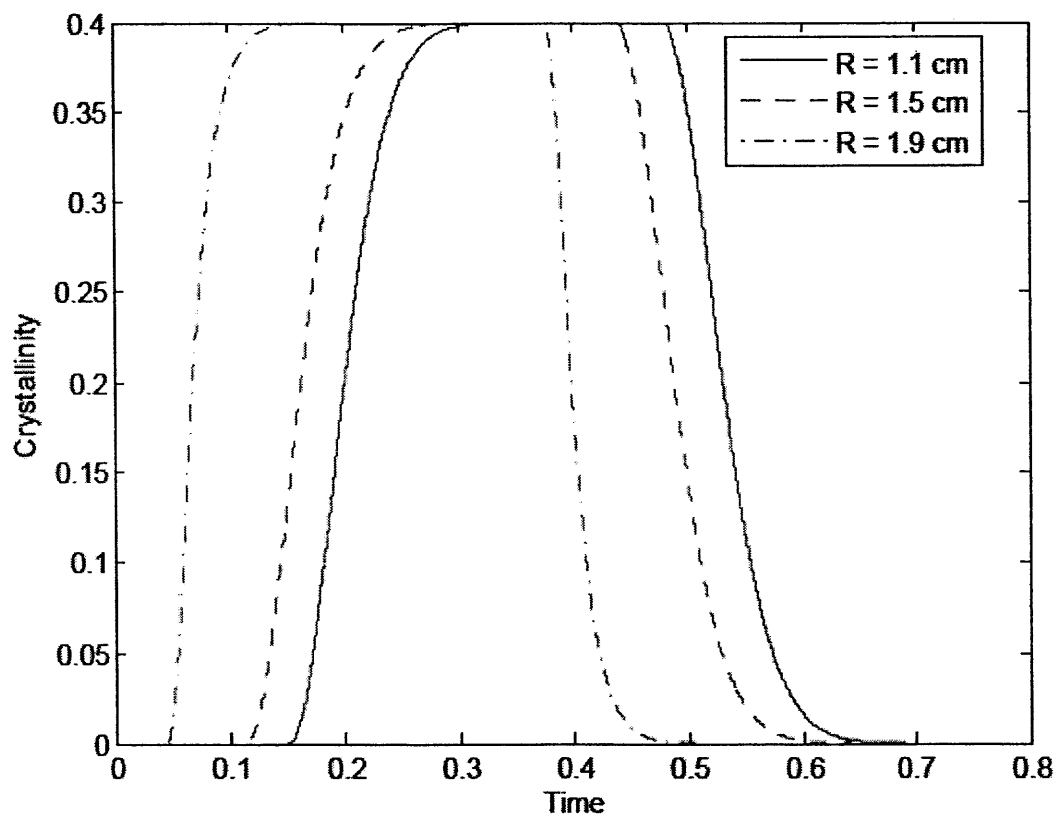
Figure 6.6 The crystallinity variation with time in the inflation and extension of the tube where there is no change in the pressure difference during the cooling process.
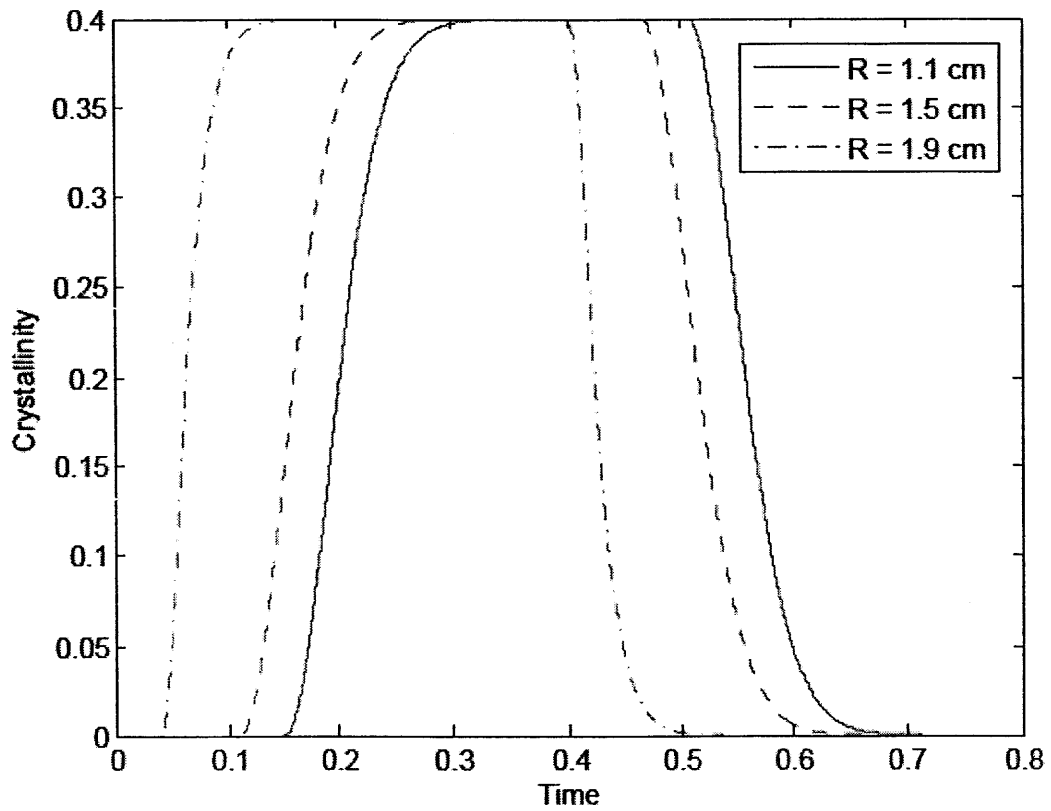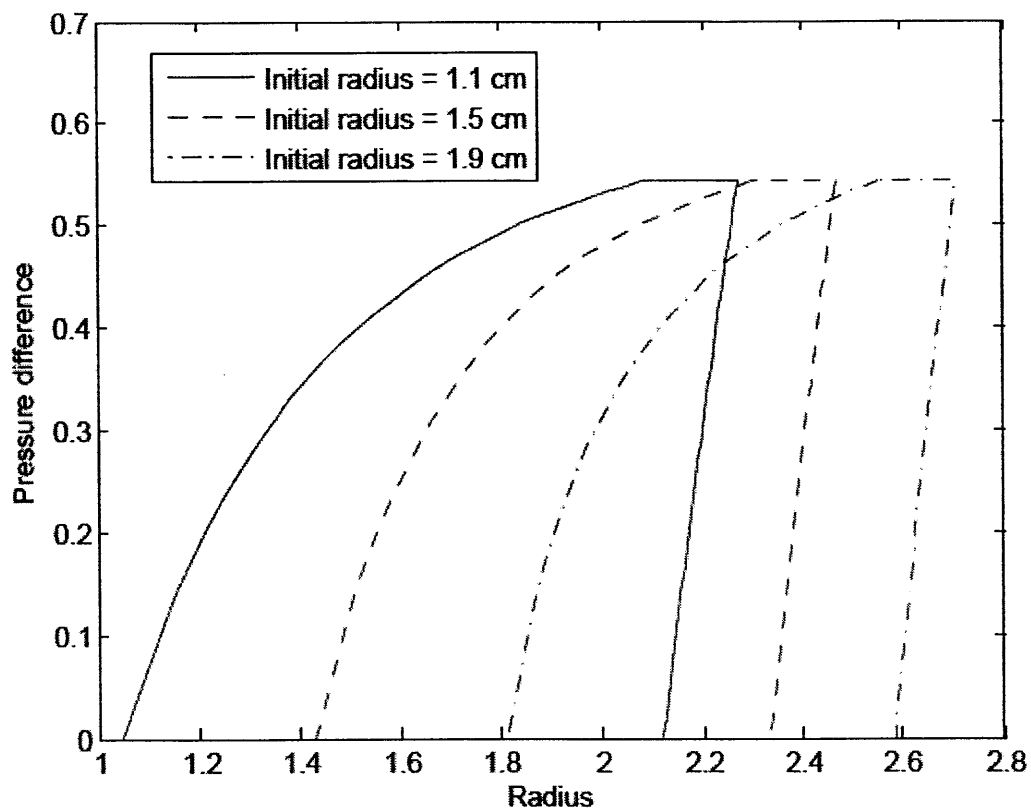
Figure 6.7 The pressure difference versus radius plot for the inflation and extension of the tube where there is no change in the pressure difference during the cooling process.

CHAPTER 7

FINITE ELEMENT MODULE FOR CRYSTALLIZABLE SHAPE MEMORY POLYMERS

7.1   Introduction

Finite element analysis is a numerical method for analyzing complex structural and thermal problems. For plastics, it is important that finite element software have good nonlinear capabilities. Often, nonlinear analysis is an add-on, not provided in the base package. Currently, there is no mathematical model available for CSMPs hence; there is no add-on available to add in of the commercial software package available. With help of the mathematical model described in the Chapter 4, it is now possible to create finite element module. Using this finite element module, finite element analysis of any processes that involves use of CSMPs can be carried out. In this chapter, the basic theory used and step by step procedure required to develop finite element module is described. Out of available commercial finite element softwares, very few allows user to include user define finite element module for newer material. ABAQUS/CAE as a finite element software package is used for simulations. Creating user subroutine (UMAT) in FORTRAN for CSMPs, finite element analysis can be carried out in ABAQUS/CAE. Required tests to validate developed user subroutine (UMAT) based on the current model is also performed.

7.2   Weak Formulation, Linearization and Stiffness Matrix

The finite element method requires the formulation of the balance laws in the form of variational principles. From the developed model in Chapter 4, it can be said that any

finite element analysis for CSMPs would be a non-linear problem and so, linearization of a weak form is essential.

7.2.1 Weak Formulation and Linearization

Balance of linear momentum is most important equation needed to be converted in to weak form to perform finite element analysis of structural problems. Following is the derivation of weak form of balance of linear momentum that can be used in finite element analysis.

Assuming displacement, $\mathbf{u}$ is given by

$$\mathbf{u} = \mathbf{x} - \mathbf{X}, \tag{7.2.1}$$

The balance of linear momentum (Equation (3.1.22)) can be rewritten in following format for body Ω

$$f(\mathbf{u}) = \int_\Omega (\rho\ddot{\mathbf{u}} - div\sigma - \mathbf{b})dv = 0. \tag{7.2.2}$$

The weak form for the balance of linear momentum can be achieved by multiplying test function, $\eta = \eta(\mathbf{x}) = \eta(\mathbf{x}, t)$ to Equation (7.2.2).

$$f(\mathbf{u}, \eta) = \int_\Omega (\rho\ddot{\mathbf{u}} - div\sigma - \mathbf{b})\cdot\eta\, dv = 0. \tag{7.2.3}$$

Using the Equation (3.1.14), assuming that body Ω is in equilibrium and using standard identities of tensor algebra, following standard format of the weak can be derived

$$f(\mathbf{u}, \eta) = \int_\Omega \sigma\cdot grad\eta\, dv - \int_\Omega \mathbf{b}\cdot\eta\, dv - \int_{\partial\Omega} \mathbf{t}\cdot\eta\, da = 0. \tag{7.2.4}$$

If we look upon η as the virtual displacement field $\delta\mathbf{u}$, defined on the current configuration then Equation (7.2.4) becomes

$$f(\mathbf{u}, \delta\mathbf{u}) = \int_\Omega \sigma\cdot grad\delta\mathbf{u}\, dv - \int_\Omega \mathbf{b}\cdot\delta\mathbf{u}\, dv - \int_{\partial\Omega} \mathbf{t}\cdot\delta\mathbf{u}\, da = 0. \tag{7.2.5}$$

The internal (mechanical) virtual work, δW_{int} and external (mechanical) virtual work, δW_{ext} can be defined as

$$\delta W_{int} = \int_{\Omega} \sigma \cdot grad\delta u \, dv,$$
$$\delta W_{ext} = \int_{\Omega} \mathbf{b} \cdot \delta \mathbf{u} \, dv - \int_{\partial\Omega} \mathbf{t} \cdot \delta \mathbf{u} \, da. \tag{7.2.6}$$

Using Equation (7.2.5) and Equation (7.2.6) principal of virtual work can be written as follows:

$$\delta W_{int} = \delta W_{ext}. \tag{7.2.7}$$

One can also derive the weak form of the balance of linear momentum in reference configuration as described below

$$f(\mathbf{u}, \eta_0) = \int_{\Omega_0} \mathbf{P} \cdot Grad\eta_0 \, dV - \int_{\Omega_0} \mathbf{B} \cdot \eta_0 \, dV - \int_{\partial\Omega_0} \mathbf{t}_0 \cdot \eta_0 \, dA = 0. \tag{7.2.8}$$

If the constitutive equation for the stress is linear in kinematic variables the finite element approximation will result in linear system of equations. However, if the constitution equation is non-linear then weak form will also be non-linear and Newton-Raphson method, an iterative method is used to solve the problem. For each iterations, it is necessary to solve linearized form of the weak form. Given a non-linear function $f(\overline{\mathbf{x}}, \Delta\mathbf{u})$ one can linearize the function with respect to some direction $\hat{\mathbf{u}}$ about some known configuration $\mathbf{x}$ as

$$f(\overline{\mathbf{x}}, \Delta\mathbf{u}) = f(\mathbf{x}, \Delta\mathbf{u}) + Df(\mathbf{x}, \Delta\mathbf{u})[\hat{\mathbf{u}}] + o(\hat{\mathbf{u}}), \tag{7.2.9}$$

where

$$Df(\mathbf{x}, \Delta\mathbf{u})[\hat{\mathbf{u}}] = \lim_{\varepsilon \to 0} \frac{f(\mathbf{x} + \varepsilon\hat{\mathbf{u}}) - f(\mathbf{x})}{\varepsilon}. \tag{7.2.10}$$

For Newton's method setting $f(\overline{\mathbf{x}}, \Delta\mathbf{u}) = 0$ and neglecting higher order terms, we get

$$Df(\mathbf{x}, \Delta\mathbf{u})[\hat{\mathbf{u}}] = -f(\mathbf{x}, \Delta\mathbf{u}). \tag{7.2.11}$$

Now, it is important to find useful form of the linearized weak form of the momentum equation. In this work, it is assumed that body force **b** and surface traction **t** are independent of the deformation of the body in consideration. So, the corresponding linearization of the external virtual work vanishes and the linearization will only affects the internal virtual work. For this work, the linearization of the weak form prescribed in reference configuration. The internal virtual work in material description can be given by:

$$\delta W_{int} = \int_{\Omega_0} \mathbf{P} \cdot Grad \delta \mathbf{u} \, dV = \int_{\Omega_0} \mathbf{S} \cdot \mathbf{F}^T Grad \delta \mathbf{u} \, dV, \tag{7.2.12}$$

where **S** is the second Piola- Kirchoff stress. Applying linearization we get

$$D_{\Delta u} \delta W_{int} = \int_{\Omega_0} \left(D_{\Delta u} \mathbf{S} \cdot \mathbf{F}^T Grad \delta \mathbf{u} + \mathbf{S} \cdot D_{\Delta u} \mathbf{F}^T Grad \delta \mathbf{u} \right) dV. \tag{7.2.13}$$

This is required equation needed to be solved.

7.2.2 Stiffness Matrix

Applying linearization defined in Equation (7.2.10) solution of Equation (7.2.13) can be achieved. Simplification leads to following useful result for the hyperelastic materials

$$D_{\Delta u} \delta W_{int} = 2 \int_{\Omega_0} \left(\mathbb{C} \mathbf{F}^T Grad \Delta \mathbf{u} \cdot \mathbf{F}^T Grad \delta \mathbf{u} \right) dV + \int_{\Omega_0} \left(Grad \Delta \mathbf{u} \mathbf{S} \cdot Grad \delta \mathbf{u} \right) dV, \tag{7.2.14}$$

where $\mathbb{C}$ is 4th order tangent stiffness matrix and can be defined as

$$\mathbb{C} = \frac{\partial \mathbf{S}}{\partial \mathbf{C}} = 2\rho_0 \frac{\partial^2 \psi}{\partial \mathbf{C}^2}. \tag{7.2.15}$$

First term in above Equation (7.2.14) is the material contribution to the tangent stiffness matrix and the second term represents geometrical contribution to the tangent stiffness matrix. In this work, ABAQUS/standard solver is used for the calculations. It requires 4th order tangent stiffness matrix defined through the Kirchoff stress tensor instead of second

Piola stress tensor. In such case, linearized form of the principal of virtual work will take following form

$$D_{\Delta u}\delta W_{int} = \int_{\Omega}\left(\tau^{J} + \mathbf{W}\tau - \tau\mathbf{D}\right)\cdot grad\delta u dV, \qquad (7.2.16)$$

while, tangent stiffness matrix $\mathbb{C}$ is defined as

$$\mathbb{C} = \frac{1}{J}\frac{\partial\tau^{J}}{\partial\mathbf{D}}. \qquad (7.2.17)$$

Here, τ^{J} is the Jawman rate of the Kirchoff stress. Keeping this fact in mind following procedure has been adopted to derive the components of the tangent stiffness matrix (See appendix A for complete derivation of tangent stiffness matrix for CSMP).

Find the equation of the Cauchy stress tensor (σ), using the stored energy function (ψ), using following equation

$$\sigma = \frac{2}{J}\mathbf{F}\frac{\partial\psi}{\partial\mathbf{C}}\mathbf{F}^{T} \qquad (7.2.18)$$

- Find the Kirchoff stress (τ), by multiplying volume ratio to Equation (7.2.18)
- Take the material time derivative of the Kirchoff stress $(\dot{\tau})$.
- Bring it to Jawman rate (τ^{J}), using following equation

$$\tau^{J} = \dot{\tau} - \mathbf{W}\tau - \tau\mathbf{W}^{T}. \qquad (7.2.19)$$

- Use Equation (7.2.17) to calculate tangent stiffness matrix.

Once stiffness matrix is derived, it is possible to create a finite element module. This particular module then will be used to carry out different finite element analysis of different realistic processes that is made from CSMP's.

7.3   Development of Finite Element Module

A finite element module that contains information regarding properties of a material is called material module. Using material module, it is possible apply material properties to a solid model. The combination of a solid model and a material module makes a material model of a part under consideration. The solid model follows instructions prescribed in a material module. A material module facilitates user to input different physical properties and related constants associated with material used to form the real object. Some finite element software provide various material modules for various commonly used materials such as metals, glass, polymers etc.. Where as some finite element software not only provide material modules for more commonly used material but also allows user to create their own material module for the specific material for which use of standard material is not appropriate.

In this chapter, the process simulation in which CSMP is used is shown. CSMPs are recently developed polymer while comparing it to other commonly used polymer such as polyethylene, polypropylene, PET, Nylon etc. Use of a material module that is made for commonly used polymer is not appropriate for our purpose. Hence, a new material module based on the constitutive equation derived in Chapter 4 is developed. The material module will be used along with different solid models made for different solids used in different processes.

In this work, ABAQUS/CAE as finite element software is used. ABAQUS/CAE allows users to create their material module for the specific material. Creating material module requires a formulation of FORTRAN code known as UMAT (User MATerial). UMAT essentially contains all required information to carry out structural analysis that may require definition of stress, strain, tangent stiffness matrix etc. A typical CSMP cycle involves temperature variation along with the phase change. Temperature change causes

phase change and latent heat is involved with phase transition phenomenon. Crystallinity also causes change in the mechanical properties such as strength. Hence, along with UMAT another FORTRAN program is needed to be written called UMATHT which includes the effect of latent heat associate with phase change and it also provides necessary information to solve heat conduction. Moreover, crystallinity is required to be defined as solution dependent state variable because it depends on the temperature and kinematic variables which change their value with time. Hence, it is important to include user subroutine called SDVINI through which crystallinity values updating is possible.

In following subsections, the templates of these subroutines along with their importance and utilities are presented. All the information prescribed here can be found in ABAQUS user material (Kindly, refer ABAQUS/CAE standard online user manual for in depth details).

7.3.1 UMAT

User-defined mechanical behavior in ABAQUS can be included by adding a user subroutine UMAT in to a library of the models. A constitutive model is programmed in a user subroutine. For finite-strain applications the interface for subroutine UMAT is implemented using Cauchy stress components ("true" stress) and integrated rate-of-deformation as the strain increment. While solving problem the user subroutine UMAT is called for each nodal points of mesh at every increment. User subroutine UMAT includes the instructions for updating stresses and solution-dependent state variables to their values at the end of the increment. It is also necessary to include the material Jacobian matrix for the mechanical constitutive model. Jacobian matrix usually defined through the variation in Kirchoff stress. Jacobian matrix prescribed in rate form is integrated numerically in the subroutine.

There is a particular way user can define the stress and strain components in ABAQUS as shown in Table 7.1.

Table 7.1 Convention Followed in ABAQUS for Stress and Strain

σ_{11} : Direct stress in the 1-direction	ε_{11} : Direct strain in the 1-direction
σ_{22} : Direct stress in the 2-direction	ε_{22} : Direct strain in the 2-direction
σ_{33} : Direct stress in the 3-direction	ε_{33} : Direct strain in the 3-direction
σ_{12} : Shear stress in the 1-2 plane	ε_{12} : Shear strain in the 1-2 plane
σ_{13} : Shear stress in the 1-3 plane	ε_{13} : Shear strain in the 1-3 plane
σ_{23} : Shear stress in the 2-3 plane	ε_{23} : Shear strain in the 2-3 plane

Moreover, for linearized elasticity matrix following relationship holds

$$\sigma = \mathbb{C}\varepsilon \quad \Rightarrow \quad \sigma_{ij} = \mathbb{C}_{ijkl}\varepsilon_{kl}. \tag{7.3.1}$$

As one can see $\mathbb{C}$ is a 4th order tensor and it contains 81 components. Due to energy consideration and geometric symmetry these 81 components reduce to 36 components. Using the Voight notations, above Equation (7.3.1) can be re written as:

$$
\begin{array}{c}
I/J \quad\quad\quad 1 \quad 2 \quad 3 \quad 4 \quad 5 \quad 6 \quad J \\
\quad\quad\quad\quad 11 \quad 22 \quad 33 \quad 12 \quad 13 \quad 23 \quad kl \quad J \\
\begin{bmatrix} \sigma_{11}=\sigma_1 \\ \sigma_{22}=\sigma_2 \\ \sigma_{33}=\sigma_3 \\ \sigma_{12}=\sigma_4 \\ \sigma_{13}=\sigma_5 \\ \sigma_{23}=\sigma_6 \end{bmatrix} =
\begin{bmatrix}
C_{11} & C_{12} & C_{13} & C_{14} & C_{15} & C_{16} \\
C_{21} & C_{22} & C_{23} & C_{24} & C_{25} & C_{26} \\
C_{31} & C_{32} & C_{33} & C_{34} & C_{35} & C_{36} \\
C_{41} & C_{42} & C_{43} & C_{44} & C_{45} & C_{46} \\
C_{51} & C_{52} & C_{53} & C_{54} & C_{55} & C_{56} \\
C_{61} & C_{62} & C_{63} & C_{64} & C_{65} & C_{66}
\end{bmatrix}
\begin{bmatrix} \varepsilon_{11}=\varepsilon_1 \\ \varepsilon_{22}=\varepsilon_2 \\ \varepsilon_{33}=\varepsilon_3 \\ \varepsilon_{12}=\varepsilon_4 \\ \varepsilon_{13}=\varepsilon_5 \\ \varepsilon_{23}=\varepsilon_6 \end{bmatrix} \\
ij \quad I
\end{array}
\tag{7.3.2}
$$

where,

$$C_{IJ} = \mathbb{C}_{ijkl} = \frac{1}{2}\left[\mathbb{C}_{ijkl} + \mathbb{C}_{ijlk}\right]. \tag{7.3.3}$$

Table 7.2 The Standard Template for UMAT

(Source: ABAQUS/CAE manual)

```
SUBROUTINE UMAT(STRESS,STATEV,DDSDDE,SSE,SPD,SCD,
1 RPL,DDSDDT,DRPLDE,DRPLDT,
2 STRAN,DSTRAN,TIME,DTIME,TEMP,DTEMP,PREDEF,DPRED,CMNAME,
3 NDI,NSHR,NTENS,NSTATV,PROPS,NPROPS,COORDS,DROT,PNEWDT,
4 CELENT,DFGRD0,DFGRD1,NOEL,NPT,LAYER,KSPT,KSTEP,KINC)
C
   INCLUDE 'ABA_PARAM.INC'
C
   CHARACTER*80 CMNAME
   DIMENSION STRESS(NTENS),STATEV(NSTATV),
1 DDSDDE(NTENS,NTENS),DDSDDT(NTENS),DRPLDE(NTENS),
2 STRAN(NTENS),DSTRAN(NTENS),TIME(2),PREDEF(1),DPRED(1),
3 PROPS(NPROPS),COORDS(3),DROT(3,3),DFGRD0(3,3),DFGRD1(3,3)

   user coding to define DDSDDE, STRESS, STATEV, SSE, SPD, SCD
   and, if necessary, RPL, DDSDDT, DRPLDE, DRPLDT, PNEWDT

   RETURN
        END
```

DDSDDE(NTENS,NTENS)

Jacobian matrix of the constitutive model. DDSDDE(I,J) defines the change in the Ith stress component at the end of the time increment caused by an infinitesimal perturbation of the Jth component of the strain increment array.

STRESS(NTENS)

This array is passed in as the stress tensor at the beginning of the increment and must be updated in this routine to be the stress tensor at the end of the increment.

STATEV(NSTATV)

An array containing the solution-dependent state variables.

SSE, SPD, SCD

Specific elastic strain energy, plastic dissipation, and "creep" dissipation, respectively. Only in a fully coupled temperature-displacement analysis.

RPL

Volumetric heat generation per unit time at the end of the increment caused by mechanical working of the material.

DDSDDT(NTENS)

Variation of the stress increments with respect to the temperature.

DRPLDE(NTENS)

Variation of RPL with respect to the strain increments.

DRPLDT

Variation of RPL with respect to the temperature.

Stiffness matrix C is denoted as DDSDDE in a UMAT. It is very essential for user to prescribe it in above mentioned format while writing UMAT.

Table 7.2 shows the standard template provided in ABAQUS user manual to create user subroutine UMAT.Using the template shown in Table 7.2 and constitutive equation derived in Chapter 4, our own UMATs (See appendix B and appendix C) are created for iso-thermal and non-isothermal processes those were simulated. Detail description of problems solved is given in following sections.

7.3.2 UMATHT

User subroutine UMATHT can be used to define the thermal constitutive behavior of the material, including internal heat generation. For example, if a material modeled can go through a complex phase change, the specific heat can be defined in user subroutine UMATHT in sufficient detail to capture the phase change. It is important that while writing UMATHT one must define the internal energy per unit mass and its variation with respect to temperature and to spatial gradients of temperature. It is also necessary to define the heat flux vector and its variation with respect to temperature and to gradients of temperature. If a material modeled can go through a complex phase change, the specific heat can be defined in user subroutine UMATHT in sufficient detail to capture the phase change. Using the template shown in Table 7.3 and based on the modeling done in Chapter 4, UMATHT that can take care of the latent heat effects (see Appendix D for UMATHT) in non-isothermal problem are developed.

Table 7.3 The Standard Template for UMATHT

(Source: ABAQUS/CAE manual)

```
SUBROUTINE UMATHT(U,DUDT,DUDG,FLUX,DFDT,DFDG,
  1 STATEV,TEMP,DTEMP,DTEMDX,TIME,DTIME,PREDEF,DPRED,
  2 CMNAME,NTGRD,NSTATV,PROPS,NPROPS,COORDS,PNEWDT,
  3 NOEL,NPT,LAYER,KSPT,KSTEP,KINC)
C
  INCLUDE 'ABA_PARAM.INC'
C
  CHARACTER*80 CMNAME
  DIMENSION DUDG(NTGRD),FLUX(NTGRD),DFDT(NTGRD),
  1 DFDG(NTGRD,NTGRD),STATEV(NSTATV),DTEMDX(NTGRD),
  2 TIME(2),PREDEF(1),DPRED(1),PROPS(NPROPS),COORDS(3)

  user coding to define U,DUDT,DUDG,FLUX,DFDT,DFDG,
  and possibly update STATEV, PNEWDT

  RETURN
        END
```

U
Internal thermal energy per unit mass.

DUDT
Variation of internal thermal energy per unit mass with respect to temperature.

DUDG(NTGRD)
Variation of internal thermal energy per unit mass with respect to the spatial gradients of temperature.

FLUX(NTGRD)
Heat flux vector.

DFDT(NTGRD)
Variation of the heat flux vector with respect to temperature.

DFDG(NTGRD,NTGRD)
Variation of the heat flux vector with respect to the spatial gradients of temperature.

STATEV(NSTATV)
An array containing the solution-dependent state variables.

7.3.3 SDVINI

SDVINI is the user subroutine through which user can define solution dependent state

variable such as crystallinity. User subroutine SDVINI can also be called to specify the

initial conditions. The user can then define all solution-dependent state variables at each

point as functions of coordinates, element number, etc. Solution dependent state variable initialized in SDVINI can be updated in UMAT and UMATHT. Using template shown in Table 7.4 user sub routines SDVINI for iso-thermal and non-iso thermal problems were created. (See appendix E and appendix F)

Table 7.4 The Standard Template for SDVINI

(Source: ABAQUS/CAE manual)

```
      SUBROUTINE SDVINI(STATEV,COORDS,NSTATV,NCRDS,NOEL,NPT,
     1 LAYER,KSPT)
C
      INCLUDE 'ABA_PARAM.INC'
C
      DIMENSION STATEV(NSTATV),COORDS(NCRDS)
      user coding to define STATEV(NSTATV)
          RETURN
          END
```

STATEV(NSTATV)
An array containing the solution-dependent state variables.

7.4 Testing of the Material Module

Once, the material module is created it is very important to test it to see if it is working correctly. There are different tests one can perform to test the material module such as single element test, single element test with oriented co-ordinate system and convergence test. In following subsection these tests are described. Above mentioned test is performed on subroutine UMAT.

7.4.1 Single Element Tensile Test

Name of the test suggests how the test is being performed. In this test solid model is constructed and then using the material model created by the user is applied to make the material model. Once the material model is created, boundary conditions are applied to the model. The solid model is then meshed to perform finite element analysis. It is important to note here that during the test meshing is done with only one element only. Once the mesh is created then finite element model is send to finite element solver for further processing. Post processor is then used to see different results obtained from the finite element solver.

The tensile test that performed here was on the cube (see Figure 7.1). There are reasons for choosing cube geometry. The first reason is: using a single 20-node brick element only, one can mesh the solid model of the cube. The other reason is: while stretching in one direction, one can observe the equal reduction in lengths of the other sides of the cube. The equal reduction is only possible with the cube geometry only.

A single element test is used to validate user subroutine UMAT. A UMAT can be tested by performing static general structural analysis. In Chapter 5, 1-D uni-axial stretching process using MATLAB were simulated. Simulating the same cycle using ABAQUS/CAE with the aid of developed UMAT and comparing its results with one obtained in Chapter 5 will be able to test UMAT. Following is the step by step procedure for simulating uni-axial stretching cycle.

Step-1. Create a solid model: A solid model can be created using standard CAD software such as Pro/ENGINEER, Solid Works, ABAQUS, AutoCAD etc. In this case, the solid model using 'part module' of the ABAQUS/CAE was created. Using extrude feature it is very easy to create cube. Figure 7.1 shows the extruded part is stored with name 'cube'.

Step-2. Create a material model: Using the UMAT developed and 'property module' of the ABAQUS/CAE material model of 'cube' can be developed. Creating a section and applying material created to it makes the material model. Applying this material module by assigning section to solid model makes the material model of 'cube' made with CSMP. (See appendix G for material module)

Step-3. Define processes: A process can be defined in 'step module' of the ABAQUS/CAE. It is known that a typical uni-axial cycle is consisting of four processes namely: Loading, Cooling/Crystallization, Unloading and Heating. Hence, four steps are required to solve the problem. However, the process here is simulated using five steps by using two steps for the heating/melting process as it needs use of smaller time steps at the end of heating process.

Step-4. Apply boundary conditions: Boundary conditions can be applied using the 'load module' of the ABAQUS/CAE. Here, object of the study is to see validity of the user subroutine UMAT hence, instead of prescribing pressure condition or force condition at surfaces or edges or at nodes, displacement boundary conditions were applied to the edges. Figure 7.2 shows the applied boundary conditions.

Step-5. Mesh the model: Using the 'mesh module' of ABAQUS/CAE solid model can be meshed to carry out solution. In this test, it is required that 'cube' is meshed with only one element. The element chosen for this test is C3D20RH: A 20-node quadratic brick, hybrid element that allows linear pressure and reduced integration.

Step-6. Solve the finite element model: Using the 'job module' of ABAQUS/CAE user subroutine UMAT can be called for solving the problem. User subroutine UMAT (umatprop1.f) is used for solving the problem.
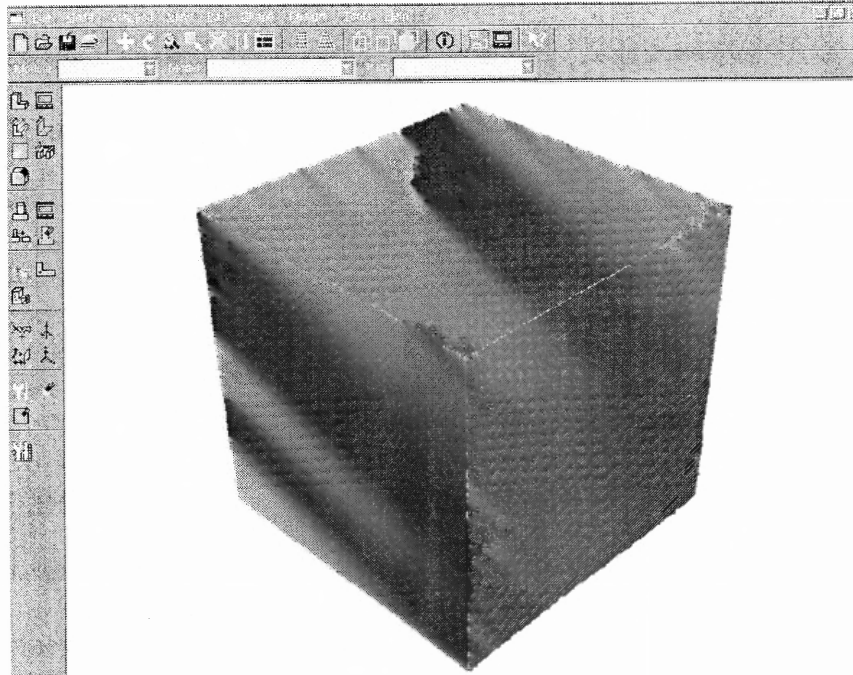
Figure 7.1 A snapshot of ABAQUS/CAE interface showing solid model of the part 'cube'. (Uni-axial tensile test)
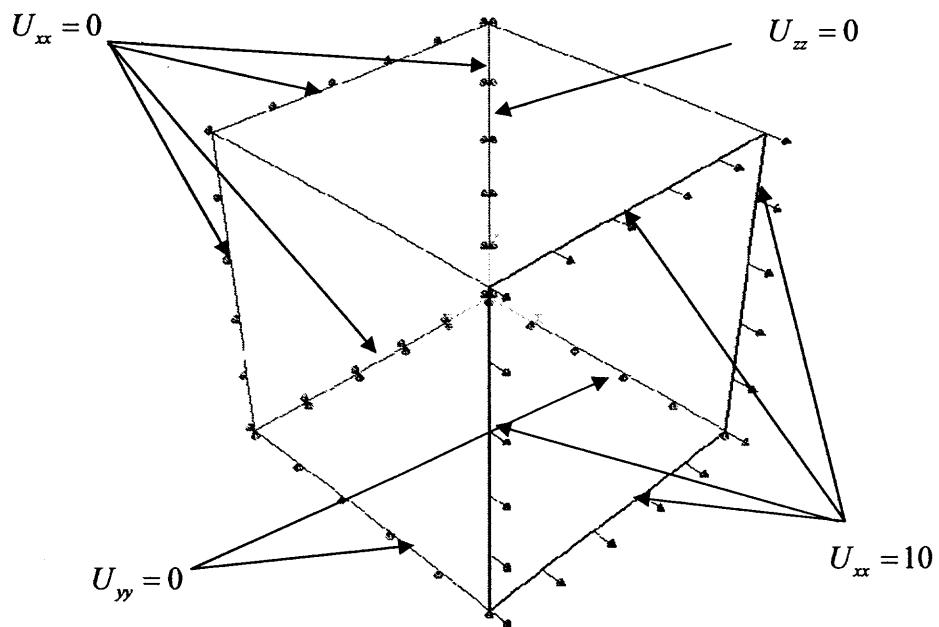
Figure 7.2 A snapshot of ABAQUS/CAE interface showing applied boundary conditions. (Uni-axial tensile test)

This completes the procedure for simulating uni-axial stretching of the single element. Using the visualization module different results can be presented. In following section the result obtained will be discussed.

7.4.2 Single Element Test with Oriented Co-ordinate System

The other test suggested by the makers of ABAQUS is to perform single element test in which local co-ordinate system is not aligned with the global co-ordinate system. If the results of the test are matching with one described in subsection 7.4.1 then it gives surety that UMAT will work with any orientation that a part can have.

For performing this test, similar procedure that was followed for the single element uni-axial stretching test with some minor differences is adopted. The first change needed to be done is after creating the part, is to orient the local co-ordinate system attached to the part. Using the 'assembly module' of ABAQUS/CAE it is easy to re-orient local co-ordinate system. Re-orienting local co-ordinate system will re-orient the part with respect to the global co-ordinate system. Figure 7.3 shows the rotated part 'cube' in the assembly module. The part is rotated to 30 degree in the counter clockwise direction with respect to z-axis. The second minor change is the boundary conditions which are applied with respect to local co-ordinate system instead of global co-ordinate system. Making these changes uni-axial tensile testing can be performed on the part with re-oriented co-ordinate system. Results obtained from this test will be compared with the test performed earlier.

7.4.3 Convergence Test

Finite element solution does not guarantee exact solutions of any problem. Using finite element method one can approximate value that is with in acceptable tolerance limit of the correct value. There are two methods to carry out finite element solution. One is

called h-method and another is p-method. In h-method, number of elements used is increased to achieve better solution where as in p-method, increasing degree of polynomial used to create shape function more correct answer can be obtained. ABAQUS/CAE allows use of linear or quadratic shape function only. Hence, only way to improve a result in ABAQUS/CAE is to use more elements. After certain iterations, very little improvement in result can be observed as solution converges to correct answer. Hence, if solution is converges to particular value with the increment in number of elements used then that answer is assumed is correct answer and method adopted to solved the problem can be considered as correct method.

To test the developed user subroutine UMAT, the convergence test is also performed. Consider a square plate with a circular hole in the middle. Applying the tensile load to the plate will create stress concentration near the hole. Increasing the number of elements near the hole region, correct value of stress near the region can be estimated. A square plate with a center circular hole has symmetry with 2 axes hence, instead of creating solid model of entire plate, only ¼ part of the plate should be enough to carry out the analysis as shown in Figure 7.4. Following is the step by step procedure for analysis.
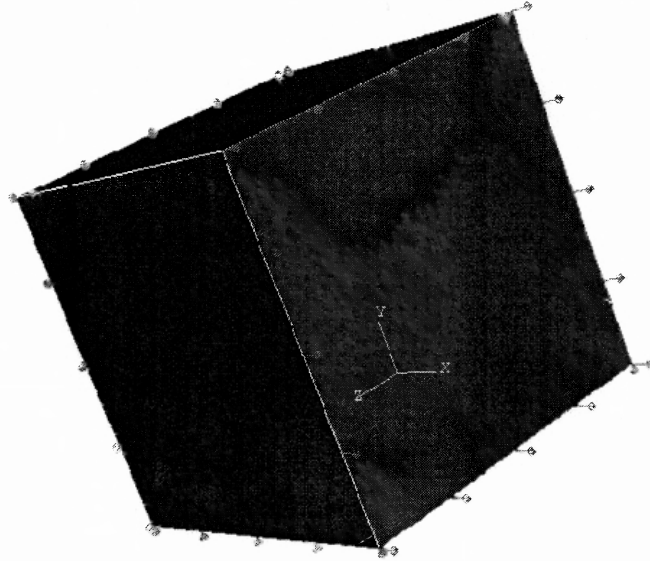
Figure 7.3 A snapshot of ABAQUS/CAE interface showing the part with re-oriented co-ordinate system. (Uni-axial tensile test with rotated co-ordinate system)

Step-1. Create a solid model: Using the part module a solid model of the plate is created. Figure 7.4 shows the solid model of ¼th part of 40mmX40mm square plate with a center hole of radius 1mm.

Step-2. Create a material model: Using the same module that used in previous test, the material model is created for the plate.

Step-3. Define processes: A process can be defined in 'step module' of the ABAQUS/CAE. For each process namely: Loading, Cooling/Crystallization, Unloading and Heating; individual step is created. During the cooling process shape of the plate is preserved. While heating moving boundary condition is de-activated.

Step-4. Apply boundary conditions: The surface on the left side of the plate is having symmetry with y axis and bottom surface of the plate is having symmetry with x-axis. Displacement can be applied to the surface on the right side of the plate. Figure 7.5 shows the applied boundary conditions. The displacement condition is deactivated in unloading and heating process.

Step-5. Mesh the model: The solid model is meshed using element called C3D20RH: A 20-node quadratic brick, hybrid element that allows linear pressure and reduced integration. Figure 7.6 shows different mesh generated for the plate.

Step-6. Solve the finite element model. Solution can be carried out as of the case of single element tensile testing. Multiple runs had to carry out for the different meshes. Total five runs C2 to C5 are carried out and the results obtained are prescribed in the following result section.
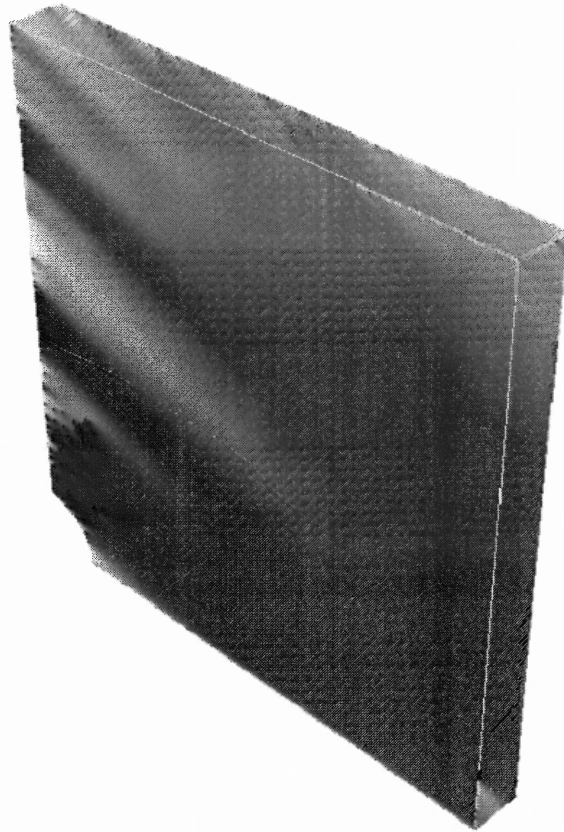
Figure 7.4 A snapshot of ABAQUS/CAE interface showing the solid model of the plate with center hole. (Convergence test)
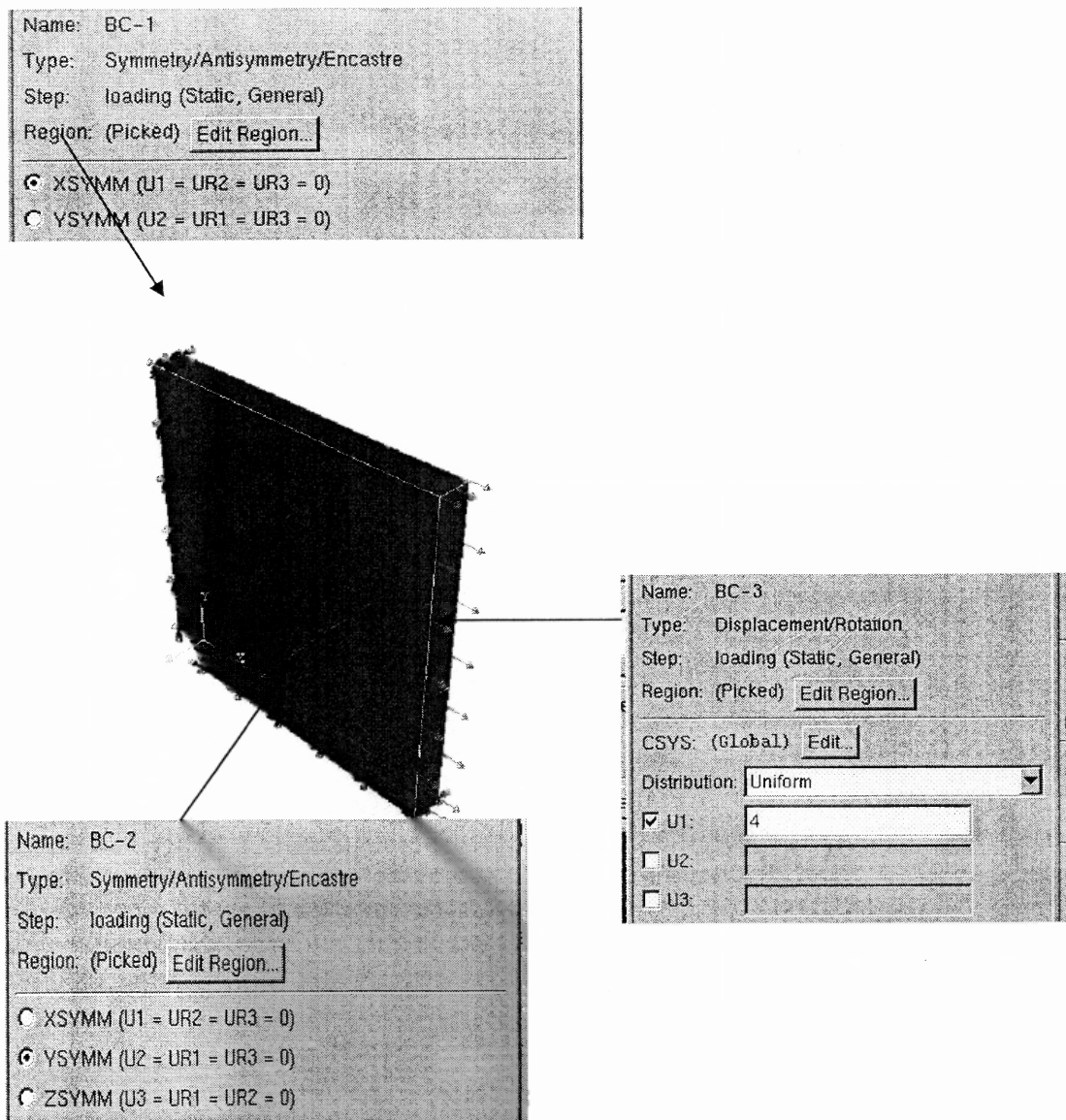
Figure 7.5 A snapshot of ABAQUS/CAE interface showing applied boundary conditions. (Convergence test)
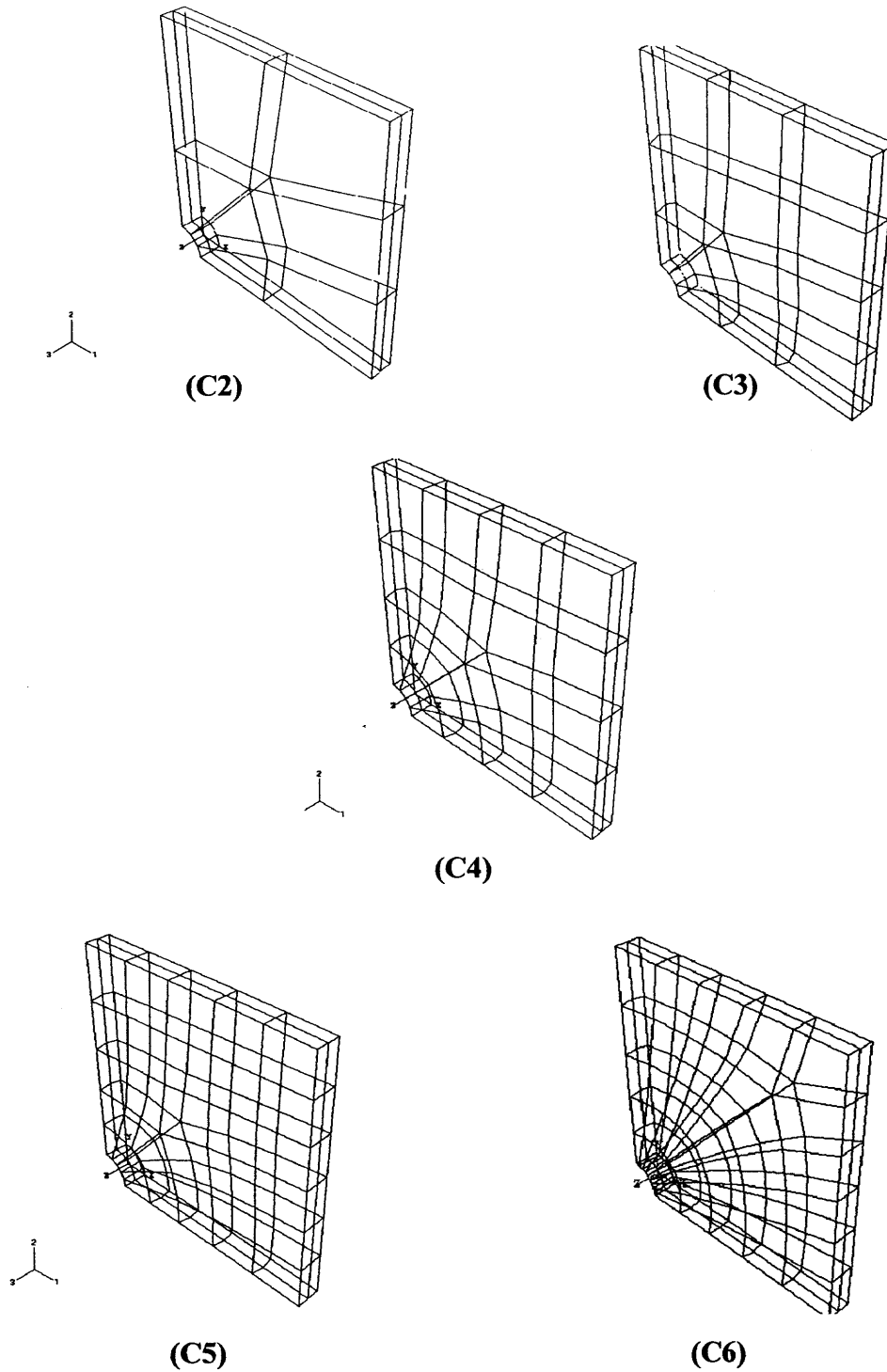
Figure 7.6 Different meshes used for convergence test runs (C2 to C6).

7.5   Results

In this section, the results obtained from various tests performed as prescribed in subsection 7.4 are presented. Three different tests were performed and for each type of tests, different set of results are obtained.
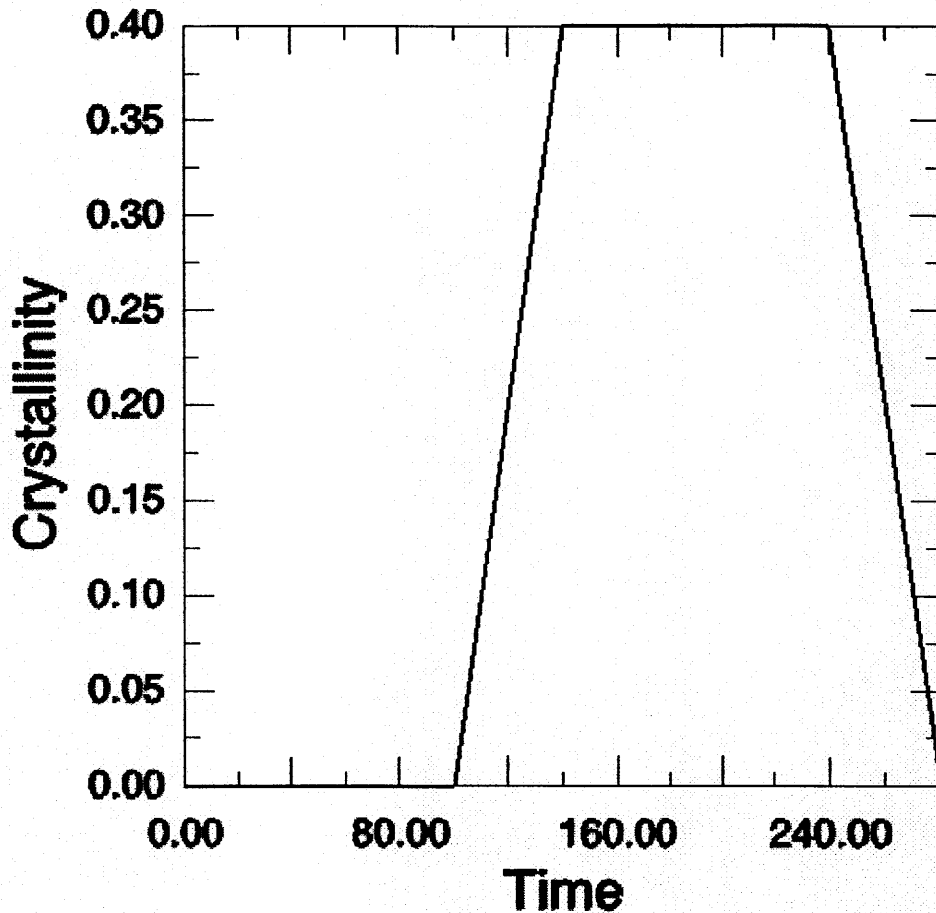
Figure 7.7 Plot of crystallinity versus time. (Single element test)

The first set of results is from the single element test. The single element test is uni-axial stretching of the cube for which the solid model is meshed with only one single element. Figure 7.7 shows the variation in the crystallinity in the element with the time. Initially, during the loading process the crystallinity is zero, while the cooling process it linearly increasing.
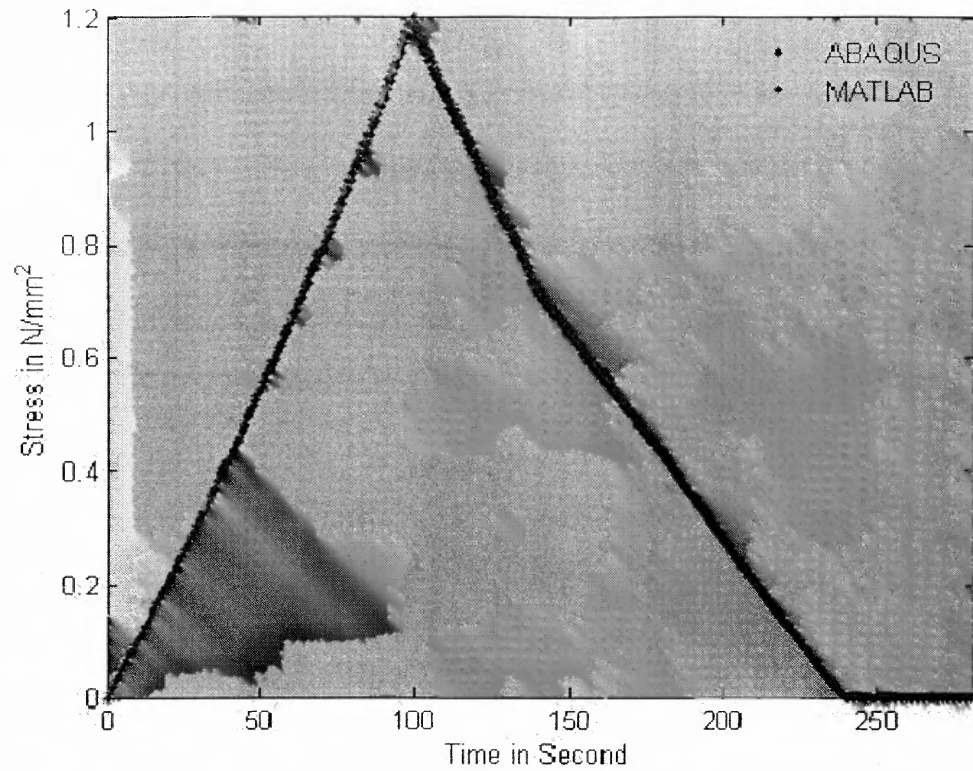
Figure 7.8 Plot of stress versus time. The results are obtained using MATLAB and ABAQUS module. (Single element test)
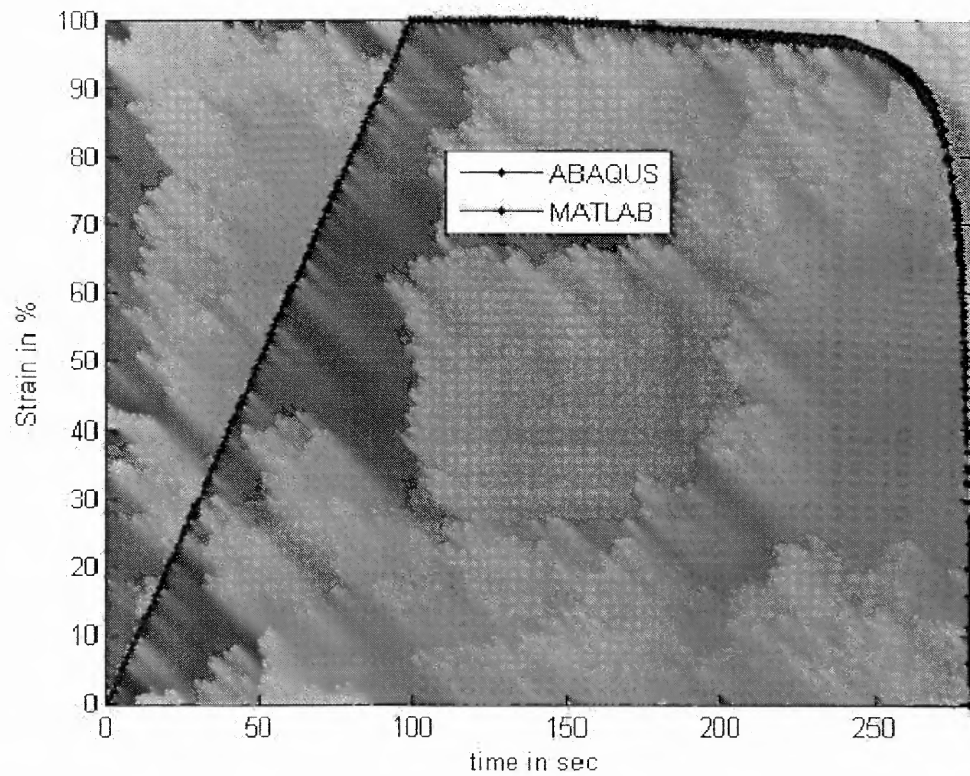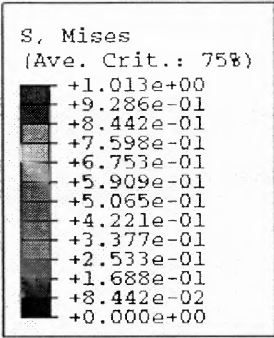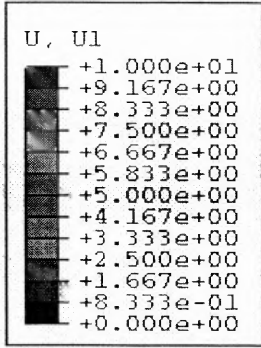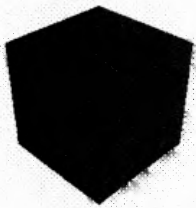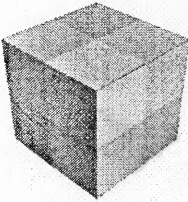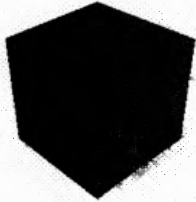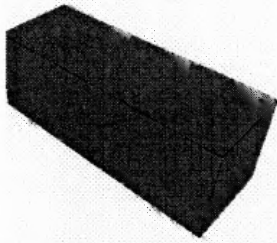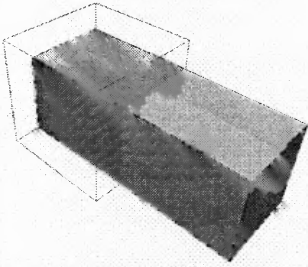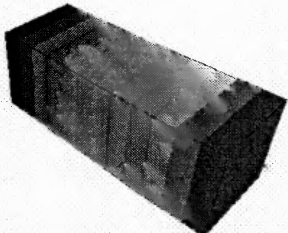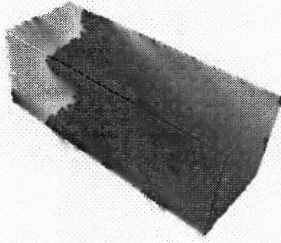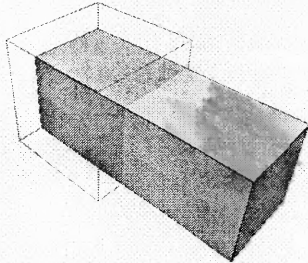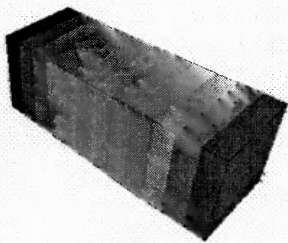
Figure 7.9 Plot of strain versus time. The results are obtained using MATLAB and ABAQUS module. (Single element test)

During the unloading process, crystallinity remains constant and during heating it linearly decreasing as designed. Figure 7.8 shows the stress variation with the time. During the loading process, the stress is increasing with increase in the strain (see Figure 7.9). While cooling significant reduction in the stress can be observed while the strain remains constant as new crystals form. Upon unloading the stress is reducing to zero yet, the strain will not go to zero and preserves the deformed shape. During heating, formed crystal melts and strain reduces to zero as material approaches to original shape. Figure 7.8 and Figure 7.9 also shows the comparisons between the results obtain from MATLAB program and the results obtained from ABAQUS matching quite closely.

MATLAB program predicts the correct answer of the 1-D problem. Figure 7.10 shows the chart where the stress fringe plots, deformations of the cube and displacement fringe plot are shown parallel with the crystallinity value at that time. At a time, stress plot in the part show only one color because the part is meshed with single element and so, all nodes in the element will have same value. Nodes on the left face of the element are constrained while the displacement boundary conditions is applied to nodes on the right face of the cube hence, equally distributed color pattern can be seen in the displacement fringe plot.

Stress	Deformation	Displacement
S, Mises (Ave. Crit.: 75%) +1.013e+00 +9.286e-01 +8.442e-01 +7.598e-01 +6.753e-01 +5.909e-01 +5.065e-01 +4.221e-01 +3.377e-01 +2.533e-01 +1.688e-01 +8.442e-02 +0.000e+00		U, U1 +1.000e+01 +9.167e+00 +8.333e+00 +7.500e+00 +6.667e+00 +5.833e+00 +5.000e+00 +4.167e+00 +3.333e+00 +2.500e+00 +1.667e+00 +8.333e-01 +0.000e+00
7.10.1.) Start: Loading process ($\alpha = 0$)		
7.10.2.) End: Loading process & Start: Cooling process($\alpha = 0$)		
7.10.3.) Intermediate time: Cooling process ($\alpha = 0.1$)		

Continued…

7.10.4.) Intermediate time: Cooling process. ($\alpha = 0.2$)
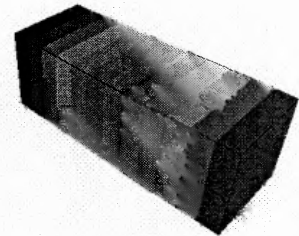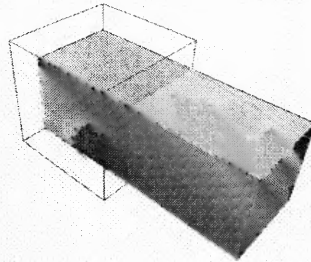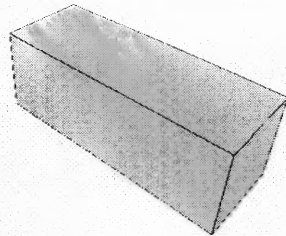
7.10.5.) Intermediate time: Cooling process($\alpha = 0.3$)
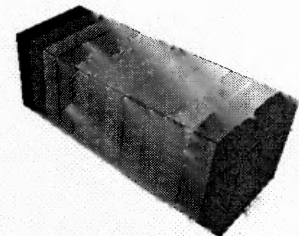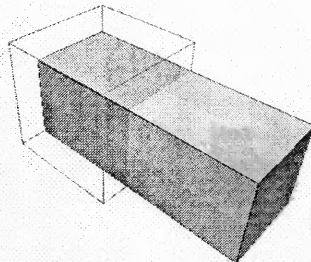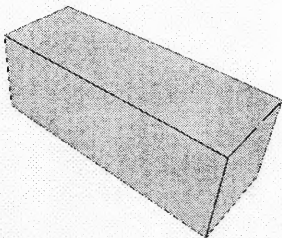
7.10.6.) End: Cooling process & Start: Unloading process. ($\alpha = 0.4$)
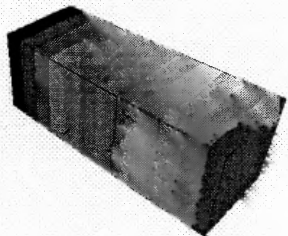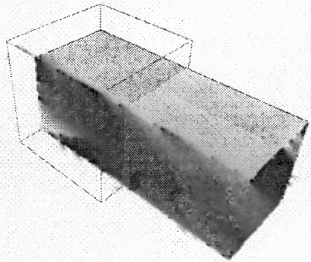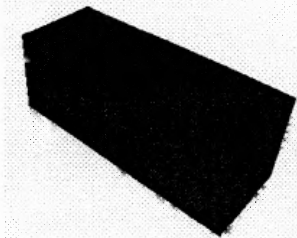
7.10.7.) End: Unloading process & Start: Heating process ($\alpha = 0.4$)

Continued…
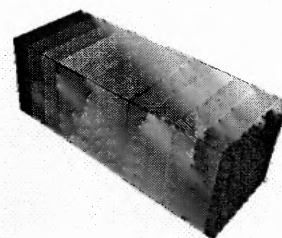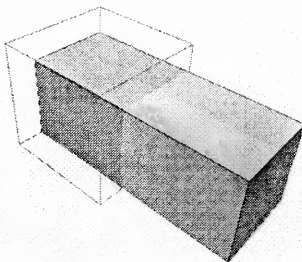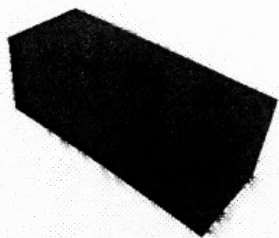
7.10.8.) Intermediate time: Heating process. ($\alpha = 0.3$)
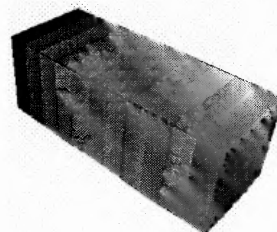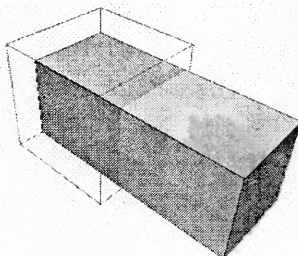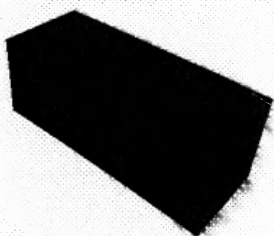
7.10.9.) Intermediate time: Heating process. ($\alpha = 0.2$)
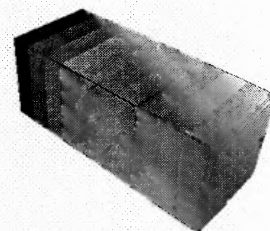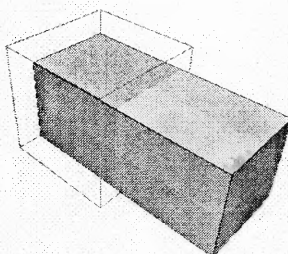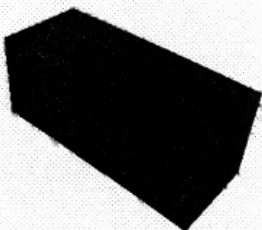
7.10.10.) Intermediate time: Heating process. ($\alpha = 0.1$)
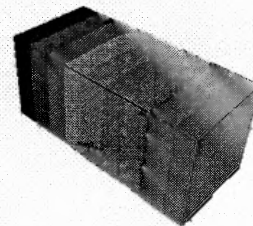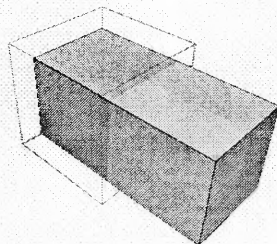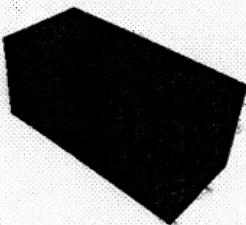
7.10.11.) Intermediate time: Heating process ($\alpha = 0.05$)

Continued…

7.10.12.) Intermediate time: Heating process ($\alpha = 0.025$)

7.10.13.) End: Heating process ($\alpha = 0$)
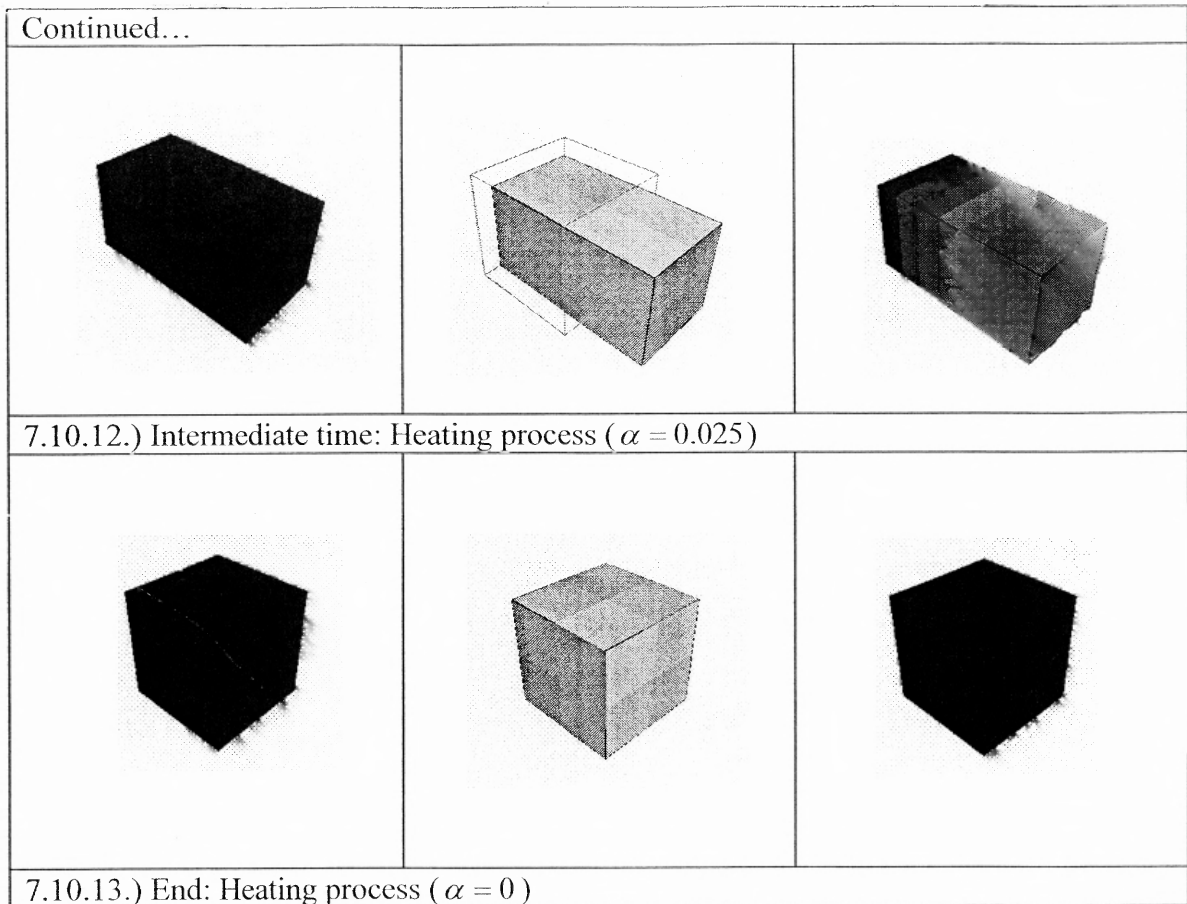
Figure 7.10 Chart shows stress fringe plots, deformed solid part with superimposed undeformed wire –framed part and displacement fringe plot for a typical uni-axial cycle for CSMP. (Single element test)

One can see from the displacement plots that nodes on the right face of the cube are moved enough to make cube length double. It produces 100% strain in the direction of stretch in the part geometry. Figure 7.11 confirms that the strain in the part is 100% after the completion of the loading cycle.

Second set of the results is from the oriented single element test. Figure 7.11 and Figure 7.12 show charts of comparison between stress fringe plots obtained through single element test and oriented single element test and displacement fringe plots obtained through same tests respectively. The comparison shows good agreement in results visually for stress fringe plots. Even the displacement plots are matching exactly.

Single element test	Oriented single element test
7.11.1.) Start: Loading process ($\alpha = 0$)	
7.11.2.) End: Loading process & Start: Cooling process($\alpha = 0$)	
7.11.3.) End: Cooling process & Start: Unloading process. ($\alpha = 0.4$)	

Continued…

7.11.4.) End: Unloading process & Start: Heating process ($\alpha = 0.4$)

7.11.5.) End: Heating process ($\alpha = 0$)
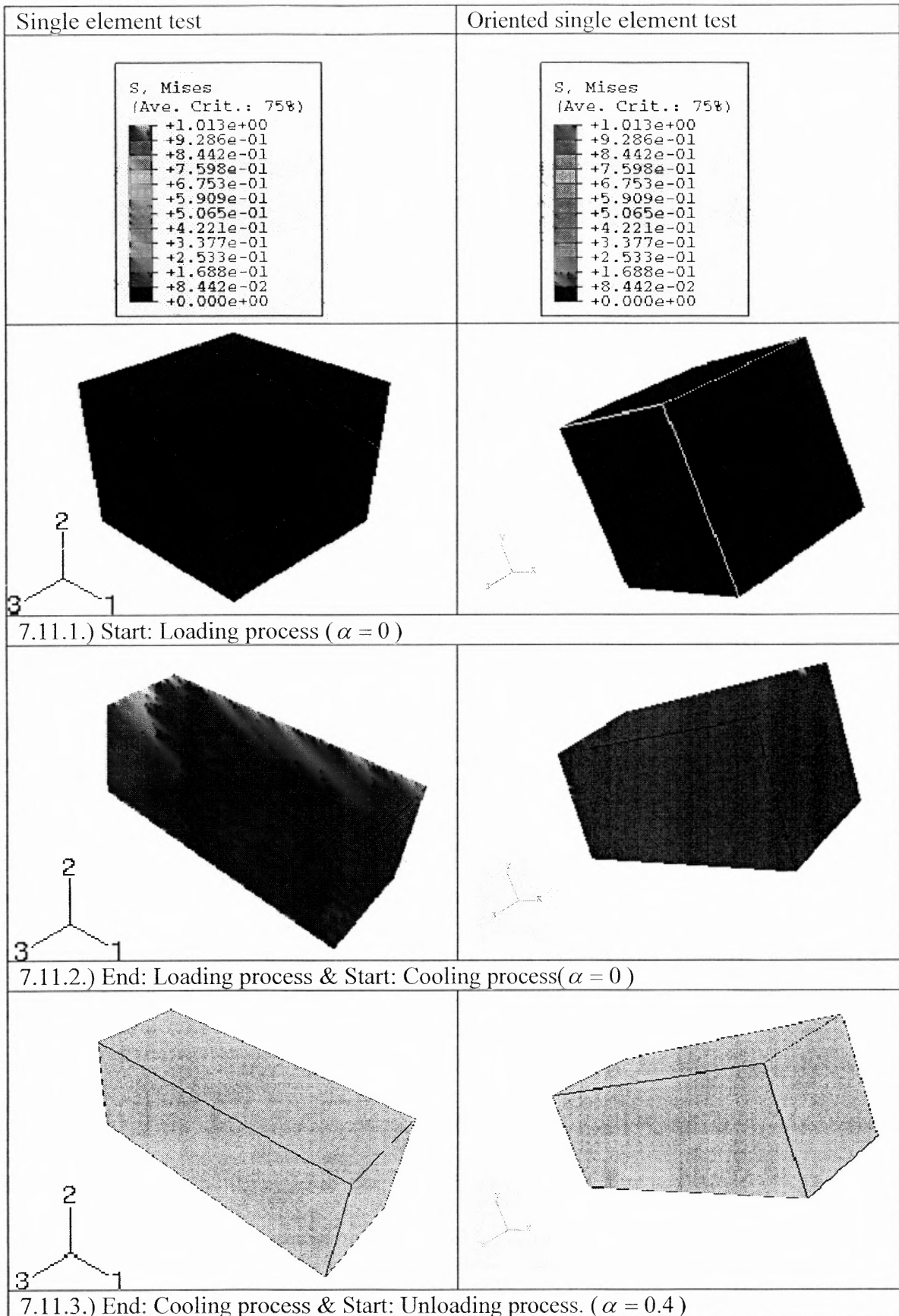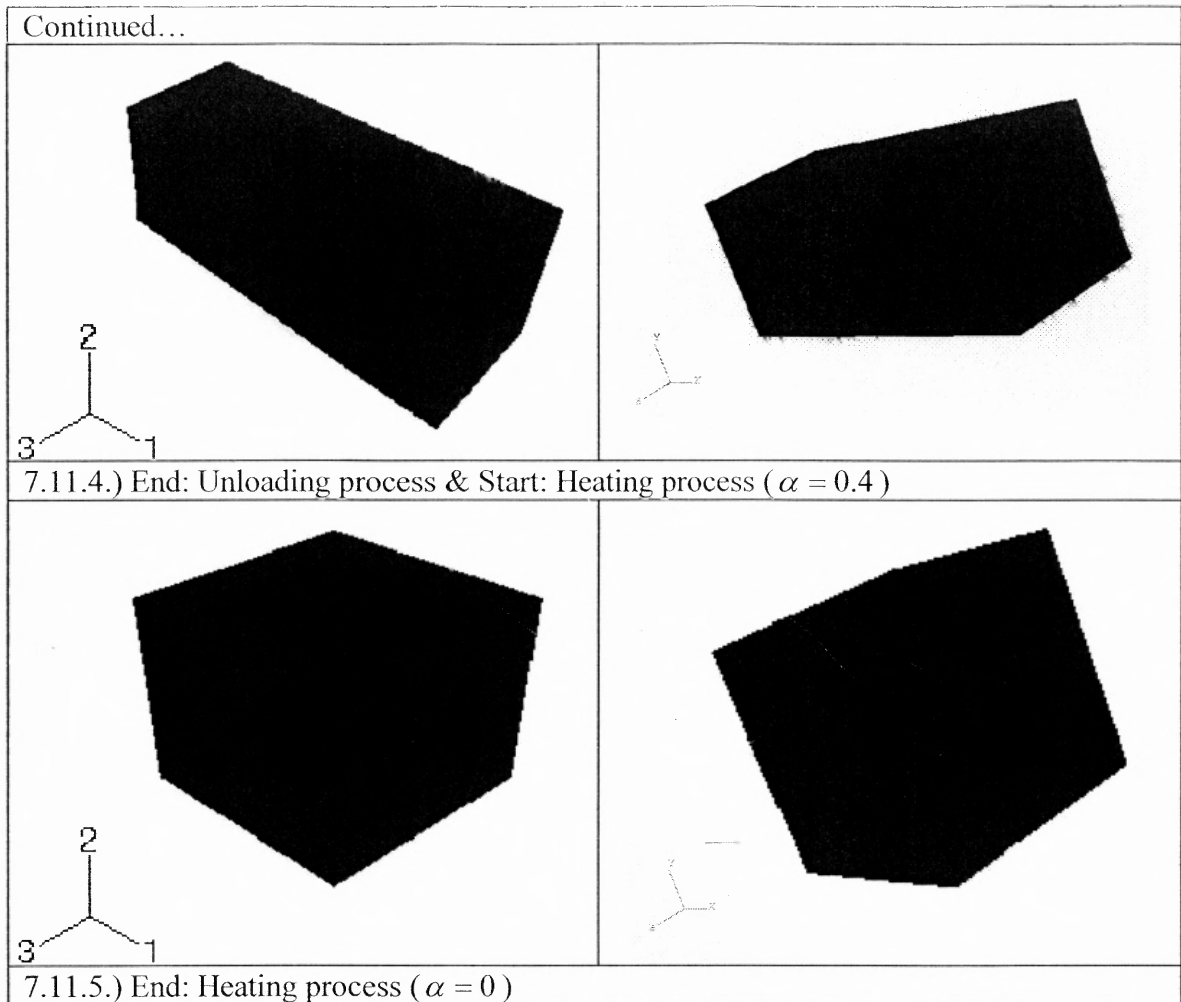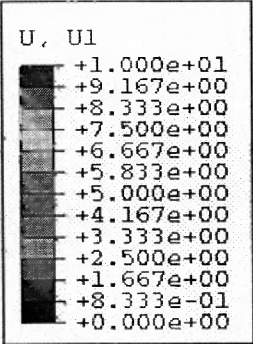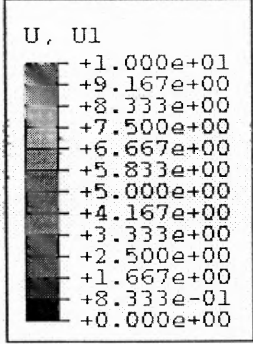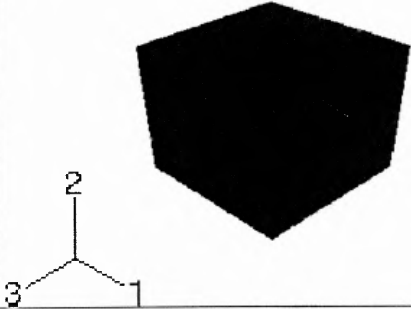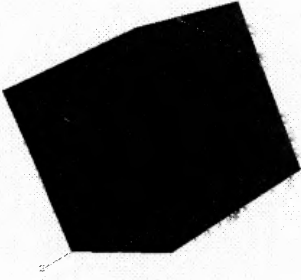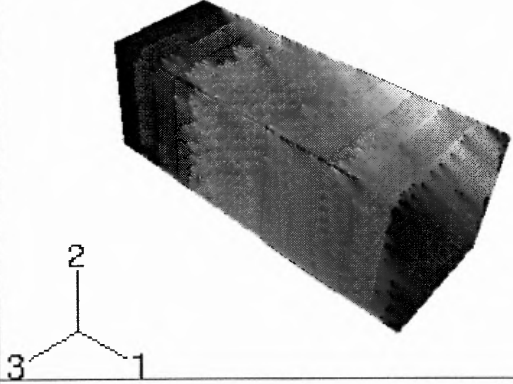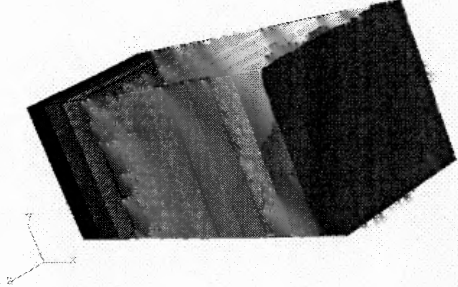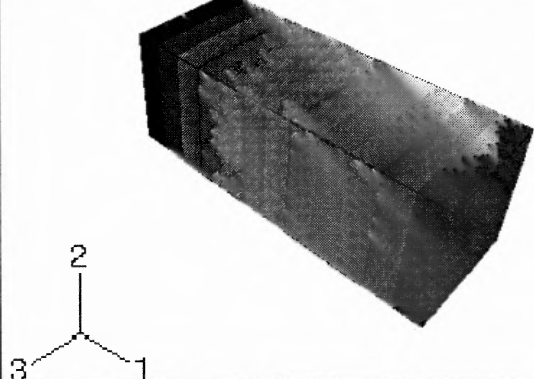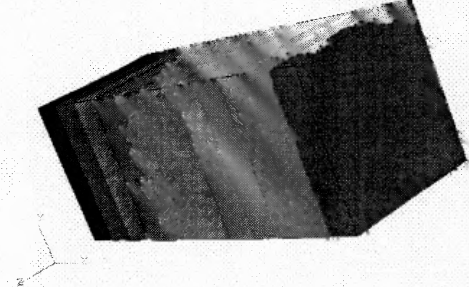
Figure 7.11 Chart shows results (stress fringe plots) obtained through single element test and oriented single element test for a typical cycle.

Single element test	Oriented single element test
U, U1 +1.000e+01 +9.167e+00 +8.333e+00 +7.500e+00 +6.667e+00 +5.833e+00 +5.000e+00 +4.167e+00 +3.333e+00 +2.500e+00 +1.667e+00 +8.333e-01 +0.000e+00	U, U1 +1.000e+01 +9.167e+00 +8.333e+00 +7.500e+00 +6.667e+00 +5.833e+00 +5.000e+00 +4.167e+00 +3.333e+00 +2.500e+00 +1.667e+00 +8.333e-01 +0.000e+00

7.12.1.) Start: Loading process ($\alpha = 0$)

7.12.2.) End: Loading process & Start: Cooling process($\alpha = 0$)

7.12.3.) End: Cooling process & Start: Unloading process. ($\alpha = 0.4$)

Continued…

7.12.4.) End: Unloading process & Start: Heating process ($\alpha = 0.4$)

7.12.5.) End: Heating process ($\alpha = 0$)

Figure 7.12 Chart shows results (displacement fringe plots) obtained, using single element and oriented single element, for a typical uni-axial cycle for CSMP. (Datum is global co-ordinate system)

Third set of the results is obtained by carrying out the convergence test. Figure 7.13 shows the plot of maximum stress in the part versus number of elements used to perform analysis. It can be infer from the plot that up to certain limit increasing number of elements result is improving drastically. However, after certain increments in number of elements used there is no significant improvement in result can be seen as the result converges to correct answer. Figure 7.14 shows the stress fringe plots for runs C2 to C6. Note that the reduction in the area of stress concentration (Area in Red) can be observed with the use of more fine meshes around the 'hole' region.
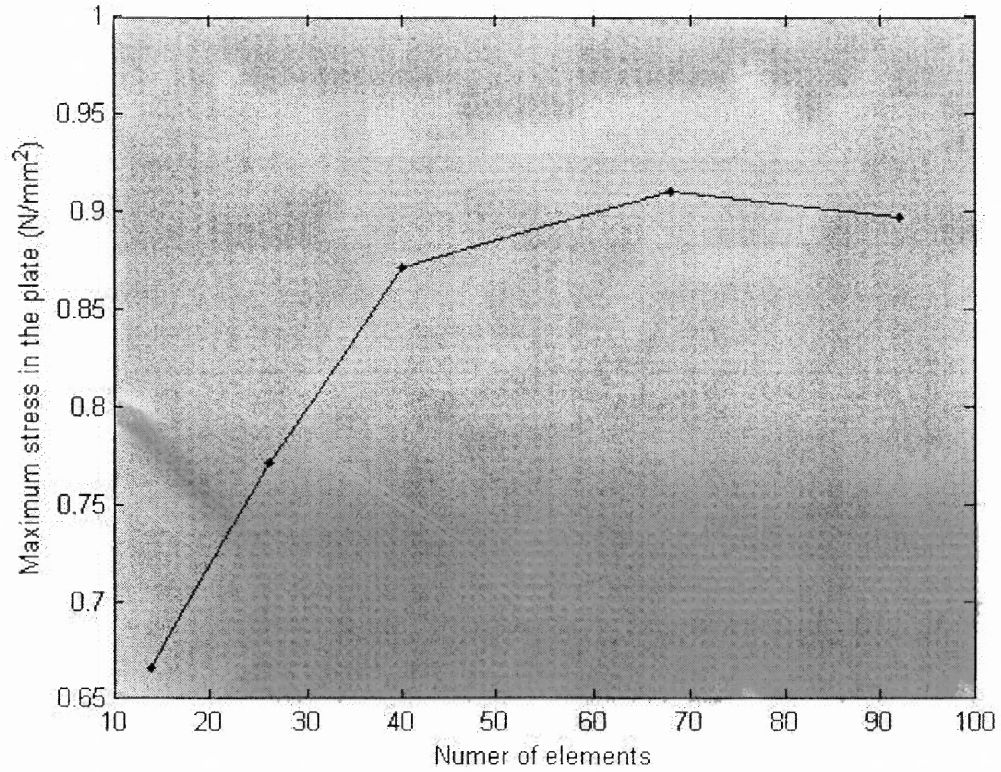
Figure 7.13 Plot of maximum stress versus number of elements used for simulating uni-axial stretching of a plate with central circular hole. (Convergence test)
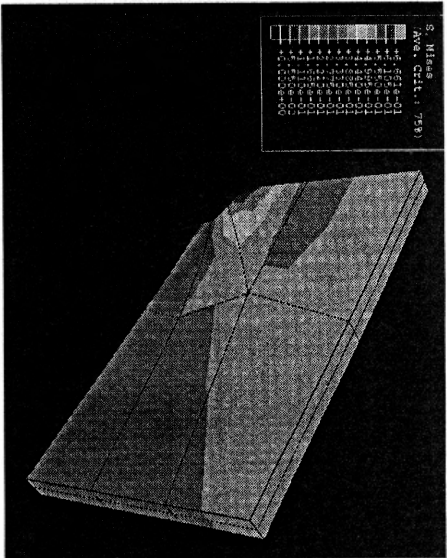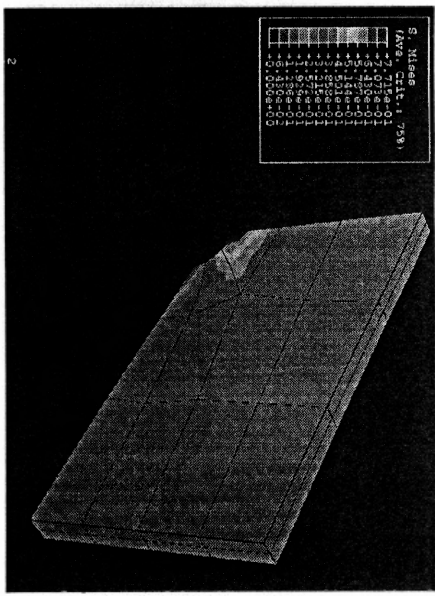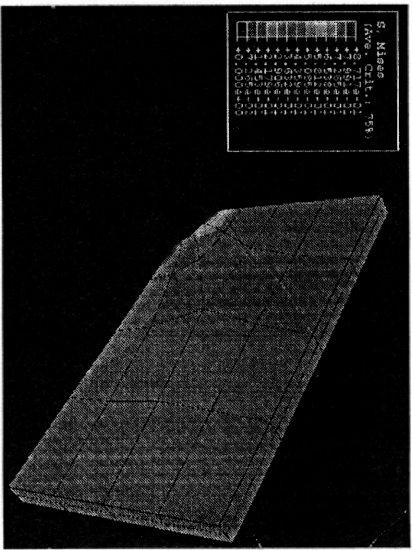
Figure 7.14 Stress fringe plots for run C2 to C6. (Convergence test)

(C2)

(C3)

(C4)

(C5)

(C6)

CHAPTER 8

APPLICATIONS OF THE FINITE ELMENT MODULE

8.1   Introduction

In this chapter, the applications of the finite element module created using the constitutive equation derived in the Chapter 4 are illustrated. To show the applicability of the module, three different simulations were carried out. The first simulation is the inflation and expansion of the hollow cylinder. The second process is also on cylindrical geometry where hollow cylinder is twisted with respect to the central axis and the third process simulated is the bending of the thin strip. All of the processes are non-linear and non-isothermal.

A material can be deformed mechanically mainly using following actions or their combinations. These actions are stretching, compression, shearing, twisting and bending. The first process involves tensile loading on the part with geometry that works well with cylindrical co-ordinates and in the second process; a material is deformed by twisting action which produces shearing effect in the elements. During the shrink fit operation the inflation and expansion of the tube occurs while twisting action can be seen in rotating actuators. In third process, a material has shape that is easy to work with in Cartesian co-ordinates and a material is deformed by bending action that produces tensile stress in some elements and compressive stress in the other elements. The strip bending is popular technique in making house hold items.

8.2   Inflation and Expansion of a Hollow Cylinder

8.2.1 Problem Definition and Solution Technique

The hollow cylinder made with CSMP experience tensile force along its central axis of revolution and at inner surface pressure is applied. These actions cause inflation and expansion of the cylinder simultaneously. Once the part is deformed, keeping the shape constant, the material is cooled by cooling inner and outer surfaces simultaneously. Once material is cooled below the transition temperature (-10^0C), the tensile force and pressure applied are removed. The original shape takes place when the material is heated at inner and outer surfaces.

The material undergoes inhomogeneous deformation and the process is non-isothermal process where primary mode of heat transfer is conduction. Following is complete step by step procedure adopted to carry out the finite element analysis of the process.

Step-1. Create a solid model: Using the part module, a solid model of the hollow cylinder is created. Figure 8.1 shows the solid model of the hollow cylinder with the 2 mm inside diameter and 3 mm diameter with 0.5mm in height. Using 'revolution' feature in part module above described geometry constructed.

Step-2. Create a material model: Using the material module developed in previous chapter material model of the cylinder is created. However, this time the non-isothermal process is under consideration and so there will be little modification is required in the material module. Material module developed for this process is presented in appendix H.
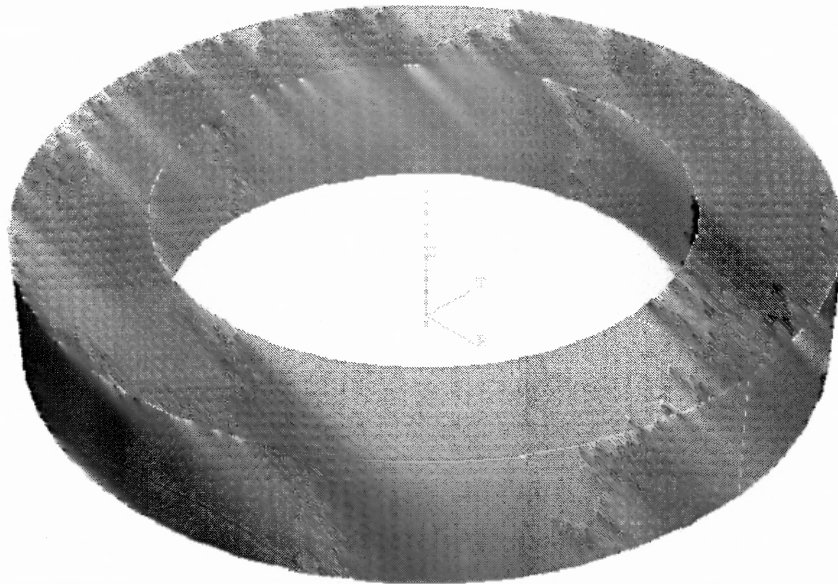
Figure 8.1 Solid model of a hollow cylinder created in ABAQUS/CAE.

Step-3. Define processes: Each process can be defined in the 'step module' of the ABAQUS/CAE. For each process namely: Loading, Cooling/Crystallization, Unloading and Heating/Melting; individual steps are created. During the cooling process, the shape of the hollow cylinder is preserved. While during the heating process the boundaries are free to retract.

Step-4. Apply boundary conditions: Figure 8.2 shows applicable boundary conditions according to the problem definition. Top face of the cylinder is stretched while the all points of the inner surface are moved equally in radial direction that causes inflation of the cylinder. The bottom part of cylinder is constrained in z direction and in angular direction. Linear variation in temperature applied at inner and outer surfaces of the cylinder. For cooling, temperature decreases linearly at both surfaces and for heating, the temperature is increasing at both surfaces where as top and bottom surfaces are considered as insulating.
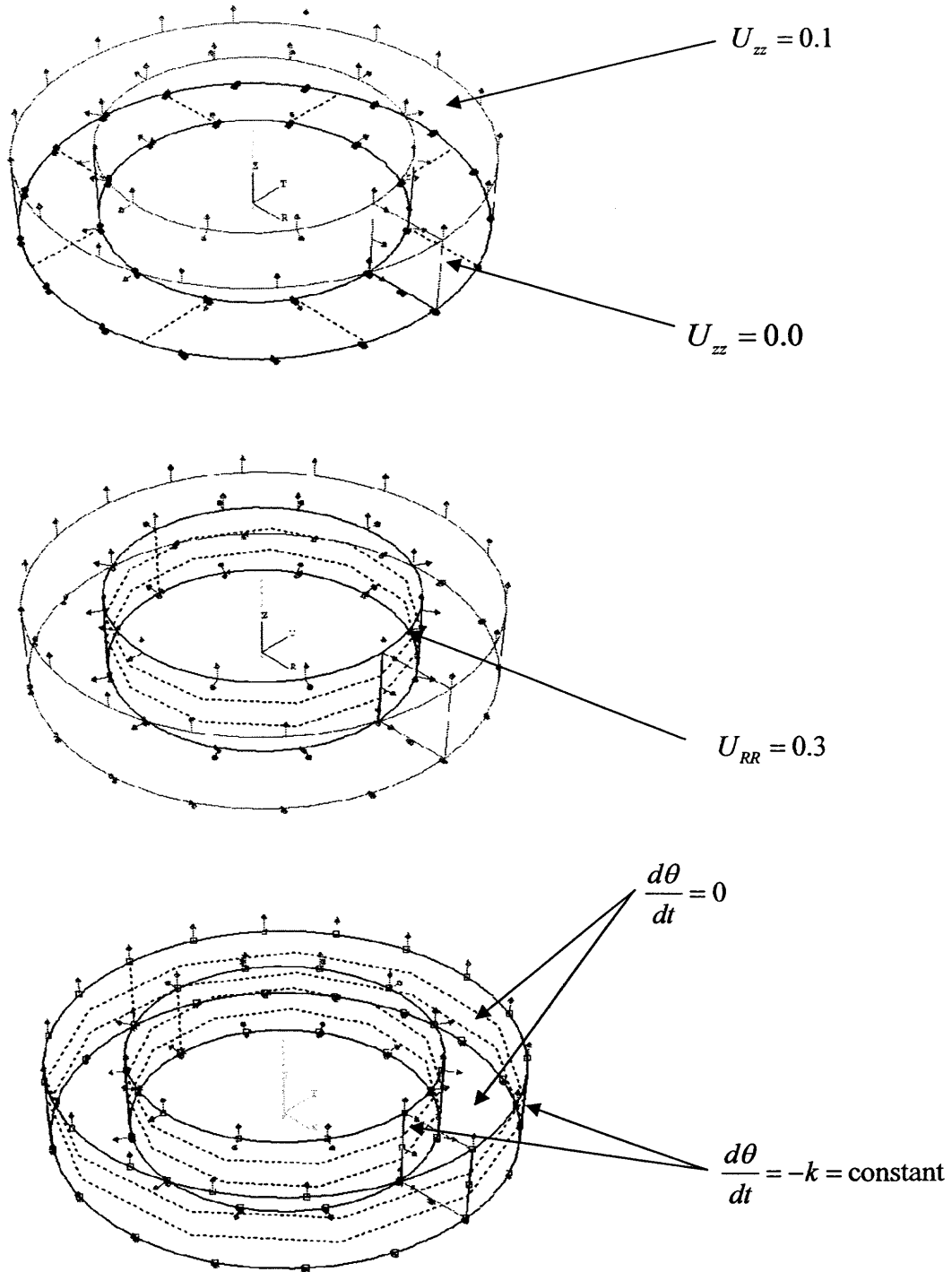
Figure 8.2 Different boundary conditions applicable to the hollow cylinder for inflating and expanding it with heat transfer going on.

Step-5. Mesh the model: The solid model is meshed using element called C3D8HT: An 8-node thermally coupled hybrid brick with shape function for trilinear displacement and temperature that only allows constant pressure.

Step-6. Solve the finite element model. Using the job module in ABAQUS/CAE, user subroutines (UMAT, UMATHT and SDVINI) can be called to carry out the solution for the process.

8.2.2 Results

In this subsection, different results obtained using the post processor module of ABAQUS/CAE are listed. To clarify the issues related with temperature and crystallinity temperature variation plot (Figure 8.3) and crystallinity variation plot (Figure 8.4) are shown.
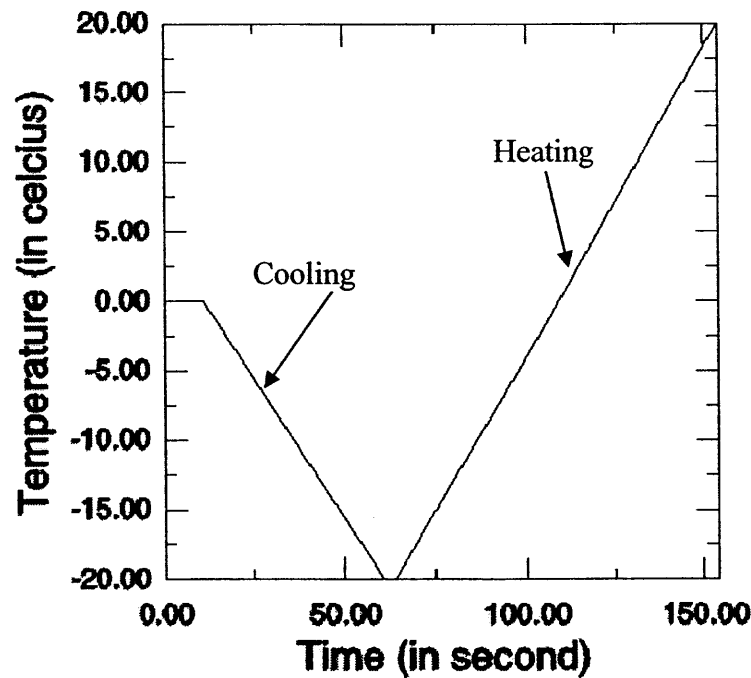
Figure 8.3 Temperature variation at the outer and inner surfaces of the hollow cylinder for the entire cycle

According to the applied boundary conditions, the linear decrease in temperature while cooling and linear increase in temperature while heating process at the inner and outer surfaces of the hollow cylinder can be observed (see Figure 8.3). During cooling new crystal forms and crystallinity reaches to its maximum value. Upon heating those formed crystal melts and crystallinity decreases. Figure 8.4 shows variation in crystallinity according to the temperature variation.
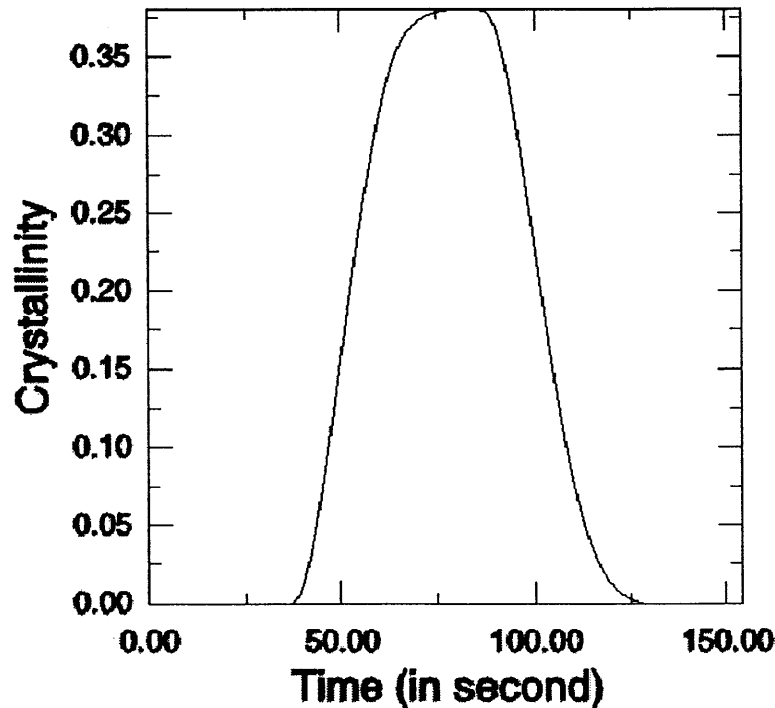
Figure 8.4 Crystallinity variation at the outer and inner surfaces of the hollow cylinder for the entire cycle.

While loading process, the temperature is kept constant and there is no temperature gradient can be seen through out the body (see Figure 8.5-A, B). During the cooling process, the temperatures at the surfaces are decreasing first and then due to conduction the temperature decreases inside (see Figure 8.5-C). During the unloading process the temperature is kept constant at the inner and outer surfaces. During this process temperature continue to decrease in the interior of the cylinder as the inner and

outer surfaces are cooler than inner part of the hollow cylinder (see Figure 8.5-D). Figure 8.5-E shows the temperature fringe plot after heating process showing that the part is heated back to obtain original shape and overall temperature of the part is well above the transition temperature.

A) Temperature fringe plot (before loading)   B) Temperature fringe plot (After loading)

C) Temperature fringe plot (After cooling)   D) Temperature fringe plot (After unloading)

NT11
+2.000e+01
+1.667e+01
+1.333e+01
+1.000e+01
+6.667e+00
+3.333e+00
-4.768e-07
-3.333e+00
-6.667e+00
-1.000e+01
-1.333e+01
-1.667e+01
-2.000e+01

E) Temperature fringe plot (After heating)   F) Legend: Temperature in Celsius
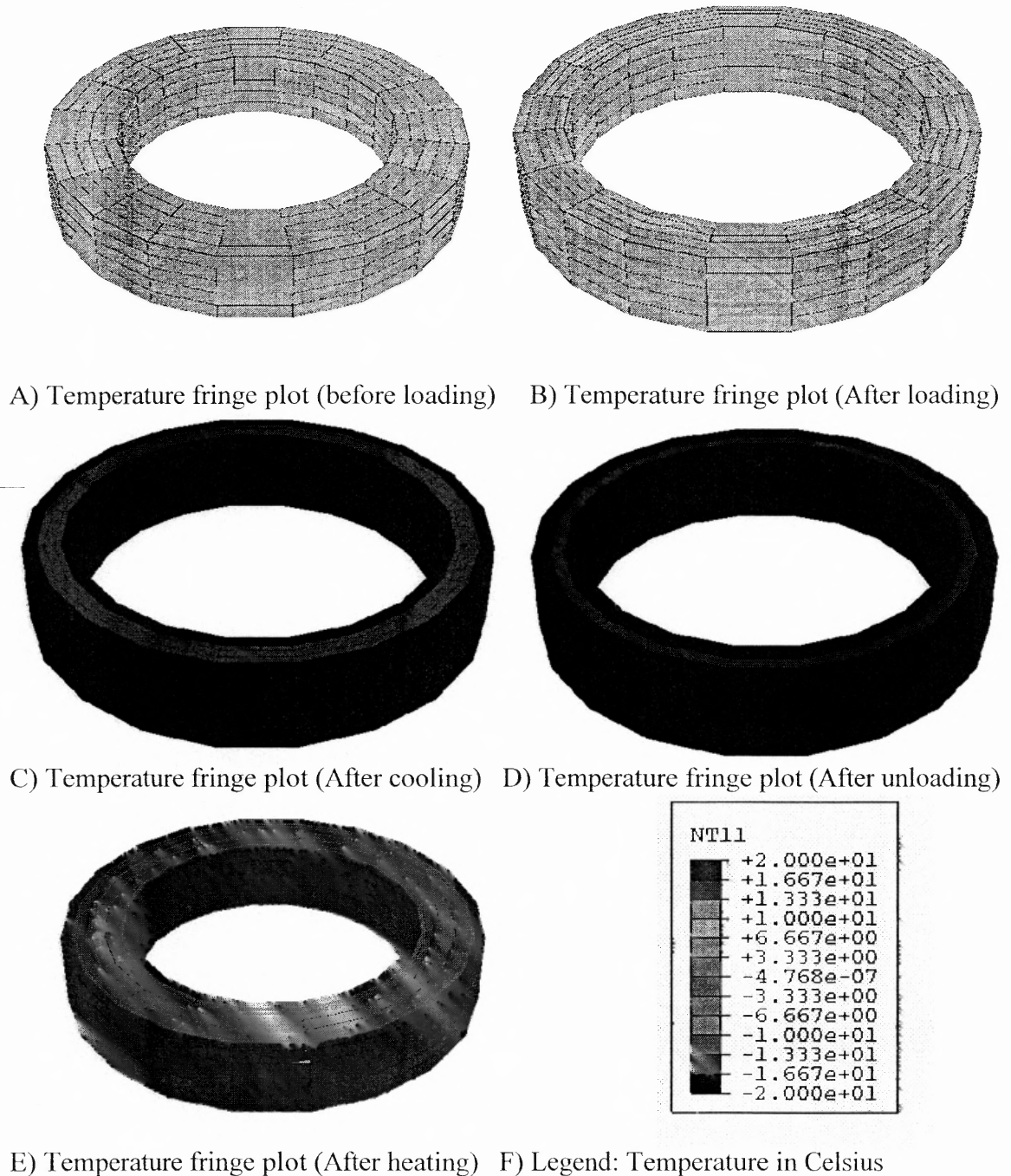
Figure 8.5 Temperature variation with in the hollow cylinder at different stages of the cycle.

Figure 8.6-A, B show that when the temperature is above the transition temperature there is no crystallinity in the part. The crystallinity increases with on cooling initially at their outer surfaces then to the interiors (see Figure 8.6-C, D). During the heating process as the temperature increases at the inner and outer surfaces, the crystallinity decreases there and then due to heat conduction crystallinity decreases to zero in the interiors as well (see Figure 8.6-E). Figure 8.7 shows the stress distribution in the hollow cylinder at various stages of the cycle. With deformation the stress increases as expected and on cooling, the stress is decreases along with the formation of the crystalline phase. Upon unloading the stress deceases further but due to variation in crystallinity in different part the stress does not go to zero. This is a consequence of the fact that this is not a homogenous deformation. On heating, crystal melts and the material goes back to its original shape and at end as there is no deformation in the amorphous phase there is any stress in the part as well. Figure 8.8 shows how material deforms and maintains the temporary shape even after unloading. It also shows that upon heating, the material takes back its original shape.
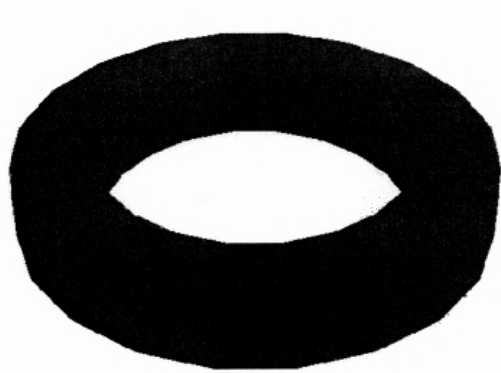
A) Crystallinity fringe plot (Before loading)   B) Crystallinity fringe plot (After loading)
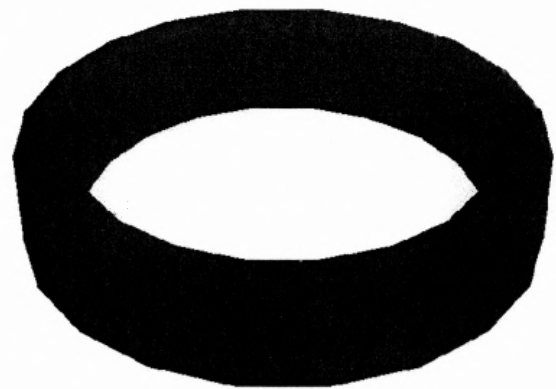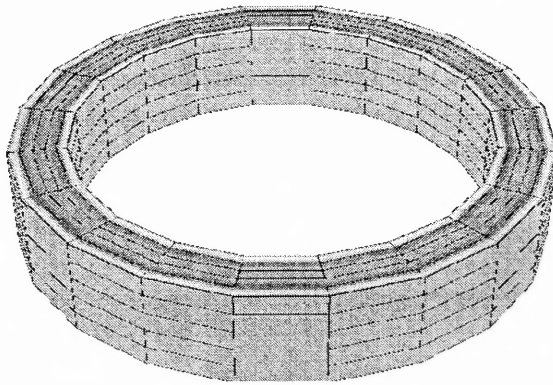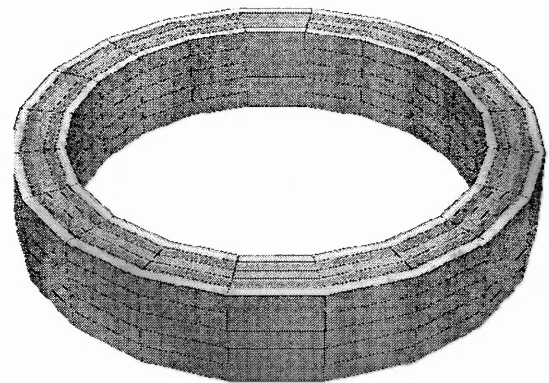
C) Crystallinity fringe plot (After cooling)   D) Crystallinity fringe plot (After unloading)
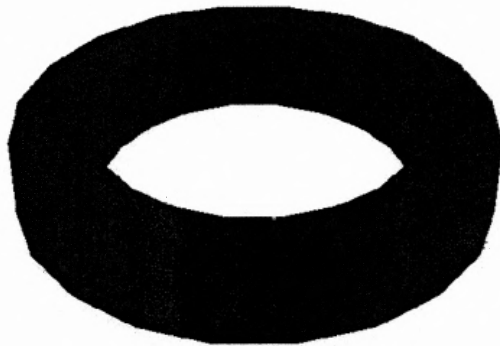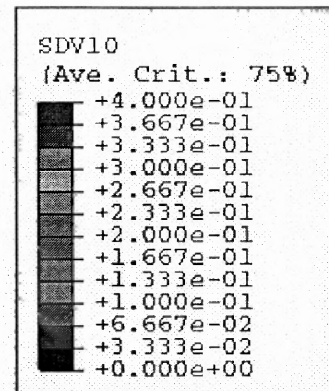
E) Crystallinity fringe plot (After heating)   F) Legend: Crystallinity

Figure 8.6 Crystallinity variation with in the hollow cylinder at different stages of the cycle.
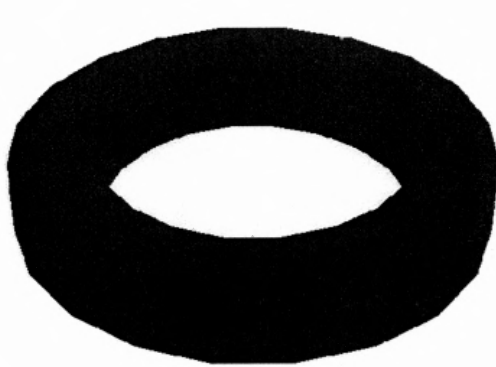
A) Stress fringe plot (Before loading)
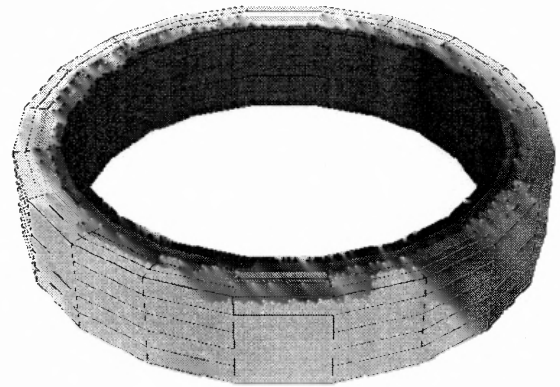
B) Stress fringe plot (after loading)
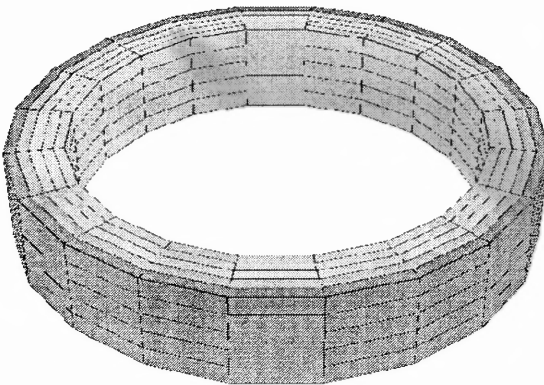
C) Stress fringe plot (After cooling)
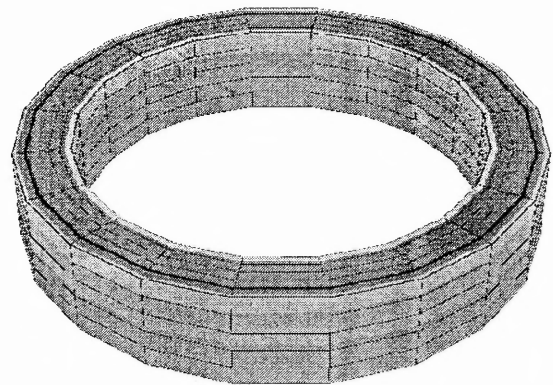
D) Stress fringe plot (after unloading)
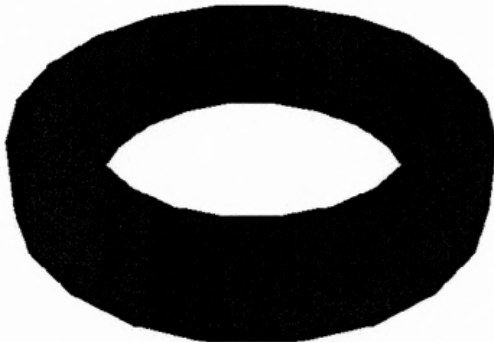
E) Stress fringe plot (after heating)
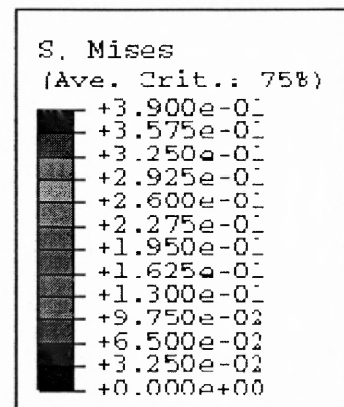
F) Legend: Stress in N/mm^2

Figure 8.7 von-Mises stress variation with in the hollow cylinder at different stages of the cycle.

A) Deformation plot (Before loading)

B) Deformation plot (After loading)

C) Deformation plot (After cooling)

D) Deformation plot (After unloading)

E) Deformation plot (After heating)

Deformed part

Undeformed part
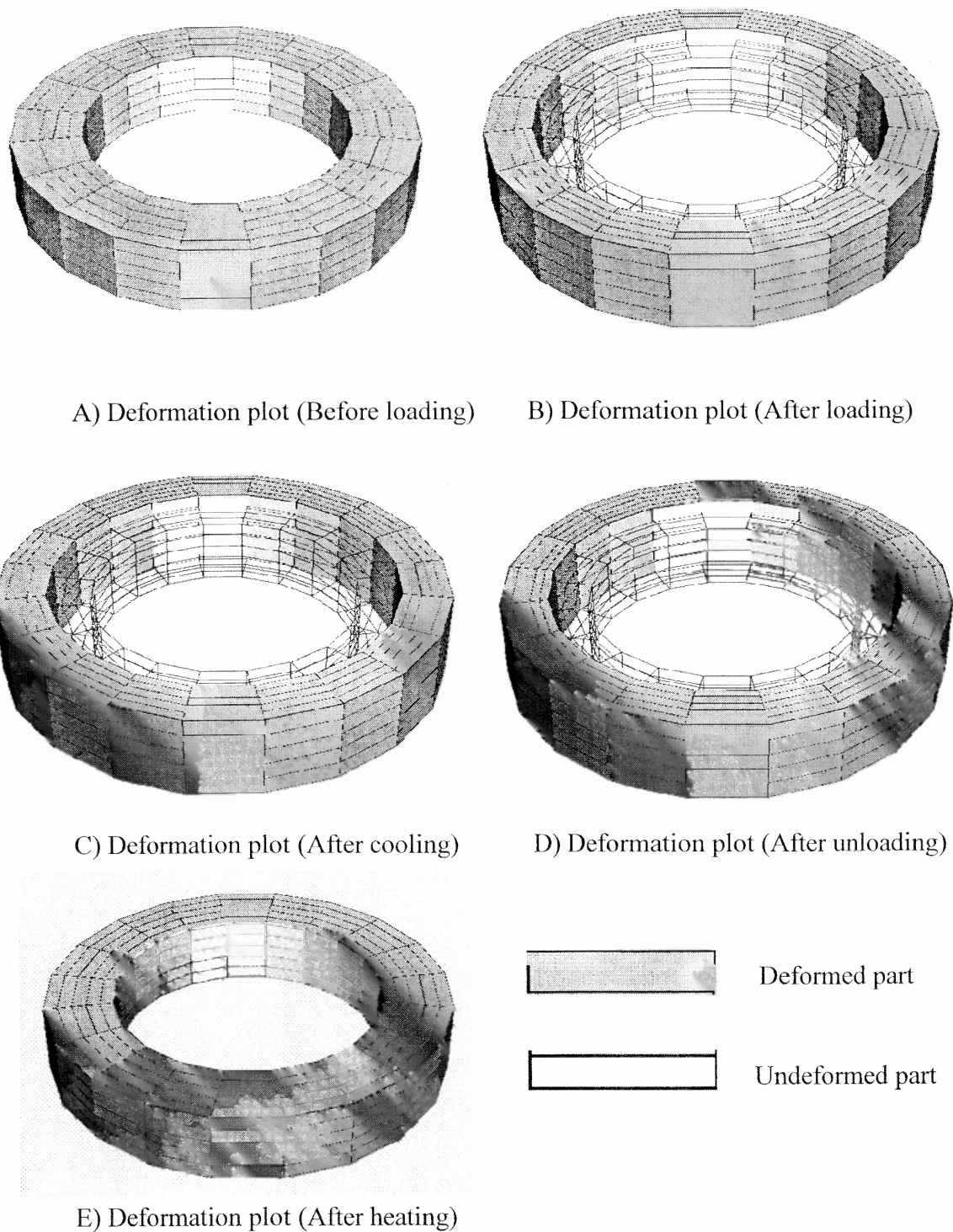
Figure 8.8 Deformation pattern of the hollow cylinder at different stages of the cycle.

8.3   Twisting of a Hollow Cylinder

8.3.1 Problem Definition and Solution Technique

The same hollow cylindrical geometry is used for this deformation cycle also. In this case, the bottom surface of the cylinder is constrained while an angular rotation is applied at the top surface. These actions will create shearing twisting in cylindrical geometry. As done in the previous problem, keeping the shape fixed, the material is then cooled from inner and outer surfaces of the cylinder to fix this temporary shape. The original shape is recovered by heating the material.

Using the procedure adopted in the previous problem, the analysis can be carried out. However, there will be little change in fourth step only.

Step-4. Apply boundary conditions: Figure 8.9 shows applicable boundary conditions according to the problem definition. Top face of the cylinder is selected for the angular rotation and the bottom surface of the cylinder is constrained in z direction and in angular direction. Linear variation in temperature applied at inner and outer surfaces of the cylinder. For cooling, temperature decreases linearly at both surfaces and for heating, the temperature is increasing at both surfaces.

8.3.2 Results

In this subsection, different results obtained using the post processor module of ABAQUS/CAE are presented. Applying rotation to the upper surface of the hollow cylinder creates a twisting action. The bottom surface is fixed and so no displacement will occur at nodes on that surface while upper surface will have maximum distortion (see Figure 8.10-A). This distortion causes stress inside the material, as shown in Figure 8.11-A. As the cooling process is done keeping the strain constant, there will be no change observed in the displacement plot (Figure 8.10-B). However, reduction in the

stress is observed due to formation of the crystals as shown in Figure 8.11-B. Upon unloading, little strain recovery is observed in the middle region of the hollow cylinder (see Figure 8.10-C) as that region is not as crystalline as the inner and outer surfaces. This is inhomogeneous deformation and crystallinity is not same everywhere due to which strain recovery at each node also varies and irregular stress pattern can be observed (see Figure 8.11-C). Upon heating full strain recovery can be observed (see Figure 8.10 and Figure 8.11).

$$U_{zz} = U_{\theta\theta} = 0$$

$$U_{\theta\theta} = 0.1$$

$$\frac{d\theta}{dt} = 0$$

$$\frac{d\theta}{dt} = -k = \text{constant}$$
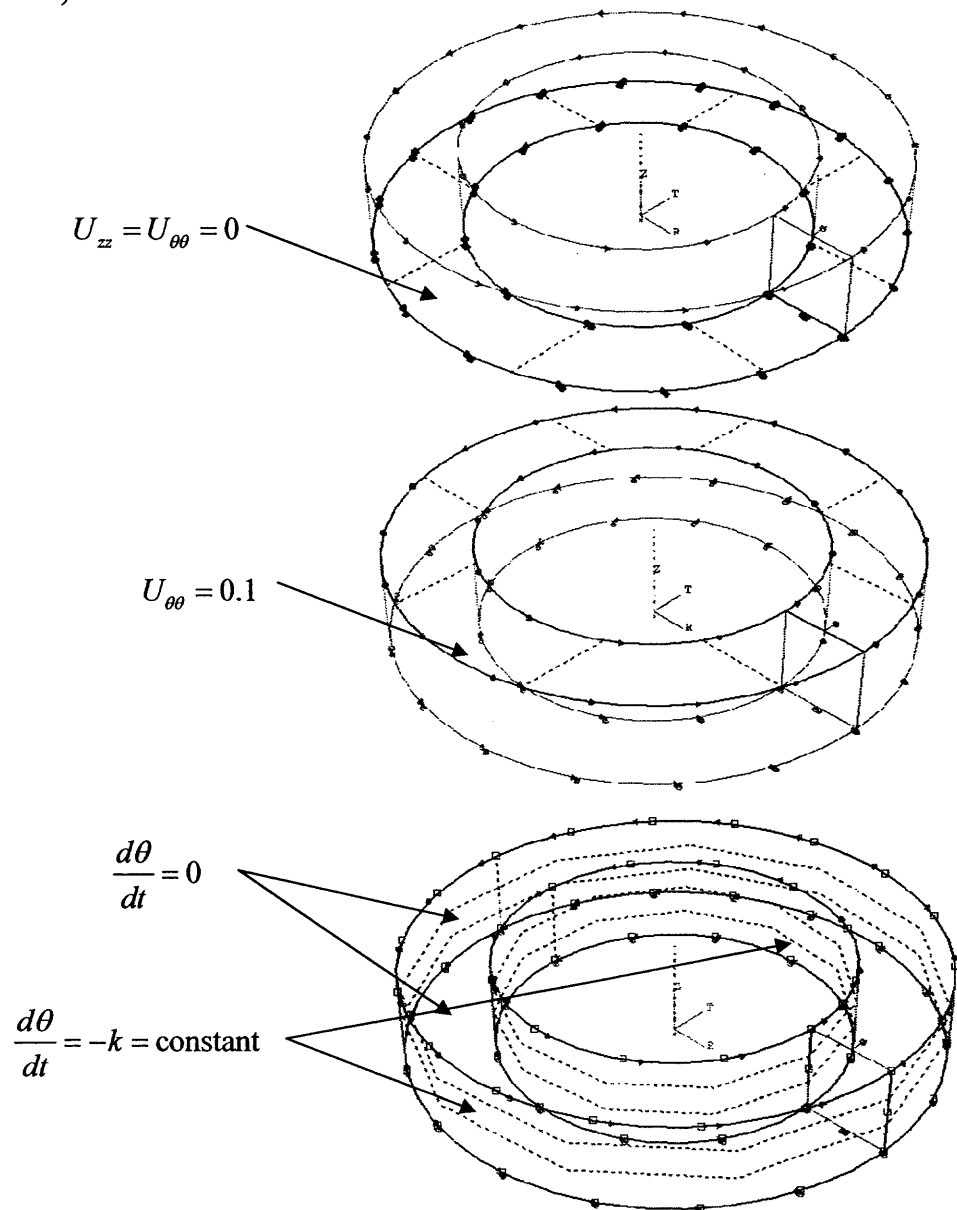
Figure 8.9 Different boundary conditions applicable to the hollow cylinder for twisting action and heat transfer.

A) After loading process   B) After cooling process

C) After unloading process   D) After heating process
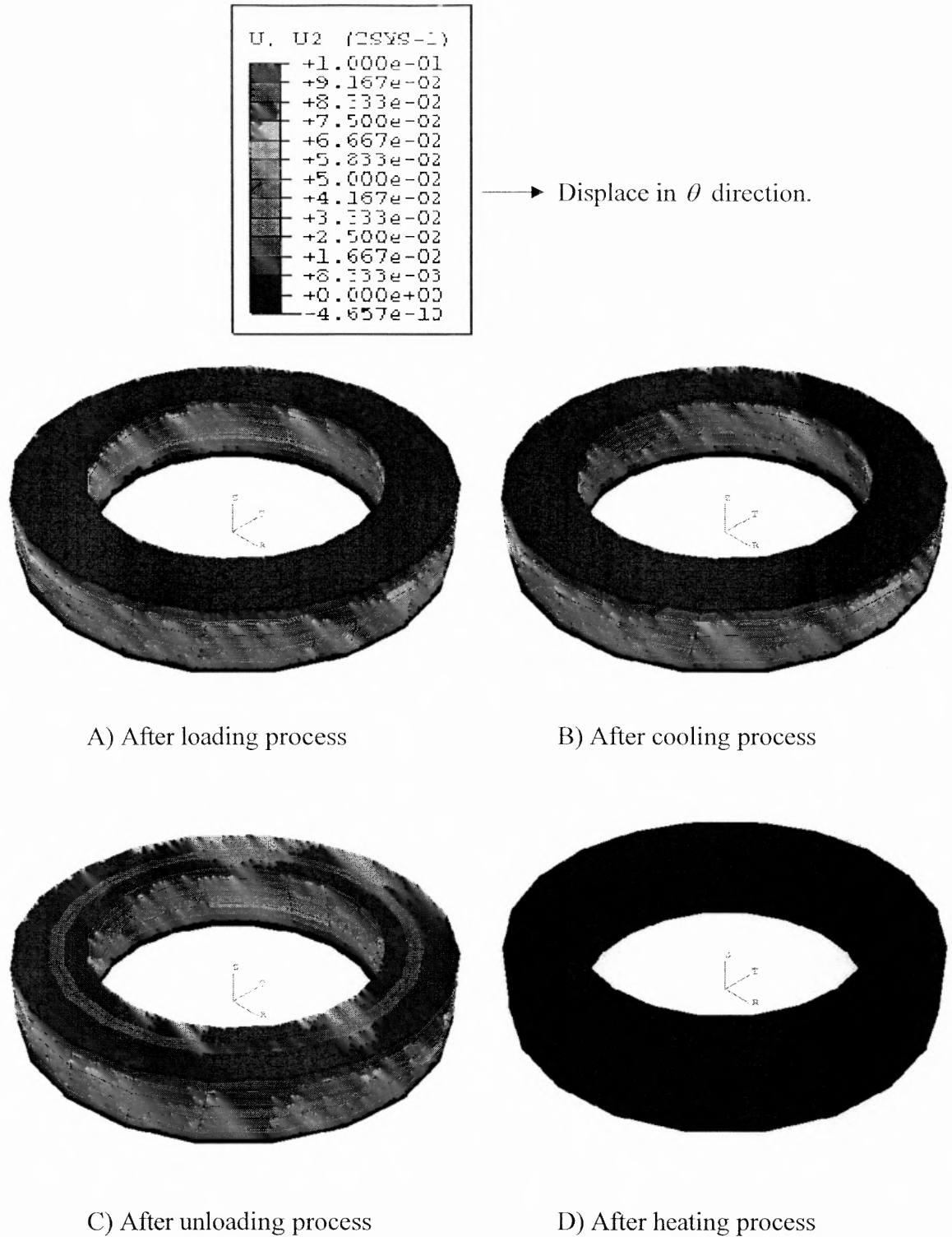
Figure 8.10 Displacement ($U_{\theta\theta}$) fringe plot for the hollow cylinder experiencing twisting moment with cooling and heating effect.

S, Mises
(Ave. Crit.: 75%)
    +2.320e-01
    +2.127e-01
    +1.933e-01
    +1.740e-01
    +1.547e-01
    +1.353e-01
    +1.160e-01
    +9.667e-02
    +7.733e-02
    +5.800e-02
    +3.867e-02
    +1.933e-02
    +0.000e+00

A) After loading process

B) After cooling process

C) After unloading process

D) After heating process
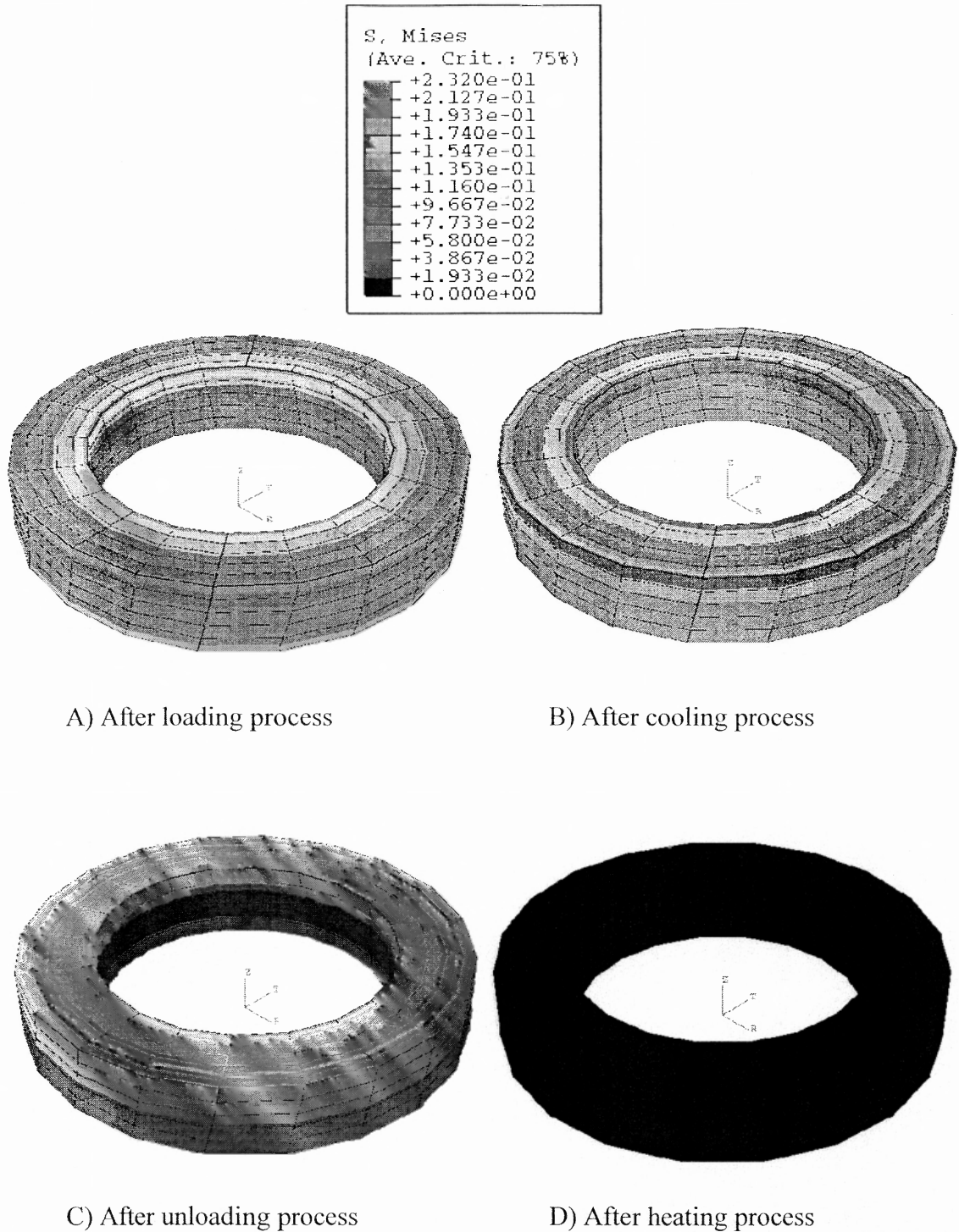
Figure 8.11 von-Mises stress fringe plot for the hollow cylinder experiencing twisting moment with cooling and heating effect.

8.4   Bending of the Thin Strip.

8.4.1 Problem Definition and Solution Technique

As the name suggests, thin strip made of CSMP is object under consideration. The thin strip is simply supported at both ends and at the midpoint of the thin strip; force is applied with the rigid V-shape punch with blunt round edge. Applying force will bend the strip and then the strip is cooled keeping the punch at the same position. The temperature of the strip reduced to -20^0C which is well below the transition temperature (-10^0C). The punch is then slowly brought back to its original position. Strip is then heated back up to 100^0C to get the original shape back. Cooling and heating is done by linearly varying temperature at the front and back surface of the plate (see Figure 8.12).

Following is complete step by step procedure adopted to carry out the finite element analysis of the process.

Step-1. Create a solid model: Using the part module a solid model of the thin strip of the dimension 100mm x 20 mm x 1mm is created (see Figure 8.12) using the extrusion command. Similarly, V-punch with 5mm nose radius is created. To save the computational time punch is considered as analytically solid object.

Step-2. Create a material model: Material module developed for this process is presented in appendix H. Applying this module to the solid model of the thin plate, the material model is constructed.

Step-3. Define processes: A process can be defined in 'step module' of the ABAQUS/CAE. For each process namely: Loading, Cooling/Crystallization, Unloading and Heating; individual step is created. As mentioned above, while cooling the punch is not retracted so that, thin strip will be in bend shape during the process. Punch is then retracted slowly and strip is heated up to 10^0C.

Step-4. Apply boundary conditions: Figure 8.13 shows applicable boundary conditions according to the problem definition. All degrees of freedom are constrained of the two edges on the back surface to create rigid support at the edges. The punch is analytically solid and hence, by applying displacement of 5 mm in Z-direction at the reference point created on the punch, the entire punch can be moved in z-direction. Linearly decreasing temperature boundary condition was applied to the front and back surfaces (as shown in Figure 8.12) for cooling the strip. For heating, the temperature variation is linear and increasing at the same surfaces.

Step-5 and step-6 are similar to those of in previous tests.
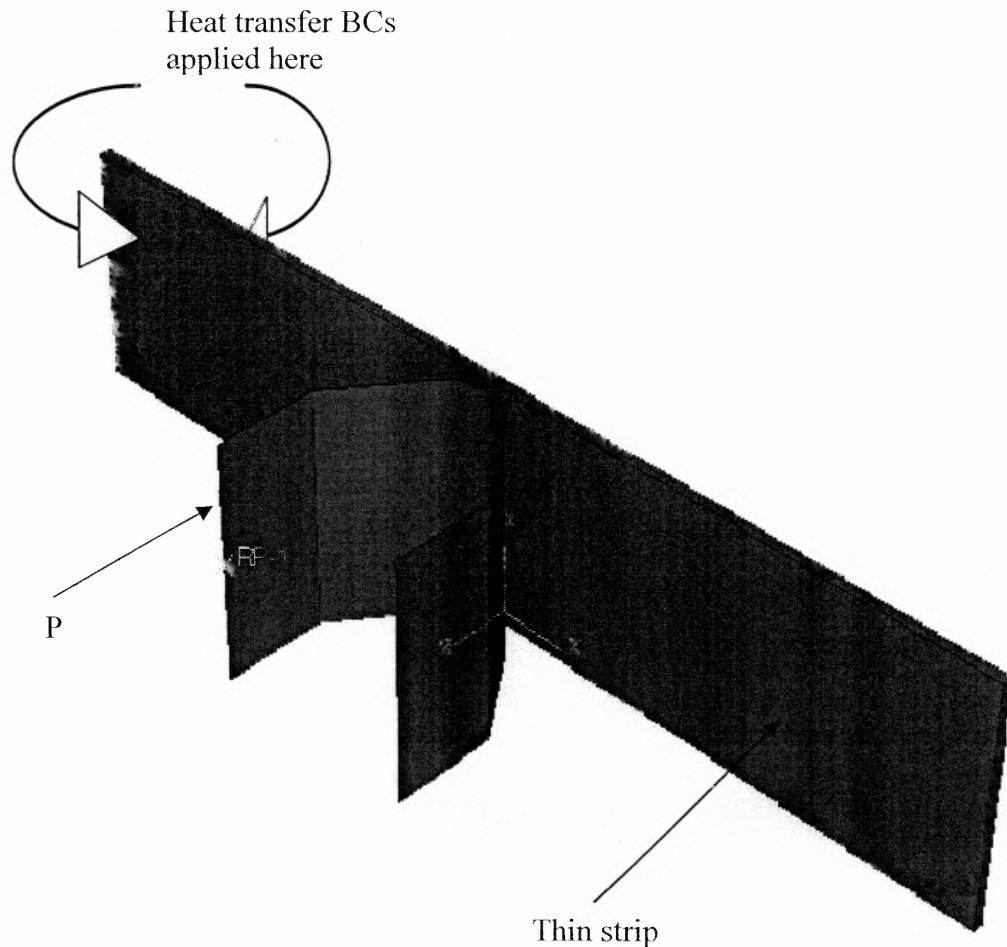
Figure 8.12 An assembly of the solid models of thin plate and the punch designed for simple bending test.

8.4.2 Results

Even in this deformation cycle also, one can see in Figure 8.14 that as middle region of the plate deforms more, the stress in that region is higher than compare to other region of the plate. Remarkable stress reduction can be observed as the crystal forms while the cooling process. Upon unloading negligible strain recovery happens and due to the variable crystallinity value at each node, and a small value of residual stress can be observed in the material. It is assumed that crystals formed last will melt first and so, upon heating when temperature exceeds transition temperature, crystallinity goes back to zero value at all nodes. As there is no stress in the amorphous region, the material goes back to its original shape.

$$U_{xx} = U_{yy} = U_{zz} = 0$$

$$U_{xx} = U_{yy} = 0,$$
$$U_{zz} = -5.$$
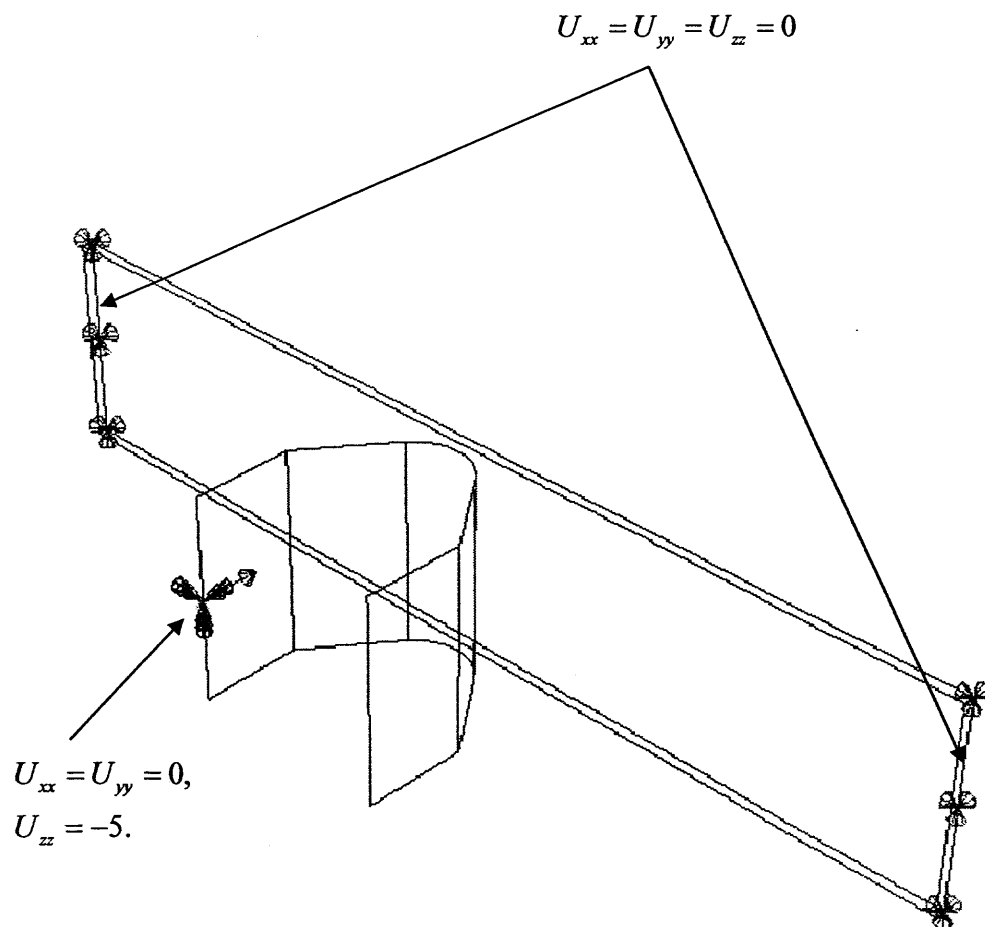
Figure 8.13 Applied boundary conditions to the thin plate and punch, required to perform simple bending test.
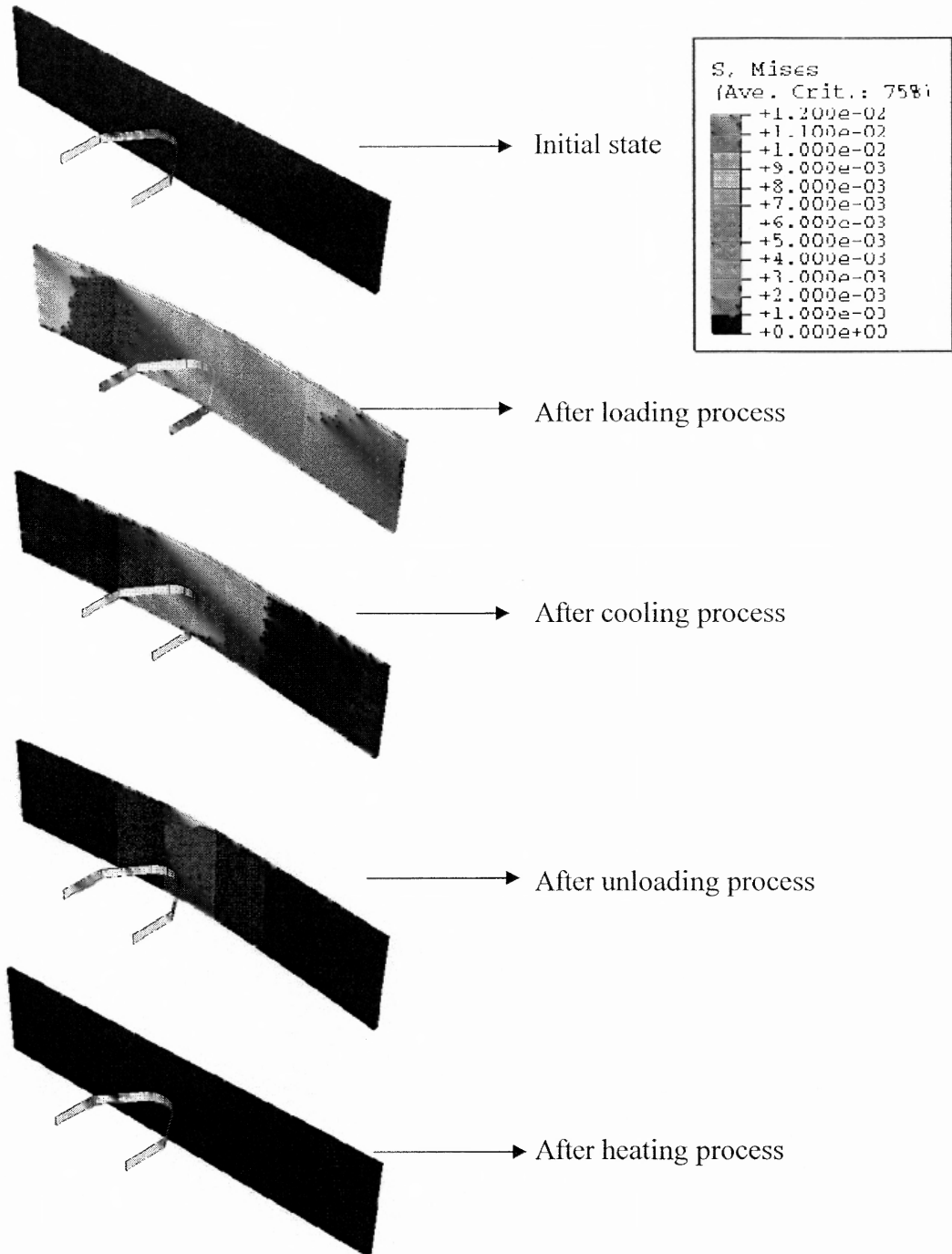
Figure 8.14 Snapshots of von-Mises stress fringe plots taken at various stage of the test.

CHAPTER 9

CONCLUSIONS AND SCOPE OF THE STUDY

9.1   Summary

The principle focus of this research was on developing a three dimensional, frame invariant, constitutive model for crystallizable shape memory polymers with emphasis on mechanics and thermodynamics associated with phase transition, anisotropy and mechanism for the return to the original shape. Toward this purpose, the following have been accomplished and presented in this dissertation:

A general framework has been developed for crystallizable shape memory polymers using the notion of natural configurations of a material and a phenomenological frame work developed for the crystallization in polymers which is flexible enough to accommodate various crystallization kinetic models.

A frame work is extended to model shape fixity of the temporary shape and shape recovery of the original shape by capturing solid to solid phase transition (amorphous phase to semi-crystalline phase and vice versa).

A finite element module for CSMPs is created based on the mathematical model developed for the CSMPs. All required tests are performed to validate the finite element module. Applications of the finite element module are presented by carrying out various simulations for various realistic processes (coupled temperature-displacement processes involving inhomogeneous deformation) those includes use of CSMPs.

In following section, the salient conclusions drawn from the present study are discussed. Following this, recommendations for future work are also listed.

9.2 Conclusions

The evolution of natural configurations of a material and the accompanying dissipation of energy developed in (Rajagopal 1995) provide the very basic theory for the phase transition phenomenon. Based on this theory, (Rao & Rajagopal) developed a framework specifically to model crystallization in polymers. Using these studies now it is possible to derive the constitutive model for the crystallizable shape memory polymers. The constitutive model which can accurately predict the behavior of CSMPs along with the mechanisms that is capable to capture shape fixity and shape recover phenomena, is developed. The anisotropy in the temporary shape due to the presence of crystals formed during the cooling process is also included in the model.

Followings are some basic ideas and theories prescribed by other researchers, essential for carrying out the current work.

- The notion of natural configurations of a material and dissipation of energy. (Rajagopal et al. 1995)

- Phase transition phenomena associated with the crystallization in polymers. (Rao and Rajagopal et al. 2002)

- The linearization and tangent stiffness calculation for the finite element formulation. (Holpzafel et al. 2000)

- Development of user subroutine (UMAT) for simulating realistic processes. (ABAQUS manual)

  The original contributions of the present work are

- A three-dimensional frame invariant constitutive model is presented for the CSMP that incorporates elements of kinematic theories, thermodynamics and polymer science.

- Solid to solid phase transitions (amorphous phase to semi-crystalline phase and vice versa) associated with CSMP's are modeled using the notion of evolving natural configuration and a developed framework for crystallization in polymers.

- Presented mechanisms associated with the shape fixity of the temporary shape and shape recovery of the original shape.

- Incorporated the mechanism responsible for anisotropy caused due to the presence of crystals in the semi-crystalline phase (temporary shape).

- A standard procedure adopted to create finite element module to carry out finite element analysis of non-linear, non-isothermal, coupled temperature-displacement problem.

- Simulated one-dimensional processes in mechanical setting using MATLAB to understand mechanical issues related to derivation of constitutive equation for CSMPs.

- Used MATLAB for simulating non-isothermal one-dimensional process to exhibit the applicability of the derived constitutive equations creating the comprehensive base for more complex study associated with complex geometries and realistic process conditions.

- Created a finite element module based on the current work by writing user subroutine UMAT, UMATHT and SDVINI in FORTRAN. The finite element module is add-on required with ABAQUS/CAE for simulating realistic processes that includes use of CSMPs.

- Performed all required test to validate the developed finite element module for user material (in this case CSMP).

- Illustrated applications of the add-on by simulating processes that are more realistic and require use of advance techniques in computer aided designing and finite element analysis.

9.3   Recommendations for Future Work

The phenomenological constitutive modeling is done at continuum level in this work and finite element analyses of the realistic processes have been carried out. However, issues related to interface is yet needed to be studied. Probably, use of scaling related techniques for modeling will be useful in conjunction with polymer science.

In the current work, some physical, mechanical and thermal properties are assumed independent of temperature and phase associated with. Further improvement in model can be made by addressing these issues.

In every finite element analyses done for the realistic processes, cooling process is assumed to take place at constant strain (shape). The constitutive equation derived is capable enough to handle constant or variable stress cooling processes. However, those simulations require more complex algorithm.

The model prediction is compared with experimental data available in literature, for 1-D processes only. For achieving better reliability more physical testing should be carried out. Results of theses tests should be used for the comparison with model prediction or the results obtained with the finite element solutions. There are some material constants associated with anisotropy in the temporary shape. Those material constants can be found by performing various mechanical tests.

APPENDIX A

DERIVATION OF TANGENT STIFFNESS MATRIX FOR CSMP

In this appendix, methodology to derive the tangent stiffness matrix from the given stored energy function (for hyper elastic material) is shown.

Stored energy function for the semi-crystalline phase can be written as:

$$\psi = \rho_0 \Psi = (1-\alpha)\left\{ C_{10}(\bar{I}_{\kappa_a} - 3) + \frac{1}{D_1}(J_{\kappa_a} - 1)^2 \right\}$$
$$+ (\alpha)\left\{ C_{20}(\bar{I}_{\kappa_{c(t)}} - 3) + \frac{1}{D_2}(J_{\kappa_{c(t)}} - 1)^2 + C_{201}(\bar{J}_1 - 1)^2 + C_{202}(\bar{K}_1 - 1)^2 \right\}$$
(A.1)

We need to find stiffness tensor matrix $\mathbb{C}$ for FEM analysis. ABAQUS need the stiffness matrix prescribed in following format.

$$\mathbb{C} = \frac{1}{J}\frac{\partial \overset{J}{\tau}}{\partial \mathbf{D}}$$
(A.2)

where, $\overset{J}{\tau}$ is Jaw-man rate of Kirchoff stress defined as:

$$\overset{J}{\tau} = \dot{\tau} - \mathbf{W}\tau - \tau\mathbf{W}^T$$
$$= \dot{J}\sigma + J\dot{\sigma} - J\mathbf{W}\sigma - J\sigma\mathbf{W}^T$$
$$= \dot{J}\sigma + J\overset{J}{\sigma}.$$
(A.3)

Putting (2) into (1) we get

$$\mathbb{C} = \sigma \otimes \mathbf{I} + \frac{\partial \overset{J}{\sigma}}{\partial \mathbf{D}}$$
(A.4)

Hence, to find $\mathbb{C}$ we need to find σ first that can be defined as:

$$\sigma = \frac{2}{J}\mathbf{F}\frac{\partial \psi}{\partial \mathbf{C}}\mathbf{F}^T.$$
(A.5)

The derivative on right hand can be written as:

$$\frac{\partial \psi}{\partial \mathbf{C}} = (1-\alpha)\left\{ C_{10}\left(\det \mathbf{C}_{\kappa_a}\right)^{-\frac{1}{3}}\left[\mathbf{I} - \frac{-1}{3}tr\mathbf{C}_{\kappa_a}\mathbf{C}_{\kappa_a}^{-T}\right] + \frac{1}{D_1}\left(J_{\kappa_a}\right)\left(J_{\kappa_a}-1\right)\mathbf{C}_{\kappa_a}^{-T}\right\}$$

$$+(\alpha)\left\{\begin{array}{l} C_{20}(\det \mathbf{C}_{\kappa_{c(t)}})^{-\frac{1}{3}}\left[\mathbf{I} - \frac{1}{3}tr\mathbf{C}_{\kappa_{c(t)}}\mathbf{C}_{\kappa_{c(t)}}^{-T}\right] \\ \\ +\frac{1}{D_2}\left(J_{\kappa_{c(t)}}\right)\left(J_{\kappa_{c(t)}}-1\right)\mathbf{C}_{\kappa_{c(t)}}^{-T} + \left(\frac{-2}{3}\right)C_{201}\overline{J}_1\left(\overline{J}_1-1\right)\mathbf{C}_{\kappa_{c(t)}}^{-T} \\ \\ +2C_{201}\left(J_{\kappa_{c(t)}}\right)^{-\frac{2}{3}}\left(\overline{J}_1-1\right)\mathbf{n}_{\kappa_{c(t)}}\otimes\mathbf{n}_{\kappa_{c(t)}} + \left(\frac{-2}{3}\right)C_{202}\overline{K}_1\left(\overline{K}_1-1\right)\mathbf{C}_{\kappa_{c(t)}}^{-T} \\ \\ +2C_{202}\left(J_{\kappa_{c(t)}}\right)^{-\frac{2}{3}}\left(\overline{K}_1-1\right)\mathbf{m}_{\kappa_{c(t)}}\otimes\mathbf{m}_{\kappa_{c(t)}} \end{array}\right\}. \qquad (A.6)$$

Using equation (A.5) and equation (A.6) Cauchy stress tensor can be written as follows:

$$\sigma = (1-\alpha)\left\{\frac{2C_{10}}{J_a}\left[\overline{\mathbf{B}}_{\kappa_a} - \frac{1}{3}tr\overline{\mathbf{B}}_{\kappa_a}\mathbf{I}\right] + \frac{1}{D_1}\left(J_{\kappa_a}-1\right)\mathbf{I}\right\}$$

$$+(\alpha)\left\{\begin{array}{l} \frac{2C_{20}}{J_C}\left[\overline{\mathbf{B}}_{\kappa_{c(t)}} - \frac{1}{3}tr\overline{\mathbf{B}}_{\kappa_{c(t)}}\mathbf{I}\right] + \frac{2}{D_2}\left(J_{\kappa_{c(t)}}-1\right)\mathbf{I} \\ \\ -\left(\frac{4}{3}\right)C_{201}\frac{\overline{J}_1}{J_{\kappa_{c(t)}}}\left(\overline{J}_1-1\right)\mathbf{I} + \frac{4C_{201}}{J_{\kappa_{c(t)}}}\left(\overline{J}_1-1\right)\overline{\mathbf{F}}_{\kappa_{c(t)}}\mathbf{n}_{\kappa_{c(t)}}\otimes\mathbf{n}_{\kappa_{c(t)}}\overline{\mathbf{F}}^T_{\kappa_{c(t)}} \\ \\ -\left(\frac{4}{3}\right)C_{202}\frac{\overline{K}_1}{J_{\kappa_{c(t)}}}\left(\overline{K}_1-1\right)\mathbf{I} + \frac{4C_{202}}{J_{\kappa_{c(t)}}}\left(\overline{K}_1-1\right)\overline{\mathbf{F}}_{\kappa_{c(t)}}\mathbf{m}_{\kappa_{c(t)}}\otimes\mathbf{m}_{\kappa_{c(t)}}\overline{\mathbf{F}}^T_{\kappa_{c(t)}} \end{array}\right\}. \qquad (A.7)$$

To get the Jawman rate of the Cauchy stress, we need to find the material time derivative of the Cauchy stress.

$$\dot{\sigma} = (1-\alpha) \left\{ \begin{array}{l} \dfrac{2C_{10}}{J_{\kappa_a}} \left[\mathbf{L}\overline{\mathbf{B}}_{\kappa_a} + \overline{\mathbf{B}}_{\kappa_a}\mathbf{L}^T - \dfrac{2}{3} tr\mathbf{D}\overline{\mathbf{B}}_{\kappa_a} - \dfrac{2}{3}\overline{\mathbf{B}}_{\kappa_a}\cdot\mathbf{DI} + \dfrac{2}{9} tr\mathbf{D}tr\overline{\mathbf{B}}_{\kappa_a}\mathbf{I} \right] \\[3mm] -\dfrac{1}{J_{\kappa_a}} \left[\overline{\mathbf{B}}_{\kappa_a} - \dfrac{1}{3} tr\overline{\mathbf{B}}_{\kappa_a}\mathbf{I} \right] + \dfrac{2}{D_1} J_{\kappa_a} tr\mathbf{DI} \end{array} \right\}$$

$$+(\alpha) \left\{ \begin{array}{l} \dfrac{2C_{20}}{J_{\kappa_{c(t)}}} \left[\mathbf{L}\overline{\mathbf{B}}_{\kappa_{c(t)}} + \overline{\mathbf{B}}_{\kappa_{c(t)}}\mathbf{L}^T - \dfrac{2}{3} tr\mathbf{D}\overline{\mathbf{B}}_{\kappa_{c(t)}} - \dfrac{2}{3}\overline{\mathbf{B}}_{\kappa_{c(t)}}\cdot\mathbf{DI} + \dfrac{2}{9} tr\mathbf{D}tr\overline{\mathbf{B}}_{\kappa_{c(t)}}\mathbf{I} \right] \\[3mm] -\dfrac{1}{J_{\kappa_{c(t)}}} \left[\overline{\mathbf{B}}_{\kappa_{c(t)}} - \dfrac{1}{3} tr\overline{\mathbf{B}}_{\kappa_{c(t)}}\mathbf{I} \right] + \dfrac{2}{D_2} J_{\kappa_{c(t)}} tr\mathbf{DI} \\[3mm] -\left(\dfrac{4}{3}\right)C_{201}\left(\dfrac{-1}{J_{\kappa_{c(t)}}}\right)\overline{J}_1\left(\overline{J}_1-1\right)tr\mathbf{DI} \\[3mm] -\left(\dfrac{4}{3}\right)C_{201}\left(\dfrac{2}{J_{\kappa_{c(t)}}}\right)\left(2\overline{J}_1-1\right)\left(\mathbf{n}_{\kappa_{c(t)}}\cdot\left[\overline{\mathbf{C}}_{\kappa_{c(t)}}\mathbf{D}+\overline{\mathbf{F}}_{\kappa_{c(t)}}^T\mathbf{D}\overline{\mathbf{F}}_{\kappa_{c(t)}}\right]\mathbf{n}_{\kappa_{c(t)}} - \dfrac{1}{3}tr\mathbf{D}\overline{J}_1\right)\mathbf{I} \\[3mm] +4C_{201}\left(\dfrac{-5}{3}\right)\dfrac{\left(\overline{J}_1-1\right)}{J_{\kappa_{c(t)}}}\overline{\mathbf{F}}_{\kappa_{c(t)}}\mathbf{n}_{\kappa_{c(t)}}\otimes\mathbf{n}_{\kappa_{c(t)}}\overline{\mathbf{F}}_{\kappa_{c(t)}}^T tr\mathbf{DI} \\[3mm] +4C_{201}\left(\dfrac{2}{J_{\kappa_{c(t)}}}\right)\left[\mathbf{n}_{\kappa_{c(t)}}\cdot\left(\overline{\mathbf{C}}_{\kappa_{c(t)}}\mathbf{D}+\overline{\mathbf{F}}_{\kappa_{c(t)}}^T\mathbf{D}\overline{\mathbf{F}}_{\kappa_{c(t)}}\right)\mathbf{n}_{\kappa_{c(t)}} - \dfrac{1}{3}tr\mathbf{D}\overline{J}_1\right]\overline{\mathbf{F}}_{\kappa_{c(t)}}\mathbf{n}_{\kappa_{c(t)}}\otimes\mathbf{n}_{\kappa_{c(t)}}\overline{\mathbf{F}}_{\kappa_{c(t)}}^T \\[3mm] +4C_{201}\left(\dfrac{1}{J_{\kappa_{c(t)}}}\right)\left(\overline{J}_1-1\right)\left[\begin{array}{l}\mathbf{L}\overline{\mathbf{F}}_{\kappa_{c(t)}}\mathbf{n}_{\kappa_{c(t)}}\otimes\mathbf{n}_{\kappa_{c(t)}}\overline{\mathbf{F}}_{\kappa_{c(t)}}^T + \overline{\mathbf{F}}_{\kappa_{c(t)}}\mathbf{Ln}_{\kappa_{c(t)}}\otimes\mathbf{n}_{\kappa_{c(t)}}\overline{\mathbf{F}}_{\kappa_{c(t)}}^T \\[2mm] +\overline{\mathbf{F}}_{\kappa_{c(t)}}\mathbf{n}_{\kappa_{c(t)}}\otimes\mathbf{Ln}_{\kappa_{c(t)}}\overline{\mathbf{F}}_{\kappa_{c(t)}}^T + \overline{\mathbf{F}}_{\kappa_{c(t)}}\mathbf{n}_{\kappa_{c(t)}}\otimes\mathbf{n}_{\kappa_{c(t)}}\overline{\mathbf{F}}_{\kappa_{c(t)}}^T\mathbf{L}^T\end{array}\right] \\[3mm] -\left(\dfrac{4}{3}\right)C_{202}\left(\dfrac{-1}{J_{\kappa_{c(t)}}}\right)\overline{K}_1\left(\overline{K}_1-1\right)tr\mathbf{DI} \\[3mm] -\left(\dfrac{4}{3}\right)C_{202}\left(\dfrac{2}{J_{\kappa_{c(t)}}}\right)\left(2\overline{K}_1-1\right)\left[\mathbf{m}_{\kappa_{c(t)}}\cdot\left[\overline{\mathbf{C}}_{\kappa_{c(t)}}\mathbf{D}+\overline{\mathbf{F}}_{\kappa_{c(t)}}^T\mathbf{D}\overline{\mathbf{F}}_{\kappa_{c(t)}}\right]\mathbf{m}_{\kappa_{c(t)}} - \dfrac{1}{3}tr\mathbf{D}\overline{K}_1\right]\mathbf{I} \\[3mm] +4C_{202}\left(\dfrac{-5}{3}\right)\dfrac{\left(\overline{K}_1-1\right)}{J_{\kappa_{c(t)}}}\overline{\mathbf{F}}_{\kappa_{c(t)}}\mathbf{m}_{\kappa_{c(t)}}\otimes\mathbf{m}_{\kappa_{c(t)}}\overline{\mathbf{F}}_{\kappa_{c(t)}}^T tr\mathbf{DI} \\[3mm] +4C_{202}\left(\dfrac{2}{J_{\kappa_{c(t)}}}\right)\left[\mathbf{m}_{\kappa_{c(t)}}\cdot\left(\overline{\mathbf{C}}_{\kappa_{c(t)}}\mathbf{D}+\overline{\mathbf{F}}_{\kappa_{c(t)}}^T\mathbf{D}\overline{\mathbf{F}}_{\kappa_{c(t)}}\right)\mathbf{m}_{\kappa_{c(t)}} - \dfrac{1}{3}tr\mathbf{D}\overline{K}_1\right]\overline{\mathbf{F}}_{\kappa_{c(t)}}\mathbf{m}_{\kappa_{c(t)}}\otimes\mathbf{m}_{\kappa_{c(t)}}\overline{\mathbf{F}}_{\kappa_{c(t)}}^T \\[3mm] +4C_{202}\left(\dfrac{1}{J_{\kappa_{c(t)}}}\right)\left(\overline{J}_1-1\right)\left[\begin{array}{l}\mathbf{L}\overline{\mathbf{F}}_{\kappa_{c(t)}}\mathbf{m}_{\kappa_{c(t)}}\otimes\mathbf{m}_{\kappa_{c(t)}}\overline{\mathbf{F}}_{\kappa_{c(t)}}^T + \overline{\mathbf{F}}_{\kappa_{c(t)}}\mathbf{Lm}_{\kappa_{c(t)}}\otimes\mathbf{m}_{\kappa_{c(t)}}C^T \\[2mm] +\overline{\mathbf{F}}_{\kappa_{c(t)}}\mathbf{m}_{\kappa_{c(t)}}\otimes\mathbf{Lm}_{\kappa_{c(t)}}\overline{\mathbf{F}}_{\kappa_{c(t)}}^T + \overline{\mathbf{F}}_{\kappa_{c(t)}}\mathbf{m}_{\kappa_{c(t)}}\otimes\mathbf{m}_{\kappa_{c(t)}}C^T\mathbf{L}^T\end{array}\right] \end{array} \right\}$$

(A.8)

Using equation(A.3) Jawman rate of Cauchy stress tensor can be written as:

$$\overset{J}{\sigma} = (1-\alpha)\left\{\frac{2C_{10}}{J_{\kappa_a}}\left(\mathbf{D}\overline{\mathbf{B}}_{\kappa_a} + \overline{\mathbf{B}}_{\kappa_a}\mathbf{D} - \frac{2}{3}tr\mathbf{D}\overline{\mathbf{B}}_{\kappa_a} - \frac{2}{3}\overline{\mathbf{B}}_{\kappa_a}\cdot\mathbf{DI} + \frac{2}{9}tr\mathbf{D}tr\overline{\mathbf{B}}_{\kappa_a}\mathbf{I}\right) + \left(\frac{2}{D_2}\right)\left(2J_{\kappa_a}-1\right)tr\mathbf{DI}\right\}$$

$$+(\alpha)\left\{\begin{array}{l}\dfrac{2C_{20}}{J_{\kappa_{c(t)}}}\left(\mathbf{D}\overline{\mathbf{B}}_{\kappa_{c(t)}} + \overline{\mathbf{B}}_{\kappa_{c(t)}}\mathbf{D} - \dfrac{2}{3}tr\mathbf{D}\overline{\mathbf{B}}_{\kappa_{c(t)}} - \dfrac{2}{3}\overline{\mathbf{B}}_{\kappa_{c(t)}}\cdot\mathbf{DI} + \dfrac{2}{9}tr\mathbf{D}tr\overline{\mathbf{B}}_{\kappa_{c(t)}}\mathbf{I}\right) \\[3mm] +\left(\dfrac{-4}{3}\right)C_{201}\dfrac{2}{J_{\kappa_{c(t)}}}\left(2\overline{J}_1-1\right)\left(\mathbf{n}_{\kappa_{c(t)}}\cdot\left[\overline{\mathbf{C}}_{\kappa_{c(t)}}\mathbf{D}+\overline{\mathbf{F}}^T_{\kappa_{c(t)}}\mathbf{D}\overline{\mathbf{F}}_{\kappa_{c(t)}}\right]\mathbf{n}_{\kappa_{c(t)}} - \dfrac{1}{3}tr\mathbf{D}\overline{J}_1\right)\mathbf{I} \\[3mm] +\left(\dfrac{-4}{3}\right)C_{202}\dfrac{2}{J_{\kappa_{c(t)}}}\left(2\overline{K}_1-1\right)\left(\mathbf{m}_{\kappa_{c(t)}}\cdot\left[\overline{\mathbf{C}}_{\kappa_{c(t)}}\mathbf{D}+\overline{\mathbf{F}}^T_{\kappa_{c(t)}}\mathbf{D}\overline{\mathbf{F}}_{\kappa_{c(t)}}\right]\mathbf{m}_{\kappa_{c(t)}} - \dfrac{1}{3}tr\mathbf{D}\overline{K}_1\right)\mathbf{I} \\[3mm] +\dfrac{8C_{201}}{J_{\kappa_{c(t)}}}\left(\mathbf{n}_{\kappa_{c(t)}}\cdot\left[\overline{\mathbf{C}}_{\kappa_{c(t)}}\mathbf{D}+\overline{\mathbf{F}}^T_{\kappa_{c(t)}}\mathbf{D}\overline{\mathbf{F}}_{\kappa_{c(t)}}\right]\mathbf{n}_{\kappa_{c(t)}} - \dfrac{1}{3}tr\mathbf{D}\overline{J}_1\right)\overline{\mathbf{F}}_{\kappa_{c(t)}}\mathbf{n}_{\kappa_{c(t)}}\otimes\mathbf{n}_{\kappa_{c(t)}}\overline{\mathbf{F}}^T_{\kappa_{c(t)}} \\[3mm] +\dfrac{8C_{202}}{J_{\kappa_{c(t)}}}\left(\mathbf{m}_{\kappa_{c(t)}}\cdot\left[\overline{\mathbf{C}}_{\kappa_{c(t)}}\mathbf{D}+\overline{\mathbf{F}}^T_{\kappa_{c(t)}}\mathbf{D}\overline{\mathbf{F}}_{\kappa_{c(t)}}\right]\mathbf{m}_{\kappa_{c(t)}} - \dfrac{1}{3}tr\mathbf{D}\overline{K}_1\right)\overline{\mathbf{F}}_{\kappa_{c(t)}}\mathbf{m}_{\kappa_{c(t)}}\otimes\mathbf{m}_{\kappa_{c(t)}}\overline{\mathbf{F}}^T_{\kappa_{c(t)}} \\[3mm] +\dfrac{4C_{201}}{J_{\kappa_{c(t)}}}\left(\overline{J}_1-1\right)\left[\begin{array}{l}\mathbf{D}\overline{\mathbf{F}}_{\kappa_{c(t)}}\mathbf{n}_{\kappa_{c(t)}}\otimes\mathbf{n}_{\kappa_{c(t)}}\overline{\mathbf{F}}^T_{\kappa_{c(t)}} + \overline{\mathbf{F}}_{\kappa_{c(t)}}\mathbf{Ln}_{\kappa_{c(t)}}\otimes\mathbf{n}_{\kappa_{c(t)}}\overline{\mathbf{F}}^T_{\kappa_{c(t)}} \\ +\overline{\mathbf{F}}_{\kappa_{c(t)}}\mathbf{n}_{\kappa_{c(t)}}\otimes\mathbf{Ln}_{\kappa_{c(t)}}\overline{\mathbf{F}}^T_{\kappa_{c(t)}} + \overline{\mathbf{F}}_{\kappa_{c(t)}}\mathbf{n}_{\kappa_{c(t)}}\otimes\mathbf{n}_{\kappa_{c(t)}}\overline{\mathbf{F}}^T_{\kappa_{c(t)}}\mathbf{D}\end{array}\right] \\[3mm] +\dfrac{4C_{202}}{J}\left(\overline{K}_1-1\right)\left[\begin{array}{l}\mathbf{D}\overline{\mathbf{F}}_{\kappa_{c(t)}}\mathbf{m}_{\kappa_{c(t)}}\otimes\mathbf{m}_{\kappa_{c(t)}}\overline{\mathbf{F}}^T_{\kappa_{c(t)}} + \overline{\mathbf{F}}_{\kappa_{c(t)}}\mathbf{Lm}_{\kappa_{c(t)}}\otimes\mathbf{m}_{\kappa_{c(t)}}\overline{\mathbf{F}}^T_{\kappa_{c(t)}} \\ +\overline{\mathbf{F}}_{\kappa_{c(t)}}\mathbf{m}_{\kappa_{c(t)}}\otimes\mathbf{Lm}_{\kappa_{c(t)}}\overline{\mathbf{F}}^T_{\kappa_{c(t)}} + \overline{\mathbf{F}}_{\kappa_{c(t)}}\mathbf{m}_{\kappa_{c(t)}}\otimes\mathbf{m}_{\kappa_{c(t)}}\overline{\mathbf{F}}^T_{\kappa_{c(t)}}\mathbf{D}\end{array}\right] \\[3mm] +\left(\dfrac{-4}{3}\right)C_{201}tr\mathbf{D}\left(\dfrac{1}{J_{\kappa_{c(t)}}}\right)\left(\overline{J}_1-1\right)\overline{\mathbf{F}}_{\kappa_{c(t)}}\mathbf{n}_{\kappa_{c(t)}}\otimes\mathbf{n}_{\kappa_{c(t)}}\overline{\mathbf{F}}^T_{\kappa_{c(t)}} \\[3mm] +\left(\dfrac{-4}{3}\right)C_{202}tr\mathbf{D}\left(\dfrac{1}{J_{\kappa_{c(t)}}}\right)\left(\overline{K}_1-1\right)\overline{\mathbf{F}}_{\kappa_{c(t)}}\mathbf{m}_{\kappa_{c(t)}}\otimes\mathbf{m}_{\kappa_{c(t)}}\overline{\mathbf{F}}^T_{\kappa_{c(t)}} \\[3mm] +\left(\dfrac{2}{D_2}\right)\left(2J_{\kappa_{c(t)}}-1\right)tr\mathbf{DI}\end{array}\right\} -\sigma tr\mathbf{D}$$

(A.9)

Equation(A.9) can be written alternatively using index notations as:

$$\overset{J}{\sigma}_{ij} = (1-\alpha)\left\{\begin{array}{l} A1\left(D_{ip}\overline{B}_{\kappa_{a}PJ} + \overline{B}_{\kappa_{a}ip}D_{pj}\right) + A2D_{pp}\overline{B}_{a_{ij}} \\ + A2\overline{B}_{\kappa_{a}pq}D_{pq}\delta_{ij} + A3D_{pp}\overline{B}_{\kappa_{a}qq}\delta_{ij} + A4D_{pp}\delta_{ij} \end{array}\right\}$$

$$+(\alpha)\left\{\begin{array}{l} A11\left(D_{ip}\overline{B}_{\kappa_{c(t)}PJ} + \overline{B}_{\kappa_{c(t)}ip}D_{pj}\right) + A21D_{pp}\overline{B}_{\kappa_{c(t)}ij} \\ + A21\overline{B}_{\kappa_{c(t)}pq}D_{pq}\delta_{ij} + A31D_{pp}\overline{B}_{c_{qq}}\delta_{ij} + A41D_{pp}\delta_{ij} \end{array}\right\}$$

$$+(\alpha)\left\{\begin{array}{l} A5cn_{p}D_{pq}n_{q}\delta_{ij} + A5fn_{p}D_{pq}fn_{q}\delta_{ij} + A6D_{pp}\delta_{ij} \\ + A51cm_{p}D_{pq}m_{q}\delta_{ij} + A51fm_{p}D_{pq}fm_{q}\delta_{ij} + A61D_{pp}\delta_{ij} \end{array}\right\} \quad (A.10)$$

$$+(\alpha)\left\{A7D_{pp}FNF_{ij} + A71D_{pp}FMF_{ij}\right\}$$

$$+(\alpha)\left\{\begin{array}{l} A8cn_{p}D_{pq}n_{q}FNF_{ij} + A8fn_{p}D_{pq}fn_{q}\delta_{ij} + A9D_{pp}FNF_{ij} \\ + A81cm_{p}D_{pq}m_{q}FNF_{ij} + A81fm_{p}D_{pq}fm_{q}\delta_{ij} + A91D_{pp}FMF_{ij} \end{array}\right\}$$

$$+(\alpha)\left\{\begin{array}{l} A10D_{ip}FNF_{pj} + A10F_{ip}D_{pq}NFT_{qj} + A10FN_{ip}D_{pq}F^{T}_{qj} + A10FNF_{ip}D_{pj} \\ + A101D_{ip}FMF_{pj} + A101F_{ip}D_{pq}MFT_{qj} + A101FM_{ip}D_{pq}F^{T}_{qj} + A101FMF_{ip}D_{pj} \end{array}\right\},$$

Where,

$$cn = \overline{\mathbf{C}}_{\kappa_{c(t)}}\mathbf{n}_{\kappa_{c(t)}}$$

$$cm = \overline{\mathbf{C}}_{\kappa_{c(t)}}\mathbf{m}_{\kappa_{c(t)}}$$

$$fn = \overline{\mathbf{F}}_{\kappa_{c(t)}}\mathbf{n}_{\kappa_{c(t)}}$$

$$fm = \overline{\mathbf{F}}_{\kappa_{c(t)}}\mathbf{m}_{\kappa_{c(t)}}$$

$$FNF = \overline{\mathbf{F}}_{\kappa_{c(t)}}\mathbf{n}_{\kappa_{c(t)}} \otimes \mathbf{n}_{\kappa_{c(t)}}\overline{\mathbf{F}}_{c}^{T}$$

$$FMF = \overline{\mathbf{F}}_{\kappa_{c(t)}}\mathbf{m}_{\kappa_{c(t)}} \otimes \mathbf{m}_{\kappa_{c(t)}}\overline{\mathbf{F}}_{c}^{T}$$

$$NFT = \mathbf{n}_{\kappa_{c(t)}} \otimes \mathbf{n}_{\kappa_{c(t)}}\overline{\mathbf{F}}_{c}^{T}$$

$$MFT = \mathbf{m}_{\kappa_{c(t)}} \otimes \mathbf{m}_{\kappa_{c(t)}}\overline{\mathbf{F}}_{c}^{T}$$

$$FN = \overline{\mathbf{F}}_{\kappa_{c(t)}}\mathbf{n}_{\kappa_{c(t)}} \otimes \mathbf{n}_{\kappa_{c(t)}}$$

$$FM = \overline{\mathbf{F}}_{\kappa_{c(t)}}\mathbf{m}_{\kappa_{c(t)}} \otimes \mathbf{m}_{\kappa_{c(t)}}$$

and

$$A1 = \left(\frac{2C_{10}}{J}\right)_{\kappa_a}, \qquad A11 = \left(\frac{2C_{20}}{J}\right)_{\kappa_{c(t)}}, \qquad A2 = \left(\frac{-4}{3}\frac{C_{10}}{J}\right)_{\kappa_a}, \qquad A21 = \left(\frac{-4}{3}\frac{C_{20}}{J}\right)_{\kappa_{c(t)}},$$

$$A3 = \left(\frac{4}{9}\frac{C_{10}}{J}\right)_{\kappa_a}, \qquad A31 = \left(\frac{4}{9}\frac{C_{20}}{J}\right)_{\kappa_{c(t)}}, \qquad A4 = \left(\frac{2}{D_1}\right)\left(2J_{\kappa_a}-1\right), \quad A41 = \left(\frac{2}{D_2}\right)\left(2J_{\kappa_{c(t)}}-1\right),$$

$$A5 = \left(\frac{-8}{3}\right)C_{201}\left(\frac{1}{J}\right)_{\kappa_{c(t)}}\left(2\overline{J}_1-1\right), \qquad A51 = \left(\frac{-8}{3}\right)C_{202}\left(\frac{1}{J}\right)_{\kappa_{c(t)}}\left(2\overline{K}_1-1\right),$$

$$A6 = \left(\frac{8}{9}\right)C_{201}\left(\frac{1}{J}\right)_{\kappa_{c(t)}}\left(2\overline{J}_1-1\right)\overline{J}_1, \qquad A61 = \left(\frac{8}{9}\right)C_{202}\left(\frac{1}{J}\right)_{\kappa_{c(t)}}\left(2\overline{K}_1-1\right)\overline{K}_1,$$

$$A7 = \left(\frac{-8}{3}\right)C_{201}\left(\frac{1}{J}\right)_{\kappa_{c(t)}}\left(\overline{J}_1-1\right), \qquad A71 = \left(\frac{-8}{3}\right)C_{202}\left(\frac{1}{J}\right)_{\kappa_{c(t)}}\left(\overline{K}_1-1\right),$$

$$A8 = (8)\frac{C_{201}}{J}_{\kappa_{c(t)}}, \qquad A81 = (8)\frac{C_{202}}{J}_{\kappa_{c(t)}}, \qquad A9 = \left(\frac{-8}{3}\right)C_{201}\left(\frac{\overline{J}_1}{J}\right)_{\kappa_{c(t)}},$$

$$A91 = \left(\frac{-8}{3}\right)C_{202}\left(\frac{\overline{K}_1}{J}\right)_{\kappa_{c(t)}}, \qquad A10 = (4)C_{201}\frac{\left(\overline{J}_1-1\right)}{J}_{\kappa_{c(t)}}, \qquad A101 = (4)C_{202}\frac{\left(\overline{K}_1-1\right)}{J}_{\kappa_{c(t)}}.$$

Using equation(A.10) in equation(A.4) stiffness matrix in index notation can be prescribed as:

$$\mathbb{C}_{ijkl} = (1-\alpha)\left\{ \begin{array}{l} A1\left(\delta_{ik}\overline{B}_{a_{lj}} + \overline{B}_{a_{ik}}\delta_{jl}\right) + A2\delta_{kl}\overline{B}_{a_{ij}} \\ + A2\overline{B}_{a_{kl}}\delta_{ij} + A3\left(tr\overline{B}_a\right)\delta_{kl}\delta_{ij} + A4\delta_{kl}\delta_{ij} \end{array} \right\}$$

$$+(\alpha)\left\{ \begin{array}{l} A11\left(\delta_{ik}\overline{B}_{c_{lj}} + \overline{B}_{c_{ik}}\delta_{jl}\right) + A21\delta_{kl}\overline{B}_{c_{ij}} \\ + A21\overline{B}_{c_{kl}}\delta_{ij} + A31\left(tr\overline{B}_c\right)\delta_{kl}\delta_{ij} + A41\delta_{kl}\delta_{ij} \end{array} \right\}$$

$$+(\alpha)\left\{ \begin{array}{l} A5cn_kn_l\delta_{ij} + A5fn_kfn_l\delta_{ij} + A6\delta_{kl}\delta_{ij} \\ + A51cm_km_l\delta_{ij} + A51fm_kfm_l\delta_{ij} + A61\delta_{kl}\delta_{ij} \end{array} \right\}$$

$$+(\alpha)\left\{ A7\delta_{kl}FNF_{ij} + A71\delta_{kl}FMF_{ij} \right\}$$

$$+(\alpha)\left\{ \begin{array}{l} A8cn_kn_lFNF_{ij} + A8fn_kfn_lFNF_{ij} + A9\delta_{kl}FNF_{ij} \\ + A81cm_km_lFMF_{ij} + A81fm_kfm_lFMF_{ij} + A91\delta_{kl}FMF_{ij} \end{array} \right\}$$

$$+(\alpha)\left\{ \begin{array}{l} A10\delta_{ik}FNF_{lj} + A10F_{ik}NFT_{lj} \\ + A10FN_{ik}F^T{}_{lj} + A10FNF_{ik}\delta_{lj} \\ + A101\delta_{ik}FMF_{lj} + A101F_{ik}MFT_{lj} \\ + A101FM_{ik}F^T{}_{lj} + A101FMF_{ik}\delta_{lj} \end{array} \right\} \qquad (A.11)$$

APPENDIX B

USER SUBROUTINE (UMAT) FOR ISOTHERMAL PROCESS

This user subroutine is for crystallizable shape memory polymer and it can be used for when it is assumed that crystallization occurs at constant temperature and constant strain.

```fortran
SUBROUTINE UMAT(STRESS,STATEV,DDSDDE,SSE,SPD,SCD,
     1 RPL,DDSDDT,DRPLDE,DRPLDT,STRAN,DSTRAN,
     2 TIME,DTIME,TEMP,DTEMP,PREDEF,DPRED,MATERL,NDI,NSHR,NTENS,
     3 NSTATV,PROPS,NPROPS,COORDS,DROT,PNEWDT,CELENT,
     4 DFGRD0,DFGRD1,NOEL,NPT,KSLAY,KSPT,KSTEP,KINC)
C
      INCLUDE 'ABA_PARAM.INC'
C
      CHARACTER*8 MATERL
      DIMENSION STRESS(NTENS),STATEV(NSTATV),
     1 DDSDDE(NTENS,NTENS),DDSDDT(NTENS),DRPLDE(NTENS),
     2 STRAN(NTENS),DSTRAN(NTENS),DFGRD0(3,3),DFGRD1(3,3),
     3 TIME(2),PREDEF(1),DPRED(1),PROPS(NPROPS),COORDS(3),DROT(3,3)
C
C ---------------------------------------------------------
C
      REAL NN,MM,NNF,MMF,FNN,FMM,FNF,FMF,C1,C2
      DIMENSION FBAR1(3,3),DFGRD2(3,3),FBAR2(3,3),
     1DFG(3,3),FIN(3,3),BAMOR(3,3),BCRY(3,3),BBARN(3,3),BBARP(3,3),
     2VECN(3),VECM(3),CBAR2(3,3),VCN(3),VCM(3),FN(3),FM(3),NN(3,3),
     3MM(3,3),FNN(3,3),FMM(3,3),NNF(3,3),MMF(3,3),FNF(3,3),FMF(3,3),
     4C1(6,6),C2(6,6)

      REAL KRON, TRBAR1, TRBAR2, J1BAR, K1BAR
C
      PARAMETER(ZE=0.D0, ON=1.D0, TW=2.D0, TH=3.D0, FO=4.D0, EI=8.D0,
     1 NI= 9.D0 )
C----------------------------------------------------------------

      C10=PROPS(1)
      D1 =PROPS(2)
      C20=PROPS(3)
      D2 =PROPS(4)
      C201 = PROPS(5)
      C202 = PROPS(6)
C
C
C   Incremental crystallinity dalph
      Dalph = 0.01
      Dalph1 = 0.001


C
C       CHECKING IF INTERMIEDIATE CONFIG NEEDS
C       TO BE INITIALIZED
C
      IF (KSTEP.EQ.2) THEN
```

```fortran
      IF (KINC.EQ.1) THEN

          STATEV(1) = DFGRD1(1,1)
          STATEV(2) = DFGRD1(1,2)
          STATEV(3) = DFGRD1(1,3)
          STATEV(4) = DFGRD1(2,1)
        STATEV(5) = DFGRD1(2,2)
        STATEV(6) = DFGRD1(2,3)
        STATEV(7) = DFGRD1(3,1)
        STATEV(8) = DFGRD1(3,2)
        STATEV(9)=  DFGRD1(3,3)
       ENDIF
          STATEV(10) = STATEV(10) + Dalph
          IF (STATEV(10).GT.0.4) THEN
            STATEV(10) = 0.4
          END IF
       ENDIF
          IF (KSTEP.EQ.4) THEN
        STATEV(10) = STATEV(10) - Dalph
      IF (STATEV(10).LT.0)THEN
       STATEV(10)=0
      END IF
      END IF


      IF (KSTEP.EQ.5) THEN
       STATEV(10) = STATEV(10) - Dalph1
       IF (STATEV(10).LT.0)THEN
        STATEV(10)=0
       END IF
       END IF


C
C       INITIALISING VALUES
C
          DFG(1,1) = STATEV(1)
          DFG(1,2) = STATEV(2)
          DFG(1,3) = STATEV(3)
          DFG(2,1) = STATEV(4)
          DFG(2,2) = STATEV(5)
          DFG(2,3) = STATEV(6)
        DFG(3,1) = STATEV(7)
        DFG(3,2) = STATEV(8)
        DFG(3,3) = STATEV(9)
        ALP = STATEV(10)

C    INVERTING DFG MATRIX
      DETF = DFG(1,1)*(DFG(2,2)*DFG(3,3) - DFG(2,3)*DFG(3,2))
     1      - DFG(1,2)*(DFG(2,1)*DFG(3,3) - DFG(2,3)*DFG(3,1))
     2      + DFG(1,3)*(DFG(2,1)*DFG(3,2) - DFG(2,2)*DFG(3,1))

      FIN(1,1) = (DFG(2,2)*DFG(3,3) - DFG(2,3)*DFG(3,2))/DETF
      FIN(2,1) = -(DFG(2,1)*DFG(3,3) - DFG(2,3)*DFG(3,1))/DETF
      FIN(3,1) = (DFG(2,1)*DFG(3,2) - DFG(2,2)*DFG(3,1))/DETF
      FIN(1,2) = -(DFG(1,2)*DFG(3,3) - DFG(1,3)*DFG(3,2))/DETF
      FIN(2,2) = (DFG(1,1)*DFG(3,3) - DFG(1,3)*DFG(3,1))/DETF
      FIN(3,2) = -(DFG(1,1)*DFG(3,2) - DFG(1,2)*DFG(3,1))/DETF
      FIN(1,3) = (DFG(1,2)*DFG(2,3) - DFG(1,3)*DFG(2,2))/DETF
```

```
      FIN(2,3) = -(DFG(1,1)*DFG(2,3) - DFG(1,3)*DFG(2,1))/DETF
      FIN(3,3) = (DFG(1,1)*DFG(2,2) - DFG(1,2)*DFG(2,1))/DETF
C
C        PRESCRIBING DEF GRAD FOR CRYSTALLINE PHASE
C
      DO  K1 = 1, 3, 1
        DO K2 = 1, 3, 1
          TEMP = ZE
          DO K3 = 1, 3, 1
            TEMP = TEMP + DFGRD1(K1,K3)*FIN(K3,K2)
          END DO
          DFGRD2(K1,K2) = TEMP
        END DO
      END DO
C
C   JACOBIAN AND DISTORTION TENSOR
C
      DET1=DFGRD1(1, 1)*DFGRD1(2, 2)*DFGRD1(3, 3)
     1 -DFGRD1(1, 2)*DFGRD1(2, 1)*DFGRD1(3, 3)
      DET2=DFGRD2(1, 1)*DFGRD2(2, 2)*DFGRD2(3, 3)
     1 -DFGRD2(1, 2)*DFGRD2(2, 1)*DFGRD2(3, 3)
      IF(NSHR.EQ.3) THEN
        DET1=DET1+DFGRD1(1, 2)*DFGRD1(2, 3)*DFGRD1(3, 1)
     1      +DFGRD1(1, 3)*DFGRD1(3, 2)*DFGRD1(2, 1)
     2      -DFGRD1(1, 3)*DFGRD1(3,1)*DFGRD1(2, 2)
     3      -DFGRD1(2, 3)*DFGRD1(3, 2)*DFGRD1(1, 1)
        DET2=DET2+DFGRD2(1, 2)*DFGRD2(2, 3)*DFGRD2(3, 1)
     1      +DFGRD2(1, 3)*DFGRD2(3, 2)*DFGRD2(2, 1)
     2      -DFGRD2(1, 3)*DFGRD2(3,1)*DFGRD2(2, 2)
     3      -DFGRD2(2, 3)*DFGRD2(3, 2)*DFGRD2(1, 1)
      END IF
      STATEV(11) = DET1
      SCALE=DET1**(-ON/TH)
      SCALE2=DET2**(-ON/TH)
      DO K1=1, 3
        DO K2=1, 3
          FBAR1(K2, K1)=SCALE*DFGRD1(K2, K1)
          FBAR2(K2, K1)=SCALE2*DFGRD2(K2, K1)
        END DO
      END DO


C********************************************************************
C   Now, we are finding the directions required for finding J1 and K1
C   for crystalline part which causes orthotropy
C   Directions are n(VECN) & m(VECM)
C        ***** verify  about (1) used in utility subroutine SPRIND
C        ***** (1) is for stress and (2) for strain tensor
C   CALCULATE LEFT CAUCHY-GREEN TENSOR
C
      BAMOR(1,1)=FBAR1(1, 1)**2+FBAR1(1, 2)**2+FBAR1(1, 3)**2
      BAMOR(2,2)=FBAR1(2, 1)**2+FBAR1(2, 2)**2+FBAR1(2, 3)**2
      BAMOR(3,3)=FBAR1(3, 3)**2+FBAR1(3, 1)**2+FBAR1(3, 2)**2
      BAMOR(1,2)=FBAR1(1, 1)*FBAR1(2, 1)+FBAR1(1, 2)*FBAR1(2, 2)
     1      +FBAR1(1, 3)*FBAR1(2, 3)
      BAMOR(2,1) = BAMOR(1,2)
      BCRY(1,1)=FBAR2(1, 1)**2+FBAR2(1, 2)**2+FBAR2(1, 3)**2
      BCRY(2,2)=FBAR2(2, 1)**2+FBAR2(2, 2)**2+FBAR2(2, 3)**2
      BCRY(3,3)=FBAR2(3, 3)**2+FBAR2(3, 1)**2+FBAR2(3, 2)**2
```

```fortran
      BCRY(1,2)=FBAR2(1, 1)*FBAR2(2, 1)+FBAR2(1, 2)*FBAR2(2, 2)
     1     +FBAR2(1, 3)*FBAR2(2, 3)
      BCRY(2,1) = BCRY(1,2)
      BAMOR(1,3) = 0.D0
      BAMOR(2,3) = 0.D0
      BAMOR(3,1) = 0.D0
      BAMOR(3,2) = 0.D0
      BCRY(1,3) = 0.D0
      BCRY(2,3) = 0.D0
      BCRY(3,1) = 0.D0
      BCRY(3,2) = 0.D0
      IF(NSHR.EQ.3) THEN
       BAMOR(1,3)=FBAR1(1, 1)*FBAR1(3, 1)+FBAR1(1, 2)*FBAR1(3, 2)
     1     +FBAR1(1, 3)*FBAR1(3, 3)
       BAMOR(3,1) = BAMOR(1,3)
       BAMOR(2,3)=FBAR1(2, 1)*FBAR1(3, 1)+FBAR1(2, 2)*FBAR1(3, 2)
     1     +FBAR1(2, 3)*FBAR1(3, 3)
       BAMOR(3,2) = BAMOR(2,3)
       BCRY(1,3)=FBAR2(1, 1)*FBAR2(3, 1)+FBAR2(1, 2)*FBAR2(3, 2)
     1     +FBAR2(1, 3)*FBAR2(3, 3)
       BCRY(3,1) = BCRY(1,3)
       BCRY(2,3)=FBAR2(2, 1)*FBAR2(3, 1)+FBAR2(2, 2)*FBAR2(3, 2)
     1     +FBAR2(2, 3)*FBAR2(3, 3)
       BCRY(3,2) = BCRY(2,3)
      END IF

C
C*****************************************************************
C   Calculating the CBAR2
      CBAR2(1,1)=FBAR2(1,1)**2+FBAR2(2,1)**2+FBAR2(3,1)**2
      CBAR2(2,2)=FBAR2(1,2)**2+FBAR2(2,2)**2+FBAR2(3,2)**2
      CBAR2(3,3)=FBAR2(1,3)**2+FBAR2(2,3)**2+FBAR2(3,3)**2
      CBAR2(1,2)=FBAR2(1,1)*FBAR2(1,2)+FBAR2(2,1)*FBAR2(2,2)
     1     +FBAR2(3,1)*FBAR2(3,2)
      CBAR2(2,1)= CBAR2(1,2)
      CBAR2(1,3) = 0.D0
      CBAR2(2,3) = 0.D0
      CBAR2(3,1) = 0.D0
      CBAR2(3,2) = 0.D0
      IF(NSHR.EQ.3) THEN
       CBAR2(1,3)=FBAR2(1,1)*FBAR2(1,3)+FBAR2(2,1)*FBAR2(2,3)
     1     +FBAR2(3,1)*FBAR2(3,3)
       CBAR2(3,1) = CBAR2(1,3)
       CBAR2(2,3)=FBAR2(1,2)*FBAR2(1,3)+FBAR2(2,2)*FBAR2(2,3)
     1     +FBAR2(3,2)*FBAR2(3,3)
       CBAR2(3,2) = CBAR2(2,3)
      END IF

C*****************************************************************
      CALL SPRIND (BAMOR, BBARP, BBARN, 1, NDI, NSHR)
      DO K1 = 1,3,1
        VECN(K1) = BBARN(K1,2)
        VECM(K1) = BBARN(K1,3)
      END DO
C*****************************************************************
C*****************************************************************
C   Finding scalars based on findings above. J1BAR, K1BAR and TRBAR1
      TRBAR1 = BAMOR(1,1) + BAMOR(2,2) + BAMOR(3,3)
```

```
      TRBAR2 = BCRY(1,1) + BCRY(2,2) + BCRY(3,3)
      J1BAR = ZE
      K1BAR = ZE
      DO K1 = 1, 3
        J1BAR = J1BAR + VECN(K1)*(CBAR2(K1,1)*VECN(1)
     1         + CBAR2(K1,2)*VECN(2) + CBAR2(K1,3)*VECN(3))
        K1BAR = K1BAR + VECM(K1)*(CBAR2(K1,1)*VECM(1)
     1         + CBAR2(K1,2)*VECM(2) + CBAR2(K1,3)*VECM(3))
      END DO
C*****************************************************************
C    Finding required vectors for DDSDDE
C     VCN = Cn, VCM= Cm, FM = Fm, FN = Fn
      DO K1 = 1, 3
        VCN(K1) = CBAR2(K1,1)*VECN(1) + CBAR2(K1,2)*VECN(2)
     1       + CBAR2(K1,3)*VECN(3)
        VCM(K1) = CBAR2(K1,1)*VECM(1) + CBAR2(K1,2)*VECM(2)
     1       + CBAR2(K1,3)*VECM(3)
        FN(K1) = FBAR2(K1,1)*VECN(1) + FBAR2(K1,2)*VECN(2)
     1       + FBAR2(K1,3)*VECN(3)
        FM(K1) = FBAR2(K1,1)*VECM(1) + FBAR2(K1,2)*VECM(2)
     1       + FBAR2(K1,3)*VECM(3)
      END DO
CC****************************************************************
CC****************************************************************
CC    Some more tensors useful in calculating DDSDDE
CC    NN = n*n, MM = m*m, FNF = Fn*nF', FMF = Fm*mF', NNF = n*nF'
CC     MMF = m*mF', FNN = Fn*n, FMM = Fm*m
CC**************************************

      DO K1 = 1, 3
        DO K2 = 1, 3
          NN(K1,K2) = VECN(K1)*VECN(K2)
          MM(K1,K2) = VECM(K1)*VECM(K2)
        END DO
      END DO
CC**************************************
      DO K1 = 1, 3
        DO K2 = 1, 3
          TEMP1 = ZE
          TEMP2 = ZE
          TEMP3 = ZE
          TEMP4 = ZE
          DO K3 = 1, 3
            TEMP1 = TEMP1 + NN(K1,K3)*FBAR2(K2,K3)
            TEMP2 = TEMP2 + MM(K1,K3)*FBAR2(K2,K3)
            TEMP3 = TEMP3 + FBAR2(K1,K3)*NN(K3,K2)
            TEMP4 = TEMP4 + FBAR2(K1,K3)*MM(K3,K2)
          END DO
          NNF(K1,K2) = TEMP1
          MMF(K1,K2) = TEMP2
          FNN(K1,K2) = TEMP3
          FMM(K1,K2) = TEMP4
        END DO
      END DO
C**************************************
      DO K1 = 1, 3
        DO K2 = 1, 3
          TEMP1 = ZE
```

```
        TEMP2 = ZE
        DO K3 = 1, 3
        FLAG1 = ZE
        FLAG2 = ZE
          DO K4 = 1, 3
            FLAG1 = FLAG1 + FBAR2(K1,K3)*NN(K3,K4)*FBAR2(K2,K4)
            FLAG2 = FLAG2 + FBAR2(K1,K3)*MM(K3,K4)*FBAR2(K2,K4)
          END DO
          TEMP1 = TEMP1 + FLAG1
          TEMP2 = TEMP2 + FLAG2
        END DO
        FNF(K1,K2) = TEMP1
        FMF(K1,K2) = TEMP2
      END DO
    END DO
C*********************************************************************
C
C   CALCULATE THE STRESS
C
    B1 = TW*C10/DET1
    B11 = TW*C20/DET2
    B2 = ( ((-TW*C10/TH)*TRBAR1/DET1) + ((TW/D1)*(DET1-ON)))
    B21 = ( ((-TW*C20/TH)*TRBAR2/DET2) + ((TW/D2)*(DET2-ON))
   1 + ((-FO/TH)*C201*J1BAR*(J1BAR-ON)/DET2)
   2 + ((-FO/TH)*C202*K1BAR*(K1BAR-ON)/DET2) )
    B31 = FO*C201*(J1BAR-ON)/DET2
    B41 = FO*C202*(K1BAR-ON)/DET2
    DO K1=1,NDI
    R1=(ON-ALP)*(B1*BAMOR(K1,K1) + B2)
    R2=ALP*((B11*BCRY(K1,K1) + B21) + B31*FNF(K1,K1) + B41*FMF(K1,K1))
    STRESS(K1) = R1 + R2

    END DO
    DO K1=NDI+1,NDI+NSHR
      IF (K1 .EQ. 4)THEN
        L1 = 1
        L2 = 2
      END IF
      IF (K1 .EQ. 5)THEN
        L1 = 1
        L2 = 3
      END IF
      IF (K1 .EQ. 6)THEN
        L1 = 2
        L2 = 3
      END IF
    R1=(ON-ALP)*(B1*BAMOR(L1,L2))
    R2= ALP*( B11*BCRY(L1,L2) + B31*FNF(L1,L2) + B41*FMF(L1,L2))

    STRESS(K1) = R1 + R2
    END DO
C
C   CALCULATE THE STIFFNESS
C*********************************************************************
C   Calculating required co-efficients
C   NOTE : A1 = B1 AND A11 = B11
    A2 = (-TW/TH)*B1
    A21 = (-TW/TH)*B11
```

```
A3 = (TW/NI)*B1
A31 = (TW/NI)*B11
A4 = (TW/D1)*(TW*DET1-ON)
A41 = (TW/D2)*(TW*DET2-ON)
A5 = (-EI/TH)*C201*(TW*J1BAR -ON)/DET2
A51 = (-EI/TH)*C202*(TW*K1BAR -ON)/DET2
A6 = (-ON/TH)*A5*J1BAR
A61 = (-ON/TH)*A51*K1BAR
A7 = (-EI/TH)*C201*(J1BAR -ON)/DET2
A71 = (-EI/TH)*C202*(K1BAR -ON)/DET2
A8 = EI*C201/DET2
A81 = EI*C202/DET2
A9 = (-ON/TH)*A8*J1BAR
A91 = (-ON/TH)*A81*K1BAR
A10 = FO*C201*(J1BAR-ON)/DET2
A101 = FO*C202*(K1BAR-ON)/DET2


C******************************************************************
C    DESCRIBING THE REQUIRED MATRIX

     DO K1 = 1, NDI+1, 1
       IF (K1 .EQ. 1) THEN
         I = 1
         J = 1
       END IF
       IF (K1 .EQ. 2) THEN
         I = 2
         J = 2
       END IF
       IF (K1 .EQ. 3) THEN
         I = 3
         J = 3
       END IF
       IF (K1 .EQ. 4) THEN
         I = 1
         J = 2
       END IF
       DO K2 = 1, NDI+1, 1
         IF (K2 .EQ. 1) THEN
           K = 1
           L = 1
         END IF
         IF (K2 .EQ. 2) THEN
           K = 2
           L = 2
         END IF
         IF (K2 .EQ. 3) THEN
           K = 3
           L = 3
         END IF
         IF (K2 .EQ. 4) THEN
           K = 1
           L = 2
         END IF
       P1=( B1*(KRON(I,K)*BAMOR(L,J)+BAMOR(I,K)*KRON(J,L)) )
       P2=(A2*(KRON(I,J)*BAMOR(K,L)) )
       P3=(A2*(KRON(K,L)*BAMOR(I,J)) )
       P4=(A3*(TRBAR1*KRON(K,L)*KRON(I,J)) )
```

```
P5=(A4*(KRON(K,L)*KRON(I,J)) )
P6=( B11*(KRON(I,K)*BCRY(L,J)+BCRY(I,K)*KRON(J,L)) )
P7=( A21*(KRON(I,J)*BCRY(K,L)) )
P8=( A21*(KRON(K,L)*BCRY(I,J)) )
P9=( A31*(TRBAR2*KRON(K,L)*KRON(I,J)) )
P10=( A41*(KRON(K,L)*KRON(I,J)) )
P11=( A5*(VCN(K)*VECN(L) + FN(K)*FN(L))*KRON(I,J) )
P12=( A6*KRON(K,L)*KRON(I,J) )
P13=( A51*(VCM(K)*VECM(L) + FM(K)*FM(L))*KRON(I,J) )
P14=( A61*KRON(K,L)*KRON(I,J) )
P15=( A7*(KRON(K,L)*FNF(I,J)) )
P16=( A71*(KRON(K,L)*FMF(I,J)) )
P17=( A8*(VCN(K)*VECN(L)+ FN(K)*FN(L))*FNF(I,J) )
P18=( A9*KRON(K,L)*FNF(I,J) )
P19=( A81*(VCM(K)*VECM(L) + FM(K)*FM(L))*FMF(I,J) )
P20=( A91*KRON(K,L)*FMF(I,J) )
P21=( A10*(KRON(I,K)*FNF(J,L) + FBAR2(I,K)*NNF(J,L)
1 + FNN(I,K)*FBAR2(L,J) + FNF(I,K)*KRON(J,L)) )
P22=( A101*(KRON(I,K)*FMF(J,L) + FBAR2(I,K)*MMF(J,L)
2 + FMM(I,K)*FBAR2(L,J) + FMF(I,K)*KRON(J,L)) )

Q1 = (ON-ALP)*(P1+P2+P3+P4+P5) + ALP*(P6+P7+P8+P9+P10+P11)
Q2 = Q1 + ALP*(P12+P13+P14+P15+P16+P17+P18+P19+P20+P21+P22)

C1(K1,K2) = Q1 + Q2

P1=( B1*(KRON(I,L)*BAMOR(K,J)+BAMOR(I,L)*KRON(J,K)) )
P2=(A2*(KRON(I,J)*BAMOR(L,K)) )
P3=(A2*(KRON(L,K)*BAMOR(I,J)) )
P4=(A3*(TRBAR1*KRON(L,K)*KRON(I,J)) )
P5=(A4*(KRON(L,K)*KRON(I,J)) )
P6=( B11*(KRON(I,L)*BCRY(K,J)+BCRY(I,L)*KRON(J,K)) )
P7=( A21*(KRON(I,J)*BCRY(L,K)) )
P8=( A21*(KRON(L,K)*BCRY(I,J)) )
P9=( A31*(TRBAR2*KRON(L,K)*KRON(I,J)) )
P10=( A41*(KRON(L,K)*KRON(I,J)) )
P11=( A5*(VCN(L)*VECN(K) + FN(L)*FN(K))*KRON(I,J) )
P12=( A6*KRON(L,K)*KRON(I,J) )
P13=( A51*(VCM(L)*VECM(K) + FM(L)*FM(K))*KRON(I,J) )
P14=( A61*KRON(L,K)*KRON(I,J) )
P15=( A7*(KRON(L,K)*FNF(I,J)) )
P16=( A71*(KRON(L,K)*FMF(I,J)) )
P17=( A8*(VCN(L)*VECN(K)+ FN(L)*FN(K))*FNF(I,J) )
P18=( A9*KRON(L,K)*FNF(I,J) )
P19=( A81*(VCM(L)*VECM(K) + FM(L)*FM(K))*FMF(I,J) )
P20=( A91*KRON(L,K)*FMF(I,J) )
P21=( A10*(KRON(I,L)*FNF(J,K) + FBAR2(I,L)*NNF(J,K)
1 + FNN(I,L)*FBAR2(K,J) + FNF(I,L)*KRON(J,K)) )
P22=( A101*(KRON(I,L)*FMF(J,K) + FBAR2(I,L)*MMF(J,K)
2 + FMM(I,L)*FBAR2(K,J) + FMF(I,L)*KRON(J,K)) )

Q1 = (ON-ALP)*(P1+P2+P3+P4+P5) + ALP*(P6+P7+P8+P9+P10+P11)
Q2 = Q1 + ALP*(P12+P13+P14+P15+P16+P17+P18+P19+P20+P21+P22)

C2(K1,K2) = Q1 + Q2

DDSDDE(K1,K2) = (ON/TW)*(C1(K1,K2)+C2(K1,K2))
  END DO
```

```
END DO
IF (NSHR .EQ. 3) THEN
DO K1 = 1, NDI+1, 1
  IF (K1 .EQ. 1) THEN
    I = 1
    J = 1
  END IF
  IF (K1 .EQ. 2) THEN
    I = 2
    J = 2
  END IF
  IF (K1 .EQ. 3) THEN
    I = 3
    J = 3
  END IF
  IF (K1 .EQ. 4) THEN
    I = 1
    J = 2
  END IF
  DO K2 = NDI+NSHR-1, NDI+NSHR, 1
    IF (K2 .EQ. 5) THEN
      K = 1
      L = 3
    END IF
    IF (K2 .EQ. 6) THEN
      K = 2
      L = 3
    END IF
P1=( B1*(KRON(I,K)*BAMOR(L,J)+BAMOR(I,K)*KRON(J,L)) )
P2=(A2*(KRON(I,J)*BAMOR(K,L)) )
P3=(A2*(KRON(K,L)*BAMOR(I,J)) )
P4=(A3*(TRBAR1*KRON(K,L)*KRON(I,J)) )
P5=(A4*(KRON(K,L)*KRON(I,J)) )
P6=( B11*(KRON(I,K)*BCRY(L,J)+BCRY(I,K)*KRON(J,L)) )
P7=( A21*(KRON(I,J)*BCRY(K,L)) )
P8=( A21*(KRON(K,L)*BCRY(I,J)) )
P9=( A31*(TRBAR2*KRON(K,L)*KRON(I,J)) )
P10=( A41*(KRON(K,L)*KRON(I,J)) )
P11=( A5*(VCN(K)*VECN(L) + FN(K)*FN(L))*KRON(I,J) )
P12=( A6*KRON(K,L)*KRON(I,J) )
P13=( A51*(VCM(K)*VECM(L) + FM(K)*FM(L))*KRON(I,J) )
P14=( A61*KRON(K,L)*KRON(I,J) )
P15=( A7*(KRON(K,L)*FNF(I,J)) )
P16=( A71*(KRON(K,L)*FMF(I,J)) )
P17=( A8*(VCN(K)*VECN(L)+ FN(K)*FN(L))*FNF(I,J) )
P18=( A9*KRON(K,L)*FNF(I,J) )
P19=( A81*(VCM(K)*VECM(L) + FM(K)*FM(L))*FMF(I,J) )
P20=( A91*KRON(K,L)*FMF(I,J) )
P21=( A10*(KRON(I,K)*FNF(J,L) + FBAR2(I,K)*NNF(J,L)
1 + FNN(I,K)*FBAR2(L,J) + FNF(I,K)*KRON(J,L)) )
P22=( A101*(KRON(I,K)*FMF(J,L) + FBAR2(I,K)*MMF(J,L)
2 + FMM(I,K)*FBAR2(L,J) + FMF(I,K)*KRON(J,L)) )

Q1 = (ON-ALP)*(P1+P2+P3+P4+P5) + ALP*(P6+P7+P8+P9+P10+P11)
Q2 = Q1 + ALP*(P12+P13+P14+P15+P16+P17+P18+P19+P20+P21+P22)

C1(K1,K2) = Q1 + Q2
```

```
P1=( B1*(KRON(I,L)*BAMOR(K,J)+BAMOR(I,L)*KRON(J,K)) )
P2=(A2*(KRON(I,J)*BAMOR(L,K)) )
P3=(A2*(KRON(L,K)*BAMOR(I,J)) )
P4=(A3*(TRBAR1*KRON(L,K)*KRON(I,J)) )
P5=(A4*(KRON(L,K)*KRON(I,J)) )
P6=( B11*(KRON(I,L)*BCRY(K,J)+BCRY(I,L)*KRON(J,K)) )
P7=( A21*(KRON(I,J)*BCRY(L,K)) )
P8=( A21*(KRON(L,K)*BCRY(I,J)) )
P9=( A31*(TRBAR2*KRON(L,K)*KRON(I,J)) )
P10=( A41*(KRON(L,K)*KRON(I,J)) )
P11=( A5*(VCN(L)*VECN(K) + FN(L)*FN(K))*KRON(I,J) )
P12=( A6*KRON(L,K)*KRON(I,J) )
P13=( A51*(VCM(L)*VECM(K) + FM(L)*FM(K))*KRON(I,J) )
P14=( A61*KRON(L,K)*KRON(I,J) )
P15=( A7*(KRON(L,K)*FNF(I,J)) )
P16=( A71*(KRON(L,K)*FMF(I,J)) )
P17=( A8*(VCN(L)*VECN(K)+ FN(L)*FN(K))*FNF(I,J) )
P18=( A9*KRON(L,K)*FNF(I,J) )
P19=( A81*(VCM(L)*VECM(K) + FM(L)*FM(K))*FMF(I,J) )
P20=( A91*KRON(L,K)*FMF(I,J) )
P21=( A10*(KRON(I,L)*FNF(J,K) + FBAR2(I,L)*NNF(J,K)
1 + FNN(I,L)*FBAR2(K,J) + FNF(I,L)*KRON(J,K)) )
P22=( A101*(KRON(I,L)*FMF(J,K) + FBAR2(I,L)*MMF(J,K)
2 + FMM(I,L)*FBAR2(K,J) + FMF(I,L)*KRON(J,K)) )

Q1 = (ON-ALP)*(P1+P2+P3+P4+P5) + ALP*(P6+P7+P8+P9+P10+P11)
Q2 = Q1 + ALP*(P12+P13+P14+P15+P16+P17+P18+P19+P20+P21+P22)

C2(K1,K2) = Q1 + Q2

DDSDDE(K1,K2) = (ON/TW)*(C1(K1,K2)+C2(K1,K2))
 END DO
END DO
DO K1 = NDI+NSHR-1, NDI+NSHR, 1
  IF (K1 .EQ. 5) THEN
    I = 1
    J = 3
  END IF
  IF (K1 .EQ. 6) THEN
    I = 2
    J = 3
  END IF
  DO K2 = 1, NDI+NSHR, 1
    IF (K2 .EQ. 1) THEN
      K = 1
      L = 1
    END IF
    IF (K2 .EQ. 2) THEN
      K = 2
      L = 2
    END IF
    IF (K2 .EQ. 3) THEN
      K = 3
      L = 3
    END IF
    IF (K2 .EQ. 4) THEN
      K = 1
      L = 2
```

```
      END IF
      IF (K2 .EQ. 5) THEN
        K = 1
        L = 3
      END IF
      IF (K2 .EQ. 6) THEN
        K = 2
        L = 3
      END IF
    P1=( B1*(KRON(I,K)*BAMOR(L,J)+BAMOR(I,K)*KRON(J,L)) )
    P2=(A2*(KRON(I,J)*BAMOR(K,L)) )
    P3=(A2*(KRON(K,L)*BAMOR(I,J)) )
    P4=(A3*(TRBAR1*KRON(K,L)*KRON(I,J)) )
    P5=(A4*(KRON(K,L)*KRON(I,J)) )
    P6=( B11*(KRON(I,K)*BCRY(L,J)+BCRY(I,K)*KRON(J,L)) )
    P7=( A21*(KRON(I,J)*BCRY(K,L)) )
    P8=( A21*(KRON(K,L)*BCRY(I,J)) )
    P9=( A31*(TRBAR2*KRON(K,L)*KRON(I,J)) )
    P10=( A41*(KRON(K,L)*KRON(I,J)) )
    P11=( A5*(VCN(K)*VECN(L) + FN(K)*FN(L))*KRON(I,J) )
    P12=( A6*KRON(K,L)*KRON(I,J) )
    P13=( A51*(VCM(K)*VECM(L) + FM(K)*FM(L))*KRON(I,J) )
    P14=( A61*KRON(K,L)*KRON(I,J) )
    P15=( A7*(KRON(K,L)*FNF(I,J)) )
    P16=( A71*(KRON(K,L)*FMF(I,J)) )
    P17=( A8*(VCN(K)*VECN(L)+ FN(K)*FN(L))*FNF(I,J) )
    P18=( A9*KRON(K,L)*FNF(I,J) )
    P19=( A81*(VCM(K)*VECM(L) + FM(K)*FM(L))*FMF(I,J) )
    P20=( A91*KRON(K,L)*FMF(I,J) )
    P21=( A10*(KRON(I,K)*FNF(J,L) + FBAR2(I,K)*NNF(J,L)
   1 + FNN(I,K)*FBAR2(L,J) + FNF(I,K)*KRON(J,L)) )
    P22=( A101*(KRON(I,K)*FMF(J,L) + FBAR2(I,K)*MMF(J,L)
   2 + FMM(I,K)*FBAR2(L,J) + FMF(I,K)*KRON(J,L)) )

    Q1 = (ON-ALP)*(P1+P2+P3+P4+P5) + ALP*(P6+P7+P8+P9+P10+P11)
    Q2 = Q1 + ALP*(P12+P13+P14+P15+P16+P17+P18+P19+P20+P21+P22)

    C1(K1,K2) = Q1 + Q2

    P1=( B1*(KRON(I,L)*BAMOR(K,J)+BAMOR(I,L)*KRON(J,K)) )
    P2=(A2*(KRON(I,J)*BAMOR(L,K)) )
    P3=(A2*(KRON(L,K)*BAMOR(I,J)) )
    P4=(A3*(TRBAR1*KRON(L,K)*KRON(I,J)) )
    P5=(A4*(KRON(L,K)*KRON(I,J)) )
    P6=( B11*(KRON(I,L)*BCRY(K,J)+BCRY(I,L)*KRON(J,K)) )
    P7=( A21*(KRON(I,J)*BCRY(L,K)) )
    P8=( A21*(KRON(L,K)*BCRY(I,J)) )
    P9=( A31*(TRBAR2*KRON(L,K)*KRON(I,J)) )
    P10=( A41*(KRON(L,K)*KRON(I,J)) )
    P11=( A5*(VCN(L)*VECN(K) + FN(L)*FN(K))*KRON(I,J) )
    P12=( A6*KRON(L,K)*KRON(I,J) )
    P13=( A51*(VCM(L)*VECM(K) + FM(L)*FM(K))*KRON(I,J) )
    P14=( A61*KRON(L,K)*KRON(I,J) )
    P15=( A7*(KRON(L,K)*FNF(I,J)) )
    P16=( A71*(KRON(L,K)*FMF(I,J)) )
    P17=( A8*(VCN(L)*VECN(K)+ FN(L)*FN(K))*FNF(I,J) )
    P18=( A9*KRON(L,K)*FNF(I,J) )
    P19=( A81*(VCM(L)*VECM(K) + FM(L)*FM(K))*FMF(I,J) )
```

```
      P20=( A91*KRON(L,K)*FMF(I,J) )
      P21=( A10*(KRON(I,L)*FNF(J,K) + FBAR2(I,L)*NNF(J,K)
     1 + FNN(I,L)*FBAR2(K,J) + FNF(I,L)*KRON(J,K)) )
      P22=( A101*(KRON(I,L)*FMF(J,K) + FBAR2(I,L)*MMF(J,K)
     2 + FMM(I,L)*FBAR2(K,J) + FMF(I,L)*KRON(J,K)) )

      Q1 = (ON-ALP)*(P1+P2+P3+P4+P5) + ALP*(P6+P7+P8+P9+P10+P11)
      Q2 = Q1 + ALP*(P12+P13+P14+P15+P16+P17+P18+P19+P20+P21+P22)

      C2(K1,K2) = Q1 + Q2

      DDSDDE(K1,K2) = (ON/TW)*(C1(K1,K2)+C2(K1,K2))
        END DO
      END DO

      END IF

      RETURN
      END
C*********************************************************************
C    Necessary Kronecker Delta function is defined below
      REAL FUNCTION KRON(P,Q)
      INTEGER P, Q
      IF (P .EQ. Q) THEN
      KRON = 1
      ELSE
      KRON = 0
      END IF
      RETURN
      END
```

APPENDIX C

USER SUBROUTINE (UMAT) FOR NON-ISOTHERMAL PROCESS

This subroutine can be used for simulation of the process that uses part made from crystallizable shape memory polymer.

═══

```
SUBROUTINE UMAT(STRESS,STATEV,DDSDDE,SSE,SPD,SCD,
  1 RPL,DDSDDT,DRPLDE,DRPLDT,STRAN,DSTRAN,
  2 TIME,DTIME,TEMP,DTEMP,PREDEF,DPRED,MATERL,NDI,NSHR,NTENS,
  3 NSTATV,PROPS,NPROPS,COORDS,DROT,PNEWDT,CELENT,
  4 DFGRD0,DFGRD1,NOEL,NPT,KSLAY,KSPT,KSTEP,KINC)
C
   INCLUDE 'ABA_PARAM.INC'
C
   CHARACTER*8 MATERL
   DIMENSION STRESS(NTENS),STATEV(NSTATV),
  1 DDSDDE(NTENS,NTENS),DDSDDT(NTENS),DRPLDE(NTENS),
  2 STRAN(NTENS),DSTRAN(NTENS),DFGRD0(3,3),DFGRD1(3,3),
  3 TIME(2),PREDEF(1),DPRED(1),PROPS(NPROPS),COORDS(3),DROT(3,3)
C
C ------------------------------------------------------------
C
   REAL NN,MM,NNF,MMF,FNN,FMM,FNF,FMF,C1,C2
   DIMENSION FBAR1(3,3),DFGRD2(3,3),FBAR2(3,3),
  1DFG(3,3),FIN(3,3),BAMOR(3,3),BCRY(3,3),BBARN(3,3),BBARP(3,3),
  2VECN(3),VECM(3),CBAR2(3,3),VCN(3),VCM(3),FN(3),FM(3),NN(3,3),
  3MM(3,3),FNN(3,3),FMM(3,3),NNF(3,3),MMF(3,3),FNF(3,3),FMF(3,3),
  4C1(6,6),C2(6,6)

   REAL KRON, TRBAR1, TRBAR2, J1BAR, K1BAR, G, GG, TR, MA, MB, MC
  1    CT1, CT2, CT3, CT4, CT
C
   PARAMETER(ZE=0.D0, ON=1.D0, TW=2.D0, TH=3.D0, FO=4.D0, EI=8.D0,
  1 NI= 9.D0, TE = 10.D0 )
C------------------------------------------------------------

   C10=PROPS(1)
   D1 =PROPS(2)
   C20=PROPS(3)
   D2 =PROPS(4)
   C201 = PROPS(5)
   C202 = PROPS(6)
   RHO = PROPS(7)
   LH = PROPS(8)

   CT = TW*RHO*LH
   CT1 = C10/CT
   CT2 = C20/CT
   CT3 = C201/CT
   CT4 = C202/CT
```

───

```
C
C
C   Incremental crystallinity dalph
      G = 0.1
      GG = 0.1
      TR = -10
      MA = STATEV(10)

C
C         CHECKING IF INTERMIEDIATE CONFIG NEEDS
C         TO BE INITIALIZED
C

          IF (TEMP.LT.TR) THEN
            Dalph = G*(STATEV(10)-(0.4))
     1     *((1-(TEMP/TR))+CT1*(STATEV(14)-TH))
            STATEV(13) = Dalph
            STATEV(10) = STATEV(10) + Dalph
            IF (STATEV(10).GT.(0.4)) THEN
              STATEV(10) = (0.4)
              STATEV(13) = 0
            END IF
            IF (STATEV(10).LT.ZE) THEN
              STATEV(10) = 0
              STATEV(13) = 0
            END IF
            IF (STATEV(11).EQ.1) THEN
          IF (STATEV(10).GT.0) THEN
            STATEV(11) = 0
            STATEV(12) = 1
          END IF
            END IF


          IF (STATEV(12).EQ.1) THEN
            STATEV(1) = DFGRD1(1,1)
            STATEV(2) = DFGRD1(1,2)
            STATEV(3) = DFGRD1(1,3)
            STATEV(4) = DFGRD1(2,1)
        STATEV(5) = DFGRD1(2,2)
        STATEV(6) = DFGRD1(2,3)
        STATEV(7) = DFGRD1(3,1)
        STATEV(8) = DFGRD1(3,2)
        STATEV(9) = DFGRD1(3,3)
        STATEV(12) = 2
      ENDIF

    ENDIF

          IF (TEMP.GT.TR) THEN
            IF (STATEV(12).EQ.2)THEN
              Dalph = GG*(-STATEV(10))
     1       *( (1-(TEMP/TR)) - CT1*(STATEV(14)-TH)
     2       + CT2*(STATEV(15)-TH)
     3       + CT3*(STATEV(16)-ON)**2 + CT4*(STATEV(17)-ON)**2)
              STATEV(10) = STATEV(10)+Dalph
              STATEV(13) = Dalph
              IF (STATEV(10).LT.0)THEN
```

```fortran
              STATEV(10)= 0
              STATEV(13) = 0
          END IF
          IF (STATEV(10).GT.(0.4))THEN
              STATEV(10)= 0
              STATEV(13) = 0
          END IF
        END IF
    ENDIF

    MB = STATEV(10)
    MC = MB - MA
    IF (MC .EQ. 0) THEN
      STATEV(13) = 0
    END IF

C
C      INITIALISING VALUES
C
      DFG(1,1) = STATEV(1)
      DFG(1,2) = STATEV(2)
      DFG(1,3) = STATEV(3)
      DFG(2,1) = STATEV(4)
      DFG(2,2) = STATEV(5)
      DFG(2,3) = STATEV(6)
   DFG(3,1) = STATEV(7)
   DFG(3,2) = STATEV(8)
   DFG(3,3) = STATEV(9)
   ALP = STATEV(10)

C    INVERTING DFG MATRIX
   DETF = DFG(1,1)*(DFG(2,2)*DFG(3,3) - DFG(2,3)*DFG(3,2))
  1    - DFG(1,2)*(DFG(2,1)*DFG(3,3) - DFG(2,3)*DFG(3,1))
  2    + DFG(1,3)*(DFG(2,1)*DFG(3,2) - DFG(2,2)*DFG(3,1))

   FIN(1,1) = (DFG(2,2)*DFG(3,3) - DFG(2,3)*DFG(3,2))/DETF
   FIN(2,1) = -(DFG(2,1)*DFG(3,3) - DFG(2,3)*DFG(3,1))/DETF
   FIN(3,1) = (DFG(2,1)*DFG(3,2) - DFG(2,2)*DFG(3,1))/DETF
   FIN(1,2) = -(DFG(1,2)*DFG(3,3) - DFG(1,3)*DFG(3,2))/DETF
   FIN(2,2) = (DFG(1,1)*DFG(3,3) - DFG(1,3)*DFG(3,1))/DETF
   FIN(3,2) = -(DFG(1,1)*DFG(3,2) - DFG(1,2)*DFG(3,1))/DETF
   FIN(1,3) = (DFG(1,2)*DFG(2,3) - DFG(1,3)*DFG(2,2))/DETF
   FIN(2,3) = -(DFG(1,1)*DFG(2,3) - DFG(1,3)*DFG(2,1))/DETF
   FIN(3,3) = (DFG(1,1)*DFG(2,2) - DFG(1,2)*DFG(2,1))/DETF
C
C      PRESCRIBING DEF GRAD FOR CRYSTALLINE PHASE
C
   DO  K1 = 1, 3, 1
     DO K2 = 1, 3, 1
       EMP0 = ZE
       DO K3 = 1, 3, 1
         EMP0 = EMP0 + DFGRD1(K1,K3)*FIN(K3,K2)
       END DO
       DFGRD2(K1,K2) =  EMP0
     END DO
   END DO
C
C JACOBIAN AND DISTORTION TENSOR
```

```
C
      DET1=DFGRD1(1, 1)*DFGRD1(2, 2)*DFGRD1(3, 3)
     1  -DFGRD1(1, 2)*DFGRD1(2, 1)*DFGRD1(3, 3)
      DET2=DFGRD2(1, 1)*DFGRD2(2, 2)*DFGRD2(3, 3)
     1  -DFGRD2(1, 2)*DFGRD2(2, 1)*DFGRD2(3, 3)
      IF(NSHR.EQ.3) THEN
        DET1=DET1+DFGRD1(1, 2)*DFGRD1(2, 3)*DFGRD1(3, 1)
     1       +DFGRD1(1, 3)*DFGRD1(3, 2)*DFGRD1(2, 1)
     2       -DFGRD1(1, 3)*DFGRD1(3,1)*DFGRD1(2, 2)
     3       -DFGRD1(2, 3)*DFGRD1(3, 2)*DFGRD1(1, 1)
        DET2=DET2+DFGRD2(1, 2)*DFGRD2(2, 3)*DFGRD2(3, 1)
     1       +DFGRD2(1, 3)*DFGRD2(3, 2)*DFGRD2(2, 1)
     2       -DFGRD2(1, 3)*DFGRD2(3,1)*DFGRD2(2, 2)
     3       -DFGRD2(2, 3)*DFGRD2(3, 2)*DFGRD2(1, 1)
      END IF

      SCALE=DET1**(-ON/TH)
      SCALE2=DET2**(-ON/TH)
      DO K1=1, 3
        DO K2=1, 3
          FBAR1(K2, K1)=SCALE*DFGRD1(K2, K1)
          FBAR2(K2, K1)=SCALE2*DFGRD2(K2, K1)
        END DO
      END DO

C*****************************************************************
C   Now, we are finding the directions required for finding J1 and K1
C   for crystalline part which causes orthotropy
C   Directions are n(VECN) & m(VECM)
C        ***** verify  about (1) used in utility subroutine SPRIND
C        ***** (1) is for stress and (2) for strain tensor
C   CALCULATE LEFT CAUCHY-GREEN TENSOR
C
      BAMOR(1,1)=FBAR1(1, 1)**2+FBAR1(1, 2)**2+FBAR1(1, 3)**2
      BAMOR(2,2)=FBAR1(2, 1)**2+FBAR1(2, 2)**2+FBAR1(2, 3)**2
      BAMOR(3,3)=FBAR1(3, 3)**2+FBAR1(3, 1)**2+FBAR1(3, 2)**2
      BAMOR(1,2)=FBAR1(1, 1)*FBAR1(2, 1)+FBAR1(1, 2)*FBAR1(2, 2)
     1    +FBAR1(1, 3)*FBAR1(2, 3)
      BAMOR(2,1) = BAMOR(1,2)
      BCRY(1,1)=FBAR2(1, 1)**2+FBAR2(1, 2)**2+FBAR2(1, 3)**2
      BCRY(2,2)=FBAR2(2, 1)**2+FBAR2(2, 2)**2+FBAR2(2, 3)**2
      BCRY(3,3)=FBAR2(3, 3)**2+FBAR2(3, 1)**2+FBAR2(3, 2)**2
      BCRY(1,2)=FBAR2(1, 1)*FBAR2(2, 1)+FBAR2(1, 2)*FBAR2(2, 2)
     1    +FBAR2(1, 3)*FBAR2(2, 3)
      BCRY(2,1) = BCRY(1,2)
      BAMOR(1,3) = 0.D0
      BAMOR(2,3) = 0.D0
      BAMOR(3,1) = 0.D0
      BAMOR(3,2) = 0.D0
      BCRY(1,3) = 0.D0
      BCRY(2,3) = 0.D0
      BCRY(3,1) = 0.D0
      BCRY(3,2) = 0.D0
      IF(NSHR.EQ.3) THEN
        BAMOR(1,3)=FBAR1(1, 1)*FBAR1(3, 1)+FBAR1(1, 2)*FBAR1(3, 2)
     1       +FBAR1(1, 3)*FBAR1(3, 3)
        BAMOR(3,1) = BAMOR(1,3)
        BAMOR(2,3)=FBAR1(2, 1)*FBAR1(3, 1)+FBAR1(2, 2)*FBAR1(3, 2)
```

```
1      +FBAR1(2, 3)*FBAR1(3, 3)
    BAMOR(3,2) = BAMOR(2,3)
    BCRY(1,3)=FBAR2(1, 1)*FBAR2(3, 1)+FBAR2(1, 2)*FBAR2(3, 2)
1      +FBAR2(1, 3)*FBAR2(3, 3)
    BCRY(3,1) = BCRY(1,3)
    BCRY(2,3)=FBAR2(2, 1)*FBAR2(3, 1)+FBAR2(2, 2)*FBAR2(3, 2)
1      +FBAR2(2, 3)*FBAR2(3, 3)
    BCRY(3,2) = BCRY(2,3)
    END IF


C
C*******************************************************************
C    Calculating the CBAR2
    CBAR2(1,1)=FBAR2(1,1)**2+FBAR2(2,1)**2+FBAR2(3,1)**2
    CBAR2(2,2)=FBAR2(1,2)**2+FBAR2(2,2)**2+FBAR2(3,2)**2
    CBAR2(3,3)=FBAR2(1,3)**2+FBAR2(2,3)**2+FBAR2(3,3)**2
    CBAR2(1,2)=FBAR2(1,1)*FBAR2(1,2)+FBAR2(2,1)*FBAR2(2,2)
1      +FBAR2(3,1)*FBAR2(3,2)
    CBAR2(2,1)= CBAR2(1,2)
    CBAR2(1,3) = 0.D0
    CBAR2(2,3) = 0.D0
    CBAR2(3,1) = 0.D0
    CBAR2(3,2) = 0.D0
    IF(NSHR.EQ.3) THEN
      CBAR2(1,3)=FBAR2(1,1)*FBAR2(1,3)+FBAR2(2,1)*FBAR2(2,3)
1        +FBAR2(3,1)*FBAR2(3,3)
      CBAR2(3,1) = CBAR2(1,3)
      CBAR2(2,3)=FBAR2(1,2)*FBAR2(1,3)+FBAR2(2,2)*FBAR2(2,3)
1        +FBAR2(3,2)*FBAR2(3,3)
      CBAR2(3,2) = CBAR2(2,3)
    END IF


C*******************************************************************
    CALL SPRIND (BAMOR, BBARP, BBARN, 1, NDI, NSHR)
    DO K1 = 1,3,1
      VECN(K1) = BBARN(K1,2)
      VECM(K1) = BBARN(K1,3)
    END DO
C*******************************************************************
C*******************************************************************
C    Finding scalars based on findings above. J1BAR, K1BAR and TRBAR1
    TRBAR1 = BAMOR(1,1) + BAMOR(2,2) + BAMOR(3,3)
    STATEV(14) = TRBAR1
    TRBAR2 = BCRY(1,1) + BCRY(2,2) + BCRY(3,3)
    STATEV(15) = TRBAR2
    J1BAR = ZE
    K1BAR = ZE
    DO K1 = 1, 3
      J1BAR = J1BAR + VECN(K1)*(CBAR2(K1,1)*VECN(1)
1          + CBAR2(K1,2)*VECN(2) + CBAR2(K1,3)*VECN(3))
      K1BAR = K1BAR + VECM(K1)*(CBAR2(K1,1)*VECM(1)
1          + CBAR2(K1,2)*VECM(2) + CBAR2(K1,3)*VECM(3))
    END DO
    STATEV(16) = J1BAR
    STATEV(17) = K1BAR
C*******************************************************************
C    Finding required vectors for DDSDDE
C    VCN = Cn, VCM= Cm, FM = Fm, FN = Fn
```

```
      DO K1 = 1, 3
        VCN(K1) = CBAR2(K1,1)*VECN(1) + CBAR2(K1,2)*VECN(2)
     1       + CBAR2(K1,3)*VECN(3)
        VCM(K1) = CBAR2(K1,1)*VECM(1) + CBAR2(K1,2)*VECM(2)
     1       + CBAR2(K1,3)*VECM(3)
        FN(K1) = FBAR2(K1,1)*VECN(1) + FBAR2(K1,2)*VECN(2)
     1       + FBAR2(K1,3)*VECN(3)
        FM(K1) = FBAR2(K1,1)*VECM(1) + FBAR2(K1,2)*VECM(2)
     1       + FBAR2(K1,3)*VECM(3)
      END DO
CC*******************************************************************
CC*******************************************************************
CC    Some more tensors useful in calculating DDSDDE
CC    NN = n*n, MM = m*m, FNF = Fn*nF', FMF = Fm*mF', NNF = n*nF'
CC    MMF = m*mF', FNN = Fn*n, FMM = Fm*m
CC**************************************

      DO K1 = 1, 3
        DO K2 = 1, 3
          NN(K1,K2) = VECN(K1)*VECN(K2)
          MM(K1,K2) = VECM(K1)*VECM(K2)
        END DO
      END DO
CC**************************************
      DO K1 = 1, 3
        DO K2 = 1, 3
          EMP1 = ZE
          EMP2 = ZE
          EMP3 = ZE
          EMP4 = ZE
          DO K3 = 1, 3
            EMP1 = EMP1 + NN(K1,K3)*FBAR2(K2,K3)
            EMP2 = EMP2 + MM(K1,K3)*FBAR2(K2,K3)
            EMP3 = EMP3 + FBAR2(K1,K3)*NN(K3,K2)
            EMP4 = EMP4 + FBAR2(K1,K3)*MM(K3,K2)
          END DO
          NNF(K1,K2) = EMP1
          MMF(K1,K2) = EMP2
          FNN(K1,K2) = EMP3
          FMM(K1,K2) = EMP4
        END DO
      END DO
C**************************************
      DO K1 = 1, 3
        DO K2 = 1, 3
          EMP1 = ZE
          EMP2 = ZE
          DO K3 = 1, 3
          FLAG1 = ZE
          FLAG2 = ZE
            DO K4 = 1, 3
              FLAG1 = FLAG1 + FBAR2(K1,K3)*NN(K3,K4)*FBAR2(K2,K4)
              FLAG2 = FLAG2 + FBAR2(K1,K3)*MM(K3,K4)*FBAR2(K2,K4)
            END DO
          EMP1 = EMP1 + FLAG1
          EMP2 = EMP2 + FLAG2
          END DO
          FNF(K1,K2) = EMP1
```

```
      FMF(K1,K2) = EMP2
    END DO
  END DO
C*******************************************************************
C
C   CALCULATE THE STRESS
C
    B1 = TW*C10/DET1
    B11 = TW*C20/DET2
    B2 = ( ((-TW*C10/TH)*TRBAR1/DET1) + ((TW/D1)*(DET1-ON)))
    B21 = ( ((-TW*C20/TH)*TRBAR2/DET2) + ((TW/D2)*(DET2-ON))
   1 + ((-FO/TH)*C201*J1BAR*(J1BAR-ON)/DET2)
   2 + ((-FO/TH)*C202*K1BAR*(K1BAR-ON)/DET2) )
    B31 = FO*C201*(J1BAR-ON)/DET2
    B41 = FO*C202*(K1BAR-ON)/DET2
    DO K1=1,NDI
    R1=(ON-ALP)*(B1*BAMOR(K1,K1) + B2)
    R2=ALP*((B11*BCRY(K1,K1) + B21) + B31*FNF(K1,K1) + B41*FMF(K1,K1))
    STRESS(K1) = R1 + R2

    END DO
    DO K1=NDI+1,NDI+NSHR
      IF (K1 .EQ. 4)THEN
        L1 = 1
        L2 = 2
      END IF
      IF (K1 .EQ. 5)THEN
        L1 = 1
        L2 = 3
      END IF
      IF (K1 .EQ. 6)THEN
        L1 = 2
        L2 = 3
      END IF
    R1=(ON-ALP)*(B1*BAMOR(L1,L2))
    R2= ALP*( B11*BCRY(L1,L2) + B31*FNF(L1,L2) + B41*FMF(L1,L2))

    STRESS(K1) = R1 + R2
    END DO
C
C   CALCULATE THE STIFFNESS
C*******************************************************************
C   Calculating required co-efficients
C   NOTE : A1 = B1 AND A11 = B11
    A2 = (-TW/TH)*B1
    A21 = (-TW/TH)*B11
    A3 = (TW/NI)*B1
    A31 = (TW/NI)*B11
    A4 = (TW/D1)*(TW*DET1-ON)
    A41 = (TW/D2)*(TW*DET2-ON)
    A5 = (-EI/TH)*C201*(TW*J1BAR -ON)/DET2
    A51 = (-EI/TH)*C202*(TW*K1BAR -ON)/DET2
    A6 = (-ON/TH)*A5*J1BAR
    A61 = (-ON/TH)*A51*K1BAR
    A7 = (-EI/TH)*C201*(J1BAR -ON)/DET2
    A71 = (-EI/TH)*C202*(K1BAR -ON)/DET2
    A8 = EI*C201/DET2
    A81 = EI*C202/DET2
```

```
      A9 = (-ON/TH)*A8*J1BAR
      A91 = (-ON/TH)*A81*K1BAR
      A10 = FO*C201*(J1BAR-ON)/DET2
      A101 = FO*C202*(K1BAR-ON)/DET2


C*******************************************************************
C    DESCRIBING THE REQUIRED MATRIX

     DO K1 = 1, NDI+1, 1
       IF (K1 .EQ. 1) THEN
         I = 1
         J = 1
       END IF
       IF (K1 .EQ. 2) THEN
         I = 2
         J = 2
       END IF
       IF (K1 .EQ. 3) THEN
         I = 3
         J = 3
       END IF
       IF (K1 .EQ. 4) THEN
         I = 1
         J = 2
       END IF
       DO K2 = 1, NDI+1, 1
         IF (K2 .EQ. 1) THEN
           K = 1
           L = 1
         END IF
         IF (K2 .EQ. 2) THEN
           K = 2
           L = 2
         END IF
         IF (K2 .EQ. 3) THEN
           K = 3
           L = 3
         END IF
         IF (K2 .EQ. 4) THEN
           K = 1
           L = 2
         END IF
         P1=( B1*(KRON(I,K)*BAMOR(L,J)+BAMOR(I,K)*KRON(J,L)) )
         P2=(A2*(KRON(I,J)*BAMOR(K,L)) )
         P3=(A2*(KRON(K,L)*BAMOR(I,J)) )
         P4=(A3*(TRBAR1*KRON(K,L)*KRON(I,J)) )
         P5=(A4*(KRON(K,L)*KRON(I,J)) )
         P6=( B11*(KRON(I,K)*BCRY(L,J)+BCRY(I,K)*KRON(J,L)) )
         P7=( A21*(KRON(I,J)*BCRY(K,L)) )
         P8=( A21*(KRON(K,L)*BCRY(I,J)) )
         P9=( A31*(TRBAR2*KRON(K,L)*KRON(I,J)) )
         P10=( A41*(KRON(K,L)*KRON(I,J)) )
         P11=( A5*(VCN(K)*VECN(L) + FN(K)*FN(L))*KRON(I,J) )
         P12=( A6*KRON(K,L)*KRON(I,J) )
         P13=( A51*(VCM(K)*VECM(L) + FM(K)*FM(L))*KRON(I,J) )
         P14=( A61*KRON(K,L)*KRON(I,J) )
         P15=( A7*(KRON(K,L)*FNF(I,J)) )
         P16=( A71*(KRON(K,L)*FMF(I,J)) )
```

```
P17=( A8*(VCN(K)*VECN(L)+ FN(K)*FN(L))*FNF(I,J) )
P18=( A9*KRON(K,L)*FNF(I,J) )
P19=( A81*(VCM(K)*VECM(L) + FM(K)*FM(L))*FMF(I,J) )
P20=( A91*KRON(K,L)*FMF(I,J) )
P21=( A10*(KRON(I,K)*FNF(J,L) + FBAR2(I,K)*NNF(J,L)
1 + FNN(I,K)*FBAR2(L,J) + FNF(I,K)*KRON(J,L)) )
P22=( A101*(KRON(I,K)*FMF(J,L) + FBAR2(I,K)*MMF(J,L)
2 + FMM(I,K)*FBAR2(L,J) + FMF(I,K)*KRON(J,L)) )


Q1 = (ON-ALP)*(P1+P2+P3+P4+P5) + ALP*(P6+P7+P8+P9+P10+P11)
Q2 = Q1 + ALP*(P12+P13+P14+P15+P16+P17+P18+P19+P20+P21+P22)


C1(K1,K2) = Q1 + Q2


P1=( B1*(KRON(I,L)*BAMOR(K,J)+BAMOR(I,L)*KRON(J,K)) )
P2=(A2*(KRON(I,J)*BAMOR(L,K)) )
P3=(A2*(KRON(L,K)*BAMOR(I,J)) )
P4=(A3*(TRBAR1*KRON(L,K)*KRON(I,J)) )
P5=(A4*(KRON(L,K)*KRON(I,J)) )
P6=( B11*(KRON(I,L)*BCRY(K,J)+BCRY(I,L)*KRON(J,K)) )
P7=( A21*(KRON(I,J)*BCRY(L,K)) )
P8=( A21*(KRON(L,K)*BCRY(I,J)) )
P9=( A31*(TRBAR2*KRON(L,K)*KRON(I,J)) )
P10=( A41*(KRON(L,K)*KRON(I,J)) )
P11=( A5*(VCN(L)*VECN(K) + FN(L)*FN(K))*KRON(I,J) )
P12=( A6*KRON(L,K)*KRON(I,J) )
P13=( A51*(VCM(L)*VECM(K) + FM(L)*FM(K))*KRON(I,J) )
P14=( A61*KRON(L,K)*KRON(I,J) )
P15=( A7*(KRON(L,K)*FNF(I,J)) )
P16=( A71*(KRON(L,K)*FMF(I,J)) )
P17=( A8*(VCN(L)*VECN(K)+ FN(L)*FN(K))*FNF(I,J) )
P18=( A9*KRON(L,K)*FNF(I,J) )
P19=( A81*(VCM(L)*VECM(K) + FM(L)*FM(K))*FMF(I,J) )
P20=( A91*KRON(L,K)*FMF(I,J) )
P21=( A10*(KRON(I,L)*FNF(J,K) + FBAR2(I,L)*NNF(J,K)
1 + FNN(I,L)*FBAR2(K,J) + FNF(I,L)*KRON(J,K)) )
P22=( A101*(KRON(I,L)*FMF(J,K) + FBAR2(I,L)*MMF(J,K)
2 + FMM(I,L)*FBAR2(K,J) + FMF(I,L)*KRON(J,K)) )


Q1 = (ON-ALP)*(P1+P2+P3+P4+P5) + ALP*(P6+P7+P8+P9+P10+P11)
Q2 = Q1 + ALP*(P12+P13+P14+P15+P16+P17+P18+P19+P20+P21+P22)


C2(K1,K2) = Q1 + Q2


DDSDDE(K1,K2) = (ON/TW)*(C1(K1,K2)+C2(K1,K2))
  END DO
END DO
IF (NSHR .EQ. 3) THEN
DO K1 = 1, NDI+1, 1
  IF (K1 .EQ. 1) THEN
    I = 1
    J = 1
  END IF
  IF (K1 .EQ. 2) THEN
    I = 2
    J = 2
  END IF
  IF (K1 .EQ. 3) THEN
```

```
        I = 3
        J = 3
      END IF
      IF (K1 .EQ. 4) THEN
        I = 1
        J = 2
      END IF
      DO K2 = NDI+NSHR-1, NDI+NSHR, 1
        IF (K2 .EQ. 5) THEN
          K = 1
          L = 3
        END IF
        IF (K2 .EQ. 6) THEN
          K = 2
          L = 3
        END IF
      P1=( B1*(KRON(I,K)*BAMOR(L,J)+BAMOR(I,K)*KRON(J,L)) )
      P2=(A2*(KRON(I,J)*BAMOR(K,L)) )
      P3=(A2*(KRON(K,L)*BAMOR(I,J)) )
      P4=(A3*(TRBAR1*KRON(K,L)*KRON(I,J)) )
      P5=(A4*(KRON(K,L)*KRON(I,J)) )
      P6=( B11*(KRON(I,K)*BCRY(L,J)+BCRY(I,K)*KRON(J,L)) )
      P7=( A21*(KRON(I,J)*BCRY(K,L)) )
      P8=( A21*(KRON(K,L)*BCRY(I,J)) )
      P9=( A31*(TRBAR2*KRON(K,L)*KRON(I,J)) )
      P10=( A41*(KRON(K,L)*KRON(I,J)) )
      P11=( A5*(VCN(K)*VECN(L) + FN(K)*FN(L))*KRON(I,J) )
      P12=( A6*KRON(K,L)*KRON(I,J) )
      P13=( A51*(VCM(K)*VECM(L) + FM(K)*FM(L))*KRON(I,J) )
      P14=( A61*KRON(K,L)*KRON(I,J) )
      P15=( A7*(KRON(K,L)*FNF(I,J)) )
      P16=( A71*(KRON(K,L)*FMF(I,J)) )
      P17=( A8*(VCN(K)*VECN(L)+ FN(K)*FN(L))*FNF(I,J) )
      P18=( A9*KRON(K,L)*FNF(I,J) )
      P19=( A81*(VCM(K)*VECM(L) + FM(K)*FM(L))*FMF(I,J) )
      P20=( A91*KRON(K,L)*FMF(I,J) )
      P21=( A10*(KRON(I,K)*FNF(J,L) + FBAR2(I,K)*NNF(J,L)
     1 + FNN(I,K)*FBAR2(L,J) + FNF(I,K)*KRON(J,L)) )
      P22=( A101*(KRON(I,K)*FMF(J,L) + FBAR2(I,K)*MMF(J,L)
     2 + FMM(I,K)*FBAR2(L,J) + FMF(I,K)*KRON(J,L)) )

      Q1 = (ON-ALP)*(P1+P2+P3+P4+P5) + ALP*(P6+P7+P8+P9+P10+P11)
      Q2 = Q1 + ALP*(P12+P13+P14+P15+P16+P17+P18+P19+P20+P21+P22)

      C1(K1,K2) = Q1 + Q2

      P1=( B1*(KRON(I,L)*BAMOR(K,J)+BAMOR(I,L)*KRON(J,K)) )
      P2=(A2*(KRON(I,J)*BAMOR(L,K)) )
      P3=(A2*(KRON(L,K)*BAMOR(I,J)) )
      P4=(A3*(TRBAR1*KRON(L,K)*KRON(I,J)) )
      P5=(A4*(KRON(L,K)*KRON(I,J)) )
      P6=( B11*(KRON(I,L)*BCRY(K,J)+BCRY(I,L)*KRON(J,K)) )
      P7=( A21*(KRON(I,J)*BCRY(L,K)) )
      P8=( A21*(KRON(L,K)*BCRY(I,J)) )
      P9=( A31*(TRBAR2*KRON(L,K)*KRON(I,J)) )
      P10=( A41*(KRON(L,K)*KRON(I,J)) )
      P11=( A5*(VCN(L)*VECN(K) + FN(L)*FN(K))*KRON(I,J) )
      P12=( A6*KRON(L,K)*KRON(I,J) )
```

```
P13=( A51*(VCM(L)*VECM(K) + FM(L)*FM(K))*KRON(I,J) )
P14=( A61*KRON(L,K)*KRON(I,J) )
P15=( A7*(KRON(L,K)*FNF(I,J)) )
P16=( A71*(KRON(L,K)*FMF(I,J)) )
P17=( A8*(VCN(L)*VECN(K)+ FN(L)*FN(K))*FNF(I,J) )
P18=( A9*KRON(L,K)*FNF(I,J) )
P19=( A81*(VCM(L)*VECM(K) + FM(L)*FM(K))*FMF(I,J) )
P20=( A91*KRON(L,K)*FMF(I,J) )
P21=( A10*(KRON(I,L)*FNF(J,K) + FBAR2(I,L)*NNF(J,K)
1 + FNN(I,L)*FBAR2(K,J) + FNF(I,L)*KRON(J,K)) )
 P22=( A101*(KRON(I,L)*FMF(J,K) + FBAR2(I,L)*MMF(J,K)
2 + FMM(I,L)*FBAR2(K,J) + FMF(I,L)*KRON(J,K)) )

 Q1 = (ON-ALP)*(P1+P2+P3+P4+P5) + ALP*(P6+P7+P8+P9+P10+P11)
 Q2 = Q1 + ALP*(P12+P13+P14+P15+P16+P17+P18+P19+P20+P21+P22)

 C2(K1,K2) = Q1 + Q2

 DDSDDE(K1,K2) = (ON/TW)*(C1(K1,K2)+C2(K1,K2))
  END DO
 END DO
 DO K1 = NDI+NSHR-1, NDI+NSHR, 1
   IF (K1 .EQ. 5) THEN
     I = 1
     J = 3
   END IF
   IF (K1 .EQ. 6) THEN
     I = 2
     J = 3
   END IF
   DO K2 = 1, NDI+NSHR, 1
     IF (K2 .EQ. 1) THEN
       K = 1
       L = 1
     END IF
     IF (K2 .EQ. 2) THEN
       K = 2
       L = 2
     END IF
     IF (K2 .EQ. 3) THEN
       K = 3
       L = 3
     END IF
     IF (K2 .EQ. 4) THEN
       K = 1
       L = 2
     END IF
     IF (K2 .EQ. 5) THEN
       K = 1
       L = 3
     END IF
     IF (K2 .EQ. 6) THEN
       K = 2
       L = 3
     END IF
   P1=( B1*(KRON(I,K)*BAMOR(L,J)+BAMOR(I,K)*KRON(J,L)) )
   P2=(A2*(KRON(I,J)*BAMOR(K,L)) )
   P3=(A2*(KRON(K,L)*BAMOR(I,J)) )
```

P4=(A3*(TRBAR1*KRON(K,L)*KRON(I,J)))
P5=(A4*(KRON(K,L)*KRON(I,J)))
P6=(B11*(KRON(I,K)*BCRY(L,J)+BCRY(I,K)*KRON(J,L)))
P7=(A21*(KRON(I,J)*BCRY(K,L)))
P8=(A21*(KRON(K,L)*BCRY(I,J)))
P9=(A31*(TRBAR2*KRON(K,L)*KRON(I,J)))
P10=(A41*(KRON(K,L)*KRON(I,J)))
P11=(A5*(VCN(K)*VECN(L) + FN(K)*FN(L))*KRON(I,J))
P12=(A6*KRON(K,L)*KRON(I,J))
P13=(A51*(VCM(K)*VECM(L) + FM(K)*FM(L))*KRON(I,J))
P14=(A61*KRON(K,L)*KRON(I,J))
P15=(A7*(KRON(K,L)*FNF(I,J)))
P16=(A71*(KRON(K,L)*FMF(I,J)))
P17=(A8*(VCN(K)*VECN(L)+ FN(K)*FN(L))*FNF(I,J))
P18=(A9*KRON(K,L)*FNF(I,J))
P19=(A81*(VCM(K)*VECM(L) + FM(K)*FM(L))*FMF(I,J))
P20=(A91*KRON(K,L)*FMF(I,J))
P21=(A10*(KRON(I,K)*FNF(J,L) + FBAR2(I,K)*NNF(J,L)
1 + FNN(I,K)*FBAR2(L,J) + FNF(I,K)*KRON(J,L)))
P22=(A101*(KRON(I,K)*FMF(J,L) + FBAR2(I,K)*MMF(J,L)
2 + FMM(I,K)*FBAR2(L,J) + FMF(I,K)*KRON(J,L)))

Q1 = (ON-ALP)*(P1+P2+P3+P4+P5) + ALP*(P6+P7+P8+P9+P10+P11)
Q2 = Q1 + ALP*(P12+P13+P14+P15+P16+P17+P18+P19+P20+P21+P22)

C1(K1,K2) = Q1 + Q2

P1=(B1*(KRON(I,L)*BAMOR(K,J)+BAMOR(I,L)*KRON(J,K)))
P2=(A2*(KRON(I,J)*BAMOR(L,K)))
P3=(A2*(KRON(L,K)*BAMOR(I,J)))
P4=(A3*(TRBAR1*KRON(L,K)*KRON(I,J)))
P5=(A4*(KRON(L,K)*KRON(I,J)))
P6=(B11*(KRON(I,L)*BCRY(K,J)+BCRY(I,L)*KRON(J,K)))
P7=(A21*(KRON(I,J)*BCRY(L,K)))
P8=(A21*(KRON(L,K)*BCRY(I,J)))
P9=(A31*(TRBAR2*KRON(L,K)*KRON(I,J)))
P10=(A41*(KRON(L,K)*KRON(I,J)))
P11=(A5*(VCN(L)*VECN(K) + FN(L)*FN(K))*KRON(I,J))
P12=(A6*KRON(L,K)*KRON(I,J))
P13=(A51*(VCM(L)*VECM(K) + FM(L)*FM(K))*KRON(I,J))
P14=(A61*KRON(L,K)*KRON(I,J))
P15=(A7*(KRON(L,K)*FNF(I,J)))
P16=(A71*(KRON(L,K)*FMF(I,J)))
P17=(A8*(VCN(L)*VECN(K)+ FN(L)*FN(K))*FNF(I,J))
P18=(A9*KRON(L,K)*FNF(I,J))
P19=(A81*(VCM(L)*VECM(K) + FM(L)*FM(K))*FMF(I,J))
P20=(A91*KRON(L,K)*FMF(I,J))
P21=(A10*(KRON(I,L)*FNF(J,K) + FBAR2(I,L)*NNF(J,K)
1 + FNN(I,L)*FBAR2(K,J) + FNF(I,L)*KRON(J,K)))
P22=(A101*(KRON(I,L)*FMF(J,K) + FBAR2(I,L)*MMF(J,K)
2 + FMM(I,L)*FBAR2(K,J) + FMF(I,L)*KRON(J,K)))

Q1 = (ON-ALP)*(P1+P2+P3+P4+P5) + ALP*(P6+P7+P8+P9+P10+P11)
Q2 = Q1 + ALP*(P12+P13+P14+P15+P16+P17+P18+P19+P20+P21+P22)

C2(K1,K2) = Q1 + Q2

DDSDDE(K1,K2) = (ON/TW)*(C1(K1,K2)+C2(K1,K2))

```
      END DO
      END DO

      END IF

      RETURN
      END
C*************************************************************************
C     Necessary Kronecker Delta function is defined below
      REAL FUNCTION KRON(P,Q)
      INTEGER P, Q
      IF (P .EQ. Q) THEN
      KRON = 1
      ELSE
      KRON = 0
      END IF
      RETURN
      END
```

APPENDIX D

USER SUBROUTINE (UMATHT) FOR NON-ISOTHERMAL PROCESS

This subroutine is to incorporate heat transfer and phase transition associated with the

crystallizable shape memory polymer.

==

```fortran
SUBROUTINE UMATHT(U,DUDT,DUDG,FLUX,DFDT,DFDG,STATEV,TEMP,DTEMP,
1 DTEMDX,TIME,DTIME,PREDEF,DPRED,CMNAME,NTGRD,NSTATEV,PROPS,NPROPS,
2 COORDS,PNEWDT,NOEL,NPT,LAYER,KSPT,KSTEP,KINC)
C
C
   INCLUDE 'ABA_PARAM.INC'
C
   CHARACTER*80 CMNAME
C
   DIMENSION DUDG(NTGRD),FLUX(NTGRD),DFDT(NTGRD),DFDG(NTGRD,NTGRD),
1 STATEV(NSTATEV),DTEMDX(NTGRD),TIME(2), PREDEF(1),DPRED(1),
2 PROPS(NPROPS),COORDS(3)
C
C
   COND = PROPS(1)
   SPECHT = PROPS(2)
C
C   INPUT SPECIFIC HEAT
C
   DUDT = SPECHT
   DU = DUDT*DTEMP
   U = U + DU
C
C   INPUT FLUX = -[K]*{DTEMDX}; CONDUCTIVITY MULTIPLIED WITH TEMP
C                              DIFFERNCE
   DO I = 1, NTGRD
     FLUX(I) = -COND*DTEMDX(I)
   END DO
C
C   INPUT ISOTROPIC CONDUCTIVITY
C
   DO I = 1,NTGRD
     DFDG(I,I) = -COND
   END DO
C
   RETURN
   END
```

APPENDIX E

USER SUBROUTINE (SDVINI) FOR ISOTHERMAL PROCESS

This subroutine is used to prescribe initial conditions for isothermal processes that uses

part made with crystallizable shape memory polymer.

```fortran
SUBROUTINE SDVINI(STATEV,COORDS,NSTATV,NCRDS,NOEL,NPT,LAYER,KSPT)
C
      INCLUDE 'ABA_PARAM.INC'
C
      DIMENSION STATEV(NSTATV),COORDS(NCRDS)
C
      STATEV(1)=1.D0
      STATEV(2)=0.D0
      STATEV(3)=0.D0
      STATEV(4)=0.D0
      STATEV(5)=1.D0
      STATEV(6)=0.D0
      STATEV(7)=0.D0
      STATEV(8)=0.D0
      STATEV(9)=1.D0
      STATEV(10)=0.D0
      STATEV(11)=1.D0


      RETURN

      END
```

APPENDIX F

USER SUBROUTINE (SDVINI) FOR NON-ISOTHERMAL PROCESS

This subroutine is used to prescribe initial conditions for non-isothermal processes that uses part made with crystallizable shape memory polymer.

```fortran
SUBROUTINE SDVINI(STATEV,COORDS,NSTATV,NCRDS,NOEL,NPT,LAYER,KSPT)
C
    INCLUDE 'ABA_PARAM.INC'
C
    DIMENSION STATEV(NSTATV),COORDS(NCRDS)
C
    STATEV(1)=1.D0
    STATEV(2)=0.D0
    STATEV(3)=0.D0
    STATEV(4)=0.D0
    STATEV(5)=1.D0
    STATEV(6)=0.D0
    STATEV(7)=0.D0
    STATEV(8)=0.D0
    STATEV(9)=1.D0
    STATEV(10)=0.D0
    STATEV(11)=1.D0
    STATEV(12)=0.D0
    STATEV(13)=0.D0
    STATEV(14)=0.D0
    STATEV(15)=0.D0
    STATEV(16)=0.D0
    STATEV(17)=0.D0

    RETURN

    END
```

APPENDIX G

THE MATERIAL MODULE FOR ISO THERMAL PROCESS

The following module is used with user subroutines given in appendix B and appendix E.

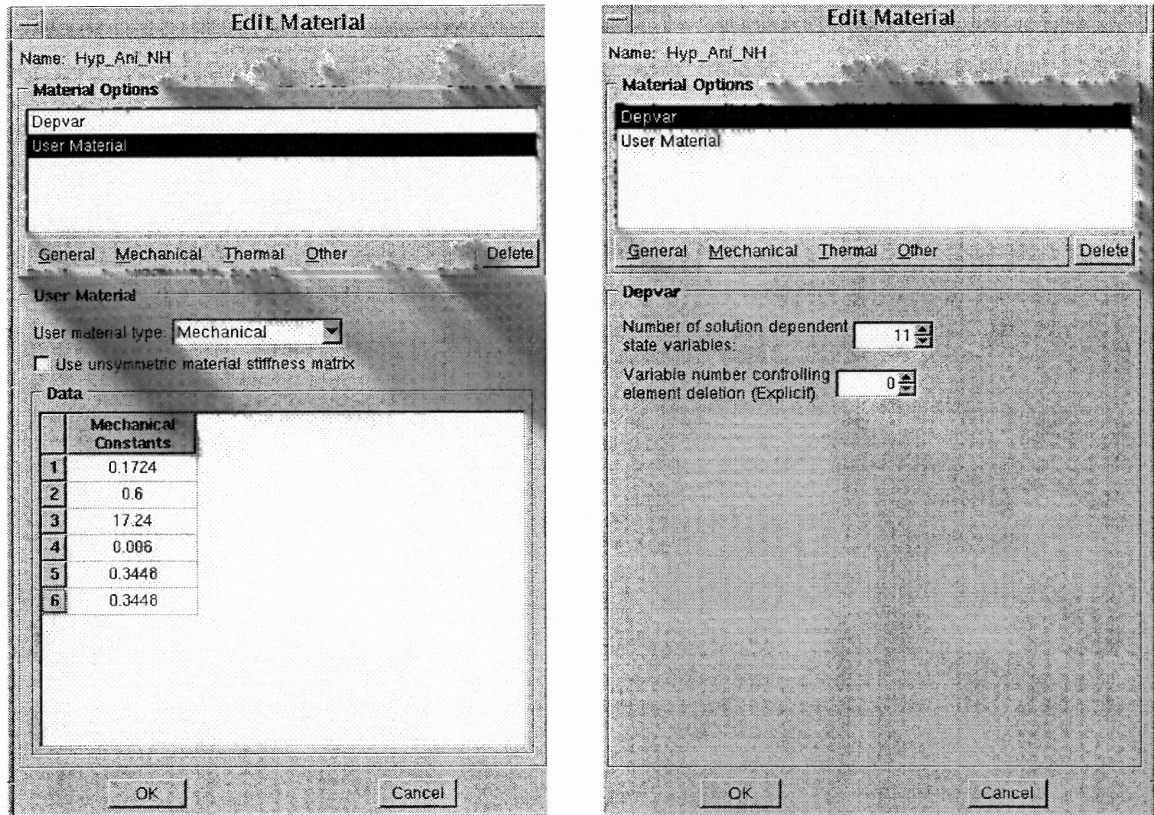Snapshots shown below are taken from ABAQUS/CAE window.

Figure G.1 Snap shots of the material module created in ABAQUS for iso-thermal process that includes use of crystallizable shape memory polymers.

MATERIAL MODULE NON-ISOTHERMAL PROCESS

The following module is used with user subroutines given in appendix C, appendix D and appendix F.
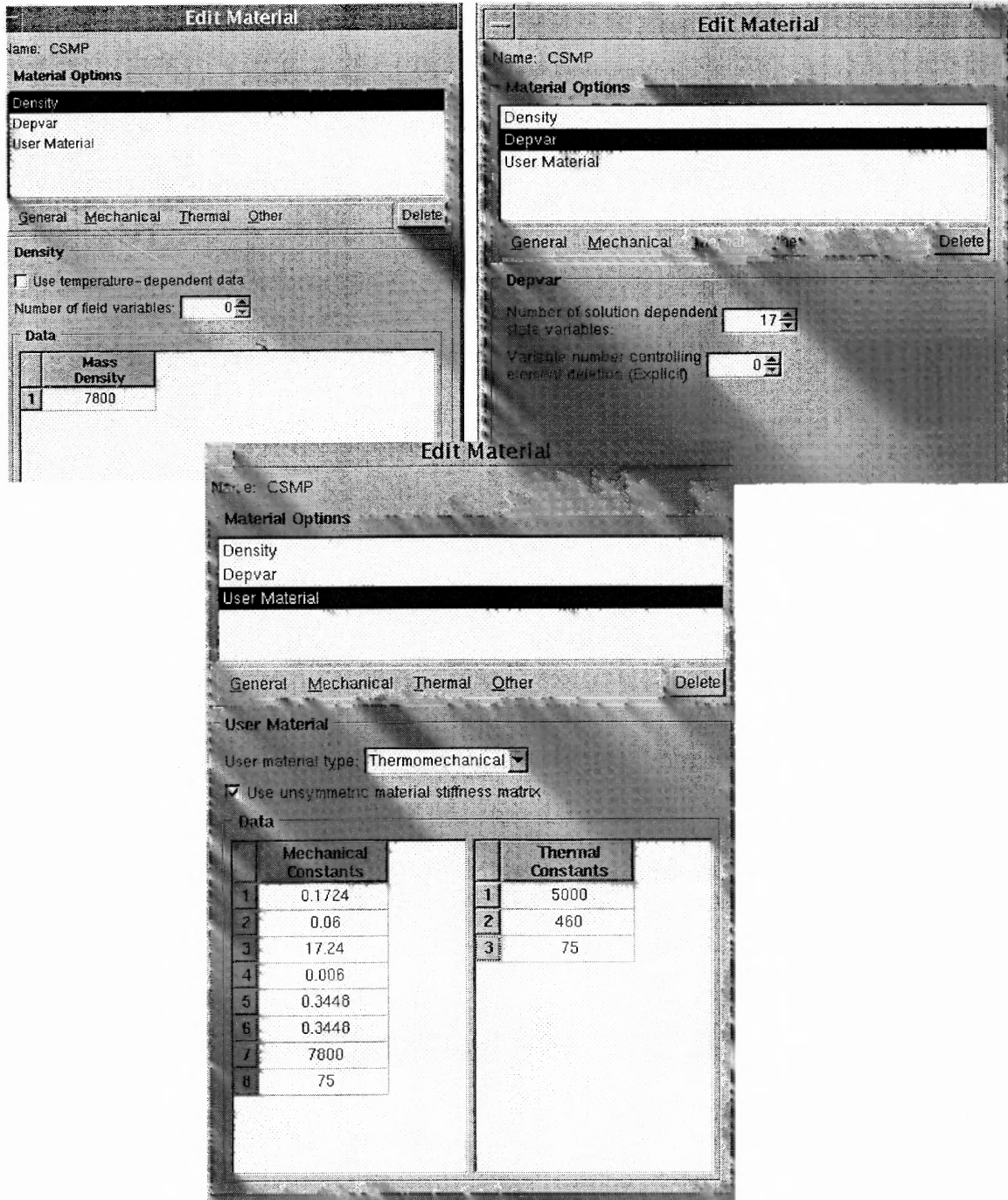

Figure H.1 Snap shots of the material module created in ABAQUS for non iso-thermal process that includes use of crystallizable shape memory polymers.

REFERENCES

Atkin R. J. and Craine, R. E., 1976. Continuum theory of mixtures: basic theory and historical development, *Q. J. Mech. Appl. Math.*, **29**, 209-244.

Bankoff S. G., 1964. Heat Conduction or Diffusion with Phase Change, *Advances in Chemical Engineering*, **5**, 75-150.

Barot G. and Rao I. J., 2005. Modeling the Film Casting Process Using a Continuum Model for Crystallization in Polymers, , *International Journal of Non-Linear Mechanics*, **40**, 7, 939-955.

Barot G. and Rao I. J., 2006. Constitutive Modeling of the Mechanics Associated with Crystallizable Shape Memory Polymers, *ZAMP*, 1-30.

Bowen R. M., Theory of the mixtures, 1975. In Eringen, A.C.(ed.), Continuum Physics vol.III, Academic Press, New York.

Crank J. 1984. *Free and Moving Boundary Problems*, Clarendoss Press, Oxford

Davis K.A., Burdick J.A., 2003. Photoinitiated Crosslinked Degradable Copolymer Network for Tissue Engineering Applications, *Biomaterial*, **24**, 2485–2495.

Eder G., Janeschitz-Kriegel H., Liedauer S. and Krobath G., 1990. Crystallization Process Under Quiescent and Moving Polymer Melt Under Heat Transfer Conditions, *Progress in Polymer Science*, **15**, 629-714.

Fasano A. and Primicero M., 1979. Free Boundary Problems for Nonlinear Equations with Nonlinear Free Boundary Conditions, *Journal of Mathematical Analysis and Applications*, **72**, 247-273.

Feynman R. P., 1989. *The Feynman Lectures on Physics*, Vol-I, Addison-Wesley.

Flory P. J., 1953. *Principles of polymer chemistry*, Cornell University Press, Ithaca, 432-494.

Flory P. J., 1961. Thermodynamic Relations for High Elastic Materials, *Transactions of the Faraday Society*, **57**, 829-838

Flory P. J., Yoon D.Y. and Dill K. A., 1984. The Interphase in Lamellar Semi-Crystalline Polymers, *Macromolecules*, **17**, 862-868.

Gedde U. W., 1995. *Polymer Physics*, Chapman Hall, London.

Green A. E. and Naghdi P. M., 1977. On thermodynamics and the nature of the second law, *Proc. Roy. Soc. London* **A 357**, 253-270.

Holpzafel G., 2000. *Non-Linear Solid Mechanics*, Wiley, NJ.

Jeong H.M., Lee S.Y., Kim B.K., 2000. Shape Memory Polyurethane Containing Amorphous Reversible Phase, *Journal of Material Science*, **35**, 1579-1583.

Irie M., 1998. *Shape Memory Polymers: in Shape Memory Materials. Ed. Otsuka and Wayman, C. M.*, Cambridge University Press, Cambridge.

Kim B. K., Lee S.Y. and Xu M., 1996. Polyurethanes having Shape Memory Effects, *Polymer*, **37**, 5781-5793.

Kim B. K., Lee S. Y., Lee J. S., Baek S. H., Choi Y. J., Lee J. O. and Xu M., 1998. Polyurethane Ionomers having Shape Memory Eeffects, *Polymer*, **39**, 2803–2808.

Kim B. K., Shin Y. J., Cho S. M. and Jeong H. M., 2000. Shape-Memory Behavior of Segmented Polyurethanes with an Amorphous Reversible Phase: The Effect of Block Length and Content, *Journal of Polymer Science, part B*, **38**, 2652-2657.

Kuwabara K., Kaji H., Horii F., Basset DC. and Olley R. H., 1997. Solid-state 13C NMR Analysis of the Crystalline-noncrystalline Structure for Metallocene-catalyzed linear low-density polyethylene, *Macromolecules*, **30**, 7516-7521.

Lame M. M. and Clapeyron B.P.E., 1831. Memoire Sur La Solidification Par Refroidissement D'un Globe Liquide, *Annales Chimie Physique*, **47**.

Landau L. D., 1967. *Collected Papers*, Gordon and Breach, New York.

Lendlein A., Schmidt A.M., Langer R., 2001. AB-polymer networks based on oligo (ε-caprolactone) segments showing shape-memory properties, *Proceedings of National Academy of Science, USA*, **98**, 842-847.

Lendlein A. and Kelch S., 2002(a). Shape Memory Polymers, *Angew.Chem.Int.ed.*, **41**, 2034-2057.

Lendlein, A., Langer, R., 2002(b). Biodegradable elastic shape-memory polymers for potential biomedical applications. *Science*, **296**, 1673-1676.

Lin J. R. and Chen L. W., 1999. Shape-Memorized Crosslinked Ester-Type Polyurethane and Its Mechanical Viscoelastic Model, *Journal of Applied Polymer Science*, **73**, 1305-1319.

Liu C.D., Chun S.B., Mather P.T., 2002. Chemically Cross-linked Polycyclooctene: Synthesis, Characterization, and Shape Memory Behavior, *Macromolecules*, **35**, 9868-9874.

Mandelkern L., 1964. *Crystallization of Polymers*, McGraw Hill, New York.

Mandelkern L., Glotin M. and Benson R. A., 1981. Supermolecular Structure and Thermodynamic Properties of Linear and Branched Polyethylenes under Rapid Crystallization Conditions, *Macromolecules*, **14**, 22-34.

Monkman G. J., 2000. Advances in Shape memory actuation, *Mechatronics*, **10**, 489-498.

Müllner P., 1999. Book Review: Shape Memory Alloys. Edited by K. Otsuka and C.M. Wayman, Cambridge University Press, ISBN 0-521-44487-X (hardcover), 284 pp. +xiv. , *Materials Science and Engineering A*, **268**, 1-2, 15, 246-247

Muralikrishna J. and Rajagopal K. R., 2004. A Thermodynamic Framework for the Constitutive Modeling Asphalt Concrete: Theory and Application, *Journal of Materials in Civil Engineering*, **16**, 2, 155-166

Ogden R. W., 1984. *Non-Liner Elastic Deformation*, Dover, NY.

Pippard A. B., 1957. *Elements of Classical Thermodynamics for Advance Students of Physics*, Cambridge University Press.

Poilane C., Delobelle P., Lexcellent C., Hayashi S. and Tobushi H., 2000. Analysis of the Mechanical Behavior of Shape Memory Polymer Membrane by Nanoindentation, Bulging and Point Membrane Deflection Tests, *Thin Solid Films*, **379**, 156-165.

Rajagopal K. R., 1995. Multiple Configurations in Continuum Mechanics, *(Technical Report No. 6)*, Pitttsburgh, PA: University of Pittusburgh.

Rajagopal K. R. and Srinivasa A. R., 1995. Inelastic Behavior of Solids: Part-I-Twinning, *International Journal of Plasticity*, **11**, 653-678.

Rajagopal K. R. and Srinivasa A. R., 1998. Inelastic Behavior of Materials: Part-I-Theoretical underpinnings, *International Journal of Plasticity*, **14**, 945-967.

Rajagopal K. R. and Srinivasa A. R., 1999. On the Thermodynamics of Shape Memory Wires, *ZAMP*, **50**, 459-496.

Rajagopal K. R. and Srinivasa A. R., 2000. A Thermodyanamic Framework for Rate Type Fluids Model, *Journal of Non-Newotnian Fluid Mechanics*, **88**, 207-227.

Rajagopal K. R. and Srinivasa A. R., 2001. Modeling Anisotropic Fluids Within the Framework of Bodies with Multiple Natural Configurations, *Journal of Non-Newtonian Fluid Mechanics*,99,2,109-124.

Rajagopal K.R. and Tao L., 1995. *Mechanics of Mixtures*, World Scientific, New Jersey.

Rajagopal K. R. and Wineman A.S., 1992. A Constitutive Equation for Nonlinear Solids which Undergo Deformation Induced Microstructural Changes. *International Journal of Plasticity*, **8**, 385-395

Rao I. J., 2002. Constitutive Modeling of Crystallizable Shape Memory Polymers, *ANTEC 2002 Annual Technical Conference; San Francisco, CA*,1-5.

Rao I. J., 2004. On the Modeling of Quiescent Crystallization of Polymer Melts, *Polymer Engineering and Science*, **44**, 1, 123-130.

Rao I. J. and Rajagopal K. R., 2000. Phenomenological Modeling of Crystallization in Polymers Using the Notion of Multiple Natural Configuration, **2**, 73-94.

Rao I. J. and Rajagopal K. R., 2002. A Thermodynamic Framework for the Study of Crystallization in Polymers, *ZAMP*, **53**, 365-406.

Rao I. J. and Rajagopal K. R., 2005. Simulation of the Film Blowing Process for Semicrystalline Polymer, *Mechanics of Advanced Materials and Structures*, **12**, 2, 129-146.

Rubinstein L. I., 1971. The Stefen Problem, *Translations of Mathematics Monographs*, **27**, A.M.S., Providence, Rhode Island.

Spencer A. J. M., 1972. *Deformation of Fiber-Reinforced Materials*, Clarendon Press, Oxford.

Stefen J., 1891. On the Theory of Formation of Ice, in Particular in the Polar Sea, *Annalen der Physik und Chemie, (Wiedemann)*, **42**, 269-286.

Tey S. J., Huang W. M., Sokolowski W. M., 2001. Influence of Long-Term Storage in Cold Hibernation on Strain Recovery and Recovery Stress of Polyurethane Shape Memory Foam, *Smart Materials and Structures*, **10**, 321-325.

Tobushi H., Hara H., Yamada E. and Hayashi S., 1996. Thermo-mechanical Properties in a Thin Film of a Shape Memory Polymer of Polyurethane Series, *Smart Materials and Structures*, **5**, 483-491.

Tobushi H., Okumura K., Hayashi S. and Ito N., 2001. Thermomechanical Constitutive Model of Shape Memory Polymer, *Mechanics of Materials*, **33**, 545-554.

Treolar L. R. G., 1976. *The Physics of Rubber Elasticity*, Oxford University Press, Oxford.

Truesdell C., 1957. Sulle basi della thermomeccanica, *Rendiconti Lincei*, **22**, 33-38.

Truesdell, C., 1991. *A First Course in Rational Continuum Mechanics*, Academic Press.

Truesdell C. and Noll W., 1965. *The Non-Linear Field Theories of Mechanics*, In *Handbuch der Physik*, **3**, Springer, Berlin.

Wang M. and Zhang L., 1999. Recovery as a measure of oriented crystalline structure in poly(etherester)s based on poly(ethylene oxide) and poly(ethylene terephthalate) used as shape memorypolymers, *Journal of Polymer Science B*, **37**, 101-112.

Wunderlich B., 1976. *Macromolecular Physics Vol.2 Crystal Nucleation, Growth and Annealing*, Academic Press, New York.